Zeitschrift: IABSE reports of the working commissions = Rapports des commissions de travail AIPC = IVBH Berichte der Arbeitskommissionen

Band: 11 (1971)

Rubrik: Introductory reports

Nutzungsbedingungen

Die ETH-Bibliothek ist die Anbieterin der digitalisierten Zeitschriften auf E-Periodica. Sie besitzt keine Urheberrechte an den Zeitschriften und ist nicht verantwortlich für deren Inhalte. Die Rechte liegen in der Regel bei den Herausgebern beziehungsweise den externen Rechteinhabern. Das Veröffentlichen von Bildern in Print- und Online-Publikationen sowie auf Social Media-Kanälen oder Webseiten ist nur mit vorheriger Genehmigung der Rechteinhaber erlaubt. Mehr erfahren

Conditions d'utilisation

L'ETH Library est le fournisseur des revues numérisées. Elle ne détient aucun droit d'auteur sur les revues et n'est pas responsable de leur contenu. En règle générale, les droits sont détenus par les éditeurs ou les détenteurs de droits externes. La reproduction d'images dans des publications imprimées ou en ligne ainsi que sur des canaux de médias sociaux ou des sites web n'est autorisée qu'avec l'accord préalable des détenteurs des droits. En savoir plus

Terms of use

The ETH Library is the provider of the digitised journals. It does not own any copyrights to the journals and is not responsible for their content. The rights usually lie with the publishers or the external rights holders. Publishing images in print and online publications, as well as on social media channels or websites, is only permitted with the prior consent of the rights holders. Find out more

Download PDF: 02.04.2026

ETH-Bibliothek Zürich, E-Periodica, https://www.e-periodica.ch

I

RAPPORTS INTRODUCTIFS / EINFÜHRUNGSBERICHTE / INTRODUCTORY REPORTS

The Ultimate Load Behaviour of Plate Girders Loaded in Shear

Comportement à la ruine des poutres à âme pleine soumises au cisaillement

Traglastverhalten schubbeanspruchter Blechträger

K.C. ROCKEY
M.Sc., Ph.D., C.Eng., F.I.C.E.
Professor of Civil and Structural Engineering
University College, Cardiff, England

M. ŠKALOUD
Doc., C.Sc., Ing.
Senior Research Fellow
Czechoslovak Academy of Sciences
Institute of Theoretical and Applied Mechanics
Prague, Czechoslovakia

1. INTRODUCTION

The paper presents a Plastic Method of Design for Plate Girder Webs which allows for the influence of flange rigidity upon the post buckled behaviour of webs. The design procedure which is based on a study of the behaviour of 40 plate girders tested by the authors, has been checked against other experimental data available in the Technical Press. Because the present design procedure allows for the influence of flange stiffness upon the post buckled behaviour of shear webs it is more accurate than existing design methods.

Although plastic design methods have been developed for linear and flat slab structures, the majority of specifications used for the design of plate girders are still based on the concept of a limiting elastic stress. Since such design methods cannot result in optimum structures there has been an urgent need for a plastic collapse method for plate girders whose webs buckle prior to failure. The present paper presents a method for calculating the ultimate load of plate girders loaded in shear which allows for the influence which the stiffness of the flange members has upon the post buckled behaviour of the webplates.

Previous studies (1-5) involving the elastic post buckled behaviour of webplates loaded in shear have shown that the post-buckled behaviour of a shear panel is greatly influenced by the influence of the flexural rigidity of the flanges and the stiffness of the vertical stiffeners.

The theoretical study of Leggett and Hopkins on the behaviour of infinitely long plates showed how the stress distribution and the inclination of the waves developed in the buckled web varied significantly with both the flexural stiffness of the flanges and the cross sectional area of the vertical stiffeners.

In 1957, Rockey[3] reported on an extensive study of the elastic post buckled behaviour of shear webs having aspect ratios (b/d) of 2 and 3. This study established that if the flange flexural stiffness was such that the flange stiffness parameter $I/_b 3_t$ was less than the value given by equation (1) then due to the inward deflection of the flanges the depth of the buckles increased considerably.

$$I/_b 3_t = A\left(\frac{\tau}{\tau_{cr}} - 1\right) \quad \ldots\ldots\ldots\ldots\ldots (1)$$

where A = 0.00035.

As a result of subsequent studies by Djubek[4], Rockey and Martin[5], it was noted that the minimum value of A in equation 1 varied with the aspect ratio b/d in the manner shown in Figure 1.

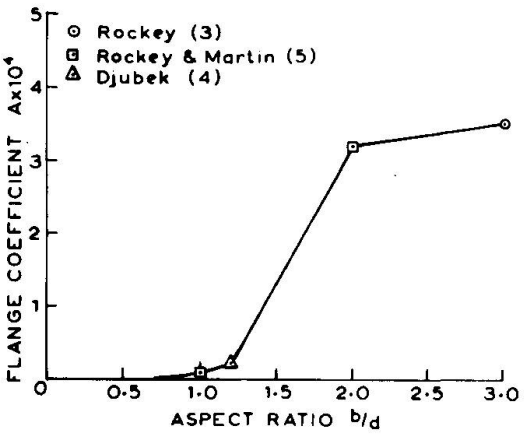

FIG. 1. VARIATION OF THE COEFFICIENT A IN EQUATION (1) WITH THE ASPECT RATIO b/d

In 1960, Basler and his colleagues (6-9) at Lehigh presented an ultimate method of design for shear webs for the particular case where the flanges are considered to be very flexible. They assumed that due to the flexibility of the flanges the buckles slip into the off diagonal form shown in Figure 2(a) and that failure occurs when the shaded area yields.

Using this structural model, Basler obtained the following expression for the ultimate load of a shear panel :-

$$W_{ult} = dt\left[\tau_{cr} + \frac{\sqrt{3}\,\tau_{yw}}{2\sqrt{1+\alpha^2}}\left(1 - \frac{\tau_{cr}}{\tau_{yw}}\right)\right] \quad \ldots\ldots\ldots\ldots\ldots (2)$$

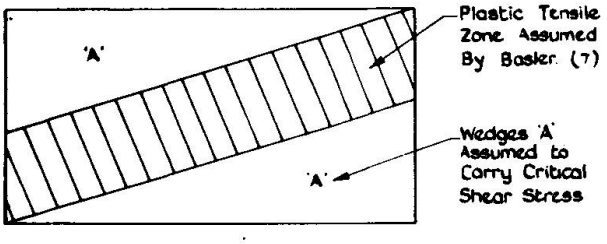

FIG. 2(a) COLLAPSE MODE ASSUMED IN BASLER THEORY.

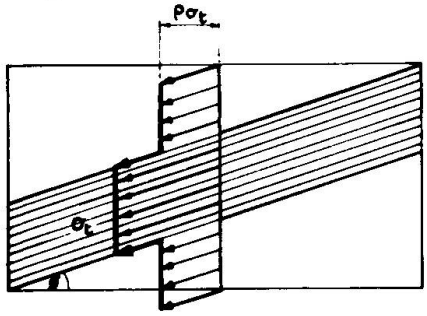

FIG. 2(b) MODIFIED BASLER TENSION FIELD MODEL ADOPTED BY OSTOPENKO; ρ = ½ TAKEN AS A TYPICAL VALUE

The results of this most interesting and valuable work have been used as the basis of the current design procedures used in the U.S.A. (10). However, it will be shown later in the present paper that the collapse model assumed by Basler is not correct and that it can result in both unduly conservative (safe) and understrength structures.

At the Conference of Steel Bridges (11), held in London in 1968 and later at the I.A.B.S.E. Conference (12) held in New York, the authors of the present paper presented the results of tests on 24 model girders, and showed that failure occurred when the girders

developed the collapse mechanism shown in Figure 3; the web yielding throughout the diagonal strip together with the development of

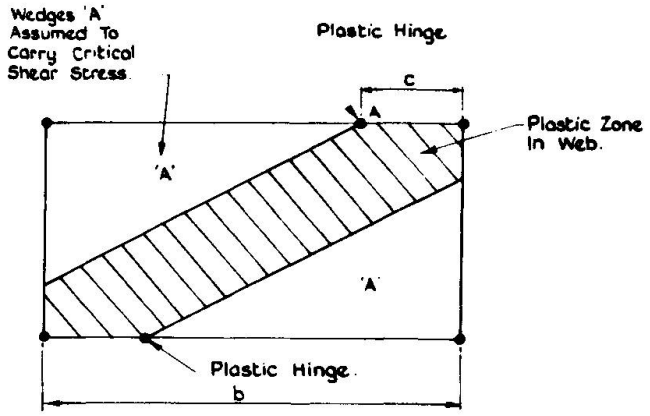

FIG 3(a) COLLAPSE MODEL PROPOSED BY ROCKEY & SKALOUD (12)

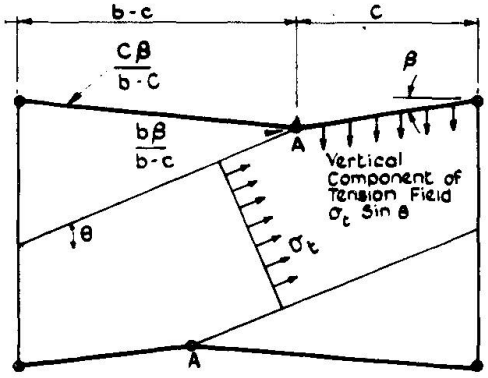

FIG 3(b) BEAM MECHANISM ASSUMED IN PROPOSED ROCKEY AND SKALOUD METHOD

plastic hinges in the flanges. It was also noted that the position of these plastic hinges varied with the flexibility of the flanges; with increasing flange stiffness the position of the plastic hinge (Q) moving towards the mid span position.

Figure 4 shows the possible modes of failure which can occur. In particular it is of interest to note that if the diagonal tension

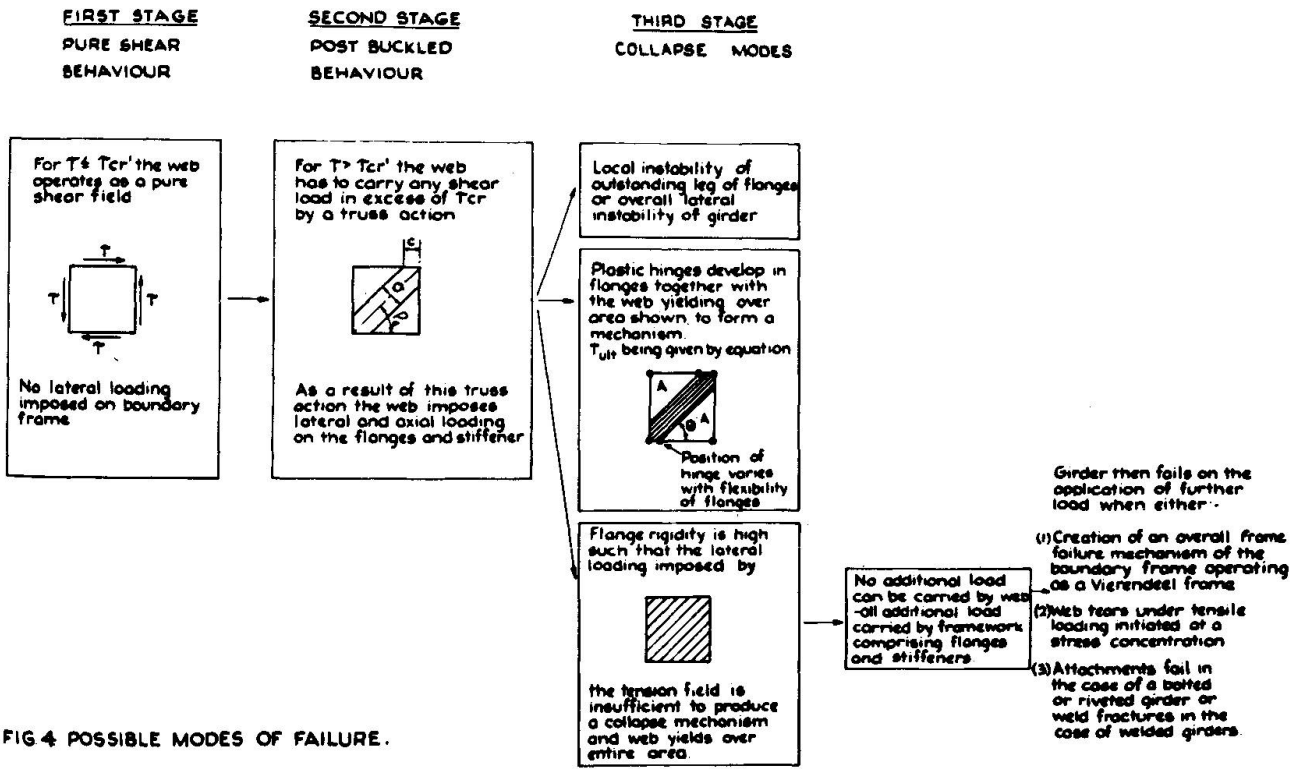

FIG 4 POSSIBLE MODES OF FAILURE.

loading is insufficient to develop plastic hinges in the flanges, then after the web has yielded any additional load has to be carried by the boundary framework, comprising the flanges and the stiffeners, acting as a Vierendeel girder.

At the same I.A.B.S.E. Conference, Fujii (13) presented a paper in which he presented a modification of Basler's theory. This modified theory involves the development of plastic hinges at mid span of the panel together with hinges over the stiffeners. It will be shown later that the modified model as proposed by Fujii, although recognising the part played by the flanges in the collapse of the girder, does not take into account the influence of the flange stiffness upon the position of the plastic hinge, and, therefore, Fujii's model is unable to deal with all of the failure modes and consequently gives results less satisfactory than the model proposed by the authors.

In August, 1969, Chern and Ostapenko (14) presented a new version of the Basler Collapse Mechanism. The model assumed by Chern and Ostapenko was similar to that assumed by Basler except for the fact that they allowed for the variation in σ_t across the section, see Figure 2(b). Furthermore, Ostapenko and Chern suggested that it would be more appropriate to use the value of τ_{cr} corresponding to the condition of the two edges supported by the flanges being clamped and the transverse edges being simply supported. They also discussed the value of ρ to be assumed in the modified tension field model, suggesting that for Practical Girders ρ should be taken as 0.5. Clearly if $\rho = 1.0$, then one would have the effect of a full tension field. It is this arbitrary choice in ρ and the fact that their tension band σ is still identical with Basler's so not allowing for the effect of flange rigidity which is the weakness in the Chern and Ostapenko approach, but with the influence of the flange flexibility parameter being clarified by the authors' present study; then as suggested by Chern and Ostapenko their model could be improved.

Chern and Ostapenko drew special attention to the frame action which occurs when the web yields and suggested a simple procedure to determine the magnitude of load required to produce this simple Vierendeel frame action.

2. EXPERIMENTAL INVESTIGATION

The experimental studies reported by the authors comprise three test series; series I and II dealing with the tests conducted by the authors and series III dealing with earlier tests made by one of the authors (15). The design details of the girders tested are given in Figure 5 and a summary of the dimensions of the girders and

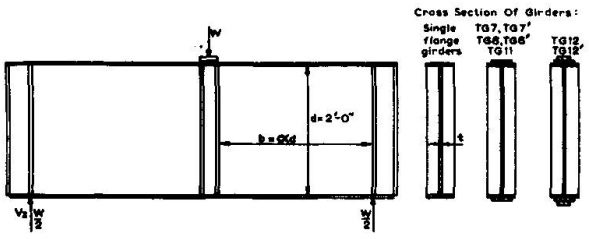

FIG. 5a. DETAILS OF SERIES I GIRDERS

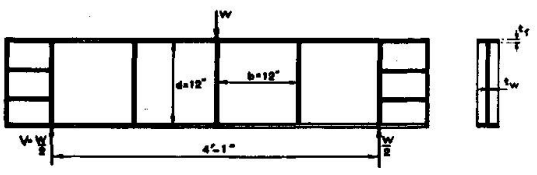

FIG. 5b. DETAILS OF SERIES II GIRDERS.

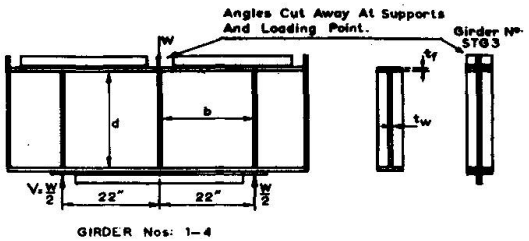

GIRDER Nos: 1–4

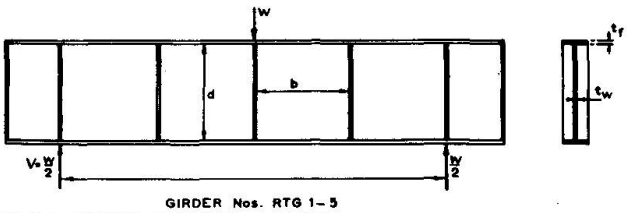

GIRDER Nos. RTG 1–5

FIG. 5c. DETAILS OF SERIES III GIRDERS.

the test data is given in Tables 1 - 3. It is beyond the scope of this paper to give a report on the testing procedure, and a full discussion of the test data obtained from these tests, but this information is available in reference (16).

2.1. DISCUSSION OF THE TEST RESULTS

Series I Girders

Table I gives the ultimate loads obtained from the 24 series I girders. Now since for each of the panel ratios examined, only the flexural stiffness of the flanges varied, the influence of flange stiffness upon the ultimate load carrying capacity of the girders is clearly demonstrated. It will be observed that the ultimate shear stress increases with the flange stiffness parameter ($I/_b{}^3{}_t$) until it reaches the shear yield stress indicating that the web has yielded over its complete surface.

Girder TG1 was very well instrumented, an electrical resistance strain gauge being attached at regular intervals along the flanges and demec gauge points placed across the compression diagonal of each of the web panels. Figure 6 shows the bending strains which were developed in the compression flange of girder TG1. It is of interest to note that at an applied load of 22.5 tons little bending of the flange had occurred but that after increasing to the ultimate load of 23.5 tons and then unloading there is a considerable plastic residue indicative of a plastic hinge having been developed. In the case of Panel W2 of Girder TG1, this plastic hinge is seen to have occurred at a distance of 0.25d. from the end stiffeners.

TABLE 1

Series I Girders. Aspect Ratio b/d = 1 b = 24in. d = 24in.

Girder No	Web Thickness t (in)	Flange* Dimensions in x in	$I/_b{}^3{}_t$ Units of 10^{-6}	W_{exp} Tons	% Gain Over Minimum Value Obtained with that Aspect Ratio	W_B Tons	W_{exp}/W_B
TG 1	0.107	4 x 0.185	1.47	22.6	0	34.26	1.43
TG 1[1]	0.107	4 x 0.187	1.47	24	6	32.63	1.36
TG 2	0.107	4 x 0.258	3.5	25.2	11.5	32.44	1.29
TG 2[1]	0.107	4 x 0.253	3.5	23.5	4	33.08	1.41
TG 3	0.108	4 x 0.495	27.9	28.5	26	34.48	1.21
TG 3[1]	0.108	4 x 0.497	27.9	27	19.5	32.25	1.19
TG 4	0.107	4 x 0.625	54.5	31.8	41	31.35	0.986
TG 4[1]	0.107	4 x 0.623	54.5	30.3	34	34.90	1.15
TG 13	0.103	4 x 0.997	224	41.7	84	34.66	0.831
Series I Girders. Aspect Ratio b/d = 1.5 b = 36in. d = 24in.							
TG 5[1]	0.103	8 x 0.375	7.35	23.4	0	29.22	1.12
TG 5	0.103	8 x 0.374	7.35	26.0	11	27.39	1.17
TG 6	0.103	8 x 0.644	34	28.4	21	30.55	1.07
TG 6[1]	0.103	8 x 0.635	34	26.7	14	26.43	0.99
TG 7	0.103	8 x 0.644 and 7 x 0.376	129	35.5	52	29.59	0.833
TG 7[1]	0.103	8 x 0.637 and 7 x 0.380	129	38.6	65	30.96	0.802
TG 8	0.103	8 x 0.639 and 7 x 0.62	254	40.3	72.5	30.44	0.755
TG 8[1]	0.103	8 x 0.644 and 7 x 0.634	254	41.4	76.5	30.41	0.735
Series I Girders. Aspect Ratio b/d = 2.0							
TG 9[1]	0.103	8 x 0.388	3.1	24.05	0	23.36	0.951
TG 9	0.103	8 x 0.388	3.1	24.55	2	25.0	1.04
TG 10	0.103	8 x 0.640	14.3	25.7	77	23.31	0.907
TG 11*	0.103	8 x 0.640 and 6 x 0.625	98.4	35.5	47.5	25.44	0.717
TG 12	0.103	9 x 0.780 and 8 x 0.62 and 7 x 0.489	384	45.7	90	23.22	0.508
TG 12[1]	0.103	9 x 0.767 and 8 x 0.63 and 7 x 0.501	384	49.2	104	24.00	0.488
Series I Girders. Aspect Ratio b/d = 0.79 b = 19in. d = 24in.							
TG 0	0.057	4 x 0.254	13.4				

* TG 11 had a depth d of 24.25".

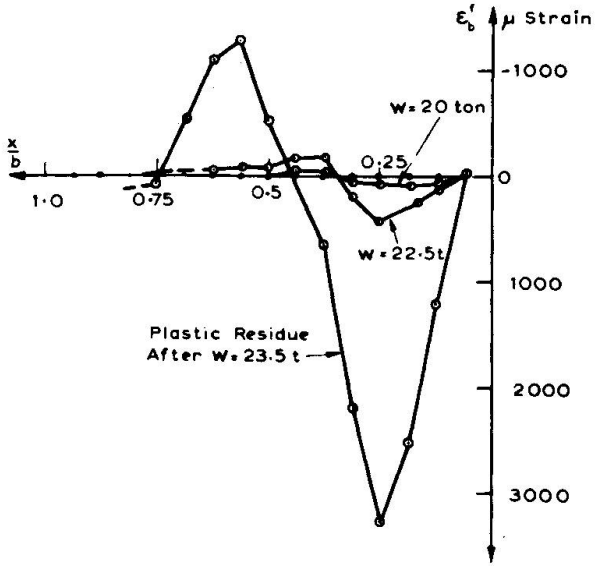

FIG. 6. COMPRESSION FLANGE BENDING STRAINS. GIRDER TG1 - PANEL W2.

Figure 7 shows the residual web deflections remaining in panel W1 after failure together with the diagonal mid plate tensile strains, acting across the diagonal AB which were measured at various loads. It is important to note that the wave inclination is along the diagonal and that the web strains are also reasonably symmetric about the diagonal since Basler, in the model shown in Figure 2, has assumed a different model.

It is also of interest to note that at an applied load of 20 tons which was 83.5% of the failure load, the diagonal membrane stresses are still elastic.

Figure 8 shows girder TG4 after it had been tested to failure, whilst Figure 9 gives the plastic residual deformations in the flanges and the residual diagonal membrane strains in the webs.

In the case of panel W1 it is seen that the plastic hinge is now 0.405 d from the end stiffener. Thus we see that as a result of increasing the flexural rigidity of the flange, the position of the hinge has moved closer to the mid section of the panel. The variation of the position of the hinge in the compression flange with the I/b^3t parameter has been plotted in Figure 10 from which it will be noted that as $I/b^3t \to \infty$ so the c/b ratio approaches 0.5. It will be noted from Figure 11 that if a residual strain of 1000 micro-strain is taken to indicate full plasticity, then the width of the fully yielded diagonal tensile band intercepts close to the position of the plastic hinges which have developed in the flanges, thus showing that the plastic collapse model proposed, see Figures 3 and 4, is completely realistic. Referring to Figure 9, it will be noted that the collapse mechanism is similar to that shown in Figure 12(a), with a plastic hinge developed at all corners. However, it should be appreciated that when the web collapses the framework develops a Vierendeel Mechanism as shown in Figure 12(b). It is clear that on combining Figures 12(a) and 12(b) one achieves the Mechanism obtained in Figure 12(c), which is of the same form as that given in Figure 9.

The series I test programme had established the basis of the design method but it was desirable that further tests be conducted on multi-bay girders to study the influence of panel continuity and to obtain data from girders having different depth/thickness ratios. With these two factors in mind the test girders comprising the Series II programme were designed, for details see Figure 5 and Tables 2 and 3. Two web thicknesses were chosen, the depth/thickness of the thickest plate giving a high buckling stress whereas the thinner plate provided web panels in which the critical load was sufficiently low to ensure that the post buckled action dominated; the buckling shear stresses for the square panels, assuming simply supported edges, being 1.13 and 5 tons/in^2 respectively. The test data obtained from this test programme was most useful in confirming and extending the basis of the theory which resulted from Series I study. Figure 13 compares the residual contour plots which were obtained in a panel of girder TG15 with that occurring in a panel of girder TG19. It will be noted from Table 2 that Girders TG15 and 19 were similar in all respects except for the thickness of the flange members. It will be seen that in the case of girder TG19, the web had developed a uniform tension field, consisting of 8 half waves which covered the whole web, whereas in the case of TG15 a less well defined

TABLE 2

Series II Girders. All panels of Aspect Ratio b/d = 1.0 b = 12m d = 12in.

Girder No	Web Thickness t (in)	Flange Dimensions in x in	I/b^3t Units of 10^{-6}	Type of Failure	$\frac{c}{b}$ exp	$\frac{c}{b}$ th	W_{exp} Tons	W_{RS} Tons	$\frac{\tau_{cr}}{\tau_y}$	$\frac{\tau_{ult}}{\tau_y}$	$\frac{\tau_{exp}}{\tau_{yw}}$	$\frac{V_B}{V_{exp}}$	$\frac{V_{RS}}{V_{exp}}$
TG 14	0.038	3 x 0.123	7.4	Mechanism, Figure 4	0.23	0.316	5.09	4.63	0.138	0.619	0.681	0.978	0.910
TG 15	0.038	3 x 0.197	23.5	Mechanism, Figure 4	0.35	0.418	5.89	5.78	0.138	0.773	0.788	0.845	0.982
TG 16	0.038	3 x 0.254	60.2	Mechanism, Figure 4	0.488	0.50	6.28	6.72	0.138	0.899	0.840	0.793	1.07
TG 17*	0.038	3 x 0.367	190	Mechanism, Figure 4	0.467	0.50	7.82	6.72	0.138	0.899	1.045	0.637	0.859*
TG 18*	0.038	3 x 0.510	471	Web has yielded, Frame Mechanism	0.50	0.50	10.10	6.72	0.138	0.899	1.35	0.493	0.665*
TG 19	0.038	3 x 0.611	835	" " " "	0.50	0.50	10.9	6.72	0.138	0.899		0.456	
TG 20	0.08	3 x 0.128	3.35	Premature Failure Flange Collapse due to Bending Stress > σ_{yf}		0.168	10.23	11.63	0.576	0.710	0.624	1.34	1.14
TG 21	0.08	3 x 0.192	11.9	Mechanism, Figure 4	0.296	0.269	14.25	12.95	0.576	0.790	0.870	0.961	0.909
TG 22	0.08	3 x 0.255	29.3	Mechanism, Figure 4	0.367	0.457	15.8	15.38	0.576	0.939	0.964	0.866	0.974
TG 23	0.08	3 x 0.363	95.2	Mechanism, Figure 4	0.484	0.50	16.3	15.95	0.576	0.973	0.995	0.840	0.978
TG 24*	0.08	3 x 0.510	236.4	Web has Yielded, Frame Mechanism	0.50	0.50	19.3	15.95	0.576	0.973	1.18	0.709	0.826*
TG 25*	0.08	3 x 0.612	408.6	" " " "	0.5	0.5	20.8	15.95	0.576	0.973	1.27	0.658	0.766*

* For these Girders $\tau_{exp}/\tau_{yw} > 1$ ∴ Frame Mechanism involved

TABLE 3

SERIES III GIRDERS

Girder No	Aspect Ratio	Web Thickness t in.	Web depth d in.	Web width b in.	Flange Dimen. in. x in. *	Girder No	Type of Failure	W_{exp} Tons	$\frac{\tau_{cr}}{\tau_{yw}}$	$\frac{\tau_{ult}}{\tau_{yw}}$	$\frac{\tau_{exp}}{\tau_{yw}}$
STG 1	1.85	0.079	11	21.7	5 x 0.312	STG 1	Mechanism Figure 4	12.0	0.445	0.834	0.771
STG 2	1.98	0.063	9.95	19.75	5 x 0.25	STG 2	" " 4	7.9	0.304	0.743	0.627
STG 3	1.98	0.056	10	19.8	5 x 0.187 plus 2½"x2½"x5/16" Angles.	STG 3	Fully developed tension field, frame mechanism.	20.0	0.251	0.814	> 1.0
STG 4	1.98	0.049	9.9	19.60	4 x 0.250	STG 4	Mechanism Figure 4	7.0	0.206	0.590	0.786
RTG 1	1.0	0.05	12	12	3 x 0.177	RTG 1	Mechanism Figure 4	8.0	0.215	0.578	0.730
RTG 2	1.0	0.05	12	12	3 x 0.183	RTG 2	" " 4	8.15	0.215	0.586	0.744
RTG 3	1.0	0.0375	12	12	3 x 0.183	RTG 3	" " 4	4.85	0.164	0.709	0.667
RTG 4	1.0	0.0375	10	10	3 x 0.183	RTG 4	" " 4	11.7	0.378	0.610	0.808
RTG 5	0.94	0.064	11.7	11	3 x 0.187						

Tension Field consisting of only 3 half waves had been developed. In the case of girder TG19 the tensile forces imposed by the membrane field upon the boundary members had been insufficient to develop plastic hinges in the flanges, thus the web was able to develop the full diagonal tension action.

In such cases there are two distinct phases; in the first phase the post buckled behaviour develops until the web has yielded over its complete surface, the flange remaining elastic. Once this stage has been reached additional shear load can only be carried by the framework and failure will result when the framework, comprising the flanges and the stiffeners, acting like a Vierendeel Frame, develops sufficient hinges to form a mechanism, such as that shown in Figure 12(c).

An alternative failure is encountered in aluminium girders when, because of the materials reduced ductibility under the tensile strains. Figure 14 shows a typical aluminium girder with very stiff flanges, which has experienced a tensile failure in the web.

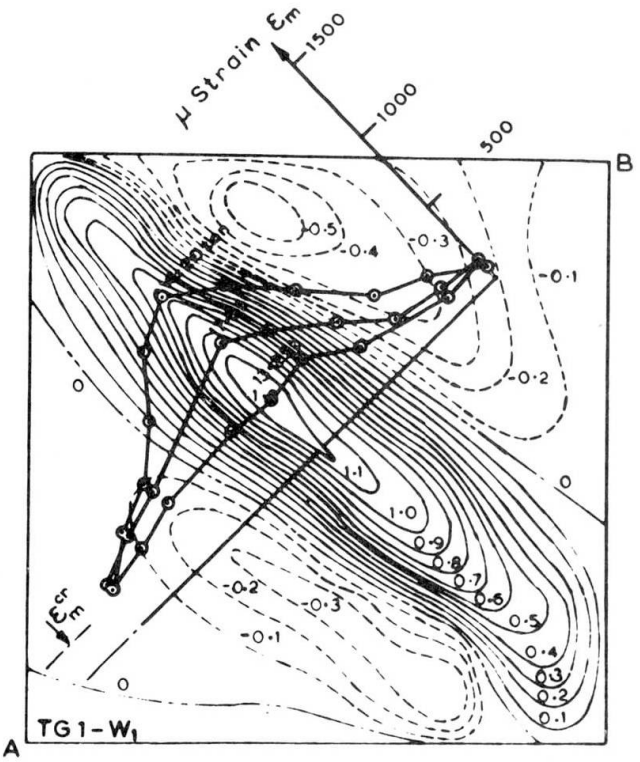

FIG.7. Tensile strains developed across diagonal AB of panel W1 in girder TG1 together with the residual web deflections which remained after failure.

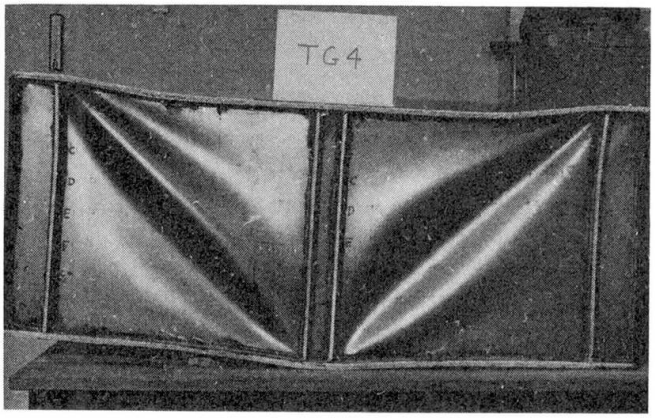

FIG.8. Girder TG4 after test to failure. Note well developed hinges.

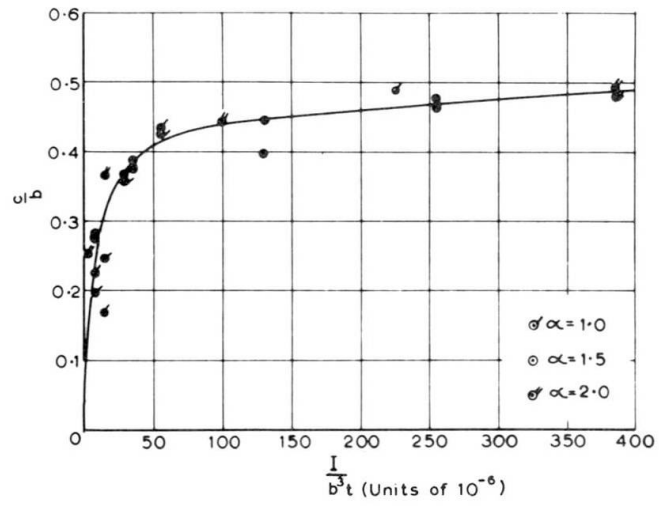

FIG.10. VARIATION OF THE POSITION OF THE PLASTIC HINGE REPRESENTED BY THE PARAMETER c/b, AND THE FLANGE FLEXIBILITY PARAMETER (I/b^3t).

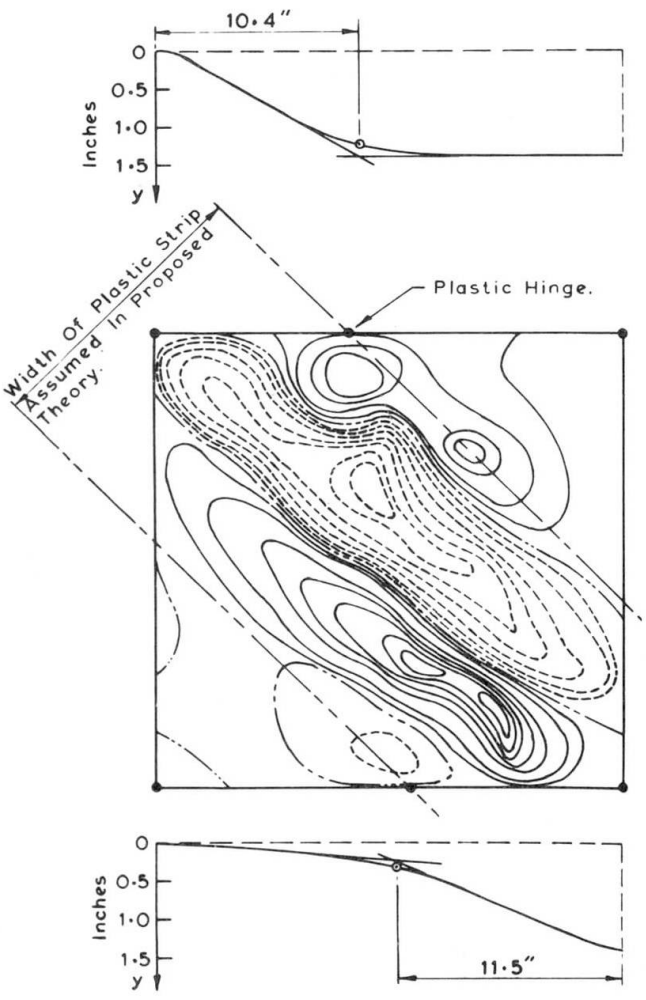

FIG.9. RESIDUAL DEFORMATIONS IN FLANGES AND WEB OF PANEL W1 OF GIRDER TG4 (Series I)

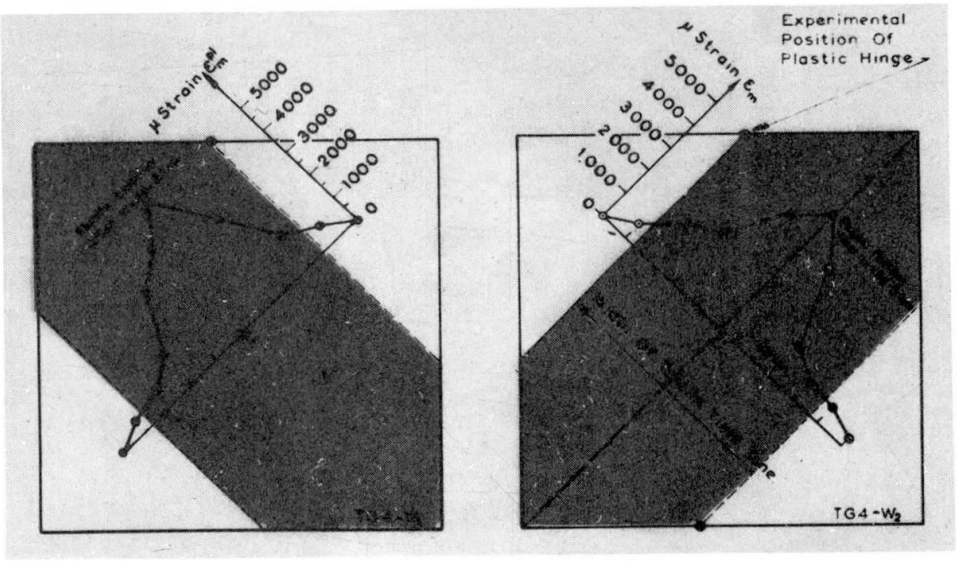

FIG. 11. RESIDUAL DIAGONAL MEMBRANE STRAINS – PANELS W_1 & W_2 OF GIRDER TG4.

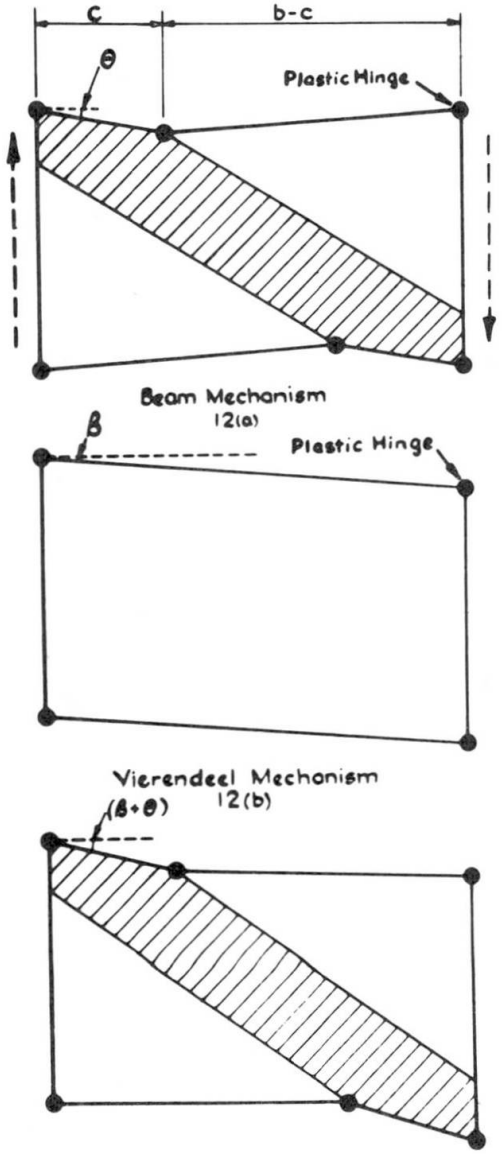

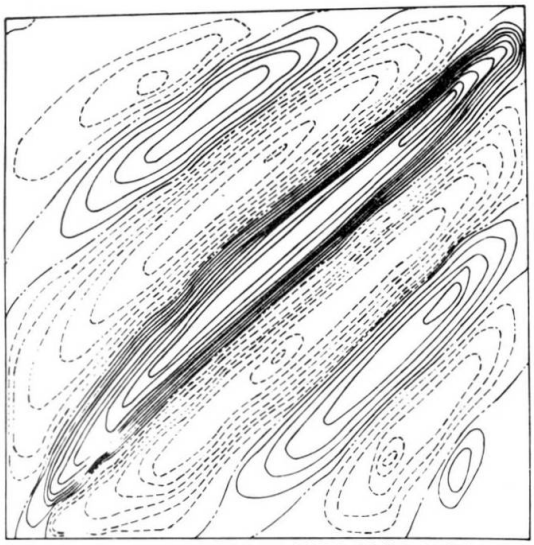

FIG. 13(a) RESIDUAL CONTOUR PLOT OF GIRDER TG 19. FLANGES VERY STRONG – WEB DEVELOPS FULL SHEAR STRENGTH.

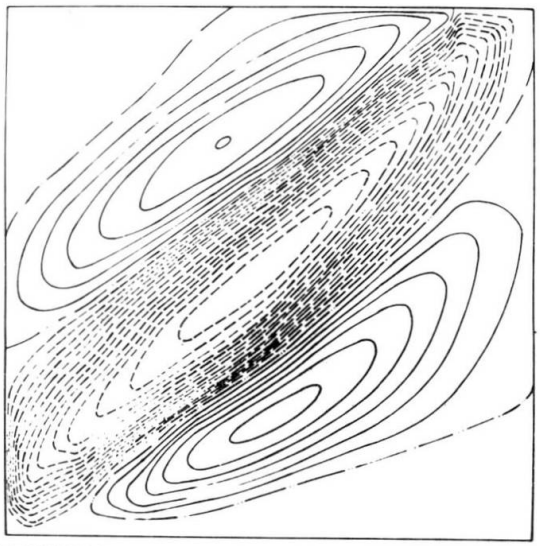

FIG. 13(b) RESIDUAL CONTOUR PLOT OF A PANEL ON GIRDER TG 15

Figures 11, 20, 22 and 24 are examples of the possible modes of failure which can be encountered in a webplate subjected to shear as shown in Figure 14.

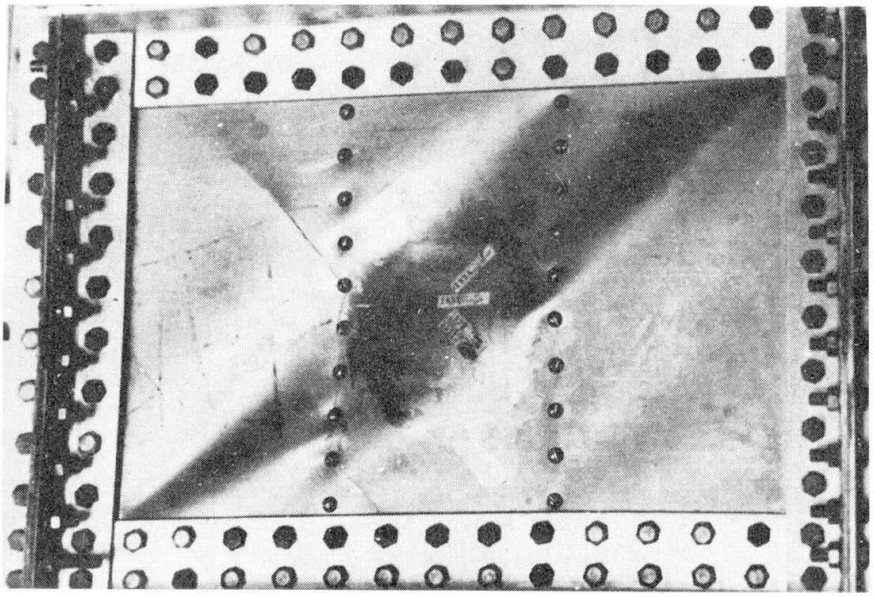

3. DESIGN CONCEPT

3.1. Introduction

The research study has shown that the behaviour of a plate girder web can be divided into three stages.

Stages I and II

In Stage I, which only applies to a perfectly flat plate, for shear stresses less than the critical buckling stress the web panels carry the applied load by a pure shear action.

The second mode of action results from the fact that in a buckled web the compressive stresses cannot increase and any additional load has to be carried by a tensile truss action. As illustrated in the preceding sections the post buckled action of a web plate is influenced by the flexural stiffness of the flanges and stiffeners; with very stiff flanges the tensile field action is uniformly distributed across the webplate, whereas with more flexible flanges the tensile field action is restricted to a diagonal band.

With normal welded plate girders which have webs with significant permanent deformations, no buckling phenomena will be observed and the loadings which are associated with Stage II occur as soon as a load is applied to the girder.

Failure occurs when the diagonal tension band, see Figure 3, yields and the boundary members develop sufficient plastic hinges to result in a failure characterised by one of the three possible forms of failure listed under Stage III, see also Figure 4.

Stage III

(a) If the lateral membrane loading on the flange is sufficient to develop plastic hinges in the flanges, then failure will be due to the development of a yielded diagonal strip together with plastic hinges in the tension and compression flanges; see Figures 3 and 4.

(b) If, however, the membrane loading corresponding to a

yielded web is not sufficient to develop plastic hinges in the flanges, then failure will occur when either :-

(1) the web material fractures, such as occurs in an aluminium web, see Figure 14, which shows a typical diagonal web fracture

(2) the frame work comprising the flanges and the stiffeners develop a 'frame' mechanism as a result of carrying further loading as a framework since the fully yielded web cannot carry any additional shear load ; see Figure 12.

(3) a third class of failure which can occur is when the compression flange buckles laterally or torsionally, or develops a local buckle in the outstanding flange of the flanges.

3.2. THEORETICAL BASIS

STAGE 1

For an initially plane web, for loading below the buckling stress, τ_{cr}, the stress state is assumed to be one of pure shear. Obviously the value of τ_{cr} will vary with the torsional rigidity of both the flanges, and the stiffeners.

Following buckling, the web is unable to withstand any further compression loading and any additional loading has to be carried by a tension field action. The present solution does not attempt to deal with the very complicated stress field which occurs in the elastic post buckled range, being solely concerned with the final collapse mode. Observations of the collapse behaviour of girders indicates that the stress and deflection distributions vary quite rapidly and significantly at loads close to the ultimate.

As shown earlier, the experimental evidence resulting from the present study is that at collapse the web develops a tension band as shown in Figure 3 in which the angle of the tension band is equal to the inclination of the geometrical diagonal and that the tension band is symmetric with respect to the geometric diagonal. The width of the diagonal tension load is assumed to be such that at its junction with the flange its edges coincide with position of the plastic hinge in the flanges. The above assumptions with respect to the inclination of the diagonal tension field will clearly result in lower bound solutions for values of $\alpha > 1$ when the flanges are stiff.

The position of the plastic hinge in the flange may be theoretically determined using the collapse mechanism shown in Figure 3(b). This mechanism assumes that the hinge coincides with the edge of the diagonal strip and that the loading consists of the vertical component of the diagonal tensile membrane stress $\sigma_t{}^y$. The solution of this simple mechanism reduces to the solution of the following cubic equation given in equation 3.

$$\left(\frac{c}{b}\right)^3 - \left(\frac{c}{b}\right)^2 + \frac{4\, z_f \sigma_{yf}}{b^2 t\, \sin^2\theta\, (\sigma_t{}^y)} = 0 \qquad \ldots\ldots\ldots\ldots (3)$$

where z_f denotes the plastic modulus for flange assembly. From a study of all experimental data from the technical literature it is

proposed that when the web buckling stress τ_{cr} is less than half the shear yield stress τ_{yw} a depth of web plate, d_e, as obtained from equation 4 be assumed to act with the flange.

$$d_e = 30(1 - \frac{2\tau_{cr}}{\tau_{yw}})t \qquad \ldots\ldots\ldots\ldots\ldots\ldots(4)$$

Thus we see that there are two stress regions, see Figures 3 and 15.

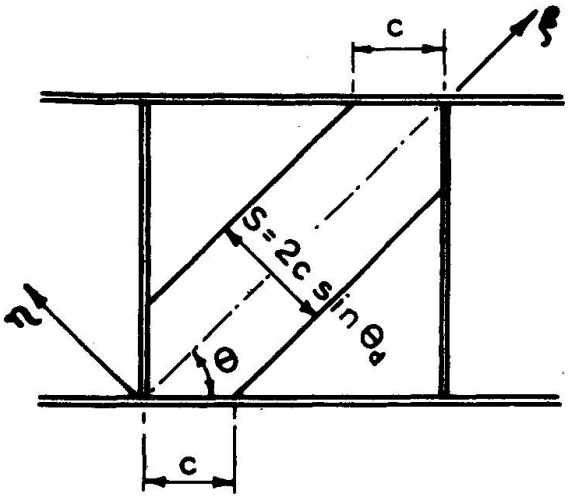

FIG. 15.

(1) two triangular wedges in which the critical shear stress is assumed to act

(2) a yielded diagonal strip

The tension stress σ_t is assumed to act uniformly over the diagonal band, yielding occurring when σ_t reaches a value σ_t^y.

The stress condition, see Figure 15, in the diagonal web strip, is given by :-

$$\sigma_\zeta = \tau_{cr} \text{ Sin } 2\theta + \sigma_t^y$$

$$\sigma_\eta = \tau_{cr} \text{ Sin } 2\theta \qquad \ldots\ldots\ldots(5)$$

$$\tau = \tau_{cr} \text{ Cos } 2\theta$$

Using the Huber Von Mises plasticity condition, the material yields when $\sigma_{mc} = \sigma_{yw}$ where

$$\sigma_{mc} = \sqrt{\sigma_\zeta^2 + \sigma_\eta^2 - \sigma_\zeta\sigma_\eta + 3\tau^2} \qquad \ldots\ldots\ldots\ldots(6)$$

Substituting equation 5 into 6 and rearranging yields

$$\sigma_t^y = -\frac{3}{2}\tau_{cr} \text{ Sin } 2\theta + \sqrt{\sigma_{yw}^2 + \tau_{cr}^2\left(\left(\frac{3}{2} \text{ Sin } 2\theta\right)^2 - 3\right)} \qquad \ldots\ldots\ldots\ldots(7)$$

The diagonal membrane tensile force will develop axial forces in both the stiffeners and the flanges, see equations 9 and 12 in the Authors' Reports (16).

The shear force V_σ carried by the diagonal strip

= width of strip x web thickness x σ_t^y x Sinθ

$$V_\sigma = 2ct \text{ Sin}^2\theta\left(-\frac{3}{2}\tau_{cr}\text{Sin}2\theta + \sqrt{\sigma_{yw}^2 + \tau_{cr}^2\left(\left(\frac{3}{2}\text{Sin}2\theta\right)^2 - 3\right)}\right) \qquad \ldots\ldots\ldots(8)$$

The total shear force $V_{ult} = V_\sigma +$ the shear force V_{cr} necessary to cause the plate to buckle.

$$V_{ult} = V_{cr} + V_\sigma = \tau_{cr}\, dt + 2ct \text{ Sin}^2\theta\left(-\frac{3}{2}\tau_{cr} \text{ Sin } 2\theta + \right.$$

$$\sqrt{\sigma_{yw}^2 + \tau_{cr}^2\left(\left(\frac{3}{2}\ \mathrm{Sin}\ 2\theta\right)^2 - 3\right)} \qquad \ldots\ldots\ldots (9)$$

and the corresponding shear stress τ_{ult} is given by

$$\tau_{ult} = \tau_{cr} + \frac{2c}{d}\ \mathrm{Sin}^2\theta\left(-\frac{3}{2}\ \tau_{cr}\ \mathrm{Sin}\ 2\theta + \sqrt{\sigma_{yw}^2 + \tau_{cr}^2\left(\left(\frac{3}{2}\ \mathrm{Sin}\ 2\theta\right)^2 - 3\right)}\right) \qquad \ldots\ldots\ldots (10)$$

The value of τ_{cr} depends on the tensile rigidity of the flanges. It is recommended that with conventional plate girders having single flat flange plates, it can be assumed that the web is simply supported along all 4 edges. However, should the flanges be of tubular construction it would be more appropriate to assume the web is clamped to the flanges and simply supported at the vertical stiffeners.

$$\text{Now} \quad \tau_{yw} = \sigma_{yw}/\sqrt{3}$$

Therefore, dividing equation 10 by τ_{yw} one obtains

$$\frac{\tau_{ult}}{\tau_{yw}} = \frac{\tau_{cr}}{\tau_{yw}} + 2\sqrt{3}\ \frac{c\alpha}{b}\ \mathrm{Sin}^2\theta\left(-\frac{\sqrt{3}}{2}\ \mathrm{Sin}\ 2\theta\left(\frac{\tau_{cr}}{\tau_{yw}}\right) + \sqrt{1 + \left(\frac{\tau_{cr}}{\tau_{yw}}\right)^2\left(\frac{3}{4}\ \mathrm{Sin}^2(2\theta) - 1\right)}\right) \qquad \ldots\ldots\ldots (12)$$

It is of interest to consider how equation (12) satisfies the following limiting conditions.

(1) Very Thin Webs and Rigid Flanges

For very thin webs $\tau_{cr} \to 0$, in which case

$$\frac{\tau_{ult}}{\tau_{yw}} = 2\sqrt{3\alpha}\ \frac{c}{b}\ \mathrm{Sin}^2\theta$$

Since for rigid flanges, $\frac{c}{b} = 0.5$, then for square web panels in which $\theta = \frac{\pi}{4}$ one obtains the value for τ_{ult} of :-

$$\frac{\sqrt{3}}{2}\ \tau_{yw} \quad \text{or} \quad \frac{\sigma_{yw}}{2}$$

which agrees with the value obtained from Wagner's Theory for a complete tension field.

(2) Very Thick Webs

When webs are very thick, then $\tau_{cr} \to \tau_{yw}$ and the terms inside the main brackets reduces to zero so that equation (12) reduces to $\tau_{ult} = \tau_{cr}$; which again is as to be expected.

(3) Very Flexible Flanges

Finally, if $\frac{c}{b} \to 0$, as would be the case if the flanges had

zero stiffness, then

$$\tau_{ult} = \tau_{cr}$$

Thus we would see that equation (12) satisfies the extreme boundary conditions exactly.

When $\sqrt{3}\,\tau_{cr}$ exceeds the limit of proportional stress of the material then the effective modulus E_r is less than the modulus of Elasticity E. This reduces the critical shear stress; and to allow for this Basler and his colleagues have recommended that τ_{cr} be replaced by τ_{cre} when $\tau_{cr} \quad \frac{0.8\,y}{\sqrt{3}}$, τ_{cre} being obtained from equation 18.

$$\frac{\tau_{cre}}{\tau_{yw}} = 1 - \frac{0.16\tau_{yw}}{\tau_{cr}}$$

Using equation (13), the relationship between the ratio τ_{ult}/τ_{yw} and the depth to thickness ratio for different values of c/b have been plotted in Figure 16 for the case of a square web plate. The values of τ_{ult}/τ_{yw} as derived from Basler's ultimate load expression, equation 2, have also been plotted using the same relationship between τ_{cre}, τ_{cr} and τ_{yw}, and it is clearly seen that for very flexible flanges Basler's equation over-estimates the strength of the girder and for relatively stiff flanges it underestimates the strength, this being particularly true for the larger values of α.

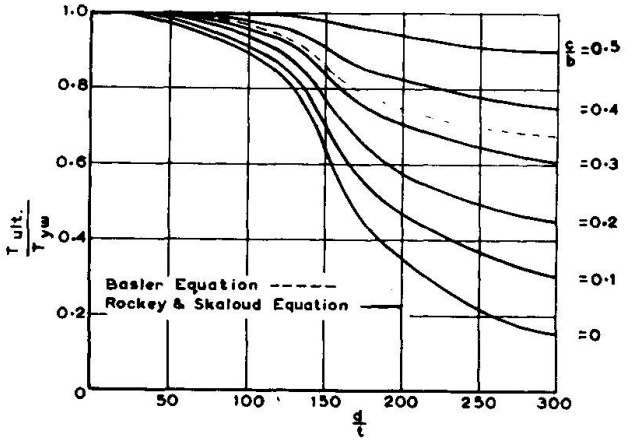

FIG. 16.

4.0. DISCUSSION OF TEST RESULTS

COMPARISON OF DESIGN PROCEDURE WITH EXPERIMENTAL DATA

In this section, the ultimate load method of design developed in the previous section will be checked against all the available experimental data.

In these tables, V_{RS} is the ultimate shear load obtained by the authors when using equation (14) together with equation (19) when $T_{cr}/T_{yw} > 0.5$.

In Tables 1 - 6, the ultimate loads predicted by the authors' Method has been compared with the experimental failure loads and the theoretical values predicted by Basler (6), Fujii (13) and Ostapenko (14).

$$\frac{T_{cre}}{T_{yw}} = 1 - 0.25\,\frac{T_{yw}}{T_{cr}} \qquad \text{.....(14)}$$

Unfortunately, it is not possible in the restricted space of the present article to refer in detail to all of the tests. However, a full discussion is available in Reference (16).

Table 2 presents the results obtained from the twelve Series II girders. These girders had web panels with an aspect ratio of one, the only variables being in the thickness of the flanges and the web material. It will be noted that for the thinner webs the predicted failure loads for girders TG14, 15 and 16 are very close to the actual failure load of the girders. With girders TG17 - 19 the flanges were thick and the web developed full plasticity without causing a plastic hinge in the flanges, failure occurring when the boundary members developed a frame mechanism. It will be noted that the τ_{exp}/τ_{yw} ratio for girders TG14 - 19 increases with an increase in flange thickness, until in the case of girders 17 - 19, it exceeds unity indicating that the web is fully yielded, and the girder is carrying the same load as a Vierendeel type structure.

In such cases the ultimate shear load is given by equation (20) in which V_f is the additional shear load necessary to cause the framework to fail a Vierendeel girder mechanism, see figure 13(c). Ignoring the presence of the yielded web but allowing for the reduction in the strength of the flanges due to the axial stresses set up in the flanges by the membrane field.

$$\text{Ultimate shear load} = V_{RS} + V_f$$

V_f can be readily determined using standard design methods for the plastic collapse of structures.

It will be noted that the proposed design procedure gives good agreement with the actual failure loads, see Tables 1 - 6.

TABLE 4

TEST DATA FROM REFERENCE 18 - SAKAI, DOI, NISHINO AND OKUMWA

GIRDER NO	$a = \frac{b}{d}$	$\frac{d}{t}$	WEB		FLANGES		V_{exp} Tons	$\frac{\tau_{exp}}{\tau_{yw}}$	V_{RS} Tons	$\frac{\tau_{cr}}{\tau_{yw}}$	$\frac{\tau_{ult}}{\tau_{yw}}$	$\frac{V_B}{V_{exp}}$	$\frac{V_F}{V_{exp}}$	$\frac{V_O}{V_{exp}}$	$\frac{V_{RS}}{V_{exp}}$
			$t \times b \times d$ mm x mm x mm	σ_{yw} Kg/mm²	$t_f \times B_f$ mm x mm	σ_{yf} Kg/mm²									
G1	2.61	55	8 x 1150 x 440	44	30 x 160	42	82	0.917	87.4	0.83	0.978	1.18	0.945	1.01	1.07
G2	2.61	55	8 x 1150 x 440	44	30 x 200	42	84	0.939	87.4	0.83	0.978	1.15	0.923	0.984	1.04
G3	2.63	60	8 x 1467 x 560	44	30 x 160	42	99	0.870	107.9	0.723	0.948	1.03	0.992	1.01	1.09
G4	3.57	70	8 x 2000 x 560	44	30 x 250	42	97	0.852	104.0	0.710	0.958	1.02	1.01	1.01	1.07
G5	2.68	70	8 x 1500 x 560	44	30 x 250	42	107	0.940	107.6	0.722	0.940	0.96	0.916	0.932	1.01
G6	1.25	70	8 x 687 x 560	44	30 x 250	42	120	1.05	112.9	0.795	0.997	0.94	0.820	0.892	0.941
G7	2.68	70	8 x 1500 x 560	44	30 x 250	42	107	0.940	107.6	0.722	0.946	0.95	0.920	0.892	1.01
G9	2.78	90	8 x 2000 x 720	44	30 x 250	42	118	0.806	117.9	0.538	0.805	0.835	1.054	0.838	0.999

It is of interest to note that Nishino and Okumwa in the discussion of their tests, write, "The plastic collapse loads increase with increase of flange area for the same web plate, whereas the theory of Basler predicts the same collapse; therefore, testing of girders with still heavier flanges may reveal the difference and lead to a clear conclusion".

It is because the design procedure proposed by the authors' of the present paper allows for the influence of flange stiffness upon the post buckled behaviour of the web, that it is capable of accurately predicting the failure load of the girders.

TABLE 5

TEST DATA FROM REFERENCE 19 - NISHINO AND OKUMMA

GIRDER NO	$a = \frac{b}{d}$	$\frac{d}{t}$	WEB $t \times b \times d$ mm x mm x mm	WEB σ_{yw} Kg/mm²	FLANGES $t_f \times B_f$ mm x mm	FLANGES σ_{yf} Kg/mm²	V_{exp} Kips	$\frac{\tau_{exp}}{\tau_{yw}}$	V_{RS} Kips	$\frac{\tau_{cr}}{\tau_y}$	$\frac{\tau_{ult}}{\tau_y}$	$\frac{V_B}{V_{exp}}$	$\frac{V_F}{V_{exp}}$	$\frac{V_O}{V_{exp}}$	$\frac{V_{RS}}{V_{exp}}$
G1	2.69	59.6	9.1 x 1450 x 543	38.0	22.4 x 301.0	44	110.5	1.02	105.8	0.826	0.976	0.904	1.06	1.02	0.958
G2	2.69	59.6	9.1 x 1450 x 543	38.0	22.4 x 220.0	44	104	0.959	105.8	0.826	0.976	0.961	0.925	1.10	1.02
G3	2.64	76.8	9.4 x 1900 x 722	38.0	22.2 x 302.0	44	124.5	0.836	134.5	0.712	0.903	1.04	1.02	1.19	1.08
G4	2.64	78.3	9.2 x 1900 x 720	38.0	22.1 x 243.0	44	114.5	0.788	126.1	0.701	0.868	1.10	-	-	1.10

TABLE 6

Test Data from Reference 20 - Longbotton and Heyman

GIRDER NO	$a = \frac{b}{d}$	$\frac{d}{t}$	WEB $t \times b \times d$ in x in x in	WEB σ_{yw} Tons/in²	FLANGES $t_f \times B_f$ in x in	FLANGES σ_{yf} Tons/in²	τ_{exp} Tons	W_{RS} Tons	$\frac{\tau_{cr}}{\tau_y}$	$\frac{\tau_{ult}}{\tau_y}$	$\frac{\tau_{exp}}{\tau_{yw}}$	$\frac{V_B}{V_{exp}}$	$\frac{V_{RS}}{V_{exp}}$
A1	1.28	94	0.056 x 6.78 x 5.25	16.7	0.25 x 1.0	18.6	5.76	5.64	0.774	0.990	1.02	0.880	0.975
A2	2.04	94	0.056 x 10.75 x 5.25	16.7	0.25 x 1.0	18.6	4.85	5.58	0.722	0.966	0.855	0.968	1.13
A4	2.1	85	0.056 x 10.0 x 4.75	16.7	0.25 x1.375	18.6	2.6	2.53	0.771	0.853	1.01	0.844	0.961

TABLE 7

TEST DATA FROM REFERENCE 9 - BASLER, YEN, MUELLER AND THURLIMANN

GIRDER NO	$a = \frac{b}{d}$	$\frac{d}{t}$	WEB $t \times b \times d$ in x in x in	WEB σ_{yw} Kips/in²	FLANGES $t_f \times B_f$ in x in	FLANGES σ_{yf} Kips/in²	$\frac{\sigma_b}{\sigma_b}$ exp	$\frac{\sigma_b}{\sigma_b}$ th	V_{exp} Kips	V_{RS} Kips	$\frac{\tau_{cr}}{\tau_y}$	$\frac{\tau_{ult}}{\tau_{yw}}$	$\frac{\tau_{exp}}{\tau_{yw}}$	$\frac{V_B}{V_{exp}}$	$\frac{V_F}{V_{exp}}$	$\frac{V_O}{V_{exp}}$	$\frac{V_{RS}}{V_{exp}}$
G6 T1	1.5	259	0.193 x 50 x 75	36.7	0.778 x 12.13	37.9	-	0.285	116	110.7	0.136	0.541	0.567	0.97	0.92	1.05	0.954
G6 T2	0.75	259	0.193 x 50 x 37.5	36.7	0.778 x 12.13	37.9	-	0.375	150	151.6	0.258	0.741	0.733	1.05	1.03	1.06	1.01
G6 T3	0.50	259	0.193 x 50 x 25	36.7	0.778 x 12.13	37.9	-	0.500	177	184.2	0.484	0.901	0.866	1.02	1.00	1.08	1.04
G7 T1	1.0	255	0.196 x 50 x 50	36.7	0.769 x 12.19	37.6	0.33	0.33	140	137.5	0.184	0.661	0.674	1.01	0.95	1.04	0.981
G7 T2	1.0	255	0.196 x 50 x 50	36.7	0.769 x 12.19	37.6	0.33	0.33	145	137.3	0.184	0.661	0.674	0.98	0.90	1.00	0.947

The very extensive tests conducted by Basler, Yen, Mueller and Thurlimann (9) at Lehigh have provided test data for deep girders having web depths of 50" the maximum web thickness being only 3/16". The girders thus had a comparatively high depth/thickness ratio and since the aspect ratio of the web panels varied from 0.5 to 3.0, the test data provides a good check for the design theory. In addition, since the girders were so large, the welding procedures adopted would be typical of those normally employed, thus the comparisons of the proposed design procedure with this experimental test data provides a most valuable check. It will be noted from Table 7 that very good correlation has been obtained between the shear failure load V_{RS} and the experimental loads. Since the I/b^3t ratio for the girders varies over a wide range, the influence of the flange flexibility parameter is well illustrated. It will be seen that the experimental ultimate load of girder G6 increase from 116 kips to 180 kips as the aspect ratio is decreased from 1.5 to 0.5, thus confirming the importance of the flange flexibility parameter.

Figures 3.7 and 3.8 or reference 9 (see also Figure 11 of Reference (7)), are particularly interesting since they show a section of girder G7 after tests T1 and T2 respectively. The mode of failure in both

cases being similar, as would be expected since the panels were nominally of identical size and subjected to identical loading. A distinct plastic hinge is visible in the compression flange of each of the panels. By making an enlargement of the picture, the approximate position of these hinges has been determined yielding c/b values of 0.3, this value being quite close to the value of c/b of 0.33 as obtained from the design procedure. In addition, Figure 3.21 of reference (9) shows the presence of the yield lines which developed in the compression flange of girder G7-T1 and from this figure a more accurate value of c/b equal to 0.33 has been obtained. The degree of agreement between this test data and the theoretical value being excellent. It is also of interest to note that whereas the plastic hinge in the compression flange is well developed, the hinges in the tension flanges are not so well defined, this again being in agreement with the findings of the authors.

In this present section, it has been fully established that the proposed design procedure for shear panels is capable of accurately predicting the failure load of such panels.

CONCLUSION

The paper presents an ultimate method of design for the collapse behaviour of plate girders loaded in shear which is substantiated by checking against experimental data.

ACKNOWLEDGEMENT

This research project has been sponsored in part by the Construction Industry Research and Information Association, in part by the British Constructional Steelwork Association and by the University College, Cardiff.

SYMBOLS

t	thickness of web plate
t_f	thickness of flange plate
d	clear depth of webplate between flanges
b	clear width of webplate between stiffeners
$\alpha = \frac{b}{d}$	aspect ratio of panel
I	flexural rigidity of flange members about an axis passing through their centroid and perpendicular to the web plate
V_{exp}	experimental ultimate shear load
V_{ult}	theoretical ultimate shear load
V_B	ultimate shear load provided by Basler collapse mechanism
V_F	ultimate shear load provided by Fujii
V_O	ultimate shear load provided by collapse mechanism proposed by Ostapenko and Chern
V_{RS}	ultimate shear load calculated by collapse mechanism presented by Authors
W	applied load
W_B	collapse load according to Basler mechanism

W_{cr} applied load resulting in buckling of webplate

W_{exp} experimental ultimate load

W_{RS} collapse load according to the Rockey, Skaloud collapse mechanism

τ applied shear stress

τ_{cr} critical shear stress $= K \frac{\pi^2}{12(1-\mu^2)} \left(\frac{t}{d}\right)^2$

where K is a non dimensional parameter

τ_{yw} shear yield stress of web material

τ_{ult} ultimate shear stress

α_{yw} tensile yield stress of web material

α_{yf} tensile yield stress of flange material

E Young's modulus of elasticity

υ Poisson's ratio

θ inclination of diagonal of panel with respect to flanges

BIBLIOGRAPHY

1. Leggett, D.M.A., & Hopkins, H.G., "The Effect of Flange Stiffness on the Stresses in a Plate Web Spar under Shear". H.M. Stationery Office, R & M No. 2434.
2. Bergman, S.G.A., "Behaviour of Buckled Rectangular Plates under the Action of Shearing Forces". Book. Stockholm, 1948.
3. Rockey, K.C., "The Influence of Flange Stiffness upon the Post Buckled Behaviour of Webplates subjected to Shear". Engineering. 20th Dec. 1957, 184, 788 - 792.
4. Djubek, J. "Stalbau Rundschau" Helt. 21-1962. Sonderheft, Osterreichische Stahlbautagung 1962. Innsbruck.
5. Rockey, K.C., & Martin, R.D., "Flange Stiffness and the Post Buckled Behaviour of Shear Webs". Civil Engineering Departmental Report, University College, Cardiff. 1967.
6. Basler, K., "Strength of Plate Girders". Ph.D. Thesis. Lehigh University, 1959.
7. Basler, K., "Strength of Plate Girders in Shear". A.S.C.E. Proc. No. 2967. ST. 7, p. 151, Octo. 1969. Part I.
8. Thurlimann, B., "Static Strength of Plate Girders". Extract Des Memoires de la Societe Royale des Sciences de Liege". Volume VIII. 1963, p. 137 - 175.
9. Basler, K., Yen, B.T., Mueller, J.A., & Thurlimann, B., "Web Buckling Tests on Welded Plate Girders". Welding Research Council Bulletin. No. 64. September 1960.
10. A.I.S.C. Specification. Adopted November 30th, 1961.
11. Rockey, K.C., "Factors Influencing Ultimate Behaviour of Plate Girders". Conference on Steel Bridges. June 24th-30th, 1968. British Constructional Steelwork Association, Institution of Civil Engineers, London.
12. Rockey, K.C., & Skaloud, M., "Influence of Flange Stiffness upon the Load Carrying Capacity of Webs in Shear". Final Report. 8th Congress New York, September, 1968. 11 pages.
13. Fujii, Tokyo. "On an Improved Theory for Dr. Basler's Theory". 8th Congress I.A.B.S.E. New York, 9-14th September, 1968. 9 pages.
14. Chern, C., & Ostapenko, A., "Ultimate Strength of Plate Girders

under Shear". Fritz Engineering Laboratory Report August, 1969. Report No. 328.7.

15. Rockey, K.C., "Ultimate Load Tests on Welded Shear Girders". Unpublished Report, 1958.
16. Rockey, K.C., & Skaloud, M., "The Ultimate Load Behaviour of Plate Girders Loaded in Shear". University College, Cardiff. Department of Civil Engineering Report - to be published.
17. Hu, P.C., Lundquist, E.R., & Batdorf, F.B., "The Effect of Small Deviations from Flatness on Effective Width and Buckling of Plates in Compression". N.A.C.A., T.N., p. 124. 1946.
18. Sakai, F., Doi, K., Nishino, F., & Okumwa, T., "Failure Tests of Plate Girders using Large Sized Models". Structural Engineering Laboratory Report. Department of Civil Engineering, University of Tokyo (1966). In Japanese.
19. Nishino, F., & Okumwa, T., "Experimental Investigation of Strength of Plate Girders in Shear". p. 451-462. 8th Congress I.A.B.S.E., New York, 1968.
20. Longbottom, E., & Heyman, J., "Experimental Verification of the Strengths of Plate Girders Designed in Accordance with the Revised British Standard 153 : Tests on Full Size and on Model Plate Girders". Inst. Civil Engineers, 1956.
21. Cook, I.T., & Rockey, K.C., "Shear Buckling of Rectangular Plates with Mixed Boundary Conditions". The Aeronautical Quarterly, Vol. XIV, March, 1963.
22. Bleich, F., "Buckling Strength of Metal Structures". McGraw Hill, 1952.
23. Rockey, K.C., "Ultimate Load Tests on Aluminium Plate Girders". Unpublished Research Data.

Leere Seite
Blank page
Page vide

Research Works on Ultimate Strength of Plate Girders and Japanese Provisions on Plate Girder Design

Recherches sur la résistance à la ruine des poutres à âme pleine et Règles Japonaises concernant les poutres à âme pleine

Forschungsbeiträge zur Tragfähigkeit von Blechträgern und Japanische Vorschriften über Blechträger

TOKIO FUJII
Dr. Chief Research Engineer, Research Inst.
Ishikawajima-Harima Heavy Industries Co., Ltd. Japan

YUHSHI FUKUMOTO
Ph.D. Associate Professor
Nagoya University, Japan

FUMIO NISHINO
Ph.D. Associate Professor
University of Tokyo, Japan

TOSHIE OKUMURA
Dr. Professor
University of Tokyo, Japan

1. INTRODUCTION

Plate Girder Committee at the Society of Steel Construction of Japan (JSSC) has been working on the general investigation of the behavior of the welded plate girder under static and dynamic loads. The purpose of the investigation was primarily to review the experimental studies which had been conducted in various countries and the results were summarized in JSSC Journals (in Japanese) Vol. 4, No. 27, 1968, pp. 1-73. The design practices of plate girders in bridges, buildings and ship structures and the current provisions of the plate girder design were also included in the volume.

In the first part of this report, the research works on the ultimate strength of plate girders which have been carried out by the authors, the Committee members of JSSC, are described independently. That is,

2.1 Ultimate Strength of Plate Girders by T. Fujii,
2.2 Lateral Collapse of Plate Girders in Bending by Y. Fukumoto, and
2.3 Load-Deformation Characteristics of Plate Girders by F. Nishino and T. Okumura.

In the second part, the current Japanese specifications for the plate girder design in railway and highway bridges, buildings and ship structures are reviewed briefly.

2. RESEARCH WORKS

2.1 Bending and Shear Strength of Plate Girders

(1) Shear Strength of Plate Girders

Fujii has introduced the theoretical formulas for calculating the ultimate shear strength of plate girder webs including the effect of the stiffness of flange plate[1][2] The results are summarized in Table 2.1.1.

Table 2.1.1 Summary of Ultimate Shear Strength of Plate Girders

Failure Mode	Requisite Condition	Ultimate Shear Force	
 $\lvert\sigma_1-\sigma_2\rvert=\sigma_{wY}$ $\sigma_2=-\tau_{cr}\sin 2\alpha$ $\alpha=45°$	$(1-\nu_{cr})<\varepsilon$	$\nu_u=1$ $\alpha=45°$	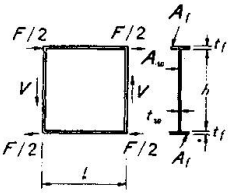
 $\lvert\sigma_1-\sigma_2\rvert=\sigma_{wY}$ $\sigma_2=-\tau_{cr}\sin 2\alpha$ $\alpha<45°$	$1-\frac{\lambda+\nu_{cr}(1+\lambda\nu_{cr})}{\sqrt{\lambda^2+(1+\lambda\nu_{cr})^2}}<\varepsilon\leq(1-\nu_{cr})$	$\nu_u=\frac{(1-\varepsilon)\nu_{cr}+\sqrt{1+\nu_{cr}^2-(1-\varepsilon)^2}}{1+\nu_{cr}^2}$ $\tan\alpha=\frac{\nu_{cr}+\sqrt{1+\nu_{cr}^2-(1-\varepsilon)^2}}{2-\varepsilon}$	$\lambda=\ell/h$: Aspect ratio α : Inclination of tension field σ_1, σ_1' : Principal stress (tension) σ_2 : Principal stress (comp.) σ_{wY} : Yield stress of web σ_{fY} : Yield stress of flange τ_{cr} : Web buckling stress $\varepsilon=\frac{8}{\lambda^2}\frac{t_f}{h}\frac{A_f\sigma_{fY}}{A_w\sigma_{wY}}$ $\nu_{cr}=\tau_{cr}/\tau_{wY}$ $\nu_u=V_u/A_w\tau_{wY}$
 $\lvert\sigma_1'-\sigma_2\rvert=\sigma_{wY}$ $\sigma_1'>\sigma_1$ $\alpha<45°$	$\varepsilon\leq 1-\frac{\lambda+\nu_{cr}(1+\lambda\nu_{cr})}{\sqrt{\lambda^2+(1+\lambda\nu_{cr})^2}}$	$\nu_u=\sqrt{\lambda^2+(1+\lambda\nu_{cr})^2}-(1-\varepsilon)\lambda$ $\tan 2\alpha=\frac{1+\lambda\nu_{cr}}{\lambda}$	

In Table 2.1.1. υ_{cr} is nondimensionalized shear buckling stress of web panel, and is given by formula (2.1.1.).

$$\upsilon_{cr}=\frac{K_s\pi^2}{12(1-\nu^2)}\left(\frac{E}{\tau_{wY}}\right)\left(\frac{t_w}{h}\right)^2,\quad \upsilon_{cr}\leq 0.5$$
$$=1-\frac{3(1-\nu^2)}{K_s\pi^2}\left(\frac{\tau_{wY}}{E}\right)\left(\frac{h}{t_w}\right)^2,\quad \upsilon_{cr}>0.5 \qquad (2.1.1)$$

where ν : Poisson's ratio, E: Young's modulus,

τ_{wY} : Yield stress of web $=\sigma_{wY}/2$ (Tresca's yielding condition is used in this theory).

K_s is a buckling coefficient depend on aspect ratio λ and constraint conditions along periphery of the panel. It seems appropriate to consider that the web is fixed along the flanges and simply supported along the vertical stiffeners, and under this condition Ostapenko gives the following formula[4]

$$K_s=\frac{5.34}{\lambda^2}+\frac{6.55}{\lambda}-13.71+14.10\lambda,\quad \lambda\leq 1.0$$
$$=8.98+\frac{6.18}{\lambda^2}-\frac{2.88}{\lambda^3},\quad \lambda>1.0 \qquad (2.1.2.)$$

In Table 3.1.1., ε is a parameter related to the effect of flange plate stiffness, and is given for any shape of flange cross section as,

$$\varepsilon=\frac{M_P^f}{\ell^2 t_w\sigma_{wY}} \qquad (2.1.3.)$$

where M_p^f is full plastic moment of flange itself.

formulas for specified sections are given in Table 2.1.2.

Table 2.1.2. ε -formulas for Specific Section of Flange Plate

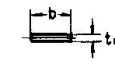	$\frac{1}{4}\frac{bt_1^2}{l^2 t_w}\left(\frac{\sigma_{fY}}{\sigma_{wY}}\right)$
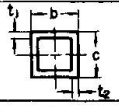	$\frac{1}{2}\frac{2bct_1+c^2t_2}{l^2 t_w}\left(\frac{\sigma_{fY}}{\sigma_{wY}}\right)$ $t_1 \ll b$, $t_2 \ll c$
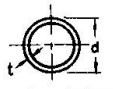	$\frac{d^2 t}{l^2 t_w}\left(\frac{\sigma_{fY}}{\sigma_{wY}}\right)$ $t \ll d$
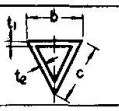	$\frac{2-\sqrt{2}}{3}\frac{1}{l^2 t_w}\left[\frac{(3bt_1-ct_2)c^2}{\sqrt{(b/2)^2+c^2}}+4ct_2\sqrt{(b/2)^2+c^2}\right]\left(\frac{\sigma_{fY}}{\sigma_{wY}}\right)$ $t_1 \ll b$, $t_2 \ll c$

Comparison of the theoretical values with the test results have already been reported at the 8th congress of IABSE in New York[2]

(2) Bending Strength of Plate Girders

Fujii has introduced the following theoretical formulas for calculating the ultimate bending strength on the assumption of lateral buckling of plate girder being prevented[1][3]

$$m_u = m_{cr} + \beta(1 - m_{cr}), \quad m_{cr} \leq 1.0$$
$$= \frac{f_s(m_{cr}-1)+(1-\xi)}{m_{cr}-\xi} \leq f_s, \quad m_{cr} > 1.0 \qquad (2.1.4.)$$

where $m = M/M_y$: nondimensionalized moment
My: flange yield moment
u : suffix for ultimate
cr : suffix for web-buckling
fs : shape factor used in plastic design

$$\xi = 2.42\left(\frac{t_w}{h}\right)\sqrt{\frac{E}{\sigma_Y}}$$

in this case $\sigma_{wY} = \sigma_{fY} = \sigma_Y$

In eq. (2.1.4.), κ_m is calculated as a simply supported rectangular plate subjected to inplane bending and is given as follows,

$$m_{cr} = \frac{K_m \pi^2}{12(1-\nu^2)}\left(\frac{t_w}{h}\right)^2\left(\frac{E}{\sigma_Y}\right)$$

$$K_m = 15.87 + 1.87/\lambda^2 + 8.6\lambda^2, \quad \lambda \leq 2/3 \qquad (2.1.5.)$$
$$= 23.9 \qquad \lambda > 2/3$$

β , in eq. (2.1.4.), is a parameter with the effective bredth of buckled web, and is given by the following formula[3]

$$\beta = 1 - \frac{(1-\xi)^2}{4(1+2A_f/A_w)} \quad \frac{(1-\xi)^3}{2(1+6A_f/A_w)} \qquad (2.1.6.)$$

where At : sectional area of flange
Aw : sectional area of web

Relations between buckling moment and ultimate moment given by eq. (2.1.4.) are graphically shown in Fig. 2.1.1.

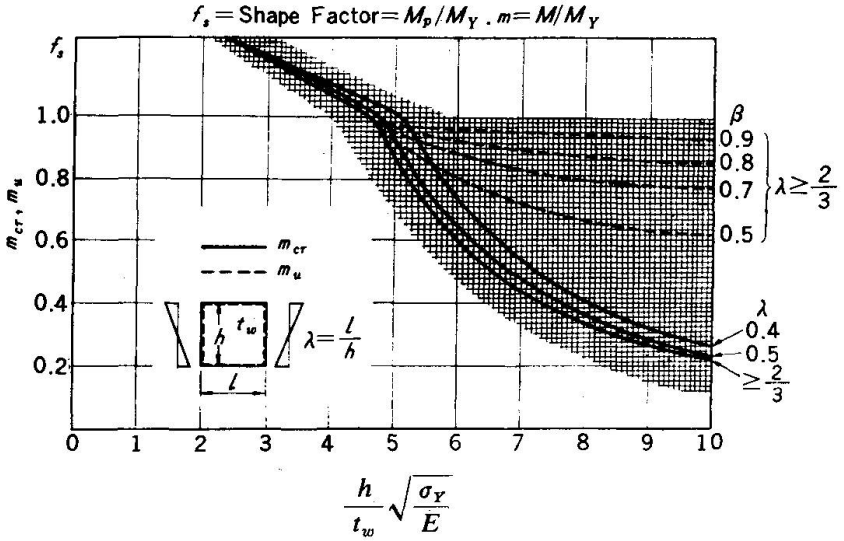

Fig. 2.1.1. Relation between Nondimensionalized Buckling Moment and Ultimate Moment

For hybrid girders, Fujii proposed to modify the results, in eqs. (2.1.4.) (2.1.5.) (2.1.6.) assuming $\sigma_Y = \sigma_{fY}$ by multiplying a correcting factor C_m; the ratio of the full plastic moment of the hybrid section to the assumed ($\sigma_Y = \sigma_{fY}$) full plastic moment,

namely,

$$M_u = C_m \, m_u \, M_Y \qquad (2.1.7.)$$

where $M_Y = S\sigma_{fY}$

S = section modulus

$$C_m = \frac{1 + \frac{t_f}{h} + \frac{1}{4}\frac{\sigma_{wY}A_w}{\sigma_{fY}A_f}}{1 + \frac{t_f}{h} + \frac{1}{4}\frac{A_w}{A_f}}$$

Comparison between theoretical and experimental results is shown in Table 2.1.3. and it shows good coincidence between them.

Table 2.1.3. Comparison of the theoretical values with the experimental results

Ref. No.	Girder No.	Experimental Values								Theoretical Values			
		λ	h/t_w	A_w s.i.	A_f s.i.	σ_Y k.s.i.	M_Y kips-inch	M_p kips-inch	M_u^x kips-inch	$\frac{h}{t_w}\sqrt{\frac{\sigma_Y}{E}}$	m_{cr}	m_u	$\frac{M_u^y}{M_u^x}$
Lehigh Univ.[5]	G2–T1	1.5	185	13.5	9.40	38	2.23×10^4	2.42×10^4	2.02×10^4	6.60	0.495	0.962	0.94
	G2–T2	0.75	"	"	"	"	"	"	2.16×10^4	"	"	"	1.01
	G4–T1	1.5	388	64.5	9.40	38	1.96×10^4	2.12×10^4	1.77×10^4	13.8	0.113	0.928	0.98
	G4–T2	0.75	"	"	"	"	"	"	1.88×10^4	"	"	"	1.03
Texas Univ.[6]	41540	1.0	147	8.82	4.187	*1 105/41.6	*2 2.15×10^4	1.94×10^4	1.63×10^4	8.76	0.282	0.916	1.04
	42540	1.0	"	"	4.173	"	"	1.93×10^4	1.65×10^4	"	"	"	1.06
				cm^2	cm^2	kg/cm^2	kg-cm	kg-cm	kg-cm				
Konishi and Others[7]	A	1.0	267	54.0	28.8	28.1	1.28×10^7	1.43×10^7	1.16×10^7	9.75	0.228	0.892	1.02
	G	1.0	200	72.0	28.8	50.0	2.47×10^7	2.83×10^7	2.40×10^7	9.76	0.227	0.873	1.11
Akita and Fujii[1]	B–1	0.988	212	20.4	14.7	27.0	3.25×10^6	3.56×10^6	3.19×10^6	7.61	0.373	0.945	1.04
	B–2	0.975	155	14.9	14.7	27.0	2.27×10^6	2.43×10^6	2.14×10^6	5.56	0.698	0.988	0.96

*1 σ_{fy}/σ_{wy}

*2 $M_y = S\sigma_{xy}$ where S is section modulus.

(3) Interaction Curve under Combined Bending and Shear

Fujii has introduced the following interaction formulas under combined bending and shear[1][3]

In the case where the web buckling is prevented, interaction formulas are given as follows,

$$M = M_{fp} + M_{wp}\sqrt{1-(V/V_p)^2}\ ,\quad M \geq M_{fp} \qquad (2.1.8.)$$

$$V = V_p \qquad M < M_{fp}$$

where

$M_{wp} = \frac{1}{4}h^2 t_w \sigma_{wY}$: Plastic moment shared by web.

$M_{fp} = (h+t_f)A_f\sigma_{fY}$: Plastic moment shared by flange.

$V_p = A_w\tau_{wY}$: Plastic shear force.

This may be diagrammatically shown by a chain line A'B'C' in Fig. 2.1.2. When a plate girder is subjected to bending moment only, the ultimate moment Mu (the point A in Fig. 2.1.2.) represents the critical value. When the web has just buckled and the tension field does not grow yet, the flanges can bear the moment denoted Mfp. The point B corresponds to this critical value. When the flanges yield under the combined bending moment and compressive force caused by the tension field action, a contribution of flange stiffness on ultimate shear force can not be expected, and this corresponds to the point C. Vu represents the critical point under shear force only. In this case, the plate girder cannot bear the bending moment because the flanges collapse at the same time.

The interaction curve can be approximated on the safe side by connecting the points A.B. C. and D. by a folded line.

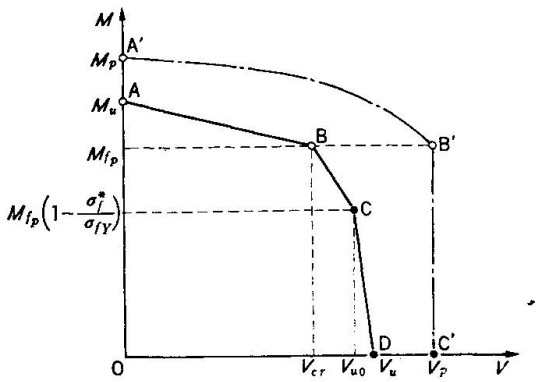

Fig. 2.1.2. Interaction Curve

At A, $M_A = M_u$, $V_A = 0$ (2.1.9.)

At B, $M_B = M_{fp}$, $V_B = V_{cr}$, (2.1.10.)

At C, $M_C = M_{fp}\left(1 - \frac{\sigma_f^*}{\sigma_{fY}}\right)$ $V_C = V_{uo}$, (2.1.11.)

where Vuo is the ultimate shearing force when ϵ is zero, and σ_f^* is compressive stress in the flanges by the action of tension field.

They can be obtained as follows[1]

$$\lambda > \frac{1}{\tau_{cr}} \frac{1-\tau_{cr}^2}{1+\tau_{cr}^2} \quad , \quad \tau_{uo} = \frac{2\tau_{cr}}{1+\tau_{cr}^2}\tau_p$$
$$\frac{\sigma_f^*}{\sigma_{fY}} = \frac{A_w \sigma_{wY}}{2A_f \sigma_{fY}} \frac{1-\tau_{cr}^2}{1+\tau_{cr}^2} \qquad (2.1.12.)$$

$$\lambda \leq \frac{1}{\tau_{cr}} \frac{1-\tau_{cr}^2}{1+\tau_{cr}^2} \quad , \quad \tau_{uo} = \left(\sqrt{\lambda^2 + (1+\lambda\tau_{cr})^2} - \lambda\right)\tau_p$$
$$\frac{\sigma_f^*}{\sigma_{fY}} = \frac{A_w \sigma_{wY}}{4A_f \sigma_{fY}} \left\{1 + \lambda\tau_{cr} - \frac{\tau_{cr}(1+\lambda\tau_{cr})}{\sqrt{\lambda^2 + (1+\lambda\tau_{cr})^2}}\right\} \qquad (2.1.13.)$$

At D, $M_D = 0$, $V_D = V_u$, (2.1.14.)

The results of girder tests conducted by Basler, Thürliman and others[5] and Cooper and others[8] under combined bending and shear are summarized in Table 2.1.4. These experimental values are compared with the theoretical interaction curves in Fig. 2.1.3. – 2.1.8[3]. The experimental values are in fairly good coincidence with the theoretical values and the interaction curves are on the safe side.

Table 2.1.4. Test Results of Girders under combined Shear and Bending

Ref. No.	Girder No.	λ	h/tw	Aw s.i.	σwY k.s.i.	Af s.i.	σfY k.s.i.	ε	Vp kips	My kips-inch	Mp kips-inch	V_u^{ex} kips	M_u^{ex} * kips-inch
Lehigh Univ. [5]	G8–T1	3.0	254	9.85	38.2	8.99	41.3	0.013	188	21,900	23,600	85.0	6,380
	G8–T3	1.5	"	"	"	"	"	"	"	"	"	116.5	13,100
	G8–T4	1.0	"	"	"	"	"	0.119	"	"	"	129.5	16,200
	G9–T1	3.0	382	6.55	44.5	9.00	41.8	0.017	146	21,100	22,700	48.0	3,600
	G9–T2	1.5	"	"	"	"	"	0.069	"	"	"	75.0	2,810
	G9–T3	"	"	"	"	"	"	"	"	"	"	79.0	8,890
	E2–T1	3.0	99	25.35	34.9	25.4	38.1	0.0178	443	48,500	54,100	377.5	47,200
	E2–T2	1.5	"	"	"	"	"	0.0713	"	"	"	378.5	42,500
	E4–T2	0.75	"	"	"	"	"	0.261	"	"	"	317	41,600
	E4–T3	0.5	"	"	"	"	"	0.587	"	"	"	322.5	44,300
Lehigh Univ. [8]	H1–T1	3.0	127	19.65	108.1	34.4	106.1	0.030	1,060	207,200	216,000	630	47,250
	H1–T2	1.5	"	"	"	"	"	0.060	"	"	"	769	28,900
	H2–T1	1.0	128	19.5	110.2	35.4	107.1	0.284	1,075	214,600	224,100	917	114,600
	H2–T2	0.5	"	"	"	"	"	1.136	"	"	"	1,125	154,700

* Values at midspan of failure panel.

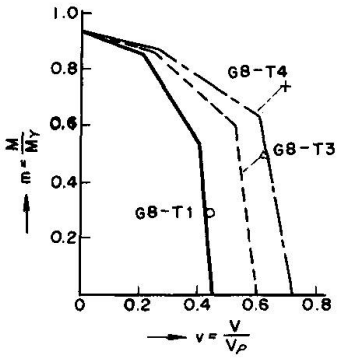

Fig. 2.1.3

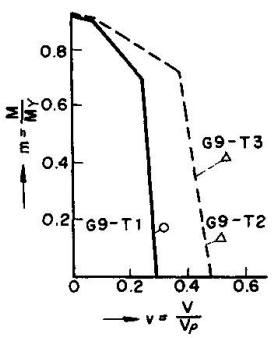

Fig. 2.1.4

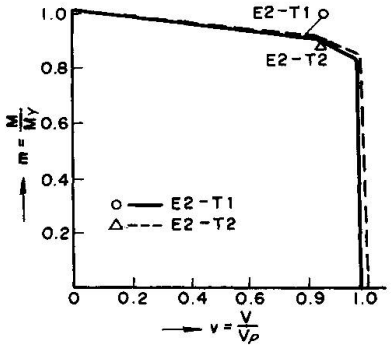

Fig. 2.1.5

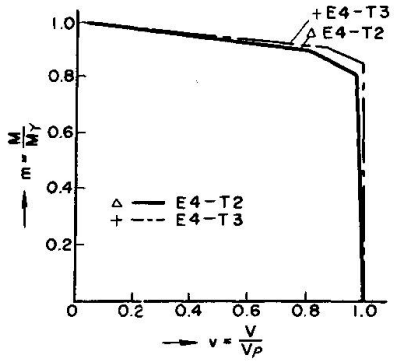

Fig. 2.1.6

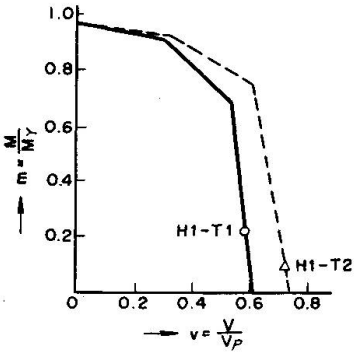

Fig. 2.1.7

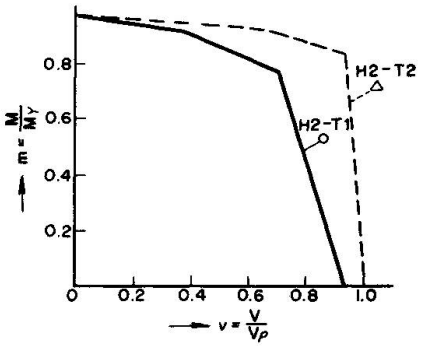

Fig. 2.1.8

References:

1) Y. Akita & T. Fujii: "Minimum Weight Design of Structures based on Buckling Strength and Plastic Collapse (1st and 2nd Report)". Selected papers from the Journal of the Society of Naval Architects of Japan Vol. 2, 1969.

2) T. Fujii: "On an Improved Theory for Dr. Basler's Theory" The Final Report of the 8th Congress of IABSE.

3) T. Fujii: "On the Ultimate Strength of Plate Girders. Japan Shipbuilding & Marine Engineering, Vol. 3, No. 3, May 1968.

4) C. Chern & A. Ostapenko: "Ultimate Strength of Plate Girders under Shear (Unsymmetrical Plate Girders)". Fritz Engineering Laboratory Report No. 328.7, August 1969.

5) K. Basler, B. Thurliman, and others: "Web Buckling Test on Welded Plate Girders" Bulletin No. 64, Welding Research Council, N. Y., 1960.

6) H. Toyoda: "Static Behaviour of Hybrid Plate Girders" Thesis for the Degree of M.S. University of Texas, Janu. 1967.

7) I. Konishi and others: "Theories and Experiments on the Load Carrying Capacity of Plate Girders" Report of Research Committee of Bridges, Steel Frames and Welding in Kansai District in Japan, July 1965 (in Japanese)

8) P. B. Cooper and others: "Welded Constructional Alloy Steel Girders" Proc. of A.S.C.E. ST1, 1964.

2.2 Lateral Collapse of Plate Girders in Bending

Ultimate strength of plate girders in bending would be governed by the following collapse mechanisms, that is, (1) excessive deformations of girders in the plane of bending, (2) local failures of the compression flange such as vertical buckling of the flange into the web and torsional buckling of the flange plate, and (3) lateral buckling of the compression flange between the unsupported length of the flange.

In this report a study which is related to the above item (3) is carried out by Fukumoto in order to clarify the interaction between the lateral collapse load of the girders and stress concentration in the compression flange and a portion of the web adjacent to it which is caused by a redistribution of the web stress in post buckling range. Comparisons are also made between the inelastic lateral buckling theory and the test results of girders with high strength steels of SM 50 (nominal yield stress σ_Y=3,200 kg/cm^2) and HT 80 (σ_Y=7,000kg/cm^2).

The Test Girders

Since the objective of this investigation is to study the interaction between the buckled web and the lateral collapse of girders under pure bending, no lateral bracings are provided for the test girders except at the both ends where the loading box beams are connected by the high strength bolts. The end conditions of test girders are, therefore, clamped laterally in the plane of the flange plates.

The detailed dimensions of the test girders are given in Fig. 2.2.1. and Table 2.2.1. Girders A and B are of SM 50 steel, girders C,D,E and F are of HT 80 and girder G is a hybrid girder with SM 50 steel in the web and HT 80 in the flange plates. The number of panels between the transverse stiffeners are two for girders D and F, and the others have three panels.

All seven girders are tested under pure bending in the setup as shown in Fig. 2.2.2. End box beams are prevented laterally at the sections where two 75 ton capacity hydraulic jacks applied loads.

Instrumentations

Fig. 2.2.3. shows the location of the strain gages to the web and flange. In the web orthogonal pairs of gages are mounted on either side of the web at the mid cross-section of each panel in order to differentiate bending and membrane strains. Gages to the flange are placed to differentiate stresses in the compression flange due to in-plane and out-of-plane bending of the girders.

The vertical and lateral deflections of the flanges are obtained through the dial gages. A dial gage rig is made to obtain the out-of-plane deformations of the web. Rotation of the compression flange is read using a clinometer for surveying. The position of measuring deflections is also shown in Fig. 2.2.3.

Test Results and Discussions

TENSION COUPON TESTS : Two coupons are cut from each slab thickness. Average values of static yield stress for each slab thickness are as follows:

SM 50	σ_Y = 4690 kg/cm^2	for t = 6 mm
	σ_Y = 3810 kg/cm^2	for t = 8 mm
	σ_Y = 3240 kg/cm^2	for t = 10 mm
HT 80	σ_Y = 6610 kg/cm^2	for t = 6 mm
	σ_Y = 7850 kg/cm^2	for t = 10 mm

LOAD-DEFORMATION CURVES : The absolute girder deflections including lateral web deflections are measured at the mid cross-sections of each panel of the girders. The deformations are recorded for the initial distorsions of the girders and for a number of loads.

Fig. 2.2.4.(a) shows the absolute deformations at the mid cross-sections of the central and adjacent side panels of girder E. Deformations are shown under the four moment values. The graphs of deformations are composed of the relative deflection of the web out-of-its plane with the flange displacements in vertical, horizontal and rotational directions.

The relative deflection of the web starts for loads from the initial distortions of the web, and with the load increased the web buckled shapes become large to continue until lateral collapse occurs in the compression flange at the maximum moment. As can be seen from this figure, the web buckled pattern in each panel become obvious with the increased loads. In the central panel the direction of the relative web deflection is opposite to the lateral displacement of the compression flange and thus the lateral movement of the flange becomes small compared to the one in the side panel due to the resultant lateral forces transmitted to the flange along the web-flange weld line. In this figure load versus vertical deflection at the span center is compared with the deflection of $v = ML^2/8EI$ by conventional beam theory.

Fig. 2.2.4.(b) shows the deformations of girder C. In this case the direction of the relative web deflection and the lateral displacement of the compression flange is the same in the central panel, but in the side panel the lateral displacement of the flange is considerably small because of the web deflection being opposite to it.

STRAIN DISTRIBUTION AND EFFECTIVE BREDTH OF THE WEB : Fig. 2.2.5. shows the distributions of the mean web strains along the sections where the deformations are measured. The mean strains are the average of the values obtained from gages on either side of the web. In Fig. 2.2.5. the linear strain distributions predicted by conventional beam theory are also shown by light lines for girders A and C, respectively. A redistribution of mean strains in the compression zone of the web is observed with the increasing loads and, consequently, a portion of the compression stress in the web are transferred to the compression flange while the girders deform laterally with the loads. The compression flange and an adjacent web portion, thus, carry bending stress which exceeds that predicted by beam theory.

Girder A was loaded up to 41.4 t-m and then the girder was completely unloaded in order to replace a damaged angle of the girder end fixtures. The presence of residual horizontal displacement of 21.5 mm in the compression flange at the span center was recorded after unloading and, therefore, in the second test the lateral collapse of the girder was observed at the relatively early stage of loading. This result may be explained in Fig. 2.2.5. in which high strain concentration can be seen in the compression flange and an adjacent web portion.

If the first moment of the compression stresses in the web and flange (Fig. 2.2.6(a)) about the neutral axis is made equal to that of the linear stresses in the effective portion (Fig. 2.2.6.(b)), the effective bredth h_e may be calculated by,

$$\sum_i \sigma_i \Delta A_i h_i = \frac{\sigma_c}{h+t} \left\{ \frac{w}{3} \left[h^3 - (h-h_e)^3 \right] + bt\left(h + \frac{t}{2}\right)^2 \right\} \qquad (2.2.1)$$

in which σ_c is the measured fiber stress in the compression flange.

Fig. 2.2.7. shows h_e/h versus M/M_{max} curves for all the test girders. The ratios of h_e to the web thickness are also taken in the ordinate. When the bending moments reach the maximum moments at which the girders fail laterally, the effective bredth may become (30 – 35) times the web thickness.

Stress concentration in the flange could be estimated using the modified stress distribution as shown in Fig. 2.2.6.(b). For HT 80 steel girders, the stress concentration factors of σ_c (Fig. 2.2.6.(b)) against the

fiber stress calculated by conventional beam theory are equal to 1.09, 1.05 and 1.03, for h_e/h=0.4, 0.5 and 0.6 in Fig. 2.2.7., respectively.

ULTIMATE MOMENT : A summary of all ultimate moments, M_{max}, is given in Table 2.2.2. The failure mode of the girders is of the lateral instability of the compression flange. A hybrid girder G has the same cross-sectional dimensions of girder C. These two girders delivered almost the same ultimate loads regardless of the different yield stresses in the web.

The yield moment M_y which is the moment initiates nominal yielding in the extreme fiber, and the critical moment M_{wcr} which is the ideal buckling moment of an isolated web panel with the panel's aspect ratio under simply supported on all sides are given in Table 2.2.2. The overall buckling moment M_{ocr} and lateral buckling moment M_{cr} which will be obtained in the subsequent sections are also listed.

OVERALL BUCKLING OF GIRDERS : The web buckling problem in bending is treated herein as the simultaneous buckling of a plate girder, that is, combined web buckling and flange torsional and lateral buckling. Boundary conditions of web plate are simply supported along vertical stiffeners, clamped along tension flange and elastic support in torsion and lateral displacement along the compression flange. Normal stress in flange due to bending of girder is taken into account for the analysis and the reduction of apparent torsional rigidity and horizontal flexural rigidity of flange due to axial compression are considered.

The buckling coefficients are obtained by solving the equation of

$$\nabla^2\nabla^2 W = \frac{\sigma_0}{D}\left(1-\alpha\frac{y}{d}\right)W_{xx} \qquad (2.2.2.)$$

with the boundary conditions of (see Fig. 2.2.8)

$w = 0,\ w_y = 0$ for y = 0 (along tension flange)

$$\left.\begin{aligned} BW_{xxxx} &= D\left[W_{yyy} + (2-\nu)W_{xxy}\right] - A_f\sigma_0(1-\alpha)W_{xx} \\ D(W_{yy} + \nu W_{xx}) &= C\left[1 - \frac{\sigma_0(1-\alpha)I_P}{C}\right]W_{xxy} \end{aligned}\right\} \text{ for y=b (along compression flange)}$$

And the deflection surface is assumed as [1]

$$W = \sum_m \left[\sum_n a_n\left(\frac{y}{d}\right)^n\right]\sin\frac{m\pi x}{a} \qquad (2.2.3.)$$

Relationships between the simultaneous buckling strength and the three independent buckling modes, torsional buckling of flange, web buckling and lateral buckling of flange, are compared with the parameters of aspect ratios and slenderness ratios of web, cross-sectional areas of flange and web, torsional rigidity of flange, flexural rigidity of flange and web.

The curves corresponding to this method are shown as the overall buckling curves in Figs. 2.2.9.(a) and (b) for test girders with HT 80 steel. For $L/r>90$ approximately, the curves become close to the lateral buckling curves. Comparisons of the test results with the overall buckling curves indicate that the curves cannot predict the lateral collapse for the range where the overall buckling would be governed by the web buckling.

LATERAL BUCKLING STRENGTH : Lateral buckling strength of plate girders in bending was treated throughly in Ref. 2 in which the contributions of lateral bending of the flange plates with one sixth of the web and St. Venant torsion were discussed in detail.

Elastic lateral buckling strength curves for the test girders are shown in Figs. 2.2.9.(a) and (b) on the assumption that the distorsion of the girder cross section does not occur at the instance of buckling. Slenderness ratio for the minor axis of the girder cross section is taken in the abscissa.

Inelastic lateral buckling strength of girders with the residual stress pattern shown in Fig. 2.2.9.(a) is obtained and the results are shown in Figs. 2.2.9.(a) and (b). The assumptions used in the analysis are the same as those made in Ref. 3. From Figs. 2.2.9.(a) and (b) the test results for girders E to G are in good agreement with the inelastic lateral buckling curves.

If St. Venant torsion is neglected, elastic lateral buckling of doubly symmetrical I sections in bending may be written as

$$\frac{\sigma_{cr}}{\sigma_Y} = \frac{1}{\alpha^2} \qquad (2.2.4.)$$

in which $\alpha = \frac{1}{\pi}\sqrt{\frac{\sigma_Y}{E}}\frac{L}{\bar{r}}$ and $\bar{r}$ is the radius of gyration of the compression flange and one sixth of the web which is defined as

$$\bar{r}^2 = \frac{I_f}{A_f + \frac{1}{6}A_w} \quad \text{with} \quad I_f = \frac{b^3 t}{12} \qquad (2.2.5.)$$

Fig. 2.2.10. shows summary of the test results and the corresponding theoretical curves. α is taken in the abscissa. Elastic buckling curves for all the test girders can then be represented reasonably by Eq. (2.2.4.)

The basic column curve

$$\frac{\sigma_{cr}}{\sigma_Y} = 1 - \frac{\alpha^2}{4} \quad \text{for } 0 < \alpha < 2 \qquad (2.2.6.)$$

is plotted in Fig. 2.2.10. And the theoretical transition curve is also shown for the girders with a residual stress pattern as in Fig. 2.2.9.(a).

From this figure, lateral collapse of the test girders in bending may occur when the moments reach the strength estimated by the inelastic lateral buckling theory including residual stresses. However, overall buckling curve may not give adequate estimation of the problem when the web buckles in several half waves.

CONCLUSIONS:

The behavior of lateral collapse of plate girders in bending was investigated for SM 50 (σ_Y=3200 kg/cm^2) and HT 80 (σ_Y=7000 kg/cm^2) steels. At the early stage of loading, the lateral and torsional deformations of the girder flanges were observed together with the buckled patterns in each web panel. Lateral deflection curves of the compression flange at failure were influenced considerably by the direction of the buckled deformation of the web. Variations of the effective sections of the web with the loads during the lateral collapse were discussed. Lateral instability of the compression flange can be estimated satisfactorily by the inelastic lateral buckling theory neglecting St. Venant torsion.

References

1) H. Yonezawa and I. Mikami, "Elastic Buckling of Plate Girders from Pure Bending", Proc. of ASCE, Vol. 94, No. EM1, Feb., 1968

2) K. Basler and B. Thurlimann, "Strength of Plate Girders in Bending", Proc. of ASCE, Vol. 87, No. St 6, Aug., 1961

3) T.V. Galambos, "Structural Members and Frames" Prentice-Hall, 1968

Table 2.2.1. Dimensions of Test Girders

Girders	Steels	d (mm)	b (mm)	w (mm)	t (mm)	L_0(mm)	Number of Panels	a_1(mm)	a_2(mm)	Stiffeners (mm)
G–A	SM50A	1000	130	6	10	4100	3	1200	450	62 x 8
G–B	SM50A	1000	120	6	8	4100	3	1200	450	51 x 8
G–C	HT80	800	110	6	10	3300	3	900	350	52 x 8
G–D	HT80	800	110	6	10	2800	2	1000	–––	52 x 8
G–E	HT80	800	130	6	10	3300	3	900	350	62 x 8
G–F	HT80	800	130	6	10	2800	2	1000	–––	62 x 8
G–G	Flange HT80 Web SM50A	800	110	6	10	3300	3	900	350	52 x 8

Table 2.2.2. Summary of Test Results and Reference Moments

Girders	Experimental	Theoretical			
	M_{max}	M_{wcr}	M_{ocr}	M_{cr}	M_y
G–A	43.6	38.5	52.7	53.8	71.7
G–B	41.0	32.8	40.2	50.5	72.3
G–C	64.4	40.4	55.2	65.1	113.9
G–D	83.4	39.9	55.2	81.1	113.9
G–E	94.8	44.8	64.1	90.8	126.2
G–F	105.1	44.2	64.1	94.6	126.2
G–G	65.5	40.4	55.2	65.1	–––

Unit in t-m

M_{wcr} : ideal buckling moment of an isolated web panel
M_{ocr} : overall buckling moment
M_{cr} : lateral buckling moment
M_y : yield moment

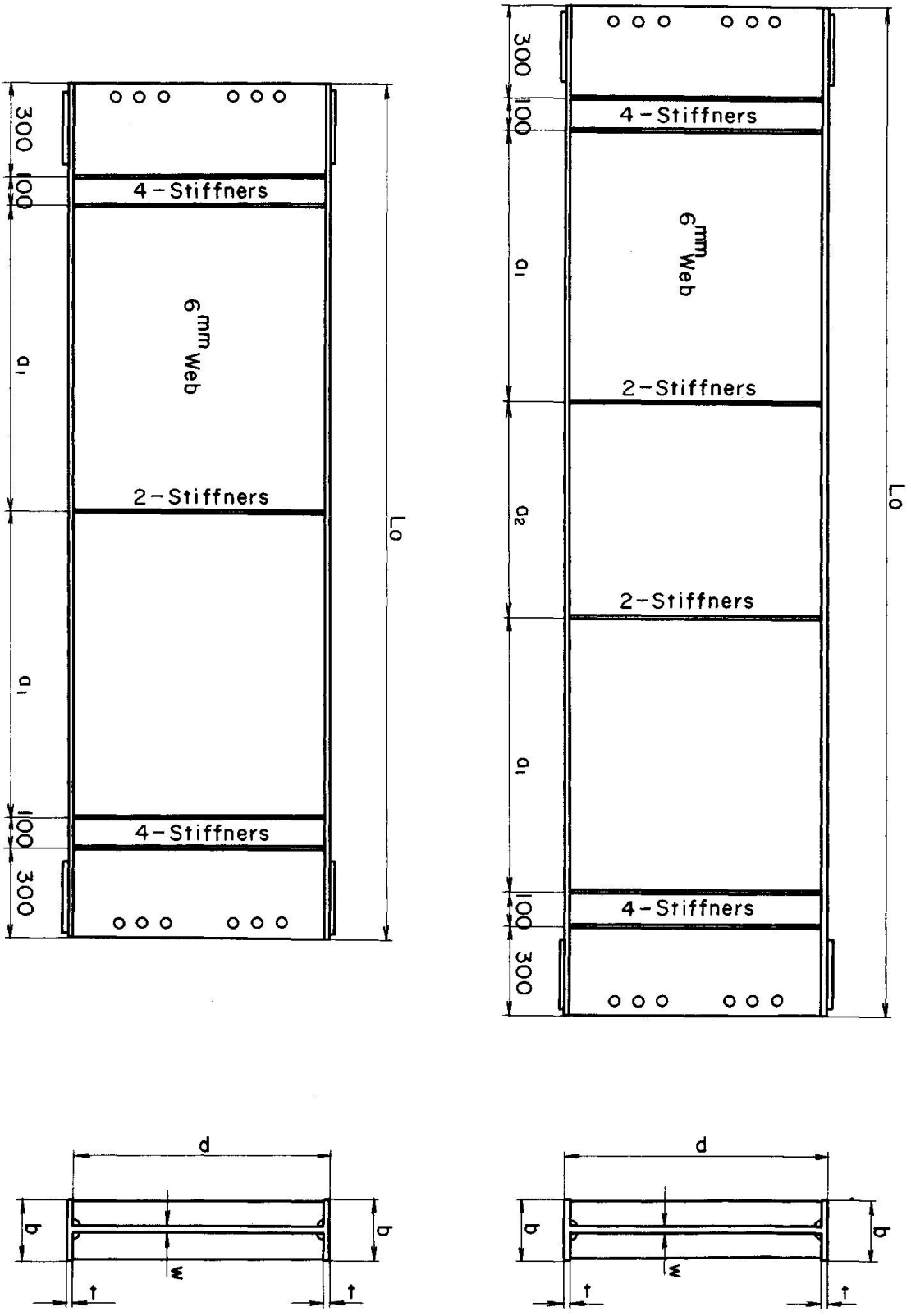

Fig. 2.2.1 Test Girders

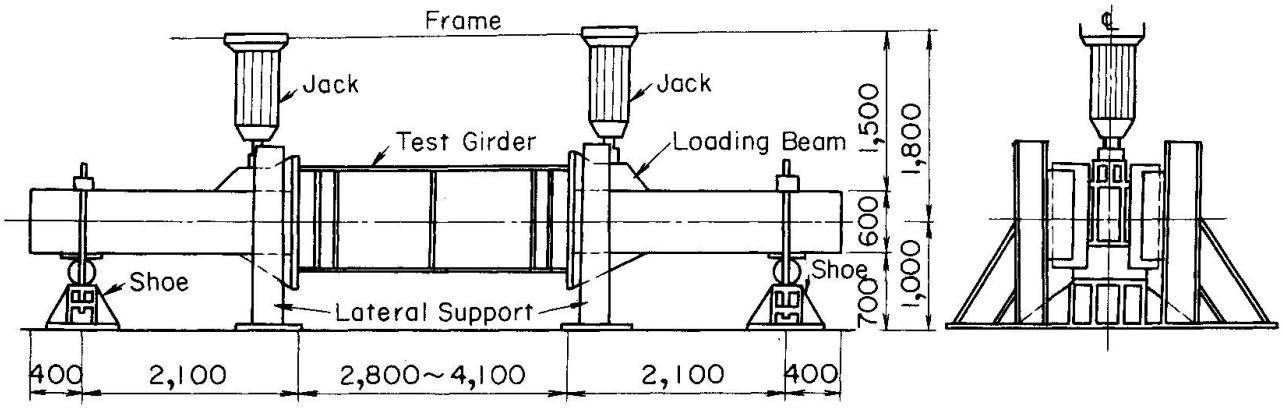

Fig. 2.2.2 Test Setup

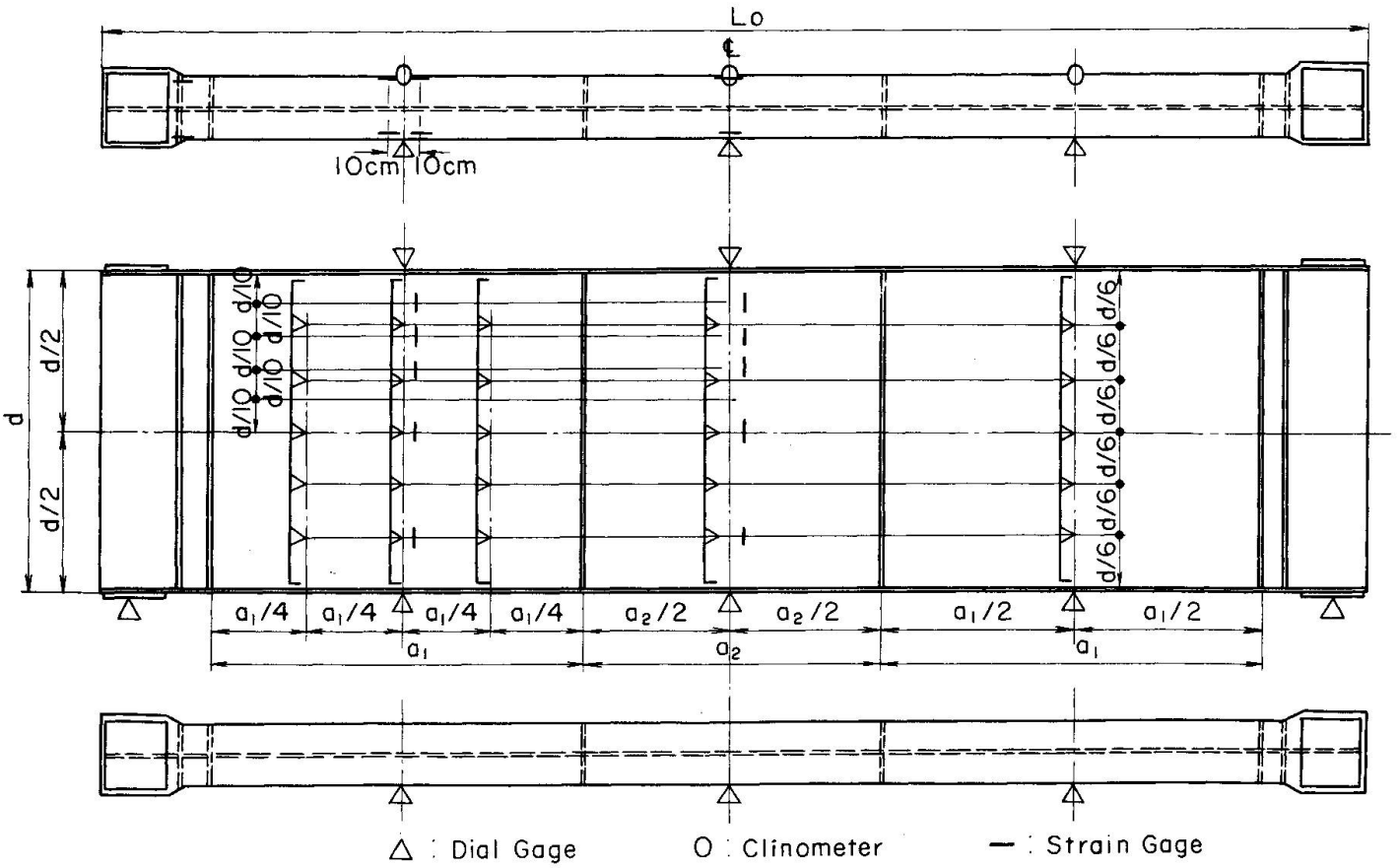

Fig. 2.2.3 Instrumentation

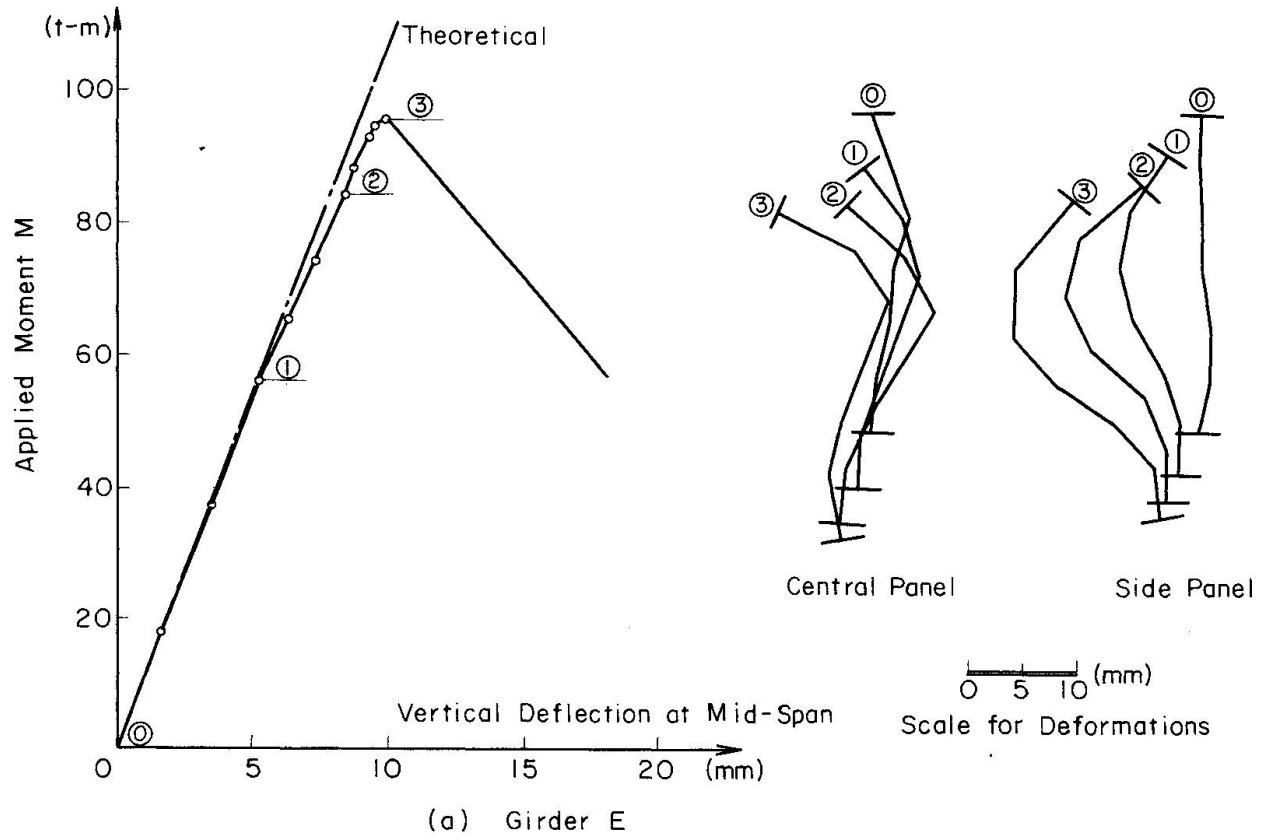

(a) Girder E

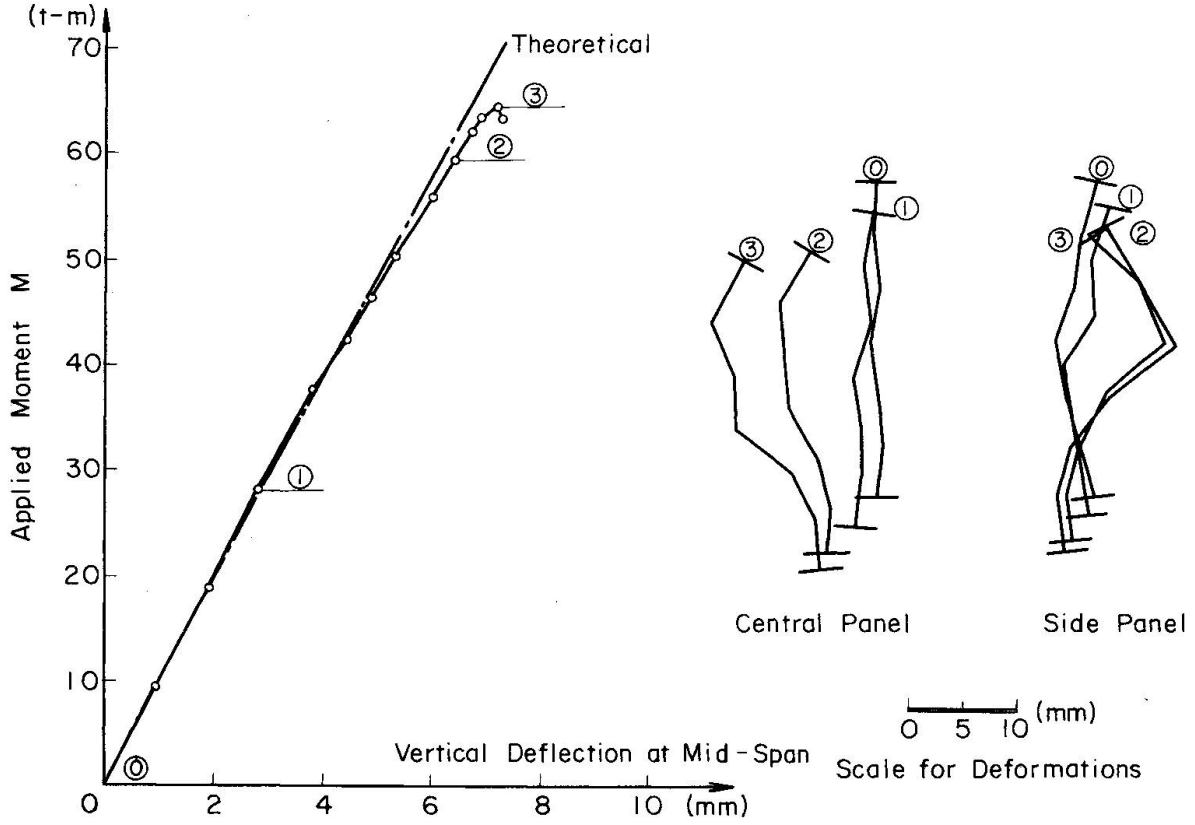

(b) Girder C

Fig. 2.2.4 Load – Deformation Relations

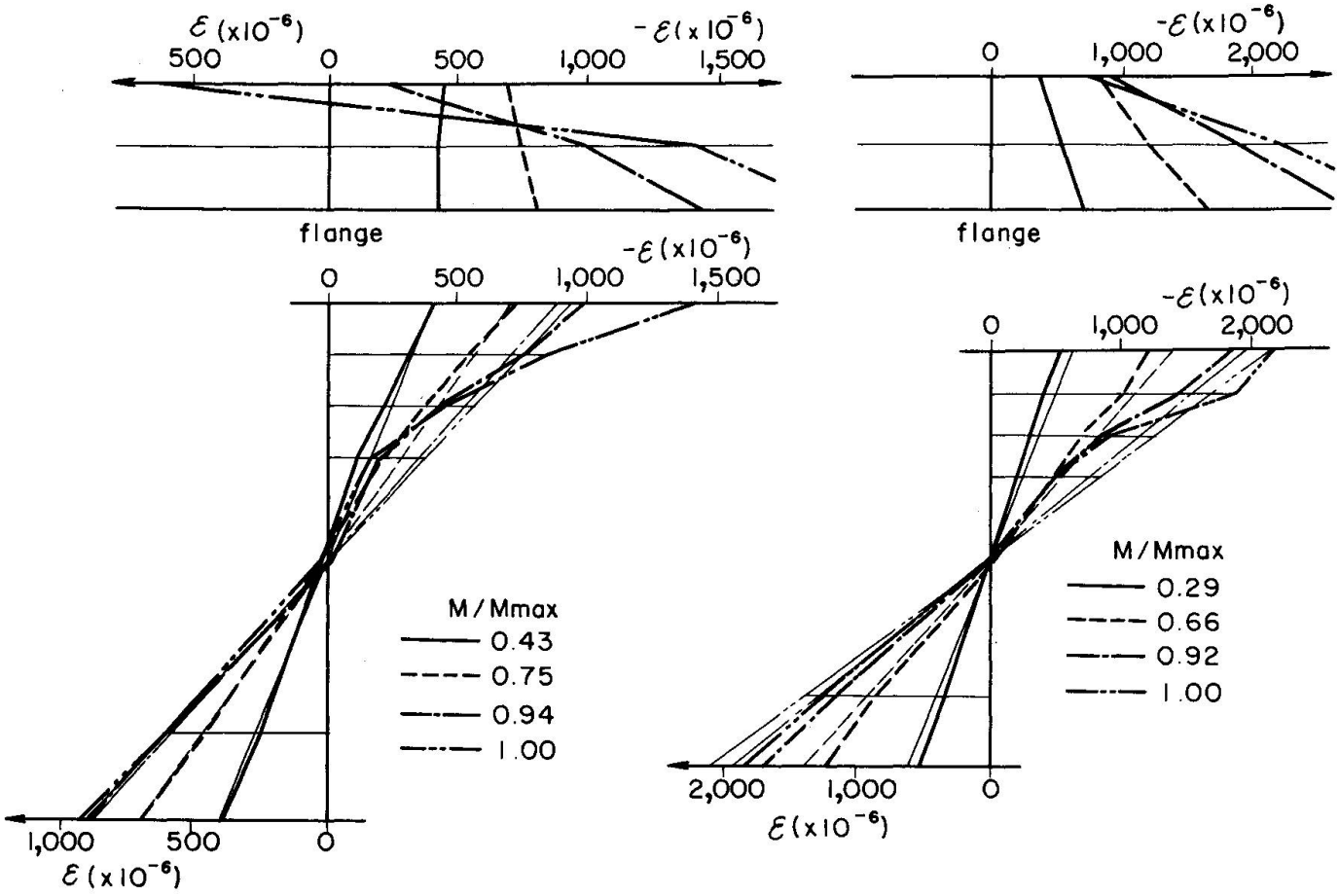

(a) Girder A (b) Girder C

Fig. 2.2.5 Strain Distribution at the Panel Center

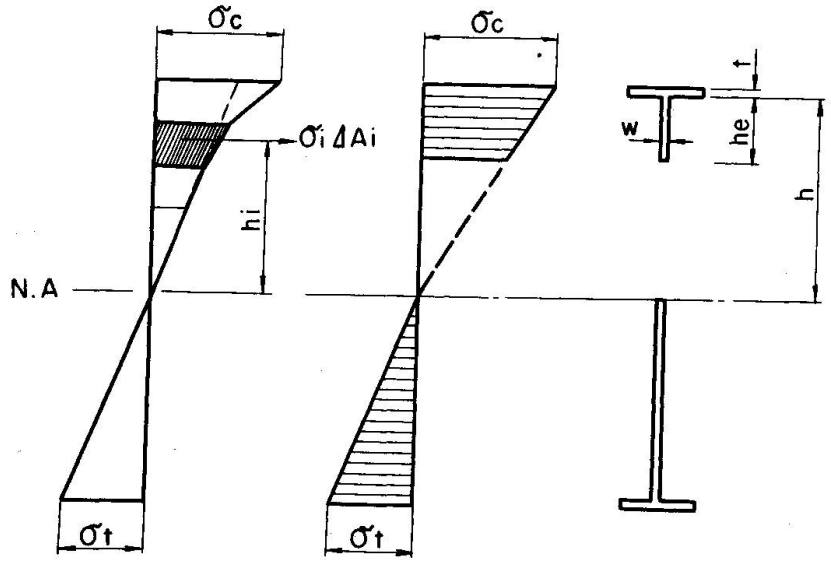

(a) (b)

Fig. 2.2.6 Modified Stress Distribution

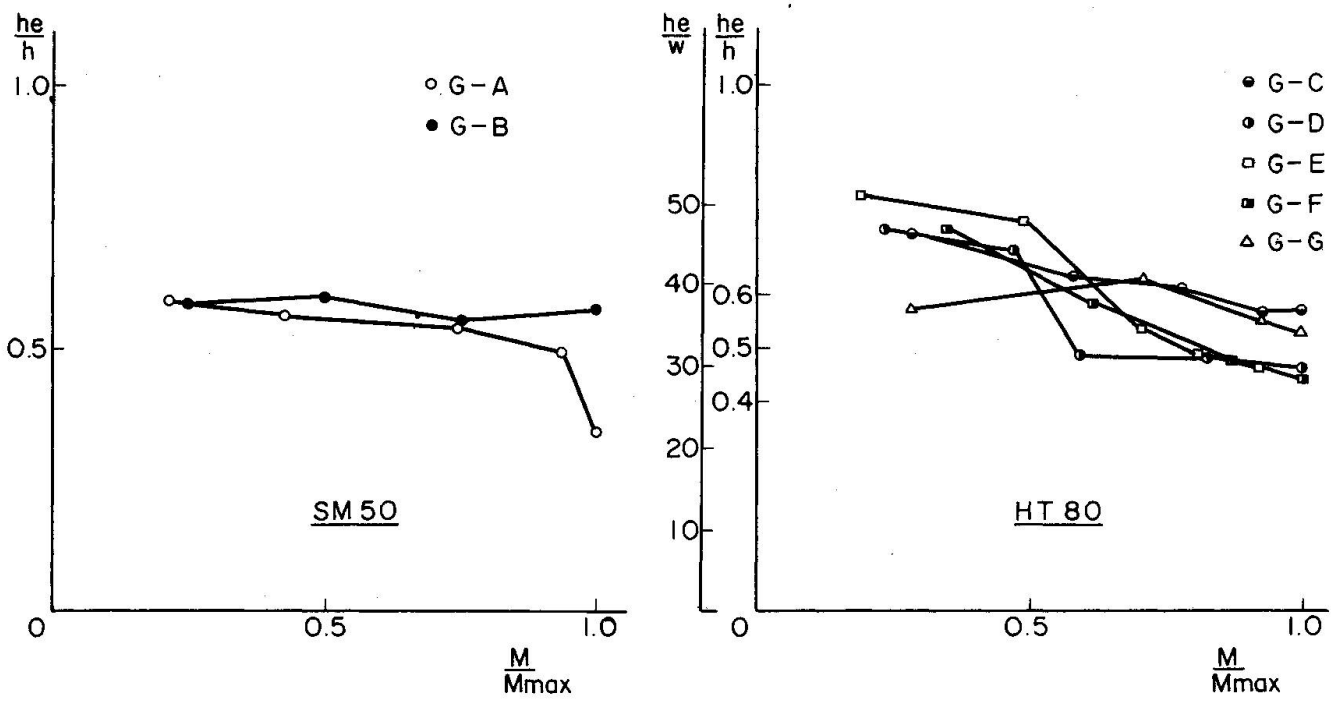

Fig. 2.2.7 Effective Bredth of Web

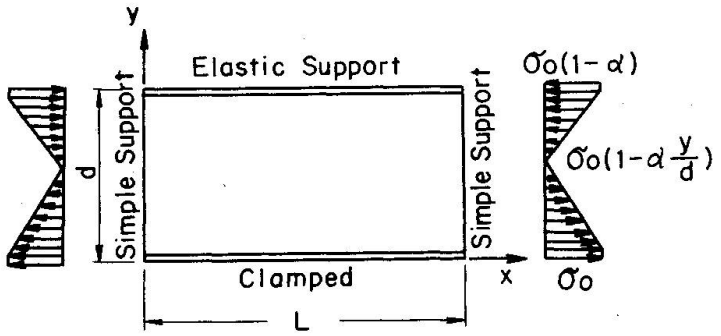

Fig. 2.2.8

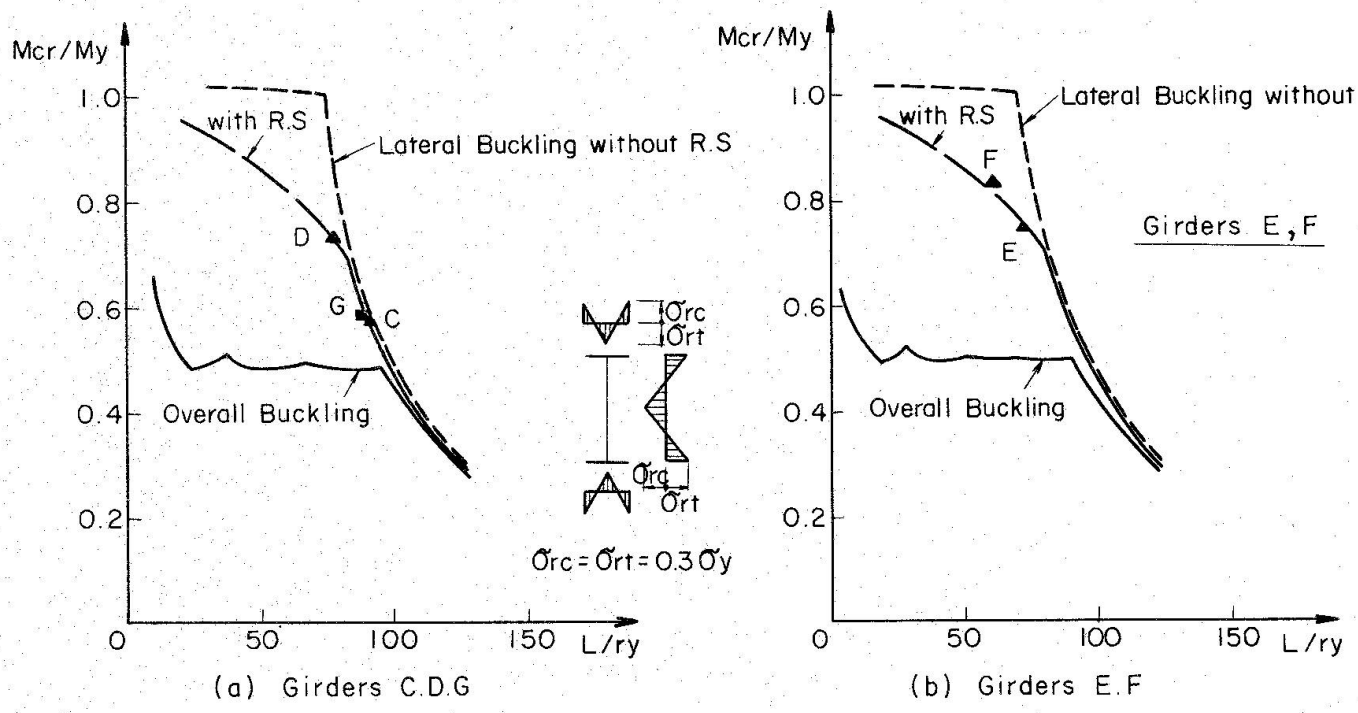

Fig. 2.2.9 Comparison of the Test Results with the Theories

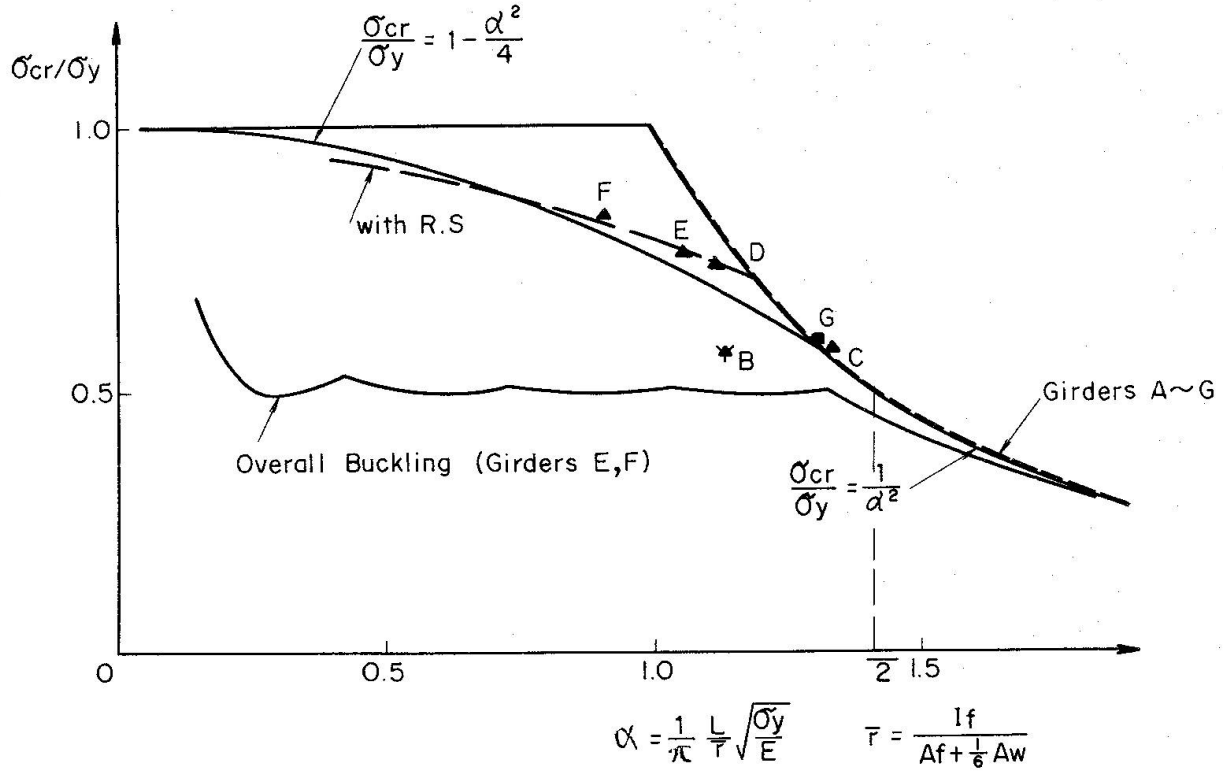

Fig. 2.2.10 Test Results and Theoretical Buckling Curves

2.3 Load-Deformation Characteristics of Plate Girders

With the increase of labor cost, there is a tendency that plate girder bridges of a relatively short span are shop-produced in large quantities. Strength of these mass-produced steel girders are studied from the two points of view; one is on the shear strength of welded built-up girders[1] and the other is on the moment carrying capacity of large size rolled I-profile beams[2]

From the economic point of view in fabrication of welded built-up girders with employment of automatic welding in mind, a design with no intermediate stiffener or a design with only horizontal stiffeners is preferred to that equipped with intermediate transverse stiffeners. Shear tests were performed by Nishino and Okumura on a series of full size plate girders with transverse stiffeners only at the supports and at the center of the test specimens where loading was applied. The depth to thickness ratios of the web plates made of a steel with yield strength of 40 kg/mm^2 ranged from 60 to 120.

The experimentally observed maximum loads exceeded the web buckling loads for all of the test girders, with exceptions of the girders with small depth-thickness ratios and failed by flange instability. Despite the comparatively small rigidity of the frameworks due to large aspect ratio of web panels of around 2.6 and in addition due to relatively smaller depth-thickness ratios of 120 at most, a large reserve of strengths above the buckling load was observed among the deeper girders, even for the girders failed by flange instability.

Although some of the design specifications restrict the use of web panels without intermediate vertical stiffeners except panels with thick plates, the tests revealed no particular ground for the restriction under static loading condition. The permissible shear stress specified in AASHO design specifications, one of the specifications which permit the use of this type of web panels, turned out to be very conservative for the test girders.

A horizontal stiffener placed at half the depth worked effectively to prevent premature buckling of the web due to shear force, suggesting a feasibility of an economical design of horizontally stiffened plate girders for shop-produced bridges in large quantities, in which no intermediate vertical stiffeners may be placed except at the points where heavy loads are concentrated.

The plastic collapse loads correlated well with the test results and represented best the experimentally obtained ultimate loads for all girders tested including the girders with d/t_w ratio of as large as 120.

Rolled I-beams in general have relatively thick web plates compared with welded built-up shapes of similar cross sectional properties and as a result the rolled shapes are inferior from the point of efficiency of cross sections. A study was carried out by Nishino and Okumura on large size rolled I-beams with the depth of 900 mm in order to study the magnitude and distribution of residual stresses inherent in the beams and their effect on the moment carrying capacity of the beams. It was found that the residual stresses present in the large size as-rolled beams are for large in magnitude compared with those present in the welded built-up sections of similar dimensions. The maximum magnitude reaches 60 to in some cases 90 percent of the yield strength and they distribute over the wide portions of the cross section. Due to the presence of large magnitude of compressive residual stresses in the web plates, there are a number of specimens in which the web plates are critical for buckling. During the bending test of full size rolled beams, it was observed that test beams behaved as if they are made of materials of different strength, which was due to the penetration of premature yielding at portions where a large magnitude of residual stress distributes. A good correlation existed between experimentally obtained moment-curvature relationship and that computed including the effect of residual stress. The fact indicates a large reduction of rigidity even at relatively small loading conditions, however, the width thickness ratios of component plates of rolled beams were so small that stability were not lost by the reduction of rigidity due to the premature yielding and as a consequence the moment carrying capacity inevitably exceeded full plastic moment. It was even noted that a beam with buckled web plates prior to the application of external loads stabilized with the increase of bending moment. The fact can be explained by the theoretical analysis of plate buckling.

References

1) F. Nishino and T. Okumura : "Experimental Investigation of Strength of Plate Girders in Shear" Final Report of 8th Congress of IABSE

2) F. Nishino and T. Okumura : "Strength of Large Size Rolled H-Beams" Annual Report of Eng. Research Inst., Faculty of Eng., Univ. of Tokyo, 1970

3 JAPANESE PROVISIONS ON PLATE GIRDER DESIGN

3.1 Steel Railway Bridges

(Excerpted from the "Specifications for Design of Steel Railway Bridges, 1970" Japanese National Railways)

(1) Thickness Requirements for Web Plates with Intermediate Transverse Stiffeners

For web plate having no longitudinal stiffeners.

Grade of Steel	SS 41 SM 41 SMA 41	SM 50	SM 50Y SM 53 SMA 50	Remarks
Minimum Thickness of Web Plate t (cm)	$\frac{D}{155}$	$\frac{D}{130}$	$\frac{D}{125}$	When the computed compressive stress at the edge of the web plate, σ, is much smaller than the allowable flange compressive stress, the value of t may be calculated by $t = 5400/\sqrt{\sigma} \leqq \frac{D}{200}$

D : clean distance between flanges of a plate girder (cm)

For web plate having one longitudinal stiffener.

Grade of Steel	SS 41 SM 41 SMA 41	SM 50	SM 50Y SM 53 SMA 50	Remarks
Minimum** Thickness of Web Plate (cm)	$\frac{D}{250}$	$\frac{D}{250}$	$\frac{D}{250}$	The gage line of longitudinal stiffener shall be about 0.2D from the toe of the compression flange

** Since plate girders in steel railway bridges are likely to vibrate through the passage of trains and are subject to high local bearing stresses combined with bending stresses when the girders directly support slippers on the top of the flanges, the above thickness requirements which may be sufficiently safe against web buckling in bending are adopted.

(2) Thickness Requirements for Web Plates without Intermediate Transverse Stiffeners

	Grade of Steel	SS 41 SM 41 SMA 41	SM 50	SM 50Y SM 53 SMA 50
Minimum Thickness of Web Plate (cm)	For web plate of a member of which flange plate directly supports sleepers and others	$\frac{D}{70}$	$\frac{D}{60}$	$\frac{D}{55}$
	For web plate of a member carrying no loads on the flange plate	$2000/\sqrt{S/A_w} \leqq \frac{D}{110}$ S : shearing force (kg) A_w : gross sectional area of web plate (cm^2)		

(3) Minimum Moment of Inertia of Stiffeners

Minimum Permissible Moment of Inertia (cm^4)	
intermediate transverse stiffener	longitudinal stiffener
$I = \frac{d_s\, t^3\, r}{11}$	$I = 2d_s\, t^3$ $(d_s/D \leqq 2)$

d_s : actual clear distance between stiffeners (cm)

t : thickness of web plate (cm)

$r = 25\left(\frac{D}{2700t\sqrt{\tau}}\right)^2 - 20 \leqq 5$ τ : mean value of shearing stresses of web plate between two adjacent stiffeners (kg/cm^2)

(4) Allowable Unit Stresses in Bending and Shear

	Allowable Unit Stress (kg/cm^2)		
	SS41 SM41 SMA41	SM 50	SM 50Y SM53 SMA50
Bending			
(1) Tension on extreme fiber(net section)	1,400	1,900	2,100
(2) Compression on extreme fiber (gross section)	1250 for $0<F\frac{\ell}{b}\leqq 28$ $1250-8.0(F\frac{\ell}{b}-28)$ for $28<F\frac{\ell}{b}\leqq 130$ $7{,}400{,}000(b/F\ell)^2$ for $130<F\frac{\ell}{b}$	1700 for $0<F\frac{\ell}{b}\leqq 24$ $1\,700-12.5(F\frac{\ell}{b}-24)$ for $24<F\frac{\ell}{b}\leqq 115$ $7{,}400{,}000(b/F\ell)^2$ for $115<F\frac{\ell}{b}$	1900 for $0<F\frac{\ell}{b}\leqq 22$ $1900-14.8(F\frac{\ell}{b}-22)$ for $22<F\frac{\ell}{b}\leqq 105$ $7{,}400{,}000(b/F\ell)^2$ for $105<F\frac{\ell}{b}$
	ℓ : unsupported length of the compression flange (cm) b : flange width (cm) $F=\sqrt{12+2\beta/\alpha}$ α = flange thickness/web thickness β = D/b		
Shear			
Web of plate girder	800	1,100	1,200

3.2 Steel Highway Bridges

(Excerpted from the "Specifications for Welded Steel Highway Bridges, 1964" Japan Road Association)

(1) Thickness Requirements for Web Plates with Intermediate Transverse Stiffeners

For web plate having no longitudinal stiffeners

Grade of Steel	SS 41	SM 50	SM 50Y SM 53	SM 58
Minimum thickness of web plate (mm)	$\frac{b}{160}$	$\frac{b}{136}$	$\frac{b}{128}$	$\frac{b}{112}$

b : clean distance between flanges of a girder

For web plate having one longitudinal stiffener.

	Portion	Grade of Steel				Remarks
		SS 41	SM 50	SM 50Y SM 53	SM 58	
Minimum Thickness of Web Plate (mm)	b_1	$\frac{b_1}{52}$	$\frac{b_1}{44}$	$\frac{b_1}{41}$	$\frac{b_1}{37}$	When the computed stresses in the portions b_1 and/or b_2 are far small as compared with the allowable stress, the values in the corresponding denominator may be multiplied by $\sqrt{\text{allowable stress}/\text{computed stress}}$
	b_2	$\frac{b_2}{95}$	$\frac{b_2}{81}$	$\frac{b_2}{76}$	$\frac{b_2}{67}$	
	b_3	$\frac{b_3}{207}$	$\frac{b_3}{176}$	$\frac{b_3}{166}$	$\frac{b_3}{146}$	
	b	$\frac{b}{259}$	$\frac{b}{220}$	$\frac{b}{207}$	$\frac{b}{183}$	

The gage line of longitudinal stiffener shall be about 0.2b from the toe of the compression flange.

For web plate having two longitudinal stiffeners.

	Portion	Grade of Steel				Remarks
		SS 41	SM 50	SM 50Y SM 53	SM 58	
Minimum Thickness of Web Plate (mm)	b_1	$\frac{b_1}{49}$	$\frac{b_1}{42}$	$\frac{b_1}{39}$	$\frac{b_1}{35}$	When the computed stresses in the portions b_1, b_2 and/or b_3 are far small as compared with the allowable stress, the values in the corresponding denominator may be multiplied by $\sqrt{\text{allowable stress}/\text{computed stress}}$
	b_2	$\frac{b_2}{55}$	$\frac{b_2}{47}$	$\frac{b_2}{44}$	$\frac{b_2}{39}$	
	b_3	$\frac{b_3}{98}$	$\frac{b_3}{83}$	$\frac{b_3}{78}$	$\frac{b_3}{69}$	
	b_4	$\frac{b_4}{202}$	$\frac{b_4}{172}$	$\frac{b_4}{162}$	$\frac{b_4}{143}$	
	b	$\frac{b}{306}$	$\frac{b}{260}$	$\frac{b}{245}$	$\frac{b}{216}$	

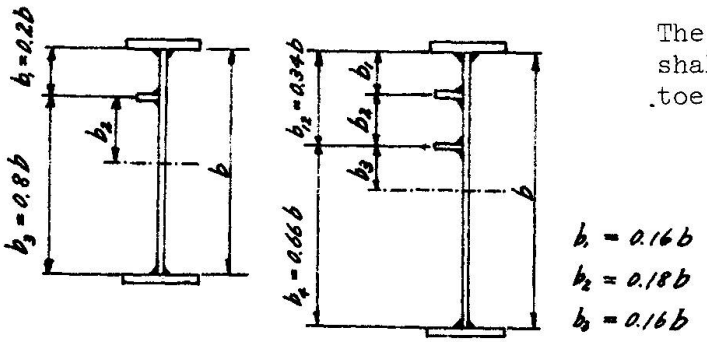

The gage lines of longitudinal stiffeners shall be about 0.16b and 0.34b from the toe of the compression flange.

(2) Thickness Requirements for Web Plates without Intermediate Transverse Stiffeners

Grade of Steel	SS 41	SS 50	SM 50
Minimum thickness of web plate (mm)	$\frac{b}{60}$	$\frac{b}{60}$	$\frac{b}{55}$

(3) Minimum Moment of Inertia of Stiffeners

Minimum permissible moment of inertia (cm^4)	
intermediate transverse stiffener	longitudinal stiffener
$I = \frac{d_o t^3 J}{11}$	$I = \ell t^3 (2.4 \frac{d^2}{\ell^2} - 0.13)$

, where d_o : actual clear distance between stiffeners (cm)

t : thickness of web plate (cm)

$J = 25\left(\frac{\ell}{d}\right)^2 - 20 \geqq 50, \qquad d = \frac{2800\ t}{\sqrt{S/A_{wg}}}$

ℓ : unsupported depth of web plate between flanges (cm)

S : shearing force applied to web plate (kg)

A_{wg} : gross sectional area of web plate (cm^2)

(4) Allowable Unit Stresses in Bending and Shear

Grade of Steel	Allowable Unit Stress (kg/cm^2)			
	SS 41	SS 50	SM 50Y SM 53	SM 58
Bending				
(1) Tension on extreme fiber(net section)	1,400	1,700	2,100	2,600
(2) Compression on extreme fiber(gross section)				
a) when compression flange is unsupported	$1{,}300 - 0.6(\ell/b)^2$ $\ell/b \leqq 30$	$1{,}600 - 0.9(\ell/b)^2$ $\ell/b \leqq 30$	$2{,}000 - 1.4(\ell/b)^2$ $\ell/b \leqq 27$	$2{,}400 - 2.0(\ell/b)^2$ $\ell/b \leqq 25$
	ℓ = unsupported length of the compression flange (cm) b = flange width (cm)			
b) when compression flange is supported laterally its full length by enbedment in concrete	1,300	1,600	2,000	2,400
Shear				
web of plate girder	800	1,000	1,200	1,500

3.3 Plate Girders in Buildings

(Excerpted from the "Specifications for the Design of Steel Structures, 1970" Architectural Institute of Japan)

(1) Check of Web Plate against Plate Buckling

(i) The check of web plate against plate buckling may be omitted provided that

$$\frac{d}{t} \leqq \frac{110}{F} \qquad (1)$$

is satisfied, where

d : clean distance between flanges of a plate girder (cm)

t : thickness of web plate (cm)

F : specified minimum yield point of the grade of steel being used (t/cm^2)

(ii) For the check of web plate against plate buckling, the web plate is sub-divided into rectangular panels of length a and depth d' as shown in Fig. 1. In case two longitudinal stiffeners are used, they must be so placed that the depths of the two subpanels near the compression flange are equal to each other (see Fig. 1).

(iii) The stress caused by external loads in the web plate panel under consideration must satisfy the following inequation:

$$\left(\frac{\sigma}{\sigma_o}\right)^2 + \left(\frac{\tau}{\tau_o}\right)^2 \leqq 1 \qquad (2) \qquad \text{, where}$$

σ : maximum compressive stress at the edge of the web plate panel (t/cm^2)
τ : average shearing stress at the web plate (t/cm^2)
σ_o : allowable plate buckling stress in bending (t/cm^2)
τ_o : allowable plate buckling stress in shear (t/cm^2)

(iv) Allowable plate buckling stress in bending δ_o

$$\sigma_o = \frac{1900}{(c_1 \frac{d'}{t})^2} f_t \qquad \text{for} \quad \frac{d'}{t} \geqq \frac{56}{c_1}$$

$$= (1.78 - 0.021\, c_1 \frac{d'}{t}) f_t \leqq f_t \qquad \text{for} \quad \frac{d'}{t} < \frac{56}{c_1} \qquad (3)$$

In case $d/t \leqq 210/\sqrt{F}$, the value of σ_o may be taken as f_t.

Notations : $c_1 = F/k_1$

$k_1 = (1 + \frac{\alpha}{6})(\alpha^3 + 3\alpha^2 + 4)$

$\alpha = 1 - \sigma_{min}/\sigma$: coefficient of compressive stress distribution(see Fig. 2)

f_t : allowable tensile stress (t/cm^2)

(v) Allowable plate buckling stress in shear.

$$\tau_o = \frac{3{,}300}{(c_2 \frac{d}{t})} \frac{f_t}{\sqrt{3}} \qquad \text{for} \quad \frac{d}{t} \geqq \frac{74}{c_2}$$

$$= (1.74 - 0.0154\, c_2 \frac{d}{t}) \frac{f_t}{\sqrt{3}} \leqq \frac{f_t}{\sqrt{3}} \qquad \text{for} \quad \frac{d}{t} < \frac{74}{c_2} \qquad (4)$$

Notations : $c_2 = F/k_2$

In case no longitudinal stiffener is used,

$$k_2 = 4.00 + \frac{5.34}{\beta^2} \quad \text{for} \quad \beta < 1.0 \qquad k_2 = 5.34 + \frac{4.00}{\beta^2} \quad \text{for} \quad \beta \geqq 1.0 \qquad (5)$$

In case one or two longitudinal stiffener is used,

$$k_2 = 4.00 + \frac{5.34}{\beta^2} + \frac{(n+1)^2 \eta}{\beta} \sqrt{\frac{8\mu}{3\beta}} \qquad \text{for } \beta < 1.0$$

$$k_2 = 5.34 + \frac{4.00}{\beta^2} + \frac{(n+1)^2 \eta}{\beta} \sqrt{\frac{8\mu}{3\beta}} \qquad \text{for } \beta \geqq 1.0 \qquad (6)$$

$\beta = a/d$ (see Fig. 2)

n = number of longitudinal stiffeners (i.e., n=1 or 2)

$\eta = \frac{d'}{d}$

$\mu = 10.9\, I_L/dt^3$

I_L : moment of inertia of longitudinal stiffener(s) (cm^4)

(2) Minimum Moment of Inertia of Intermediate Transverse Stiffeners

In case no longitudinal stiffener is used,

$$I_o = 1.1\ dt^3\left(\frac{1}{\beta^2} - 0.5\right) \qquad \text{for } \beta < 1.0$$

$$= 0.55\ dt^3 \qquad \text{for } \beta \geq 1.0 \qquad (7)$$

, where I_o denotes the required minimum moment of inertia of intermediate stiffeners.

In case one or two longitudinal stiffener is used,

$$I_o = 1.1\ dt^3\left(\frac{1}{\beta'^2} - 0.5\right) \qquad \text{for } \beta' < 1.0$$

$$= 0.55\ dt^3 \qquad \text{for } \beta' \geq 1.0 \qquad (8)$$

, where β' represents an aspect ratio a/d for which the value of τ_o computed by the use of Eq.(6) with the actual value of β is equal to that computed by the use of Eq.(5) with $\beta=\beta'$.

(3) Minimum Radius of Gyration of Longitudinal Stiffeners

$$\frac{i}{t} = C_m\{135(0.5 - \eta)^2 + 3\}\beta^{2/3}$$

$$C_m = 0.7 + \frac{1}{200(n+1)}\ \frac{i}{t}\ \frac{1}{\delta}$$

, where $0.2 \leqq \eta = \frac{d'}{d} \leqq 0.5$ for $n = 1$

$0.15 \leqq \eta = \frac{d'}{d} \leqq 0.3$ for $n = 2$

Notations :

$$\delta = \frac{A_s}{dt}$$

A_s : cross-sectional area of longitudinal stiffeners (cm^2)

---

* The minimum yield points for the six grades of steel are as follows:

Grade of Steel	SS 41	SS 50	SM 50	SM 50Y	SM 53	SM 58
Minimum Yield Point(kg/cm^2)	2,300	2,800	3,200	3,600	3,600	4,600

3.4 Ship Structures

The shape of girders used in ship structures are more complex compared to bridge or building structures. Namely, the girders are of variable cross sections and the height of webs become large at the corner connections. Furthermore, the girders have many holes in the web plate for man holes, piping holes and slots for longitudinal members.

The web height-thickness ratios of bottom transverses in wing tank are shown in Fig. 3. Fig. 4 shows the detailed dimensions of a bottom transverse in wing tank for different size (dead weight tonnages) of ships.

According to the increasing size of ships, the web height increases, on the other hand, the web thickness have hardly increased. This results the ratios h/t_w become high for huge tankers.

Thickness requirements of Nippon Kaiji Kyokai Rule (1970) for web plate of bottom transverses are as follows,

$$t_w = C_{do} + 3.5 \leq t_{min} \qquad (10)$$

where t_w : required web thickness (mm)

d_o : web height (m)

$C=C_1$: for web plate without horizontal stiffeners

$C=C_2$: for the panels between a horizontal stiffener and the bottom plate.

$C=C_3$: for the panels between horizontal stiffeners or between a horizontal stiffener and the flange plate

C_1, C_2 and C_3 are given in the table below, and when there are slots or holes, the modified C value should be used.

S*/do	≤0.2	0.4	0.6	0.8	1.0	1.5	2.0	2.5≤
C_1	2.6	4.5	5.6	6.4	7.1	7.8	8.2	8.4
C_2	2.1	3.7	4.9	5.8	6.6	7.4	7.8	8.0
C_3	3.7	6.7	8.6	9.6	10.3	10.4	10.4	10.4

* S : space of vertical stiffeners

Minimum thickness t_{min} in eq. (10) is specified in the table below.

Length of Ship (m)	105	105 – 120	120 – 135	135 – 150	150 – 165	165 – 180	180 – 195	195 – 225	225 – 275	275 –
t_{min} (mm)	8.0	8.5	9.0	9.5	10.0	10.5	11.0	11.5	12.0	12.5

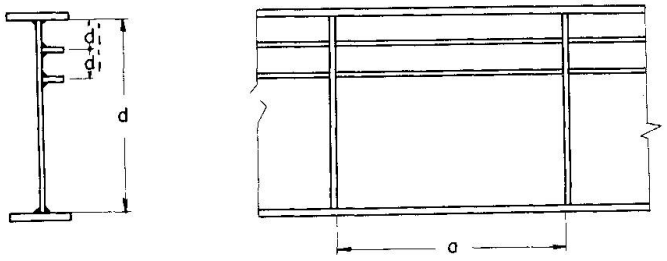

Fig. 1

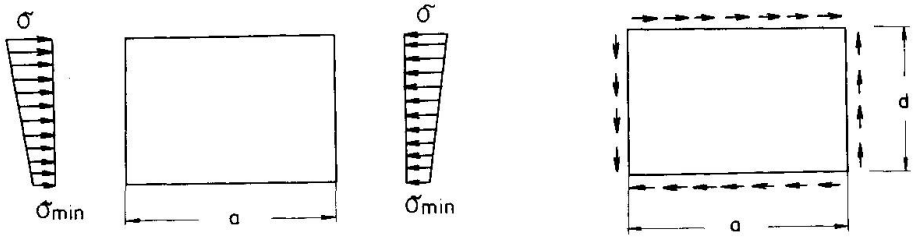

Fig. 2

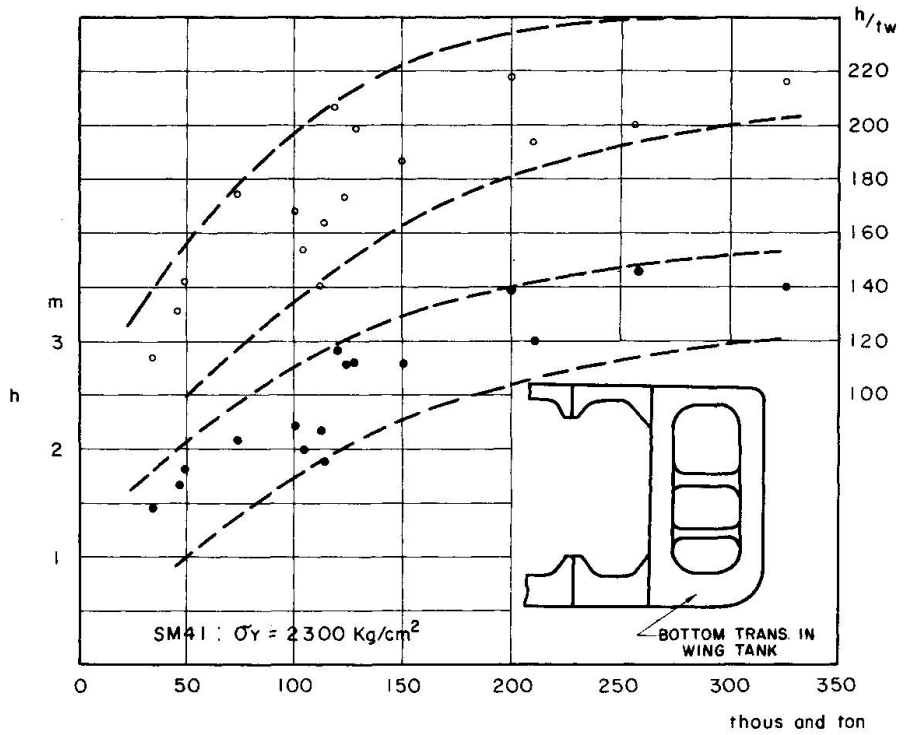

Fig. 3 Web Heights (or Web Height – Thickness Ratio) and Dead Weight Tonnages of Tankers for Bottom Transverses in Wing Tanks.

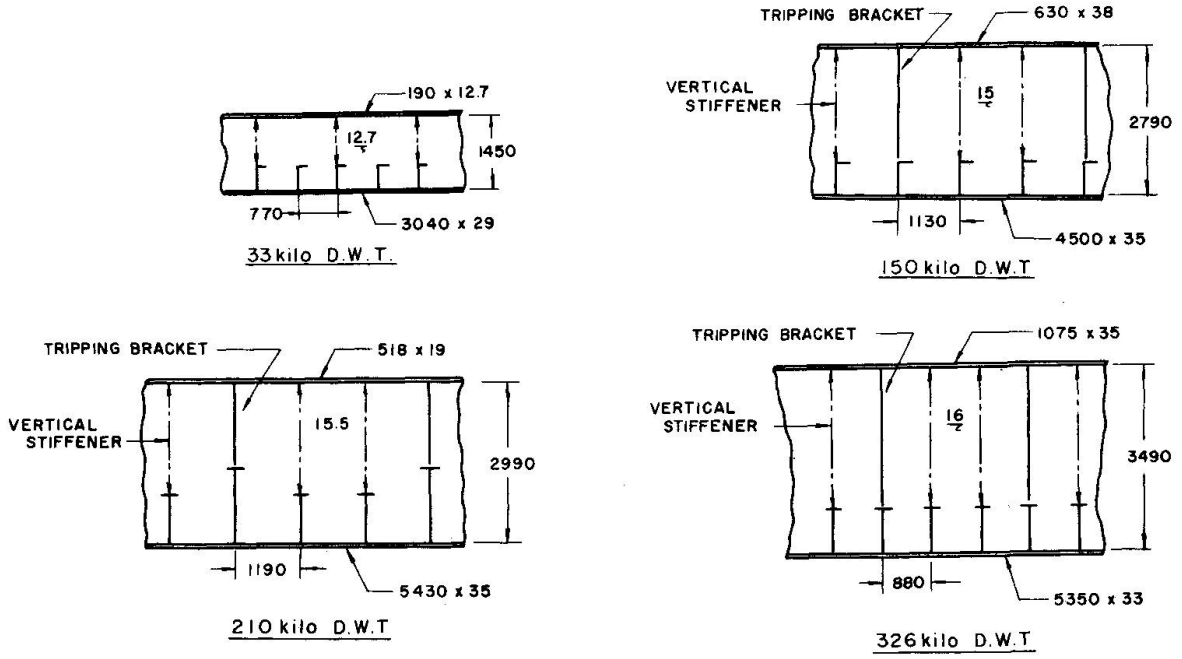

Fig. 4 Detailed Dimensions of Bottom Transverses in Wing Tanks for different Dead Weight Tonnages of Tankers.

Ultimate Strength of Stiffened Plate Girders Subjected to Shear

Résistance à la ruine des poutres à âme pleine raidies soumises au cisaillement

Tragfähigkeit ausgesteifter, schubbeanspruchter Blechträger

SADAO KOMATSU
Dr. Eng.
Professor, Department of Civil Engineering
Osaka University, Osaka, Japan

I. INTRODUCTION

For many years it was recognized that the static strength of plate girder entirely depends upon the web buckling strength. However, it has been shown by Massonnet, Rockey, Basler and other authors having been in progress since 1957 that the slender-web plate girder has its considerable inherent post-buckling strength. In several countries, the current Design Specification for transversely stiffened plate girders is based on these findings.

The present effort is part of a continuing study about the behavior of slender-web plate girder stiffened by transverse and longitudinal stiffeners, and that is concerned with the predicting of the limit strength of its panel under shear. To insure the justification of this approach, a series of proof-tests was carried out at Osaka University in the summer of 1968.

Five 7m long welded girders with 3.33mm webs, the slenderness ratios of which were 200, 225, 250, were tested. The test panels of girders had one or two longitudinal stiffeners, dividing the web into two or three subpanels of equal depth, in addition to transverse stiffeners. The stiffeners were designed by taking Prof. Skaloud's recommendations so as to allow the sufficient development of incomplete diagonal tension field.

The behavior of longitudinally stiffened slender-web girder under shear will be discussed in this report. Then the essential data of the proof-tests were compared with the predicted values. These test results as well as ones measured by several authors show excellent agreement with theoretical values obtained according to proposed method.

Finally, design recommendations based on these static studies have been formulated for plate girders subjected to shear.

II. MODE OF FAILURE UNDER SHEAR

A pure shear loading causes some kinds of failure mode chiefly dependent on the relation between the slenderness of web and the strength of smaller flange. In the case of low slenderness, a shear carrying action called "beam action" resists at the neutral axis to the pure shear. With the attainment of shear yield stress at the same place, the failure starts and then the yielding phenomenon spreads all over the web by only small increasing of the shear force. To design the girder having a comparatively slender web according to the classical beam theory based on "beam action", we need transverse stiffener spaced

close enough so that instability due to shear is excluded.

On the other hand, it has been long recognized that the pure diagonal tension develops in such a extremely thin web as those being seen in aircraft. The action of a pure diagonal tension field is quite similar to that of a diagonal member of Pratt Truss.

In the case of median slenderness, a pure shear loading results in equal tensile and compressive principal stresses up to critical shear buckling. After buckling, only a diagonal tension can carry any additional shear load. Basler and his colleagues at Lehigh University have developed "Theory of modified incomplete diagonal tension field". In the state of incomplete diagonal tension, two kinds of stress situation always exist together in the web plate. One of them corresponds to a critical shear stress, another a diagonal tensile stress. The mode of failure in this stress condition is greatly afftected by the rigidity of the boundary members and the slenderness of web plate. If the boundary members have sufficient stiffness, the diagonal tensile stress will be uniformly distributed in the web plate. So the collapse of that panel certainly occurs due to yielding all over the web plate. If the boundary member, however, do not have sufficient rigidity, yield zone is restricted to a narrow diagonal strip. The diagonal strip of the web flows plastically with the development of plastic hinges in the flange. The residual flange and web deflections shown by Prof. Rockey make it quite clear that the mode of failure is not similar to that assumed by Baslar. It should be also noted that the position of plastic hinge varies with the flange stiffness, being quite differ from Fujii's assumption.

For high flange stiffness, the plastic hing is located in the middle point of the panel length. While, its position is quite near a corner of panel for relatively flexible flange.

III. COMPUTING PROCEDURE

In order to find the ultimate strength of a plate girder under shear, the girder may be assumed to behave according to beam theory up to the critical buckling stress of web plate and then in a diagonal tension field manner up to the yielding point. With the exception of extremely low slenderness of web, for example less than 90, or extremely flexible stiffness of flange, the panel may also be assumed to be rigidly clamped along the flange.

Fig. 1 shows the relation between the extension of diagonal tension field and the deformation of panel-frame after collapse. In the same figure, γ denotes the shearing displacement and v(x) the deflection at a point x of flange due to its bending. If the tension field develops with the inclination θ to girder axis after buckling, a tensile strain ε_{tu} will be induced in the direction P"R' parallel to that of tension field.

$$\varepsilon_{tu} = \left[\gamma - \frac{V_u(x)}{a - x}\right] \sin\theta \cdot \cos\theta \qquad (1)$$

, where a is the panel length.

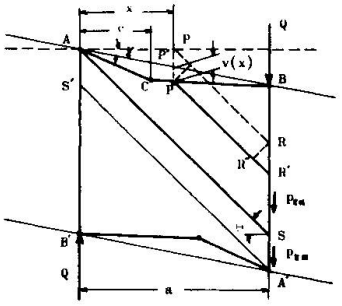

Fig. 1 Deformation of shear panel

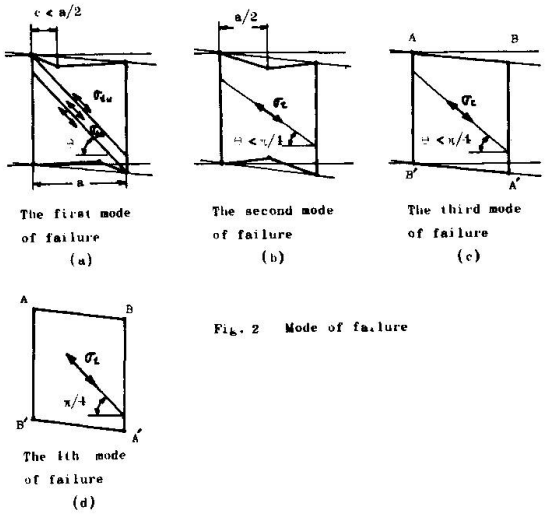

Fig. 2 Mode of failure

Corresponding tensile stress σ_{tu} will be also produced with the elastic modulus E_t.

$$\sigma_{tu} = E_t \left[\gamma - \frac{V_u(x)}{a - x} \right] \sin\theta \cdot \cos\theta \qquad (2)$$

Therefore, a distributed transverse internal force q_u acts on the flange all over the span AB.

$$q_u = E_t \left[\gamma - \frac{V_u(x)}{a - x} \right] \sin^3\theta \cdot \cos\theta \cdot t_w \qquad (3)$$

, where t_w is the thickness of web plate.
Whereas it may be assumed that both bounds A'S and AS' are scarcely deformed, a diagonal tensile stress σ_{tm} in central region may be written as follows;

$$\sigma_{tm} = E_t \gamma \sin\theta \cdot \cos\theta \qquad (4)$$

Now, two kinds of failure mode are cosidered according to the rigidity of flange. The first mode corresponding to a relatively flexible flange starts with bending collapse of flange, being accompanied by web-yielding in the central region such as shown in Fig.1. However, both upper region ABS and lower one A'B'S' remain elastic in spite of failure of girder. Neglecting the elastic deformation, the deflection of flange just after collapse may be represented by the following linear equation of coordinate x.

$$v(x) = \frac{x}{c}\Delta \qquad 0 \le x \le c$$
$$v(x) = \frac{a-x}{a-c}\Delta \qquad c \le x \le a \qquad (5)$$

Substituting v(x) into eq.(3), the transverse internal force q_u is written by

$$q_u = E_t \left(\gamma - \frac{x}{c} \cdot \frac{\Delta}{a-x} \right) \sin^3\theta \cdot \cos\theta \cdot t_w \qquad 0 \le x \le c$$

$$q_u = q_{u2} = E_t \left(\gamma - \frac{\Delta}{a-c} \right) \sin^3\theta \cdot \cos\theta \cdot t_w \qquad c \le x \le a \qquad (6)$$

, where Δ is the deflection at the point C.
Especially, at x=0

$$q_u = q_{u1} = E_t \gamma \sin^3\theta \cdot \cos\theta \cdot t_w \qquad (7)$$

For the sake of simplicity, the linear distribution of transverse internal force q_u along the coordinate axis x may be assumed as an approximation between A and C.

$$q_u = q_{u1} - (q_{u1} - q_{u2}) \frac{x}{c} \qquad (0 \le x \le c) \qquad (8)$$

By applying the principle of virtual displacement to the flange AB broken off by the transverse action q_u, a following relation can be obtained.

$$\frac{12a}{c(a-c)} M_p = cq_{u1} + (3a-c) q_{u2} \qquad (9)$$

, where M_p denotes the full plastic moment of smaller flange, being computed by following formula.

$$Mp = \frac{1}{4} \sigma_{fy} b_f t^2_f \qquad (10)$$

In above formula, σ_{fy} , b_f, and t_f denote yield stress, breadth, and thickness of flange, respectively

Substituting eqs.(6) and (7) into eq.(9), and putting

$$\bar{\eta} = E_t \Delta \sin^3\theta \cos\theta \cdot t_w / a$$

$$= \frac{q_{u1}(a-c) - \frac{4Mp}{c}}{a - \frac{c}{3}} \qquad (11)$$

Considering of equilibrium in vertical direction at the cross section AB gives a following relation,

$$Q = \int_0^a p_{zu}(x)dy(x) + \int_{a\tan\theta}^{b} p_{zm}(y)dy + \tau_{cr} bt_w \qquad (a)$$

, p_{zu} and p_{zm} are shear internal forces per unit length along the boundary at the upper and central region, respectively as shown in Fig.1. The third term represents the contribution of remaining beam action. From boundary conditions of the panel,

$$\left.\begin{aligned} p_{zu} &= \sigma_{tu} \sin\theta \cdot \cos\theta \cdot t_w \\ p_{zm} &= \sigma_{tm} \sin\theta \cdot \cos\theta \cdot t_w \end{aligned}\right\} \tag{12}$$

Then, using eqs.(12) in eq.(a),

$$Q = q_{ul} b \cdot \cot\theta - \bar{\eta}\left[1+\frac{c}{2(a-c)}\right] a + \tau_{cr} b t_w \tag{13}$$

Furthermore, the attainment of yielding in the central region causes the complete failure of plate girder, so that the diagonal tensile stress σ_{tm} can increase up to following value according to the yield criterion,

$$\sigma_{tm} = \sigma_{wy} - 2\tau_{cr} \sin 2\theta \tag{14}$$

, where σ_{wy} , τ_{cr} are yield stress and critical shear buckling stress of web, respectively.
So q_{ul} becomes as follows,

$$q_{ul} = (\sigma_{wy} - 2\tau_{cr} \sin 2\theta) \sin^2\theta \cdot t_w \tag{15}$$

Substituting eqs.(11) and (15) into eq.(13), the ultimate shear force can be finally obtained.

$$Q = \frac{1}{2}(\sigma_{wy} - 2\tau_{cr} \sin 2\theta)\left\{b \sin 2\theta - \alpha(1-\cos 2\theta)\right\} t_w + \frac{4 M_p \alpha}{c(a-c)} + \tau_{cr} b t_w \tag{16}$$

, where b and t_w are depth and thickness of web plate respectively, and

$$\alpha = \frac{a-c/2}{a-c/3} a \tag{17}$$

The inclination of diagonal tension field θ can be obtained under such condition as the shearing resistance should become maximum; that is,

$$\frac{\partial Q}{\partial \theta} = 0$$

, from which the following relation is deduced.

$$\sigma_{wy}(b \cos 2\theta - \alpha \sin 2\theta) + 2\tau_{cr}\left\{\alpha(\cos 2\theta - \cos 4\theta) - b \sin 4\theta\right\} = 0 \tag{18}$$

For this case, the inclination should be determined to satisfy above condition (18).

Then the position of plastic hinge can be determined by a following empirical formula,

$$C = \frac{1.782 \dfrac{Mp}{\sigma_{wy}\, b^2 t_w} + 0.38}{2\left(1.782 \dfrac{M_p}{\sigma_{wy} b^2 t_w} + 1\right)}\, a \qquad (19)$$

For flexible flange, Mp value is so small that the factor $\bar{\eta}$ of plastic deflection in eq.(11) takes positive value.
In such a case, the first mode of collapse as shown in Fig.2(a) will be occured. If the rigidity and strength of flange are much enough to resist elastically against the transverse internal force q_u even after yielding of web, the third or fourth mode of failure will be deduced as shown in Fig.2(c) or (d).
In these modes, the diagonal tensile stress will be uniformly distributed all over the panel. The failure of girder will be induced by complete panel-yielding, when the diagonal tensile stress σ_t will attain to the yield point. Therefore

$$p_z = p_{zu} = p_{zm} = \sigma_t \sin\theta \cdot \cos\theta \cdot t_w$$

$$= \frac{1}{2}\left(\sigma_{wy} - 2\tau_{cr} \sin 2\theta\right) \sin 2\theta \cdot t_w \qquad (20)$$

Substituting eq.(20) into eq.(a), the ultimate shear force Q can be obtained as follows,

$$Q = \left\{ \frac{1}{2}\sigma_{wy} \sin 2\theta + \tau_{cr}(1 - \sin^2 2\theta) \right\} b t_w \qquad (21)$$

According to the condition of maximum value $\partial Q / \partial \theta = 0$ again,

$$\cos 2\theta \left(\sigma_{wy} - 4\tau_{cr} \sin 2\theta \right) = 0 \qquad (22)$$

If the slenderness of web is so large that the critical shear buckling stress has a very small value and an inequality

$$\sigma_{wy} - 4\tau_{cr} \geq 0 \qquad (23)$$

can be satisfied, the fourth mode of failure will be occured. Since the inclination θ of tension field should become $\pi/4$ in such a case, the ultimate shear force Q can be readily found.

$$Q = \tau_{wy}\, b\, t_w + 4Mp/a \qquad (24)$$

The last term represents the sum of the full pastic moments at the corners A, B, A' and B'.

This means so-called Wagner's complete tension field.

However, if the slenderness of web plate is not so large as to satisfy inequality(23), the inclination should be determined by a following equation.

$$\theta\ (=\theta_0) = \frac{1}{2}\sin^{-1}\frac{\sigma_{wy}}{4\tau_{cr}} \tag{25}$$

The ultimate force Q should be, of course, calculated by eq.(21). Consequently the third mode of failure will be occured in such a case.

As an intermediate case between the first and third mode, it will be considered that the plastic hinge at the middle point of flange will be built up simultaneously with the spreading of yielded scope in the web. For such a case, the mode of failure may be called the second mode and shown in Fig.2(b). In this case, $\bar{\eta}$ takes a negative value for θ satisfying condition(18), while it has positive one for θ taking $\pi/4$ in spite of satisfying inequality(23).

Since it must be complicated to analyze rigorously such stress situation, the following approach may be useful to find ultimate load. From the condition of simultaneous collapse, the following relation may be derived.

$$M_p = \frac{a^2}{16}\left(\sigma_{wy} - 2\tau_{cr}\sin 2\theta\right)\sin^2\theta \cdot t_w \tag{26}$$

When the plastic moment M_p of flange is given, the inclination θ for such mode of failure should satisfy above eq.(26).

Thus eq.(21) can be applied again to determine the ultimate shear force, because the combined stress will be attained to yield point in entire panel immediately after collapse of flange.

The practical computing process may be carried out in such a way as shown by a block diagram as shown in Fig.3.

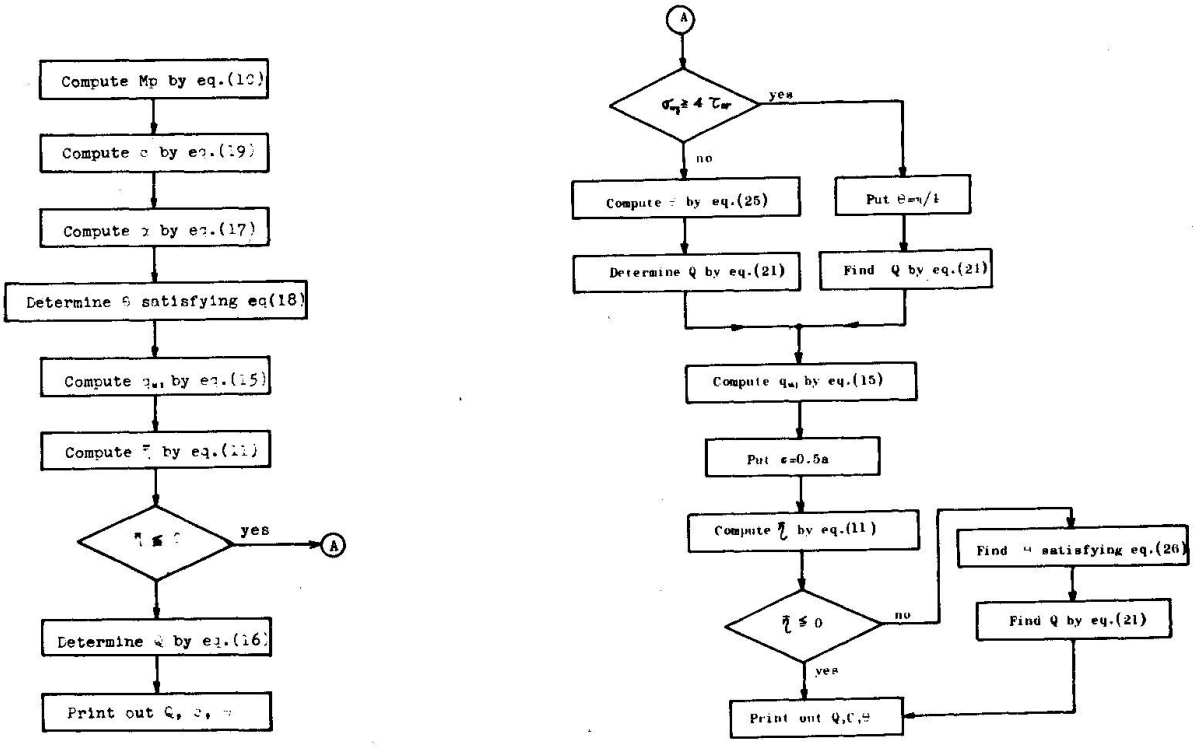

Fig. 3 Block diagram for ultimate shear force computation program

IV. PROOF TESTS

The primary purpose of the main tests was to justify the newly developed theory for the ultimate strength of unsymmetrical plate girder under shear.

Five girders could be loaded statically to fail for this purpose. Since it was unde sirable to fail in any panel other than the test-panel, the girder was designed so that the failure loads were remarkably different for adjacent panels.

4.1 Girder Specimens

Among the five girders tested, each of three girders had a one-sided longitudinal stiffener at the middle of web depth shown in Fig.4, the other had two one-sided longitudinal stiffeners on the internal trisector of the web. The test girders were connected to a rigid supporting girder by high tension bolts shown in Fig.5.

Moreover, two corner plates were welded to increase the ridigity of upper flange shown in Fig.6. The dimensions of test girders are given in Table 1.

4.2 Test Load

The load was applied by means of two oiljacks with total capacity 150tons. Five equal increments of load were taken up to two-thirds of predicted yield load, then the load was increased by 2tons at one time until failure.

4.3 Material Properties

The actual dimensions of the component plates of the test specimens were obtained from measurements on coupon plates cut from the various plates before fabrication. Table 2 shows the measured values of dimensions and the results of the tensile tests.

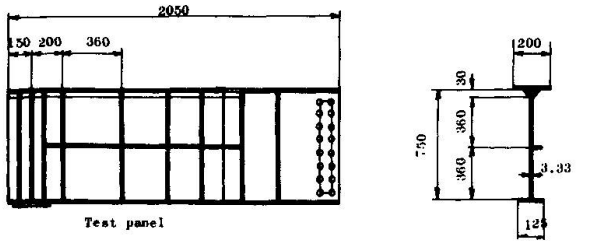

Fig. 4 Specimen A-2

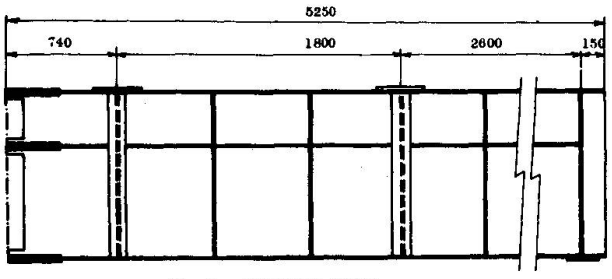

Fig. 5 Supporting girder

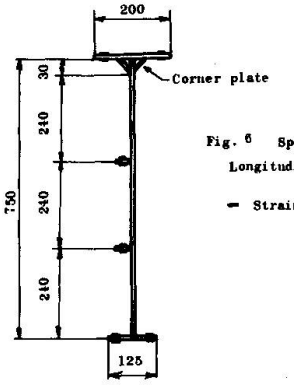

Fig. 6 Specimen A-3
Longitudinal stiffener section
35mm×1.5mm
— Strain gauge

Specimen	b cm	b_1 cm	t_w cm	b_f cm	t_f cm	a cm	n
A-1	67	32	0.333	12.5	1.0	32	1
A-2	75	36	0.333	12.5	1.0	36	1
A-3	75	24	0.333	12.5	1.0	36	2
A-4	83	40	0.333	12.5	1.0	40	1
A-5	83	26.7	0.333	12.5	1.0	40	2

b: depth of web
b_1: depth of subpanel
t_w: thickness of web
b_f: breadth of smaller flange
t_f: thickness of smaller flange
a : length of shear panel (distance between transverse stiffeners)
n : number of longitudinal stiffeners

Table 1 Dimensions of panel

Specimen	Size mm	Section area mm	Gauge distance mm	Yield load ton	Ultimate load ton	Yield stress kg/cm	Ultimate stress kg/cm	Stretch mm	Percentage of stretch %
A-1	39.93 9.93	396.505	200	15.00	21.11	3783.1	5399.7	44.0	22.0
A-2	39.95 9.85	393.508	200	14.89	21.06	3784.0	5352.0	45.0	22.5
A-3	40.00 9.65	386.000	200	14.50	20.69	3756.9	5360.1	41.0	20.5
B-1	40.07 10.69	428.348	200	15.93	24.02	3719.4	5608.2	41.0	20.5
B-2	40.07 10.79	432.355	200	15.98	24.16	3695.7	5588.1	41.0	20.5
B-3	39.87 10.61	423.021	200	16.00	23.80	3782.5	5626.2	41.0	22.5
C	50.03 14.09	704.923	200	25.70	40.10	3646.0	5688.8	44.0	22.0
D	25.25 4.44	112.110	50	5.50	6.46	4906.3	5762.2	10.5	21.0
E-1	23.17 3.33	77.156	50	3.50	4.35	4533.7	5637.9	16.5	33.0
E-2	23.20 3.35	77.72	50	3.29	4.19	4233.1	5391.1	15.5	31.0
E-3	23.17 3.33	77.156	50	3.27	4.19	4237.9	5430.6	16.0	32.0

A,B,C,D: SM50 for flange E : SM50 for web

Table 2 Tensile test of material

V. TEST RESULTS

In this paper, the typical data of many test results are shown as follows.

5.1 Deflection of Web

The lateral deflections at the middle point of each subpanel under shear were plotted against load as shown in Fig.7.

5.2 Strain of Flanges

The longitudinal strain of both flanges were plotted against load as shown in Fig.8. It can be considered that these strains were suddenly increased due to shear buckling of web plate. Therefore, actual critical shear buckling stresses may be observed from these diagrams. Thus, the experimental critical shear stresses could be seen to coincide with the theoretical ones of subpanel fixed at both longitudinal sides and simply supported at vertical sides.

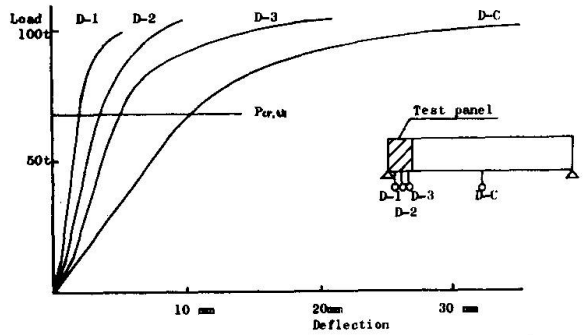

Fig. 9 Vertical deflection of girder A-2

5.3 Deflection of Girders

The deflection of several points measured by dialgages were plotted against loads as shown in Fig.9. Most curves tend to deviate from a straight line just after predicted critical shear buckling load $P_{cr,th}$ as shown in the same figures. From these facts, the theoretical values for shear buckling can be considered to be acceptable.

5.4 Strain of Longitudinal Stiffeners

The strains of longitudinal stiffeners were plotted against applied load as shown in Fig.10. After buckling of web, the longitudinal stiffeners of all test girders, except A-4, were bent upward. This behavior was caused by the fact that the membrane were pull up towards the upper flange which was more rigid than the lower one. Moreover, the longitudinal strains at the opposite side to stiffened surface of web were compressive in the case of one stiffener, or compressive at upper stiffener and tensile at lower one in the case of two stiffeners.

5.5 Strain of Transverse Stiffener

The strains of transverse stiffeners were plotted against applied load as shown in Fig.11. The strain scarcely induced in any transverse stiffener up to web buckling. The strain of transverse stiffeners as well as flanges, however, abruptly increase after buckling of web, because the frame consisting of flanges and stiffeners must bear the internal forces transfered from the buckled web.

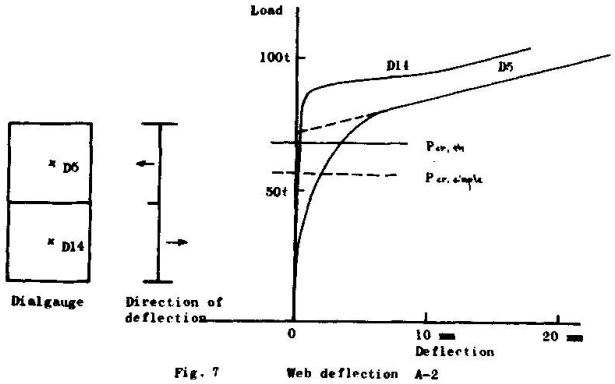

Fig. 7 Web deflection A-2

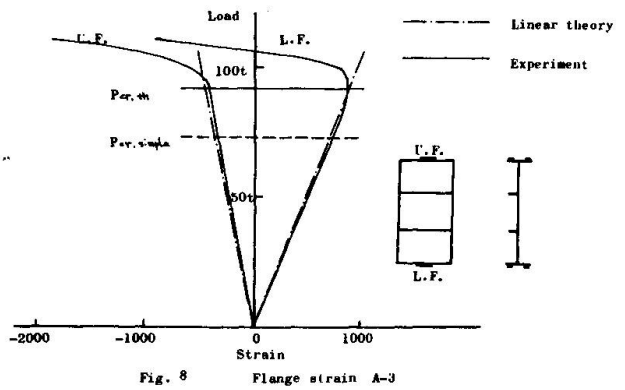

Fig. 8 Flange strain A-3

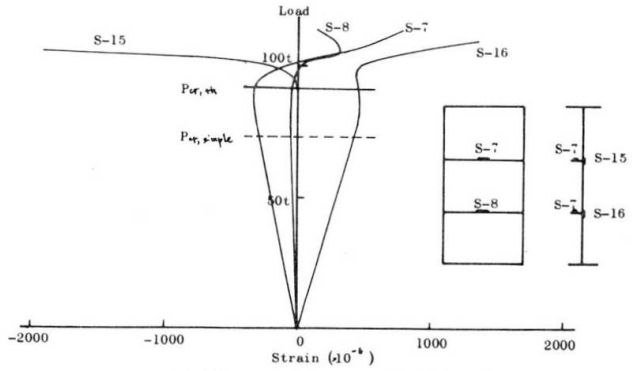

Fig. 10 Strain of longitudinal stiffeners

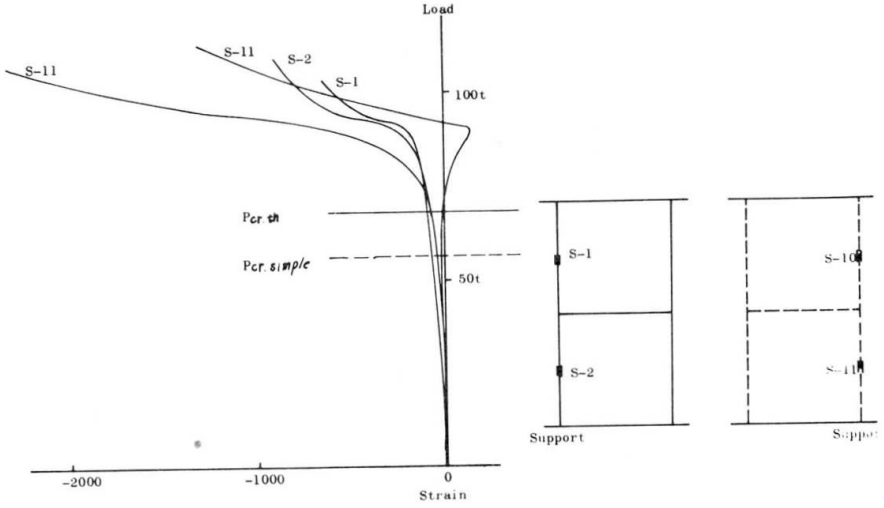

Fig. 11 Strain of traseverse stiffner A-2

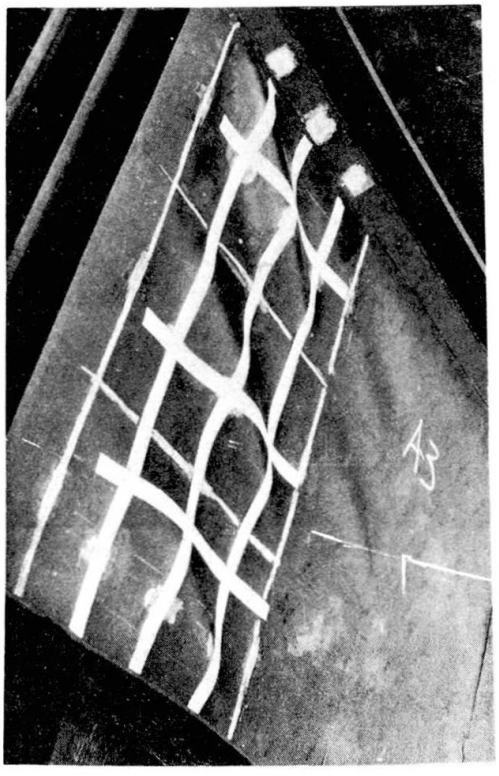

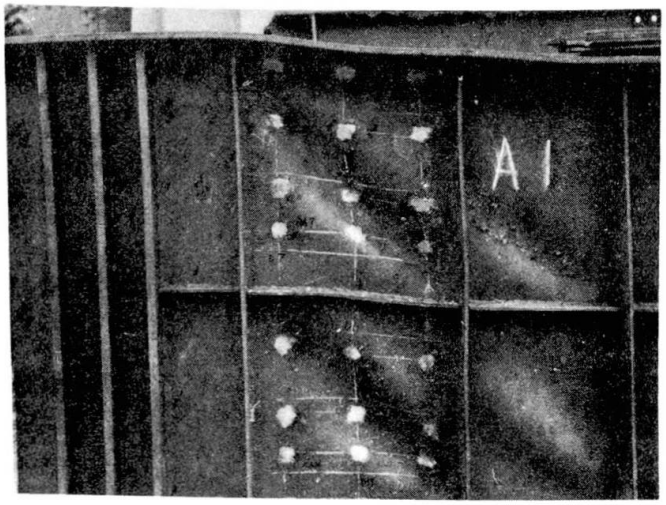

VI. COMPARISON BETWEEN PREDICTED VALUES AND EXPERIMENTAL RESULTS

The experimentally obtained ultimate load Q_{ex} were compared with the values Q_{th} based on the author's theory as shown in Table 3. It can be seen that the fairly agreement between them could be obtained.

Moreover, the strength of every stiffeners except A-4 girder may be recognized to be so enough as to resist elastically diagonal tensile stress.

In Table 3, the experimental results given by other authors also agree with author's theoretical values.

VII. REQUIREMENT FOR FLANGE STRENGTH

In order to establish a well balanced design of girder under shear, how large flange or stiffener should be adopted? Concerning with this problem, it is rational to choose such a flange as to make the girder fail in the second mode for given dimension of web plate.

Hence, for the web satisfying inequality (23), the maximum ultimate shear force Q_{max} can be given when θ is equal to $\pi/4$, that is

$$Q_{max} = \tau_{wy}\, b\, t_w + 4M_p/a \tag{27}$$

Herein, the required plastic moment $M_{p,req}$ of smaller flange may be given from eq(26) as follows,

$$M_{p,req} = \frac{a^2}{32}\left(\sigma_{wy} - 2\tau_{cr}\right) t_w \tag{28}$$

However, if inequality(23) cannot be satisfied for given web, the inclination $\theta = \theta_0$ should be decided by eq.(25). Therefore, Q_{max} takes the value given by substituting $\theta = \theta_0$ into eq.(21). In this case, a required plastic moment $M_{p,req}$ of flange should be found by a following formula.

$$M_{p,req} = \frac{a^2}{16}\left(\sigma_{wy} - 2\tau_{cr}\sin 2\theta_0\right)\sin^2\theta_0 \cdot t_w \tag{29}$$

The required full plastic moments $M_{p,req}$ of desirable flange for girder specimens can be compared with the actual ones $M_{p,act}$ in Table 3. The strength of flange in the girder at which the 3rd mode of failure was occured was too large to be appropriately and economically designed for designated web. While, in the girder collapsing in the 1st mode, the strength of flange was too small to use up the full strength of girder.

CONCLUSIONS

An approach to the limit design of thin-web plate girder with transverse and longitudinal stiffeners under shear was proposed in this paper. It was shown by analysis that there were four modes of failure any one of which would

be induced in accordance with the relative strength of flange to the web. This calculating method of ultimate strength includes both the finding of the mode of failure for designated dimension of member and the determination of ultimate strength.

It was shown that the test results given by several authors fairly agreed with the theoretical ones.

The rational design method of shear panel, especially the determination of desirable dimension of flange was indicated here.

The stiffness of longitudinal stiffener has only to be sufficient to increase the critical buckling stress as much as possible and make the stiffener remain straight up to the collapse load of girder.

REFERENCES

1. Ch. Massonnet,
Stability considerations in the design of plate girders.
Proce ASCE, vol. 86, ST 1, 1960.

2. Owen D.R.J., K.C. Rockey, and M. Skaloud,
Behaviour of longitudinally reinforced plate girders.
Prel. publication of 8th congress IABSE, 1968.

3. Rockey, K.C. and M. Skaloud,
Influence of flange stiffness upon the load carring capacity of webs in shear
Prel. publication of 8th congress IABSE, 1968.

4. Ostapenko, A., B.T. Yen, and L.S. Beedle,
Research on plate girders at Lehigh University.
Prel. publication of 8th congress IABSE, 1968.

5. Fujii, T,
On improved theory for Dr. Basler's theory
Prel. publication of 8th congress IABSE, 1968.

6. Basler, K,
Strength of plate girders in shear,
Proce. ASCE vol. 87, ST 7, 1961.

7. Basler, K., Yen, B.T., Mueller, J.A., and Thürlimann, B.
Web buckling tests on welded plate girders,
Bulletin No. 64, Welding Research Council 1960.

8. Konishi I,
Theories and experiments on the load carring capacity of plate girders
Report of Research Committee of Bridges, Steel Frames and Welding in Kansai District in Japan 1965.

9. Cooper, P.B.,
Strength of longitudinally stiffened plate girders,
Proc. ASCE, vol. 93, ST 2, 1967.

10. Patterson, P.J., J.A. Corrado, J.S. Huang, and B.T. Yen,
Proof-tests of two slender-web welded plate girders,
Fritz Engineering Laboratory Report No.327.7, 1969.

11. Schueller, W., and A. Ostapenko,
Static tests on unsymmetrical plate girders main test series
Fritz Engineering Laboratory Report No.328.6, 1968.

12. Skaloud, M.,
Design of webplates of steel girders with regard to the postbucking behaviour approximate solution
The Structural Engineer vol. xxxx, No. 9, 1962.

	Specimen	Web			Flange			a	Plastic hinge C	Mode of failure	cr, th
		b (b_1)	tw	Vwy	bf	tf	Vfy				
1	A-1	67 (32)	0.333	4,534	12.5	1.0	3,783	32	None	3rd	1758
	A-2	75 (36)	0.333	4,233	12.5	1.0	3,784	36	None	3rd	1555
	A-3	75 (24)	0.333	4,235	12.5	1.0	3,756	36	None	3rd	1842
	A-4	83 (40)	0.333	4,395	12.5	1.0	3,738	40	20.0	2nd	1450
	A-5	83 (27)	0.333	4,238	12.5	1.0	3,738	40	None	3rd	1769
2	TG-1	100	0.25	2,037	16	0.506	2,862	100	19.0	1st	145.8
	TG-1'	100	0.25	2,037	16	0.526	2,862	100	19.0	1st	145.8
	TG-2	100	0.25	2,037	20	1.008	2,862	100	19.2	1st	145.8
	TG-2'	100	0.25	2,037	20	1.012	2,862	100	19.2	1st	145.8
	TG-3	100	0.25	2,037	20	1,643	2,862	100	50.0	2nd	145.8
	TG-3'	100	0.25	2,037	20	1.642	2,862	100	50.0	2nd	145.8
	TG-4	100	0.25	2,037	20	2.016	2,862	100	50.0	2nd	145.8
	TG-4'	100	0.25	2,037	20	2.013	2,862	100	50.0	2nd	145.8
	TG-5	100	0.25	2,037	25	2.975	2,862	100	None	4th	145.8
	TG-5'	100	0.25	2,037	25	2,972	2,862	100	None	4th	145.8
3	G6-T1	127	0.49	2,580	30.8	1.975	2,665	190.5	36.6	1st	306
	G6-T2	127	0.49	2,580	30.8	1.975	2,665	95.2	47.6	2nd	435
	G6-T3	127	0.49	2,580	30.8	1.975	2,665	63.4	None	3rd	741
	G7-T1	127	0.498	2,580	30.95	1.95	2,645	127	24.4	1st	358
	G7-T2	127	0.498	2,580	30.95	1.95	2,645	127	24.4	1st	358
	G8-T1	127	0.50	2,680	30.45	1.902	2,910	381	73.2	1st	283
	G9-T1	127	0.333	3,130	30.45	1.902	2,940	381	73.4	1st	125
	G9-T2	127	0.333	3,130	30.45	1.902	2,940	190.5	36.7	1st	145
4	B	120	0.45	5,000	24.0	1.2	5,000	120	22.9	1st	328
5	F10-P1	127	0.665	2,405	39.5	3.20	1,915	190.3	95.2	2nd	579
	F10-P5	127	0.653	2,720	40.75	2.54	2,025	152.4	76.2	2nd	590
	F11-P3	240(193)	0.665	2,405	35.9	3.20	1,915	241	46.0	1st	262
	F11-P1	241(193)	0.66	2,405	36.0	3.18	1,738	335	64.0	1st	236
6	LS3-T1	127(85)	0.46	2,690	36	3.84	2,095	190	95	2nd	556

	Specimen	Longitudinal stiffener	Q_{ex} x 10^3	Q_{th} x 10^3	Q_{ex}/Q_{th}	Mp, req.	Mp, act
1	A-1	1	56.5	55.5	1.02	5.692×10^{3}	1.182×10^{4}
	A-2	1	57.5	56.8	1.01	7.630×10^{3}	1.183×10^{4}
	A-3	2	59.0	61.2	0.96	5.191×10^{3}	1.174×10^{4}
	A-4	1	63.0	63.0	1.00	1.271×10^{4}	1.168×10^{4}
	A-5	2	63.5	66.4	0.96	7.025×10^{3}	1.168×10^{4}
2	TG-1	0	15.54	14.09	1.10	1.364×10^{5}	2.931×10^{3}
	TG-1'	0	11.85	14.15	0.84 (0.97)*	1.364×10^{5}	3.167×10^{3}
	TG-2	0	16.3	16.98	0.96	1.364×10^{5}	1.454×10^{4}
	TG-2'	0	14.15	17.01	0.83 (0.90)*	1.364×10^{5}	1.466×10^{4}
	TG-3	0	19.4	19.32	1.00	1.364×10^{5}	3.863×10^{4}
	TG-3'	0	19.35	19.32	1.00 (1.00)*	1.364×10^{5}	3.858×10^{4}
	TG-4	0	22.3	21.86	1.02	1.364×10^{5}	5.816×10^{4}
	TG-4'	0	21.1	21.86	0.97 (1.00)*	1.364×10^{5}	5.799×10^{5}
	TG-5	0	31.47	31.78	0.99	1.364×10^{5}	1.583×10^{5}
	TG-5'	0	30.5	31.78	0.96 (0.98)*	1.364×10^{5}	1.580×10^{5}
3	G6-T1	0	52.5	50.6	1.03	1.005×10^{6}	8.004×10^{4}
	G6-T2	0	68.0	70.4	0.97	2.373×10^{5}	8.004×10^{4}
	G6-T3	0	80.4	81.0	0.99	4.038×10^{4}	8.004×10^{4}
	G7-T1	0	63.5	65.9	0.96	4.677×10^{5}	7.782×10^{4}
	G7-T2	0	65.8	65.9	1.00	4.677×10^{5}	7.782×10^{4}
	G8-T1	0	38.6	36.5	1.06	4.796×10^{6}	8.014×10^{4}
	G9-T1	0	21.8	21.4	1.02	4.349×10^{6}	8.096×10^{4}
	G9-T2	0	34.0	36.2	0.94	1.072×10^{6}	8.096×10^{4}
4	B	0	76.0	78.7	0.97	8.798×10^{5}	4.320×10^{4}
5	F10-P1	0	83.5	88.1	0.95	9.389×10^{5}	1.936×10^{5}
	F10-P5	0	86.2	92.8	0.93	7.303×10^{5}	1.331×10^{5}
	F11-P3	1	127.5	128.9	0.99	2.271×10^{6}	1.760×10^{5}
	F11-P1	1	111.9	105.5	1.06	4.472×10^{6}	1.582×10^{5}
6	LS3-T1	1	63.5	71.3	0.89	8.190×10^{5}	2.780×10^{5}

bl : Depth of main subpanel

C : Distance between plastic hinge and the nearest corner of panel

Mp,req.: Required plastic moment of desirable flange for given web

Mp,act : Existing plastic moment of flange

(1) Komatsu
(2) Skaloud
(3) Basler
(4) Konishi
(5) Patterson
(6) Cooper

* mean value of twin specemens

unit : cm, kg

Table 3 Comparison between experimental and theoretical ultimate load.

```
      REAL NU,KS,MU,MP,MS
      E=2.1*10.0**6
      NU=0.3
      PAI=3.141592
      DO 100 I=1,21
      READ(5,1000) B,B1,TW,SWY,BF,TF,SFY,A
 1000 FORMAT(8F8.0)
      READ(5,1001) KS,SK
 1001 FORMAT(2F8.0)
      ASP=A/B
      TWY=0.5*SWY
      WRITE(6,2000) B,TW,SWY,BF,TF,SFY,A
 2000 FORMAT(1H ,4H  B=F8.2,4H TW=F8.2,5H SWY=F8.2,4H BF=F8.2,4H TF=F8.2
     1,4H SF=F8.2,4H  A=F8.2)
      TCS=SK*PAI**2*E/12.0/(1.0-NU**2)*(TW/B1)**2
      IF(TCS-0.5*TWY) 20,20,21
   21 TCS=TWY*(1.0-3.0*(1.0-NU**2)/SK/PAI**2/E*TWY*(B1/TW)**2)
   20 CONTINUE
      TCR=KS*PAI**2*E/12.0/(1.0-NU**2)*(TW/B1)**2
      IF(TCR-0.5*TWY) 10,10,11
   11 TCR=TWY*(1.0-3.0*(1.0-NU**2)/KS/PAI**2/E*TWY*(B1/TW)**2)
   10 WRITE(6,2001) TCR,TCS
 2001 FORMAT(1H ,4HTCR=F8.2,13X,4HTCS=F8.2)
      MP =0.25*SFY*BF*TF**2
      C=(0.38+1.782*MP/SWY/B**2/TW)*0.5/(1.0+1.782*MP/SWY/B**2/TW)*A
      CA =C/A
      ALP=(A-C/2.0)/(A-C/3.0)*A
      II=1
   52 T  =0.10
      JJ=1
      BB=0.0
      STEP=0.01
      NC =1
    1 T  =T+STEP
      GO TO (2,3),II
    2 AA =SWY*(B*COS(2.0*T)-ALP*SIN(2.0*T))+2.0*TCR*(ALP*(COS(2.0*T)-COS
     1(4.0*T))-B*SIN(4.0*T))
      GO TO 4
    3 AA =MP-A**2/16.0*(SWY-2.0*TCR*SIN(2.0*T))*SIN(T)**2*TW
    4 CC =AA*BB
      IF(CC.LT.0.0) GO TO 5
      BB =AA
      NC =NC+1
      IF(NC.GT.100) GO TO 7
      GO TO 1
    5 T  =T-STEP
      JJ =JJ+1
      IF(JJ.EQ.3) GO TO 6
      STEP=STEP/10.0
      GO TO 1
    6 T  =T+0.5*STEP
    7 CONTINUE
      TH =T
      GO TO (18,19),II
   18 CONTINUE

   50 QU1=(SWY-2.0*TCR*SIN(2.0*TH))*SIN(TH)**2*TW
   51 ETB=(QU1*(A-C)-4.0*MP/C)/(A-C/3.0)
      IF(ETB) 12,12,13
   13 CONTINUE
      WRITE(6,2004)
 2004 FORMAT(1H ,11X,8H1ST MODE)
      Q  =0.5*(SWY-2.0*TCR*SIN(2.0*TH))*(B*SIN(2.0*TH)-ALP*(1.0-COS(2.0*
     1TH)))*TW
      Q  =Q+4.0*MP*ALP/C/(A-C)+TCR*B*TW
C     OUT PUT
   53 TUL=Q/B/TW
      MU =TUL/TCR
      TH=TH*180.0/PAI
      IF(SWY-4.0*TCR) 22,23,23
   22 X  =SWY/4.0/TCR
      TT =0.5*ATAN(X/SQRT(1.0-X**2))
      STM=(SWY-2.0*TCR*SIN(2.0*TT))
      PP    =A**2/16.0*STM*SIN(TT)**2*TW
      GO TO 60
   23 STM=SWY-2.0*TCR
      PP    =A**2/32.0*STM*TW
   60 CONTINUE
      WRITE(6,2002) MP,PP,ALP,QU1,ETB
 2002 FORMAT(1H ,3HMP=E14.7,8H MP,REQ=E14.7,4X,4HALP=E15.7,6X,4HQU1=E15.
     17,4X,4HETB=E15.7)
      WRITE(6,2005) Q,C,TH,TUL,MU
 2005 FORMAT(1H ,2HQ=E15.7,5X,2HC=E15.7,5X,3HTH=E15.7,5X,5HTULT=E15.7,5X
```

```
     1,3HMU=F15.7///)
 78   WRITE(6,2003)
 79 2003 FORMAT(///)
 80   GO TO 56
 81  12 IF(SWY-4.0*TCR) 14,15,15
 82  14 X  =SWY/4.0/TCR
 83   TH =0.5*ATAN(X/SQRT(1.0-X**2))
 84   Q  =(0.5*SWY*SIN(2.0*TH)+TCR*(1.0-SIN(2.0*TH)**2))*B*TW
 85   GO TO 54
 86  15 TH =PAI/4.0
 87   Q  =TWY*B*TW+4.0*MP/A
 88  54 QU1=(SWY-2.0*TCR*SIN(2.0*TH))*SIN(TH)**2*TW
 89   C  =0.5*A
 90   ETB=(QU1*(A-C)-4.0*MP/C)/(A-C/3.0)
 91   IF(ETB) 16,16,17
 92  16 IF(TH.EQ.PAI/4.0) GO TO 55
 93   WRITE(6,2006)
 94 2006 FORMAT(1H ,11X,8H3RD MODE)
 95   GO TO 53
 96  55 WRITE(6,2007)
 97 2007 FORMAT(1H ,11X,8H4TH MODE)
 98   GO TO 53
 99  17 II=2
100   GO TO 52
101  19 Q  =(0.5*SWY*SIN(2.0*TH)+TCR*(1.0-SIN(2.0*TH)**2))*B*TW
102   WRITE(6,2008)
103 2008 FORMAT(1H ,11X,8H2ND MODE)
104   GO TO 53

105  56 CONTINUE
106 100 CONTINUE
107   STOP
108   END
```

Leere Seite
Blank page
Page vide

Studies and Tests on Slender Plate Girders without Stiffeners
Shear Strength and Local Web Crippling

Etudes et essais sur les poutres à âme mince sans raidisseurs
Résistance au cisaillement et voilement de l'âme sous charges concentrées

Untersuchungen und Versuche an dünnwandigen Blechträgern
Schubfestigkeit und Stehblechbeulen unter Einzellasten

ALLAN BERGFELT
Professor
Chalmers University of Technology
Göteborg, Sweden

I. Shear test results

Summary of theories

For girders with normal web imperfections the theoretical computation of linear elastic instability does not give the real bearing capacity. For plate girders with web stiffeners better results are obtained with Wagner's [1] theory of tension fields as adjusted by Basler and Thürlimann [2] and still better as improved by Rockey and Skaloud [3].

These theories are not applicable to girders without web stiffeners or with stiffeners only at the supports. For such girders the use of Karman 's [4] equation of finite plate theory gives better results. An early approximate solution to this equation was given by Bergman [5]. During the long period of time after the publication of this paper not more than a few tests on very slender girders with end stiffeners only have been reported.

Test results on girders without intermediate web stiffeners

Unpublished reports on test results have been given by C.A.Granholm 1960-62 [6,7] and a summary has been published [8]. Further results are included in tests published by Bergfelt and Hövik [9].

The results obtained in these tests are plotted in the diagrams fig.3 and 4 (filled dots). In both diagrams comparison curves computed according to Bergman's theory [5] are shown. In fig.3 the directly computed mean τ-values are marked [10] but in fig.4 these values are reduced in order to correspond to an infinite long girder with a yield stress $\sigma_Y = 2200$ kp/cm^2, which yield stress was Bergman's base value.

As a further comparison also some values from tests on slender girders with web stiffeners are marked ($\alpha = a/h > 2$ and $h/d > 150$). Even some tests with h/d equal to 100, 120 and 140 are included. This is motivated because in these particular

cases σ_Y in the web (3800 kp/cm^2) or in the flanges (5600 kp/cm^2) was very high [11] resp. [12] and these girders therefore might show a different behaviour [11]. The characteristic values for the test are recorded in Table 1.

The comparison curves in fig. 3 and the characteristic curve in fig. 4 are based on the diagrams numbered VII 2 and VII 3 in reference [5]. These diagrams are here given in a somewhat revised form as fig. 1 and fig. 2.

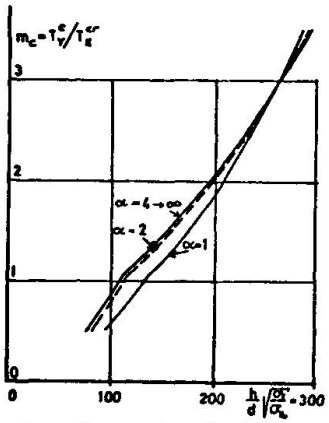

Fig. 1

Collapse shear force at web yield stress σ_Y divided by critical shear force at ideal buckling, $m_c = T_T^c / T_E^{cr}$ as function of slenderness ratios h/d made comparable by multiplying with $\sqrt{\sigma_Y/\sigma_0}$. Here σ_0 is chosen to 2200 kp/cm^2. Aspect ratios one and upwards. [5]

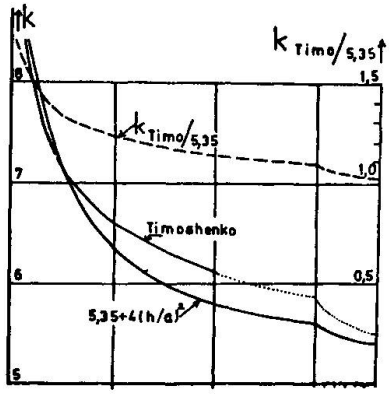

Fig. 2

Diagram over buckling coefficient k in $\tau^{cr} = k\pi^2 D/dh^2$ for different aspect ratios α of plates with hinged edges. Values calculated by S Timoshenko and the approximate curve 5,35 + 4 (h/a)^2. [5]
The right vertical scale measures the factor $k_{Timoshenko}/5,35$.

Ref.	No	h/d	α	σ_Y	t	b·t	h·d	σ	τ	$\frac{h}{d}\sqrt{\frac{\sigma_Y}{2200}}$	m_c	$m_{c\sigma}$	k_α/k	τ_{corr}
[9]	1:1	300	12	>2600	7,3	175 · 6	600 · 2	1640	467	>325	3,60	4,13	1,02	400
Bergfelt	2:2	300	2,4	(2600)	7,3	175 · 6	600 · 2	2220	635	(325)	3,62	4,16	1,18	470
-Hövik	3:1	197	17	>2600	9,8	200 · 8	590 · 3	2750	587	>215	2,04	2,25	1,01	525
	3:5	"	"	"	"	"	"	1865	620	"	"	"	"	554
	3:6	"	"	"	"	"	"	940	650	"	"	"	"	580
[5]	A2	286	2,0	2820		300 · 30	1000 · 3,5	-	655	324	3,42	4,20	1,23	437
Bergman	A6	218	3,4	2280		300 · 20	700 · 3,2	-	675	221	2,28	2,30	1,12	595
	A5	175	3,4	3030		300 · 20	700 · 4,0	-	870	206	1,75	2,16	1,12	630
[6]	E53	270	3,4(1,7)	2800	4,0	130 · 5,4	590 · 2,2	2290	470	305	3,12	3,7	1,12	353
Granholm	E54	"	3,4(1,7)	"	4,0	"	"	2350	480	"	"	"	"	362
	C	195	<7	2800	5,9		780 · 4	2820	757	220	2,00	2,35	1,04	621
	E32	187	13,4	2800	8,0	180 · 9	596 · 3,1	2240	712	210	1,92	2,21	1,02	607
	E33	"	13,4	"	8,0	"	"	2320	735	"	"	"	"	627
	E42	187	3,4	2800	8,0	200 · 10	600 · 3,1	2440	900	210	1,90	2,18	1,12	700
[2]	G8-T1	254	3,0	2700					612	281	2,84	3,31	1,14	461
Basler-Thürlim.	E1-T1	131	3,0	2940					1012	151	1,25	1,46	1,14	760
[11]	G7	119	2,6	3800	6,0	282 · 22	1080 · 9,1		1300	156	1,10	1,50	1,17	815
Nishino-	G8	121	2,6	3800	"	221 · 22	1080 · 9,1		1150	159	1,12	1,54		715
Okumura	G5	100	2,6	3800	5,5	291 · 22	899 · 9,0		1510	131	0,84	1,22	1,17	890
	G6	101	2,6	3800	"	212 · 22	900 · 8,9		1320	133	0,85	1,24		775
[12] Carskad.	C-AC2	143	5,5	2150	5,8	94 · 9,7	454 · 3,2	≈5600	845	141	1,39	1,37	1,06	810

Table 1

The test results for long girders with end stiffeners only are all lying close to the characteristic curve in fig. 4. This fact applies to the measuring values E 32, E 33 in ref. [6] as well as the values 1:1, 3:1, 3:5, 3:6 in ref. [9] marked with filled dots, compare Table 1. Some of these test results are based not only on pure shear and bending of the web, but also local web crippling under a point load and flange buckling are acting in a composite way. When σ increased from 940 to 2750 kp/cm^2 τ reduced 10 % [9].

Decimal points are marked with commas, e.g. 1,234 and 0,234 instead of 1.234 and .234. Multiplication is generally marked with a point · but in case there can be risk for mistakes the sign x is used.

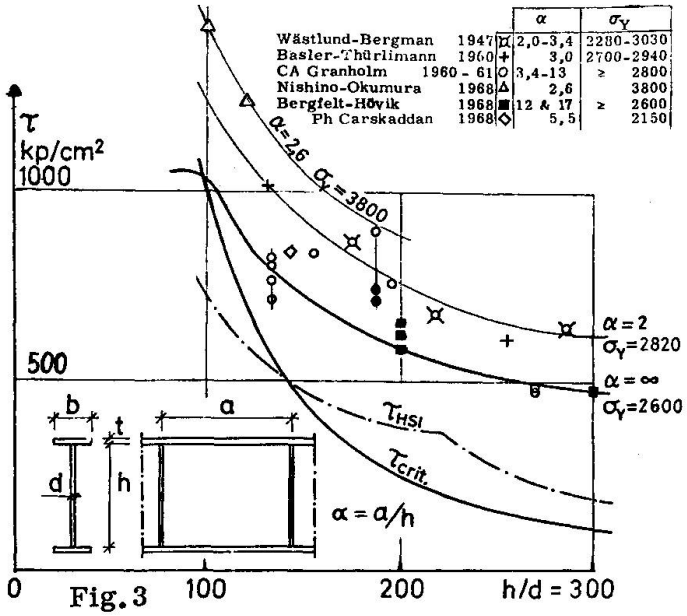

Fig. 3

Nominal shear stresses as function of the web slenderness ratio h/d. Measured test values for ultimate bearing capacity compared with $\tau_{critical}$ for elastic buckling, with allowable stresses according to provisional Swedish specifications (HSI) and with yield stresses computed according to Bergman [Ref. 2 fig. VII 2].
(The figure is copied from [10].

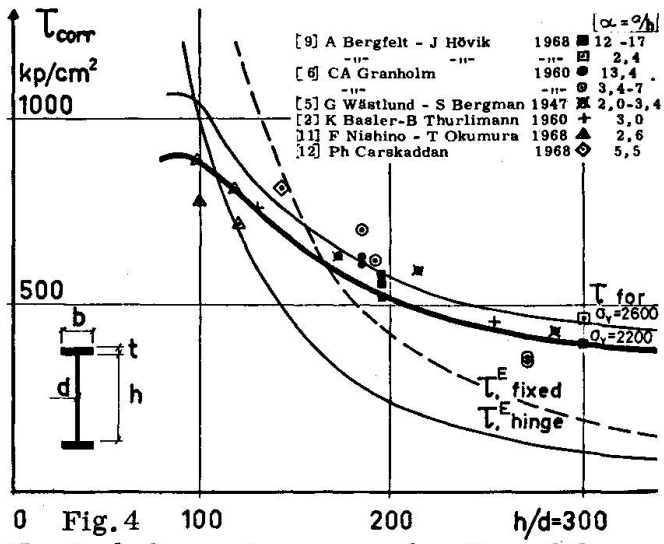

Fig. 4

Nominal shear stresses as function of the web slenderness ratio h/d.
The points computed from the test values for ultimate bearing capacity, see Table 1, are compared with Bergman's characteristic curve for $\sigma_{Y,web} = 2200$ kp/cm^2. Comparison also between characteristic curve for $\sigma_{Y,web} = 2600$ and curves of elastic buckling with a hinged web (E_{hinge}) and a restrained web (E_{fixed}).

1000 kp/cm^2 (kiloponds/sq. cm) = 1 Mp/cm^2 = 1 ton/cm^2 =
= 14,2 ksi (kilopounds/sq. in) ≈ 100 MN/m^2 (Mega Newton/sq. m) = 100 N/mm^2

The comparison results for girders with lower α-values are also lying relatively close. This might be a mere chance as the flange dimensions of the test girders were not exceptional. Most of these test results are a little too high compared to the characteristic curve indicating the neglect of consideration to the influence of flange stiffness, which is large for small α-values. Some of the results are to the contrary under the curve. For these it is pointed out in the reports that the collapse was caused by flange buckling and not by web buckling [11] or that the end stiffeners might have been insufficient [6].

For girders with end stiffeners only the influence of varying flange areas is not very important. For lower values of α the influence of varying flange areas is great as may be seen from the diagrams given by Rockey and Skaloud [3] or the computation method given in [13].

On the diagram in fig. 4 also buckling curves are shown according to linear, small-deflection theory, on the assumption of the web being hinged to the flange (k = 5,35) and of full restraint (k = 8,98). To get a better visual picture of the greatest real load in comparison with the linear theory a curve according to Bergman denoted "τ for $\sigma_Y = 2600$" is shown. The yield limits of all test girders except two were greater than 2600 kp/cm^2.

The real bearing capacity for slender webs, h/d > 150, is larger or even far larger than the linear elastic theory should give even in case of the favourable assumption of a fully restrained web. This holds true even for great initial lateral deformations of the web, e.g. h/100 or $5 \cdot 10^{-5}\, h^2/d$ (c.f. test 3:2 in [10] where δ_{init} was h/50).

II. Web Crippling

Presentation and earlier tests

Under great concentrated loads attacking on the upper flange of a plate girder it is necessary to stiffen the girder with web stiffeners. In case of small loads such as from closely spaced purlins no stiffeners are usually necessary except at the supports. With increasing web slenderness ratios it may be questioned if intermediate stiffeners are necessary or not.

Normally the demand for stiffeners is controlled by checking the vertical web stress under the load. An approximate method is to consider the load distribution length to be equal to the width of the purlin increased by the thickness of the flange and the height of the fillet welds. Another method is to distribute the load considering the flange as an elastic beam resting on elastic springs [14]. A third method is naturally to compute stresses and strains without any simplified models and taking into account the real shape of the girder. This method gives an increased amount of computing.

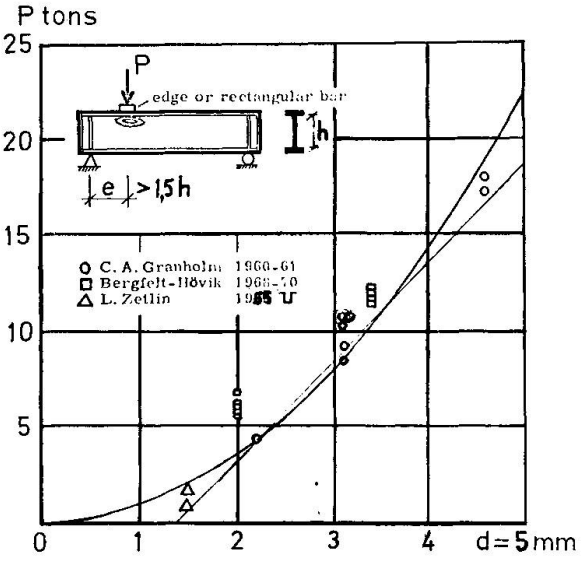

Fig. 5
The dependency of collapse load P on web thickness d , as observed by different authors. (Zetlin´s tests were performed on cold-formed ⌐⌐-shaped section.)
The figure is copied from [10].

Besides the determination of the vertical web stresses the risk of web buckling has to be investigated. A great many theoretical investigations of this phenomenia have been done [e.g.15,16]. For girders with slender webs (thickness 2 to 6 mm and h/d varying from 150 to 300) it has been shown [7] that approximate cripple failure loads are given by the simple empirical formula $P = 0,9\ d^2$, where P is the cripple load in tons and d is measured in mm. Naturally also the modulus of elasticities and the yield stresses for the flange and web material influence the static behaviour as well as the dimensions of the flanges.

In a paper the author and his co-worker J. Hövik [10] have compared tests done by us with earlier tests and the results are in support of the simplified formula according to [7], see fig. 5. In an earlier paper [9] it is suggested that the dominating importance of the web thickness d over the influence of the flange dimensions may qualitatively be explained by the theory of beam on elastic foundations in taking into account some part of the web in the computation of the stiffness of the "flange beam".

New tests on web crippling in girders without intermediate stiffeners

Despite the accurateness of the empirical curve as demonstrated by the measuring points in fig. 5 the dependency on yield strength and flange dimensions has to be taken

into account in case of deviations from the mean yield strength and in case of varying ratios of flange to web areas.

Therefore a test series has been executed with constant web dimensions 3 x 700 mm and varying flange areas from 6 x 150 mm to 15 x 300 mm.

Under each point load a knife-edge or a plate of width 100 mm was placed to transfer the load. Once the knife-edge was applied first and in the next case the plate. With this procedure the load was not increased to collapse, but the loading was interrupted at successive yielding (if possible). The yield was considered successive when the deformation at a loading stage amounted to at least 0,05 mm during the first five minutes of the stage and when it continued after 15 minutes. During earlier tests [10] this method has been considered satisfactory.

At two points on the girder, D_u and H_u repeated loading cycles were applied. For all loading cycles except one 80% of the static collapse load was used as an upper bound.

The tests are summarized in Table 2 and dimensions in Table 3. Here the values of the yield strength in tension and the results of plate bending tests of the flange material are also given. For the flanges the plate bending tests are converted into the moment at first yield and into the fully plastic moment.

Point	Span m	Flange plate materials: Nominal dim. mm	σ_Y kp/cm²	M_Y cm·kp	M_{pl} cm·kp	Knife-edge load: No	Def. mm	P tons	10 cm bar load: No	Def. mm	P tons	δ_{init} mm	Strain
B	2,4	6 x 150	3 540	3 090	4 990	2	0,8	9,7[c]	1	0,7	10,8	4,4	ϵ
B_A	1,4					1	1,6	9,7	-	-	-	0,7	
C	2,4	8 x 200	2 400	5 830	8 450	1	0,8	11,2	2	0,9	12,4	4,5	
F	2,4			5 730	8 290	2	1,3	10,3	1	0,8	10,3	9,5	
C_u	2,4	10 x 250	2 480	14 700	16 000	2	0,9	12,3	1	0,4	13,7	5,2	
G_u	2,4			14 600	15 800	1	0,5	12,3	2	0,8	13,4	4,8	
D	2,4	12 x 250	2 370	23 500	30 100	2	1,0	11,9	1	0,6	10,1	7,0	
G	2,4			23 400	29 900	1	0,6	13,8	2	0,8	14,2	3,6	
E	2,4	15 x 300	3 110	43 300	58 400	2	0,8	15,6[c]	1	0,7	15,8	4,5	
H	2,4			43 400	58 500	1	0,9	15,4[c]	-	-	-	-	
H	2,4					1	1,3	15,3	2	1,7	16,1	3,1	ϵ
B_u	9,4	10 x 250	2 480	14 500	15 700	2	2,3	12,0	1	2,1	13,1	7,7	
E_u	9,4			14 600	15 800	1	0,4	10,4	2	0,5	12,0	10,5	ϵ
H_u	2,4	10 x 250	2 480	14 800	16 000	1	(0,7)	(9,8)	2	(1,7)	(10,9)	2,4	ϵ
D_u	9,4			14 700	16 000	1	(1,7)	(9,2)*	2	(1,9)	(10,0)	0,8	ϵ
Web		3 x 700	3 320	78,9	89,3	M_Y and M_{pl} for web in kpcm/cm							

c = collapse, local straightening before test

δ_{init} = initial lateral deformations ϵ = strain measurings

( ) = load applied in 100 loading cycles (each cycle 11 min) and deflection for these loads.

* = for this loading case also 100 loading cycles to 10,2 tons (90% of the static collapse load) were made. The deflection increased from 2,60 mm in the first cycle to 2,71 mm in the last cycle.

Table 2

In the neighbourhood of each load transfer the vertical deformation of the loaded flange was measured as the displacement in relation to the other flange (in 1/1000 mm), see fig. 8. The lateral deflections of the web were also measured.

The vertical deflection of the upper flange in relation to the lower flange, centrally under the point of load attack and corresponding to 3/4 P is given in Table 2. For repeated loads corresponding to (P). This proportion of the final collapse load P was chosen because the deformation increased uniformly up to this stage. Beyond this stage the increase was discontinous owing to yield and snap buckling (fig. 10).

In some tests the strains were measured by electric strain gages. Here at most 68 gages were used, some of them united in rosettes. Every measuring point was double, symmetrically placed on each side of the web, fig. 9. The readings were collected with recorders.

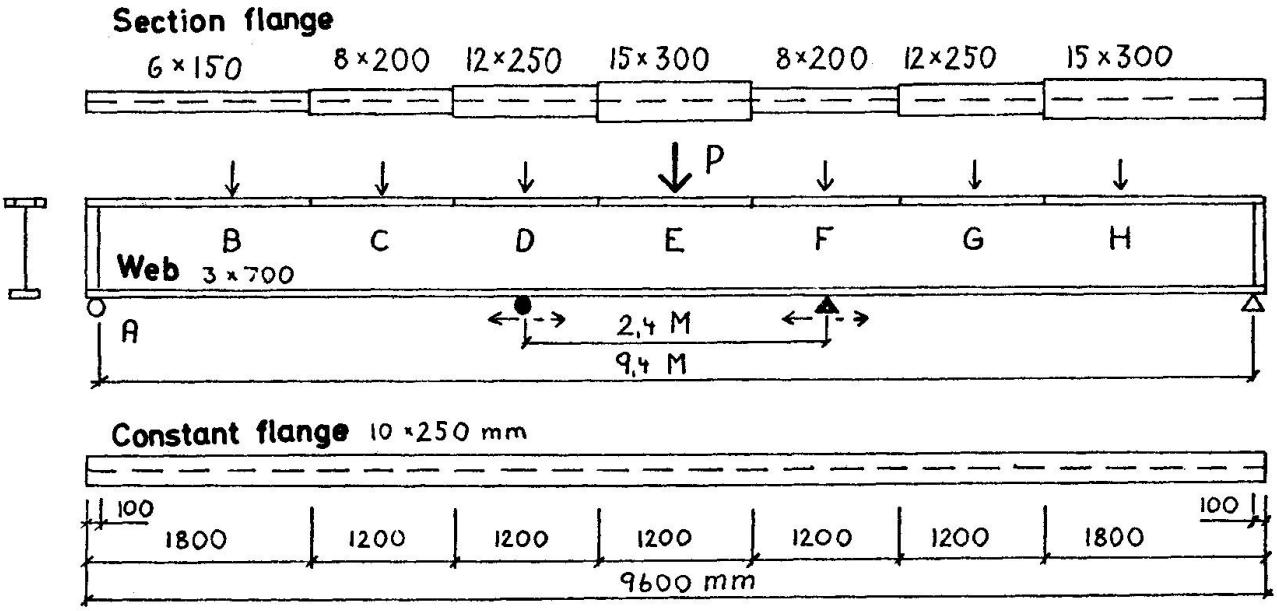

Fig. 6 Test girder

The tests were done on a girder with one flange of dimension 10 x 250 mm and the other flange welded together of sections 6 x 150, 8 x 200, 12 x 250 and 15 x 300 mm. The sections were 1,2 m long and the end sections 1,8 m. The loads were transmitted through various points on the flange of constant cross section and through the midpoints of the sections of the other flange (except in the case of end sections, see fig. 6).

The load was normally introduced by a jack with fixed attachment. In some cases the head of the jack was hinged. In the design of the arrangement of load transmittance the hinge was situated somewhat higher than the upper flange (about 0,1 h). This means that even in the case of a hinged jack the web is somewhat restrained by the flange. During most tests the free span between supports amounted to 2,4 m. Even the ends of the girder were supported.

The point loads have mainly a local influence on the flange, from which follows that the influence of the change in flange area far from the loading point is small as much as the web is continous. A check of this assumption is obtained by the results from the loading on the flange of constant area, which well accommodate the results on the other flange. That the result even for the thickest flange section 15 x 300 mm, is in detail correct, is not safeguarded.

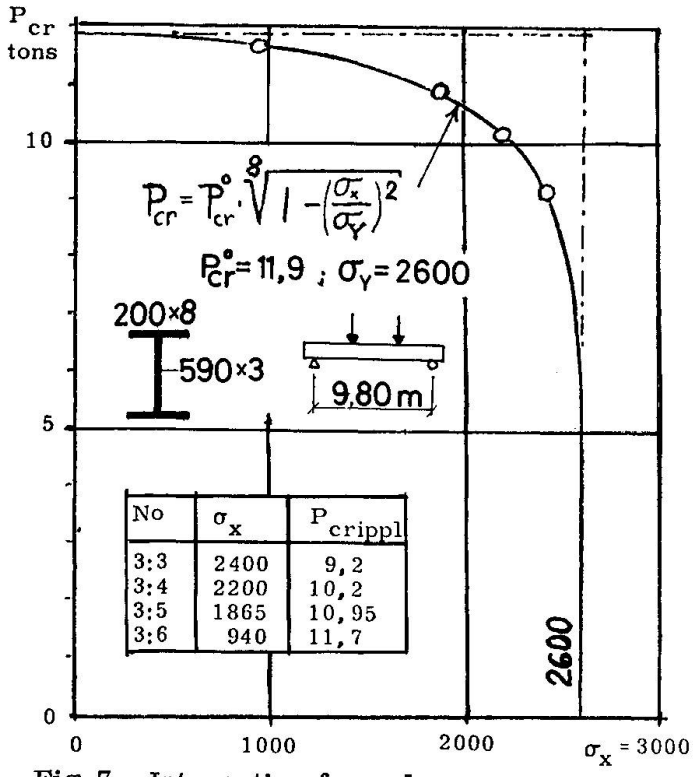

Fig. 7 Interaction formula $P_{cr} = P^{o}_{cr} [1-(\sigma/\sigma_Y)^2]^{1/8}$ from [10] compared with test values from [9].

For the chosen span width the compressive bending stresses in the flange during web crippling have amounted to between 200 and 600 kp/cm^2. (With some correction for the end supports). Earlier investigations show that for so small stresses the bending stress has a very small influence on the cripple load (cf fig. 7). Also the results in ref. [17] illustrate the small interaction, but refer to tests with loading lengths that are longer compared to the beam depth and with a relatively thick web, h/d = 40.

Test results

Certain test results as described above are aummarized in Table 2 and 3 as well as in fig. 10. Furthermore some results from strain gage measurements for the loading case B:2 are in detail shown in fig. 13.

The thickness of the web plate was measured in 220 points distributed over the whole length of the girder with an increasing number of measuring points at the points of load attack. The thickness varied between 3,19 and 3,33 mm with the mean value 3,26 ± 0,04 mm.

The initial shape of the girder was measured under each point of load attack before loading. Because of residual deformations after previous loadings etc. the initial position in some cases changed somewhat. The greatest initial lateral deflections are given in Table 2. The lateral deflections during the test were measured by a recording gauge (0,001 mm) placed 5 cm under the loaded flange. Several other points were measured from a special vertical reference plane and in case of residual buckles they were levelled in up to 400 points.

Discussion

Introductorily it was stated that the main factors caused by point loads regarded stresses and buckling. The different factors also influence each other and the risk of combined action is probable. Therefore a more complete survey of the different causes may be done as follows.

A. Web stresses under the points of load attack.

B. Web buckling under concentrated loads.

C. Web crippling, defined here as local cripples under a concentrated load, which may develop under high compressive stresses in combined action with bending stresses and local buckling.

D. The influence of A, B and C on the bearing capacity of the girder.

Fig. 8 Dial gauges for vertical displacement of the loaded flange and for lateral deflection at one point of the web.

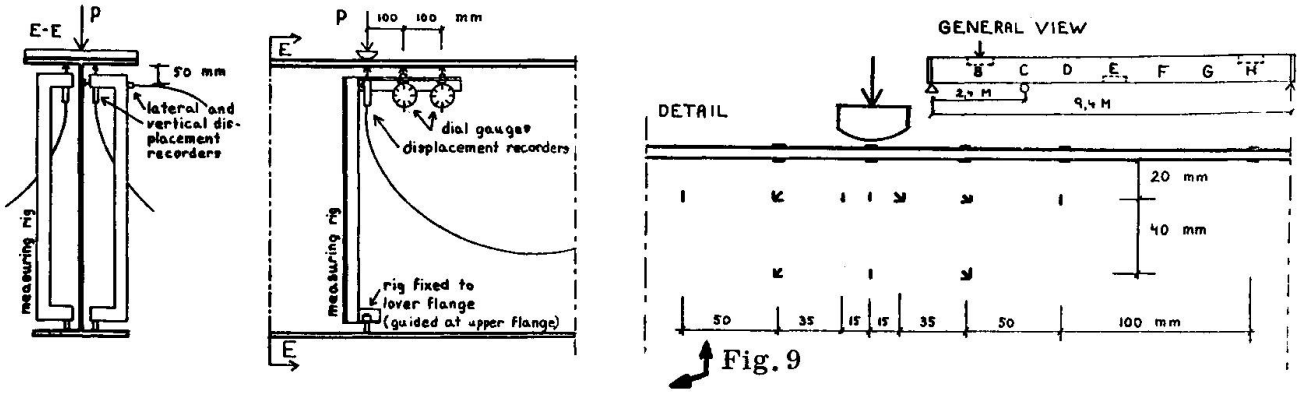

Fig. 9

Electric strain gages for test B. Similar arrangements for tests H and E_u. Strain gages were placed also on the unloaded flange. In test E_u more gages were of rosette type. Under the knife-edge there was a plate of 1,0 mm with recesses for the gages and leads.

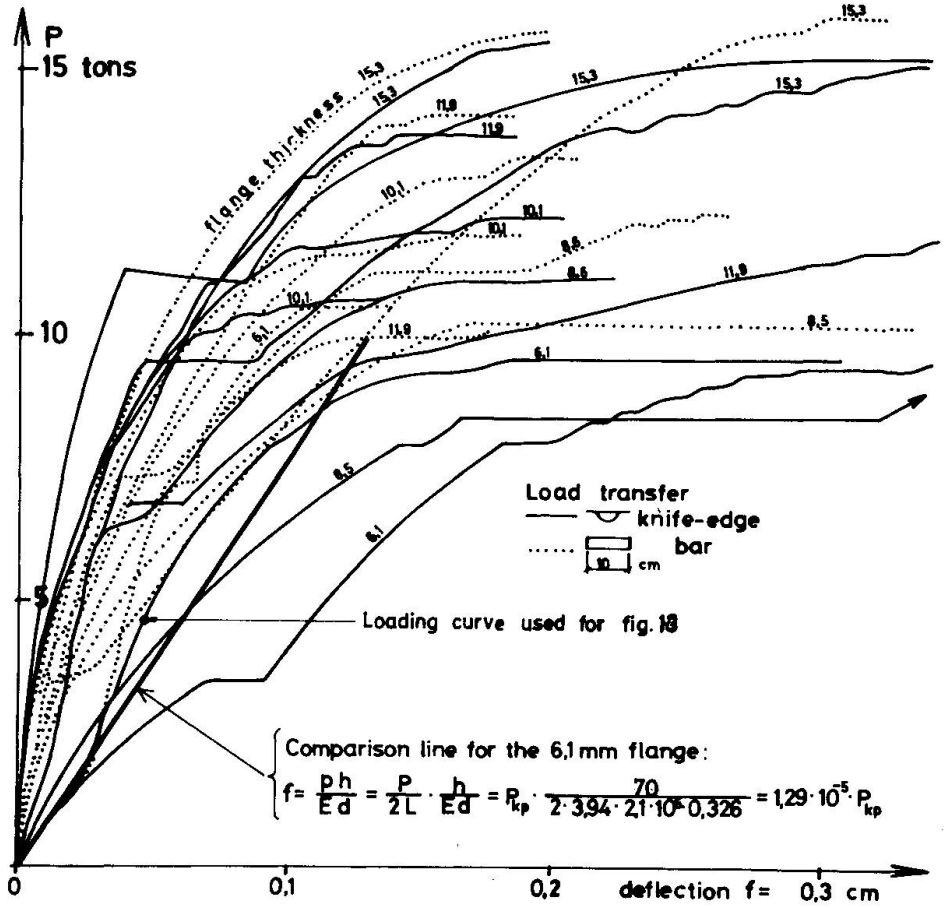

Fig. 10 Vertical deflection of the loaded flange directly under the concentrated load

	Flange mm	I_{fl} cm^4	L_o cm	I_T cm^4	$e_ö$ cm	L_{To} cm	L_T cm *
B	6,1 x 151	0,284	3,94	29,8	0,98	12,6	26,6
C	8,5 x 200	1,025	5,45	34,3	0,83	13,1	27,7
C	10,1 x 250	2,08	6,50	37,3	0,80	13,3	28,4
D	11,9 x 253	3,56	7,42	41,0	0,85	13,7	29,1
E	15,3 x 302	9,01	9,35	49,7	0,94	14,4	30,6

Table 3
Dimensions and elastic lengths L.

* For δ_o = h/100 = 7 mm
For δ_o = h/50, L_T is to be multiplied with 1,4.

A. Compressive web stresses under the point load is a factor that limits the load.

a. - Computing stresses without using a simplified theory is a difficult task for a beam with such a slender web as used here. Even small lateral deflections result in a behaviour that differs very much from case to case. Some guidance may, however, be found in treaties on solid beams as ref. [18]. In this preliminary report of the actual tests only approximate methods are used.

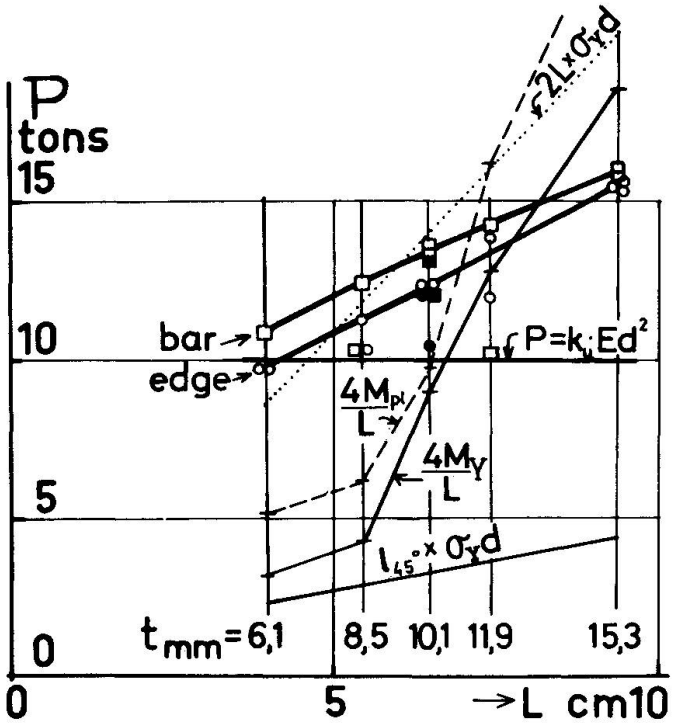

Fig. 11 Measured values of $P_{cripple}$ compared with values calculated under different assumptions. σ_Y, M_Y and M_{pl} from table 2.

b - Assuming a load distribution at an angle of 45° through the flange to the web the load is assumed limited by yield inside this region. The corresponding load is marked on fig. 11. No consideration is taken to combined action. The load calculated in this way $P = \sigma_y \cdot \ell_{45°} \cdot d$ is far below the greatest observed load (24 to 28% of it only). Even in case the yield stress is substituted by the compressive strength, the real loads by far surpass the calculated ones.

c. - For a beam on elastic foundations the distribution of the reactions, moments, etc. is given as a function of the "elastic length" L. The application to I-girders is given in [14] and a summary of the different function diagrams of interest is found in an "Appendix" to [10].

Elastic length $L = \sqrt[4]{4EI/Cd}$. Maximum web stress under the point load $\sigma = P/2Ld$. Maximum flange moment $M = PL/4$.

The moment of inertia I used in the computation of the compressive web stress is assumed to be equal to that of the flange plate $I = bt^3/12$. As to the computation of the flange bending stress and the web buckling load this value of the moment of inertia has been used as well as the resulting values when a part $(20 \cdot d)$ of the web is supposed to be included thus considering the elastic beam as a T-section*).

The spring constant C corresponding to the web support of the flange was computed according to two different assumptions. On one hand the web has been assumed to be plane and its lateral deflection has been neglected. On the other hand it has been assumed that the vertical deformation increases **) owing to an initial lateral deflection of the web with pitch h/100 (or about $5 \cdot 10^{-5} \cdot h^2/d$), which according to the measurements was a proper value.

On fig. 11 the load corresponding to maximum stress in the web directly under the point load is marked when this stress equals the yield limit e.g. $P = \sigma_Y \cdot 2Ld$. As seen the assumption that the flange plate only is load-distributing gives computed loads almost equal to or greater than the observed ones.

*) and **) see next page.

The flange has to take up the bending moment corresponding to the applied load distribution, however. On fig.11 the load corresponding to first yield and fully plastic moment is marked, that is $P = 4\ M/L$ where M is given in Table 2.

It is seen that the thinner flanges do not have sufficient bending stiffness and thus should not e.g. for the flange dimensions 6 x 150 mm carry more than 3 to 5 tons. Notwithstanding this fact the girder is able to support a maximum load of about 9,7 tons.

The computations of the collapse load illustrated in fig.12 explains this. At $P =$ $= 3$ tons the flange moment under the point load is $M = PL/4 = 3 \cdot 3,94/4 =$ $= 2,95$ tons x cm (tcm), shortly under the moment at first yield 3,09 (Table 2), where flow takes place in a small region in the outermost parts of the flange plate. With increasing load a certain strain redistribution takes place, but not until the moment for $P = 5$ tons equals about 4,91 tcm the bearing capacity of the flange is nearly exhausted. The moment then approximately equals the plastic moment 4,99 t according to Table 2. The maximum web stress is $\sigma = P/2\,Ld = 5000/2 \cdot 3,94 \cdot$ $\cdot\ 0,326 = 1950$ kp/cm^2. On fig.12 these extreme values are marked as well as moment and stress in the neighbourhood of the point of load attack computed according to the "theory of beams on elastic foundations" (from Appendix in [10].

Above $P = 5$ tons the flange functions as hinged under the point load. For an increase to $P = 7$ tons the flange functions as a hinged beam loaded with 2 tons or as two semiinfinite beams loaded each with a point load of 1 ton at the end. The increment in moment obtains its maximum value $M = 1/2 \times 2 \cdot L \cdot 0,3224 = 1,27$ tcm at a distance $\pi/4 \times L = \pi/4 \times 3,94 = 3,1$ cm from the point load.

The increment in web stress obtains the maximum value $\sigma = 1/2 \times 2000 \cdot 2/3,94 \cdot$ $\cdot\ 0,326 = 1560$ kp/cm^2. The resulting stress in the critical point is thus 1950 + 1560 =

---

*)
Different theories give values from 15 to 40 · d. From the observed folding deformations and strains in the tested web the value 20 · d is chosen here, but of course it ought to be dependent on the dimensions of the flange too.

**)
The compression under load p per unit length is for an initially plane web $f =$ $= ph/Ed$ and the spring constant is $Cd = Ed/h$. Considering flange stiffnes only L is equal to $L = \sqrt[4]{bt^3/3 \times h/d}$.

The initial deflection δ_o of a hinged strut of length ℓ causes an additional shortening $\Delta f = p \cdot \delta_o^2\ \ell/2\ EI$ due to small increase in lateral deflections. The measurements of the initial web deflections and an evaluation of flange restraint have motivated that the web as to bending may be considered as a plate hinged at two edges at a distance 0,7 h apart. The total web shortening in the case of initial deformations therefore is

$$f_{tot} = f + \Delta f = \frac{ph}{Ed}\,(1 + 4,2 \cdot \delta^2/d^2)$$

The spring constant is correspondingly diminished.

The load distribution is over a short length only. This implies that the computation as to the web behaviour as single-acting springs gives rise to great errors due to shear and plate action.

$= 3570$ kp/cm^2 and therefore it is only locally somewhat over the yield stress $\sigma_Y = 3320$ kp/cm^2 according to the fig. For further increments of load the web pressure can not increase in the region where σ_Y is surpassed.

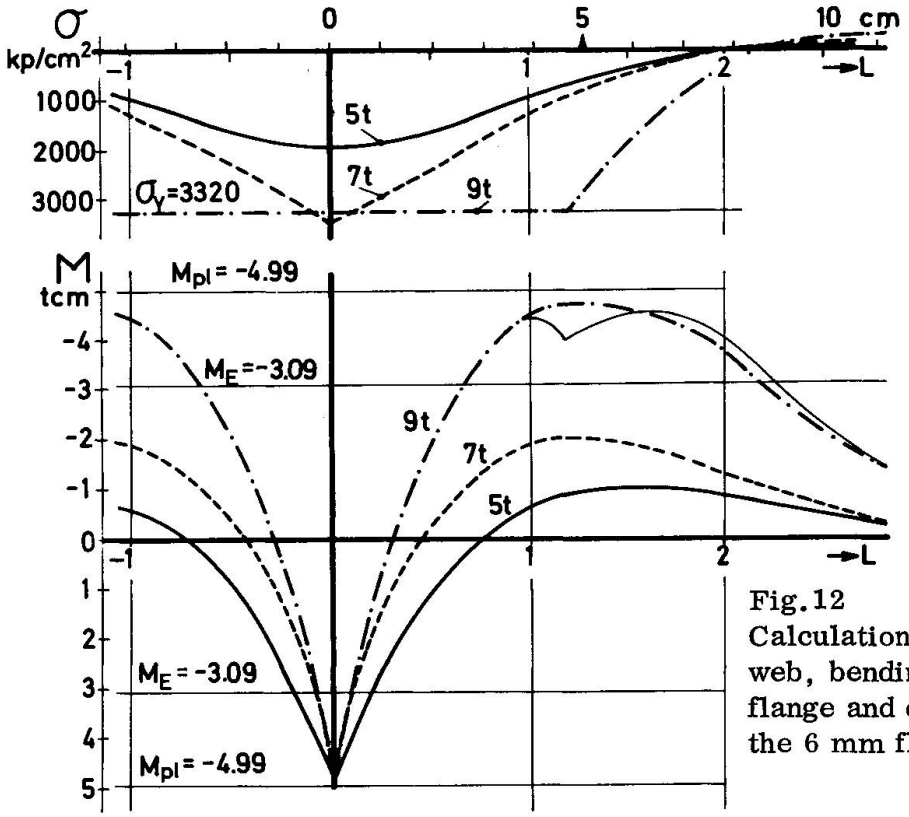

Fig. 12
Calculation of stresses in the web, bending moment in the flange and crippling load for the 6 mm flange.

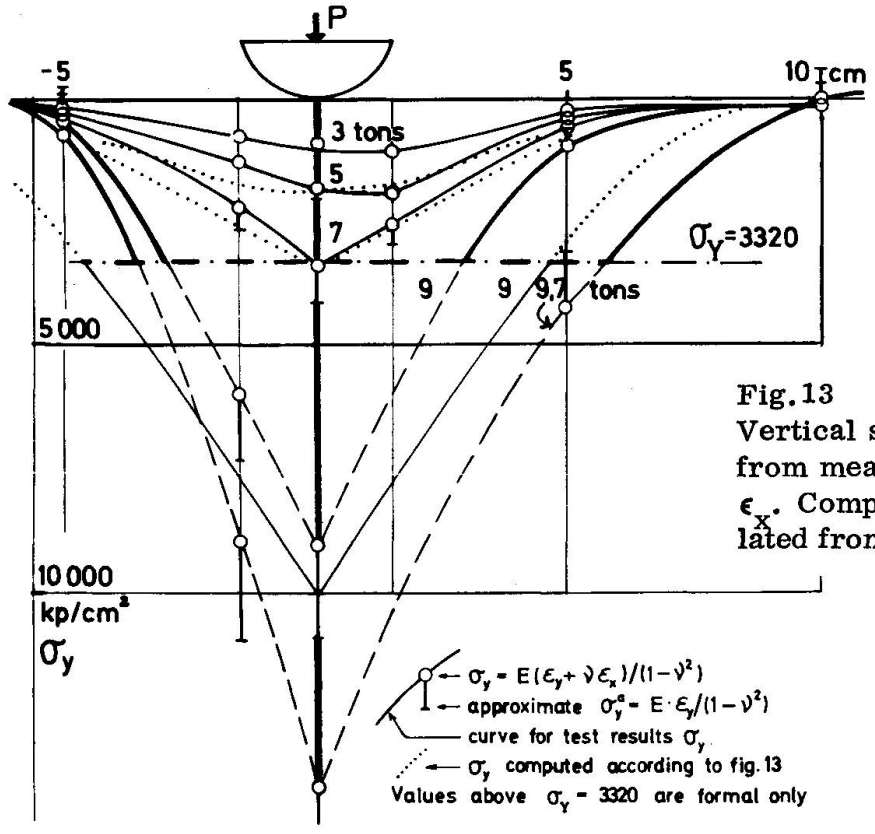

Fig. 13
Vertical stresses σ_y calculated from measured strains ϵ_y and ϵ_x. Comparison with σ_y calculated from fig. 12.

By a load increment from 7 to 9 tons the flange functions as two semiinfinite beams loaded with 1 ton at the ends and with the reactive pressure near the ends equal to the difference between σ_Y and the earlier existing stress, while the pressure further away is the same as for a beam on elastic springs. With dividing points situated at 4,7 cm from the point load the moment there is 2,0 tcm and the stress $\sigma = \sigma_5 + \sigma_{5-7} + \sigma_{7-9} = 800 + 200 + 2300 = 3300$ kp/cm^2 or approximately equal to σ_Y. The assumption of a direct change at the dividing points makes a small approximation of the calculated moments near the dividing points necessary as done on fig.12.

The moment diagram shows that the flange moment is approximately 4,7 tcm at about 4,7 cm from the point load. As the yield moment is $M_{pl} = 4,99$ tcm the load can only be increased somewhat over P = 9 tons before the bearing capacity fails if strain hardening is neglected. The real collapse load was 9,7 tons. On fig.13 the vertical stresses of test B2 is shown for different load stages. Here also the calculated stresses are shown. As seen the agreeement between the simplified theory and the experimental values are very good both regarding the maximum strain and the shape of the curves.

In fig.14 results from computations of idealized I-girders with small flange thicknesses are shown. In the same diagram the buckling load from the following section B is shown. The measured test values for knife-edge load are also plotted. It is seen that for girders with flanges thinner than about 2 d computations according to the "theory of beams on elastic foundation" limit the concentrated loads.

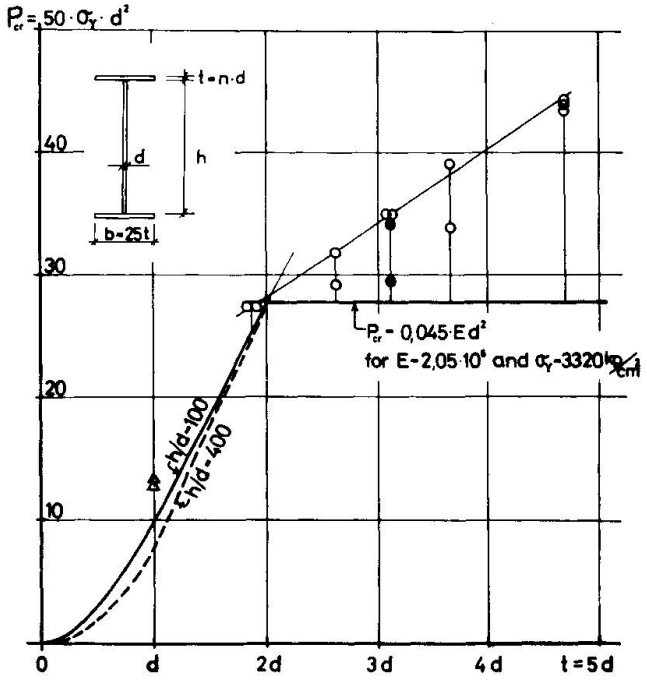

Fig.14 b → Idealized dependence on δ_{init} of the lateral deflection and of P_{cr}.

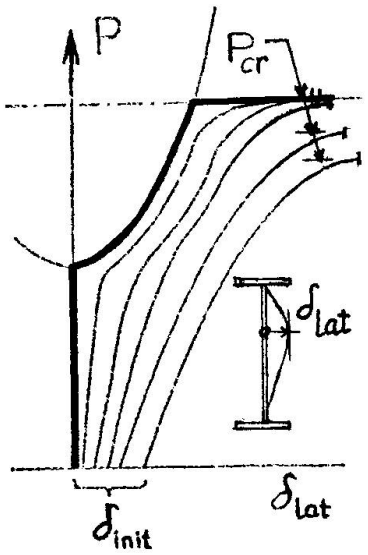

Fig.14 $P_{cripple}$ calculated for idealized girders with b = 25 t and t = n·d. For t ≤ 2 d the flange is calculated as a beam on elastic foundation (h/d = 100 and 400). For t > 2 d a straight line corresponding to the approximate formula $P_{cr} = 0,045\ Ed^2$ is shown. Values measured for knife-edge load on the test girders are marked. As further comparison (for t = d) the values measured for lipped channels and with transfer length c/a = 0,04 are plotted from [15].

In case of great flange thickness the flanges computationally are strong enough to distribute the stresses from the point load against the web without giving stresses far out of the elastic range as in the case of 6 mm flange thickness. The distribution length is so great that buckling over a greater part of the web heigt is actual, c.f. the following section B.

B. Web buckling

Some earlier theoretic derivations [15] [16] of the buckling loads of ideal plates supported along all edges may be summarized as follows

[15] .... $P_{total} = p \cdot c = K_Z \frac{c \pi^2 D}{a^2}$ and [16] .... $P_{total} = K_R \frac{a \pi^2 D}{h^2}$

The formulas can of course be used to compute a new coefficient K such that $P_{total} = K \frac{\pi^2 D}{h}$. Introducing the plate stiffness $D = \frac{Ed^3}{12(1-\nu^2)}$ one obtains

$$P_{total} = K \frac{\pi^2 Ed^3}{12(1-\nu^2)h} = k \cdot E \frac{d^2}{h/d} \quad \text{where} \quad k = \alpha K_R \frac{\pi^2}{12(1-\nu^2)}$$

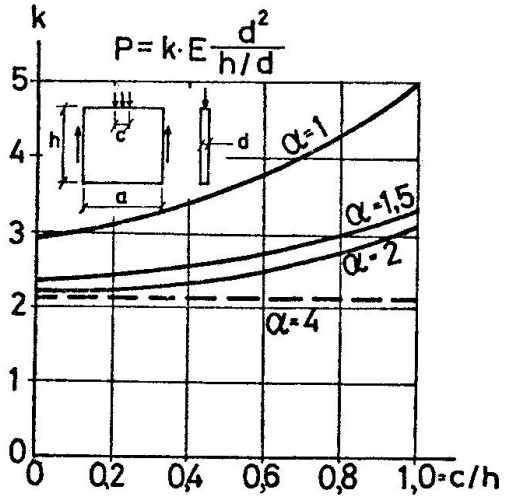

Fig. 15
Variation on buckling coefficient k with apex ratio $\alpha = a/h$ and loading length ratio c/h for a plate.

In fig. 15 the coefficient k is given as a function of α and distribution length c/h. The last ratio has been chosen instead of the more traditional c/a, as the intension is to illustrate girder behaviour and not plate action. For those α-values where both coefficients K_Z and K_R are given in [15] and [16] respectively, the values of k are the same independent of the initializing ones.

On the figure K_R has been used for $\alpha = 1$ and 1,5 and 2, while for $\alpha = 4$ there are only the clearly approximate values of K_Z given and there the mean values of K_Z for c/h = 0,06 and 0,20 have been used.

Naturally the buckling load of a plate is increased in case it is supplied with flanges to form an I-section. In [16] for a plate element with $\alpha = 1$ and c/h = 0,2 the values of the buckling coefficient are 7,75/3,48 = = 2,22 to 8,13/3,48 = 2,34 times greater in case of flanges with thickness ratios t/d = 2 to 5 than for the case of no flanges.

From the tests it can be concluded that even if the lateral web deflection may develop in a shape as assumed in [15] and [16] the final bearing capacity is limited by the great web deformations in a region of the upper part of the web directly under the point load.

From an earlier test series[9] it is clear that the expression for the buckling load $P = k \cdot E \frac{d^2}{h/d}$ is not appropriate to describe the final bearing capacity.

Fig. 16 shows the results of the tests done for different heights h, but with constant web thickness d and thus varying h/d . P is there approximately independent of the variation of d/h. Thus a better formula for collapse load would be $P = k_u Ed^2$.

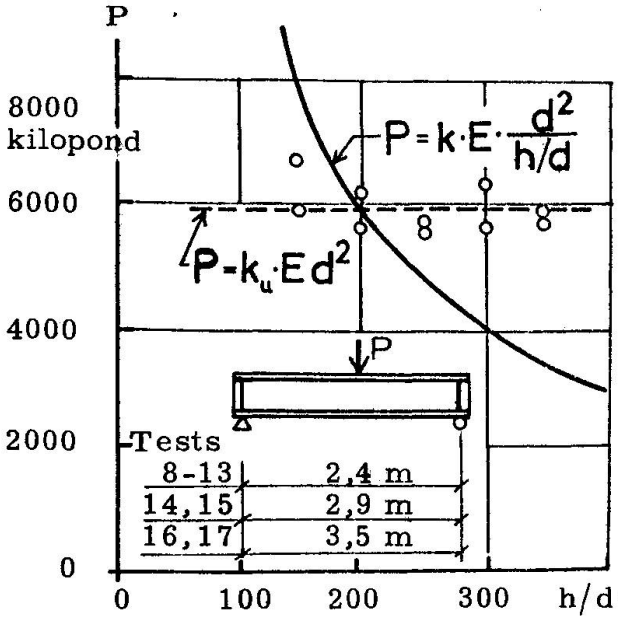

Fig. 16
Crippling loads for different web slenderness ratios. The test values are from ref. [9].

For comparison the curves $P = k \cdot E \frac{d^2}{h/d}$ and $P = k_u \cdot E \cdot d^2$ are shown. Here the coefficients k and k_u are determined to such values which give coincidence for h/d = = 200. (The web thickness was nominally 2 mm but the real thickness was greater.)

Applied to the test values the considerations in the preceding sections show that in case of strong flanges, the local compressive stresses in the web are not decisive. The flange distributes the load over such a great length in relation to the height of the girder that buckling ought to dominate, the combination probably resulting in crippling. For example in case of a flange thickness of 15 mm one obtains *) respectively $2\ L_o/h = 2 \cdot 9,35/70 = 0,27$ or $2\ L_T/h = 2 \cdot 30,6/70 = 0,88$ from Table 3.

a. - If the diagram in fig.15 is used **) with a correction for the flange thickness according to [16] one would obtain

$$P = 2,34 \cdot 2,1 \cdot 2,1 \cdot 10^6 \cdot \frac{0,326^2}{70/0,326} = 5230 \text{ kp} = 5,23 \text{ tons}$$

As the measured greatest loads varied from 15,4 to 15,8 the agreement is not good partially due to the restraint caused by the upper flange. (Correcting for the restraint with regard to the coefficient in the following section one obtains $5,23 \cdot 5,32/1,88 = 14,8$ tons.)

b. - The traditional simplified theory of buckling under a point load on the flange assumes a distribution on a length equal to the height of the girder (corresponding to a distribution at an angle of 45^o down to the axis of the center of gravity of the girder). Making the simplifying assumptions that the web of the test girder is fully restrained by the upper and hinged at the lower flange, and assuming linear variation from the loaded to the unloaded flange, one obtains

$$P = 5,32 \cdot \frac{\pi^2 EI}{(1-\nu^2)h^2} = 4,77 \cdot E \frac{d^2}{h/d}, \text{ as } I = \frac{h \cdot d^3}{12}$$

*)
It may be observed that the expression L/h corresponds to the flange flexibility parameter used in [16] multiplied with α^3 for the aspect ratio, that is $L/h = \sqrt[4]{\alpha^3 I/b^3 t}$ with the symbols of [16].

**)
At the calculations the value $E = 2,1 \cdot 10^6$ kp/cm^2 generally applied in European papers has been used. The measurings shown in Table 2 gave however the value $2,05 \cdot 10^6$ kp/cm^2.

The form of the expression is the same as above and the coefficient is corrected as to the restraint. The buckling load would be 5,07 tons, even somewhat less than the much to low value obtained above.

An increase in distribution length from h to h + 2L gives better values but they are still to low. Also plate action must be considered.

c. - The empirical formula $P = k_u \cdot Ed^2$ will give with $k_u = 0,45 \cdot 10^{-4}$ the value P = 10,0 tons.

C. Web crippling

The shear stresses for the slender webs considered here does not correspond to a linear load distribution down to the unloaded flange, but the load transmission is concentrated to the region under the point load. This fact which is verified by the strain gage measurements means that the buckling lengths are shorter and thus the buckling loads greater.

At the same time for the real girders there were some initial deviations from planeness of the web. This means that even at the start of loading the compressive stresses act in combination with bending stress.

A treatment of the test values as to this effect is in progress.

D. The influence of A, B and C on the bearing capacity of the girder

If the bending stresses or the shearing stresses in the girder on the whole are great (but still under allowed values) and are of the same sign as the local stresses the influence of combined action reduces the capacity to support a point load somewhat, and vice versa. An earlier example is shown in fig. 8. A further test value is obtained by comparison between the tests G_u and E_u where the increase in span width from 2,4 to 9,4 meters with a corresponding increase in σ_x has reduced the capacity to carry point loads from 12,3 to 10,4 tons, e.g. a reduction of about 15 %.

Summary and Conclusion

From Part I of the article is seen, in fig. 4, that tests on shear buckling of plate girders without intermediate web stiffeners support the approximate solution of ultimate bearing capacity given by Bergman [5]. The influence of coexisting bending stresses and of initial lateral deformations is small. This is in contrast to the behaviour predicted on linear small deflection theory.

In Part II formulas for crippling load are discussed and compared to new tests. The empirical formula

$$P_{cr\ tons} = 0,9 \cdot d^2_{mm} \quad \text{or} \quad P_{cr} = 0,045 \cdot Ed^2$$

gives fairly good values for the tested slenderness ratios $150 < h/d < 350$ and for web dimensions from 2 to 6 mm. This holds true for I-girders, where the web to some extent is restrained by the flange. As is seen from fig. 14 for very thin flanges, $t < 2d$ (or cold formed profiles) it is necessary to check the yield stress of the web (e.g. with

yield zones in the flange computed as for beams on elastic foundations). For thicker flanges P_{cr} increased and reached in these tests for very plane webs $P_{cr} = 0,045 \cdot Ed^2 \cdot (0,55 + 0,035\ L/d)$ or, still more approximately $P_{cr} = 0,045 \cdot Ed^2\ (0,55 + 0,22\ t/d)$. When the webs had great initial lateral deflections P_{cr} was lower, c.f. fig. 14 b, but with $0,045 \cdot Ed^2$ as lowest boundary. In some tests where the flange was thin, the load not fixed and the web thus almost hinged at the flange, there was a reduction to about 70% of the above values.

If the load was transmitted by a bar plate of the length of 30 d (or h/7) instead of by a knife edge, P_{cr} increased about 10% for thin girder flanges. This increase diminished to about 5% for the thickest flange of the tests (fig. 11). When the bar was 60d long, P_{cr} was further increased some few %.

The influence of high bending and shear stresses (allowable stresses) reduced P_{cr} only about 15% compared to values at small stresses.

For repeated loading cycles to 80% of the P_{cr} for one loading only there was no failure after 100 cycles, though snap buckling took place and strains up to 3,8 ‰ were measured for pressure and bending stresses in the web.

It is intended to do further tests.

*

REFERENCES

1 H. Wagner : Ebene Blechwandträger mit sehr dünnen Stegblech. Zeitschrift f. Flugtechn. u. Motorluftschiffahrt, vol. 20, 1929.

2 K. Basler - B. Thürlimann : Strength of plate girders. Proc. ASCE, ST 6 and 7, 1961.

3 K. C. Rockey - M. Skaloud : Influence of flange stiffeners upon the load carrying capacity of webs in shear. IABSE, New York 1968, p. 429.

4 Th. v Kármán : The engineer grapples with non-linear problems. Bull. Am. Math. Soc. vol. 46, 1940.

5 S. Bergman : Behaviour of buckled rectangular plates under the action of shearing forces. Theses, KTH, Stockholm 1948.

6 C. A. Granholm : Provning av balkar med extremt tunt liv. (Tests on girders with extremely thin web plates). Rapport 202, Inst. f. Byggnadsteknik, CTH. Göteborg 1960-61.

7 C. A. Granholm : Lättbalkar (Light girders). Teknisk Tidskrift, Stockholm 1961, p. 455.

8 Hj. Granholm : Svetsade balkkonstruktioner (Welded girders). Jernkont. Ann. 148 (1964):10. Uppsala, Sweden 1964.

9 A. Bergfelt - J. Hövik : Thin-walled deep plate girders under static loads. IABSE 1968, New York, p. 465.

10 A. Bergfelt - J. Hövik : Shear failure and local web crippling in thin-walled plate girders, Experiments 1966-69. CTH, Stål- och Träbyggnad, Int. skr. S70:11b, Göteborg 1970.

11 F. Nishino - T. Okumura : Experimental investigation on strength of plate girders in shear. IABSE, New York 1968, p. 451.

12 Ph. Carskaddan : Shear buckling of unstiffened hybrid beams. Proc. ASCE, ST 8, Aug. 1968.

13 A.Ostapenko - B.Yen - L.Beedle : Research on plate girders at Lehigh University. IABSE, New York 1968, p.441.
14 Klöppel - Lie : Beulung des rechteckigen, allseitig belasteten und einspannungsfrei gelagerten Bleches. VDI-Zeitschrift, Bd 86, H5/6, 1942.
15 L.Zetlin : Elastic instability of flat plates subjected to partial edge loads. Proc.ASCE, Vol.8, Paper 795, 1955.
16 D.K.Bagchi - K.C.Rockey : A note on the buckling of a plate girder web due to partial edge loadings. IABSE, New York 1968, p.489.
17 Ch.Schilling : Web crippling tests on hybrid beams. Proc.ASCE, ST1, Feb.1967.
18 A.W.Hendry : The stress distribution in a simply supported beam of I-section carrying a central concentrated load. Proc.Soc.for Experimental Stress Analysis, Vol.VII No 2, 1949, pp 91-102.

SUMMARY

From Part I of the paper it is seen that tests to failure on shear buckling of plate girders with thin webs without intermediate web stiffeners, fig. 4, support the approximate solution of ultimate bearing capacity already given by Bergman (5).

The tests of Part II illustrate that for these girders the failure in web crippling under concentrated loads is limited by bending and compression stresses in the web and in the flange up to a flange thickness of about twice the web thickness. For thicker flanges the web buckling dominates and the load increases slightly in proportion to flange thickness, fig. 11 and fig. 14.

RESUME

Les essais de la première partie de l'article, fig. 4, confirment les résultats de la solution approximative de Bergman (5) concernant la résistance au cisaillement.

Dans la seconde partie il est démontré que la résistance à la rupture de l'âme sous charges concentrées est limitée par les tensions de compression et de flexion dans l'âme et dans les semelles pour une épaisseur de la semelle qui est le double de l'épaisseur de l'âme (voir fig. 14). Pour des semelles plus épaisses le voilement prédomine et la charge n'augmente que faiblement pour des épaisseurs élevées de la semelle, fig 11.

ZUSAMMENFASSUNG

Im ersten Teil dieses Aufsatzes wird gezeigt, dass Versuche über die Beulung durch Querkraft, Bild 4, für Blechträger mit dünnen Stegen die approximative Lösung über das Bruchverhalten bestätigen, die schon von Bergman (5) gegeben wurde.

Die Versuche im zweiten Teil zeigen, dass das Bruchverhalten des Steges unter Punktlasten durch die Biege- und Druckspannungen im Steg und im Flansch bei einer Flanschdicke von ungefähr doppelter Stegdicke begrenzt wird. (Bild 14). Für dickere Flanschen überwiegt die Beulung, und die Last nimmt nur wenig mit erhöhten Flanschdicken zu (Bild 11).

Leere Seite
Blank page
Page vide

I

Simply Supported Long Thin Plate I-Girders without Web Stiffeners Subjected to Distributed Transverse Load

Poutres longues à âme mince sans raidisseurs, simplement appuyées et soumises à une charge uniforme

Einfach gelagerte, lange, dünnwandige Blechträger ohne Stegaussteifungen, unter gleichmässiger Belastung

TORSTEN HÖGLUND
Techn. lic.
Department of Building Statics and
Structural Engineering of the
Royal Institute of Technology
Stockholm, Sweden

1. INTRODUCTION

During the last ten years there has been a marked increase in the use of welded thin plate I-girders especially in roof constructions. This has been made possible by the use of rational methods of fabrication and design. One essential point is - in spite of the thin web - to avoid web stiffeners, which have to be manually fitted and welded and thus cause considerable costs.

The simply supported girder is a common element in roof constructions. When the load is sufficiently distributed along the girder no other vertical web stiffeners than at the supports are needed. When the girder is subjected to a few concentrated loads vertical web stiffeners are required to prevent web crippling.

This investigation deals with long simply supported plate girders with web-stiffeners at the supports loaded with distributed transverse loads. The web is then subjected to varying shear forces, distributed edge loading and bending stresses simultaneously. The simple cases of loading, constant shear, bending moment or edge loading have been studied but not this combination of all three.

Granholm [9] has made tests on web crippling and he has given the empirical formula $P = 85\ 000\ d^2$ (d in cm gives P in kp) for the buckling load. This formula has been confirmed by Bergfeldt and Hövik [5]. See fig. 1.

Shear loaded welded girders with large distance between web stiffeners ($a/h > 2.6$) have been tested by Wästlund and Bergman [17] Basler et al [1], Granholm [9], Cooper [7], Nishino-Okumara [12], Fuiji [8]. The test girders have been loaded with constant shear forces, in some tests combined with bending moment, see fig. 2 and 3.

Theoretical solutions for an infinitely long plate subjected to the action of shearing forces along the edges have been obtained by Kromm and Marguerre [10], Bergman [6] and Skaloud [15]. These theories which are based on the differential equations for large deflections gives informations of bending and membrane stresses in the elastic postbuckling range.

The research work at Lehigh University [1,2,3,4,7] on plate girders with transverse stiffeners with a spacing less than three times the girder depth (a/h < 3) has resulted in specifications for such girders [18]. The influence of the stiffeners of the flanges has been studied e.g. by Bergman [6], Fuiji [8], Rockey and Skaloud [13,14].

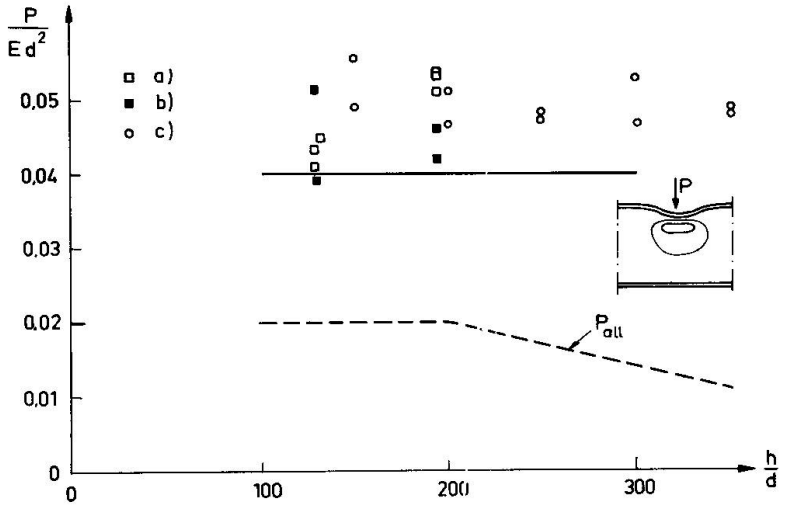

Fig. 1 Test results on web crippling. [5], [9].

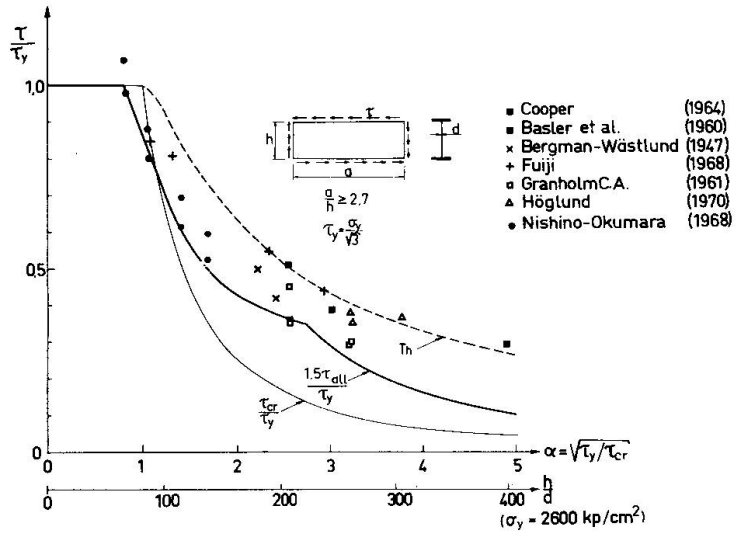

Fig. 2 Test results of welded plate girders subjected to shear. Th = theoretical ultimate load, see fig. 19.

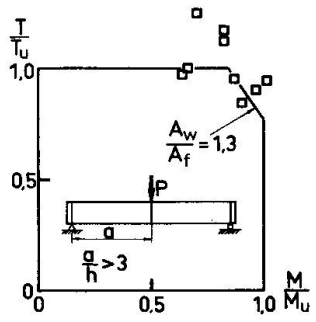

Fig. 3 Test results of welded plate girders subjected to bending and shear. Granholm [9].

$T_u = hd\,\tau_{all}$ where τ_{all} = allowable shear stress according to [19].

$$M_u = \sigma_y 2I/h\left(1 - 0{,}0005\,\frac{A_w}{A_f}\left(\frac{h}{d} - 5{,}7\sqrt{\frac{E}{\sigma_y}}\right)\right) \qquad [2]$$

In Sweden special specifications for the design of welded plate girders in roof constructions mainly loaded with dead load [19] have been in use since 1966. The draft of these specifications which contains rules for the complete design of plate girders with thin web was worked out by H. Nylander and the author by order of Gränges Hedlund AB, Stockholm. This paper is a part of the basis for these specifications. In fig. 1 and 2 test results are compared with the allowable load P_{all} regarding to web crippling and the allowable shear stress τ_{all} according to these specifications. In fig. 3 test results for girders loaded in bending and shear are compared with an interaction curve according to Basler [4].

2. TEST PROGRAM AND TEST PROCEDURE

Three girders of structural carbon steel were tested, two with 9 m span and one with 6 m span, see fig. 4.

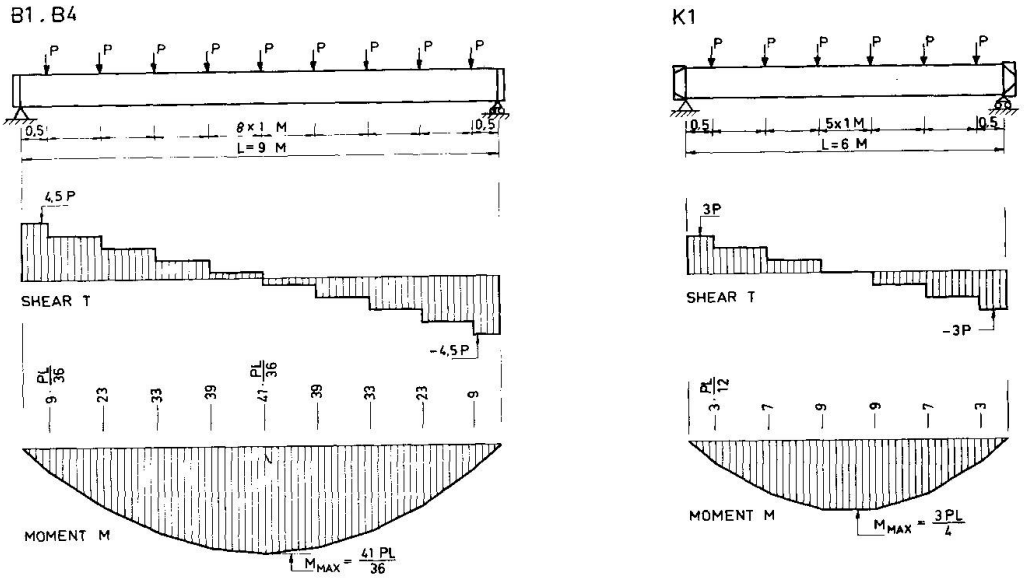

Fig. 4a Distribution of load, shearing forces and bending moment for the test girders.

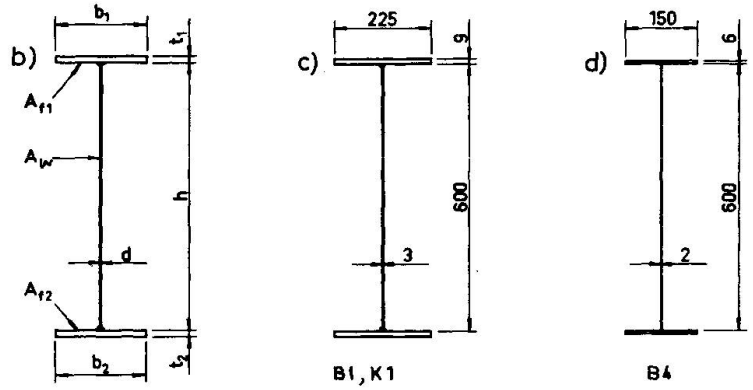

Fig. 4b-c-d. b) Notations for cross section. c) and d) Girder cross sections for the test girders.

The girders were simply supported and loaded with nine or six gravity loads with a spacing of 5/3 of the girder depth. The gravity loads were produced by levers and scales with weights, see fig. 5. The test girders were fabricated of flame cut flange and web plates in an automatic welding machine.

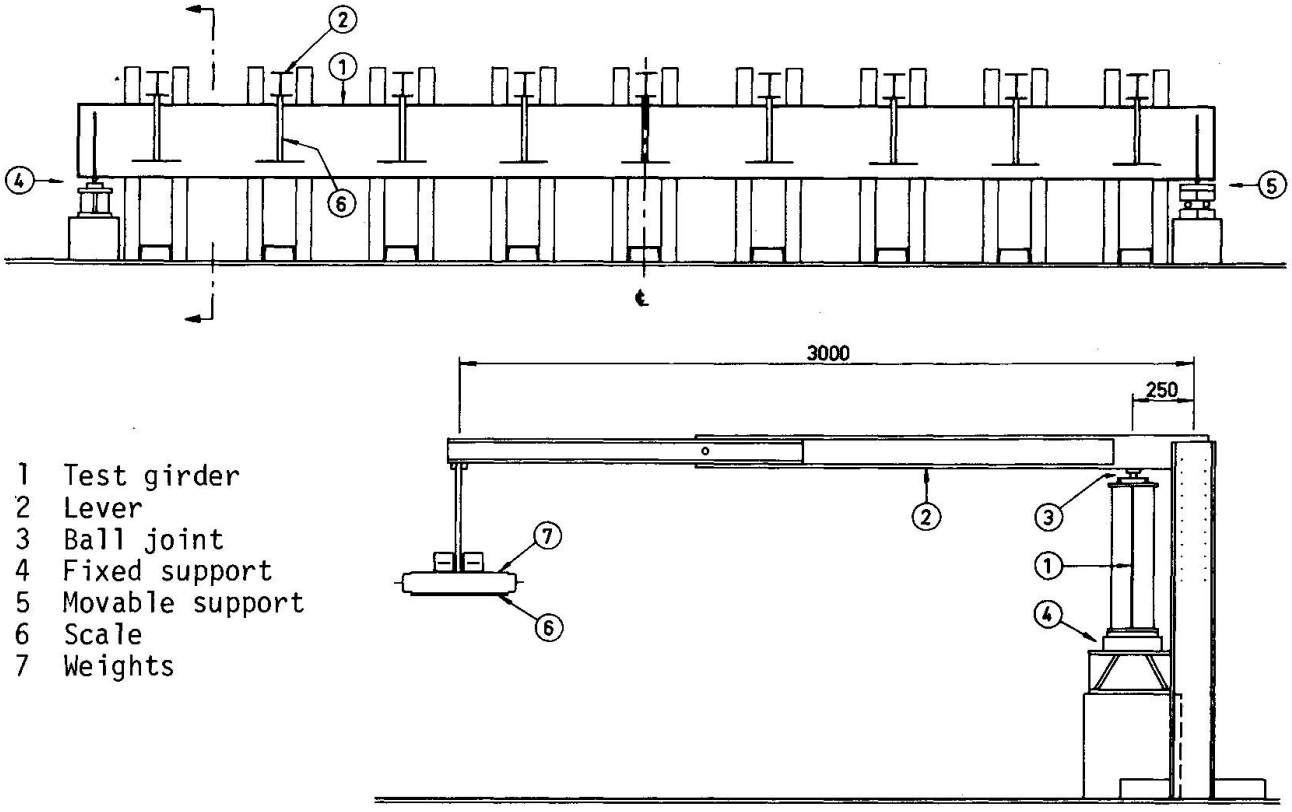

Fig. 5 Test setup.

Table 1. Cross sectional properties and yield point of the flange and the web material.

Test girder	h cm	d cm	b cm	t cm	$\frac{h}{d}$	I_x cm^4	σ_y kp/cm^2 flange	web
B1	60.0	0.286	22.6	0.99	210	46600	2944	4185
B4	60.0	0.200	15.1	0.61	300	20500	3040	2800
K1	60.0	0.286	22.6	0.99	210	46600	2944	4185

Details of the test girders are given in table 1.

The surface strains were measured with electrical strain gauges at points near the supports on the web, on the stiffeners and on the flanges. The out of plane deflections of the web were determined with a photogrammetic method.

Fig. 6, 7 and 8 show load versus midspan deflection curves for the test girders. The following reference loads are given in the figures:

$P_{\tau cr}$ = shear buckling load for the web calculated under the assumption that the web is simply supported, very long and subjected to pure shear

$P_{\sigma cr}$ = the buckling load in bending for the web at midspan section of the girders

$P_{\sigma s}$ = the bending moment $\sigma_y I/(h/2)$ at midspan.

The ultimate loads are denoted P_{Br}^{Bl} and P_{br}^{Kl}. The web deflection configuration at ultimate load is indicated in the figures.

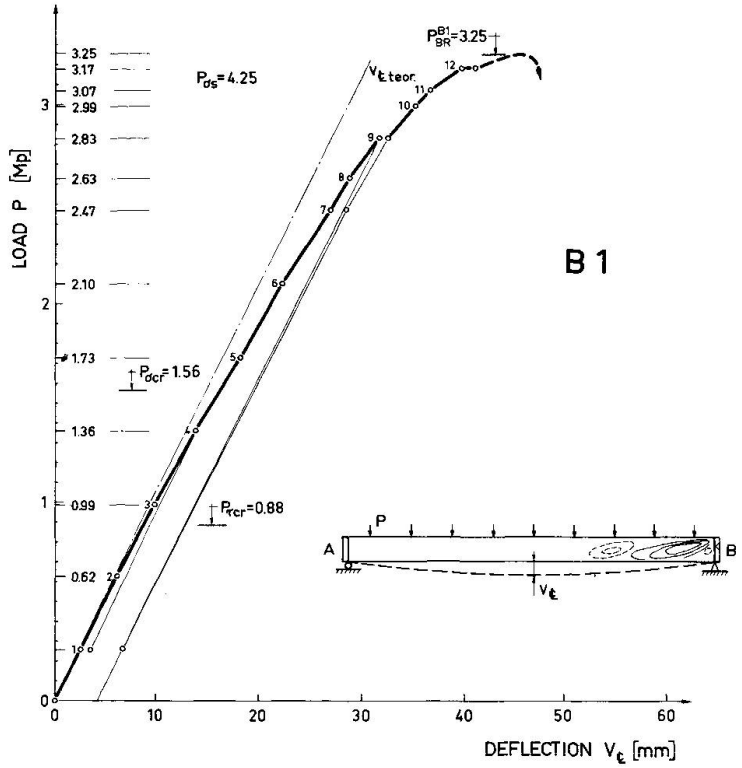

Fig. 6 Load-deflection curve of test girder B1.

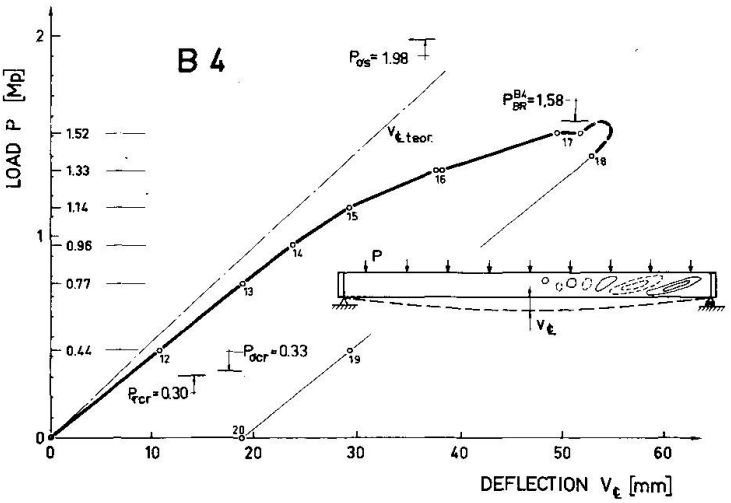

Fig. 7 Load-deflection curve of test girder B4.

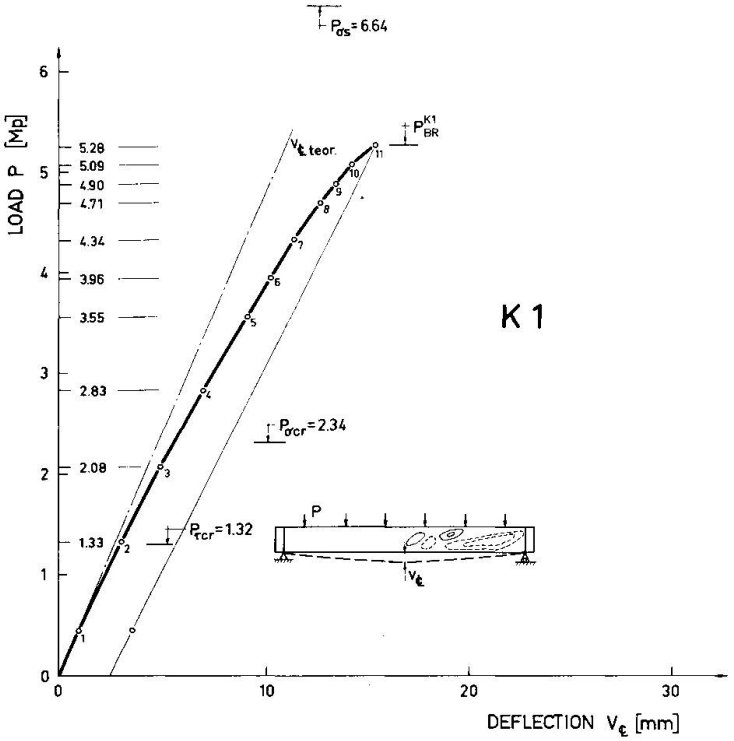

Fig. 8 Load-deflection curve of test girder K1.

3. TEST RESULT

Prior to testing, the initial deformations of the web plate were determined by photogrammetric method. The testing procedure consisted of taking new photos, dial gauges and strain readings at each load level.

The web of test girder B1 was at support A stiffened with two web stiffeners and with a single stiffener at support B.

Fig 9 and 11 show the deformation of the web of girder B1 at different loads. The principal stresses in the middle surface calculated from strain measurements at six points of the web are shown with stress vectors. Typical curves for the relation between the principal stresses and the load for two points in the web, one at each support, are shown in fig 10 and 12. As in other tests the compressive principal stress σ_2 reached a certain value near the shear buckling stress and remained approximately at this level up to the maximum load.

The web of test girder B4 and K1 was stiffened with two stiffeners at both supports. Fig. 13 shows the web deflection and fig. 14 the flange strains at support of girder B4.

The ultimate load for the three test girders varied from 3.7 to 4.7 times the shear buckling load, se table 2.

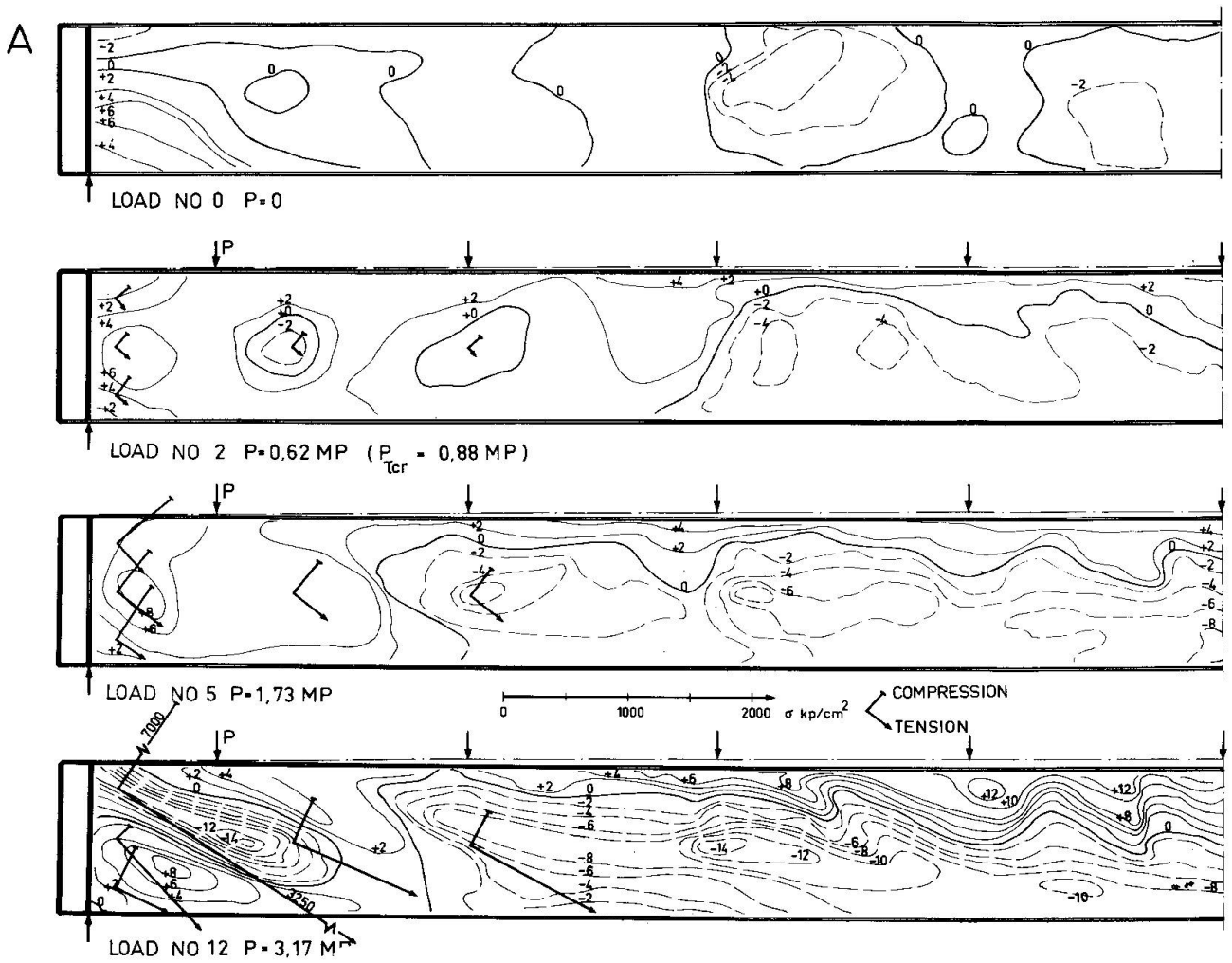

Fig. 9 Web deflection (in mm) and principal stresses in the web of test girder B1 at support A.

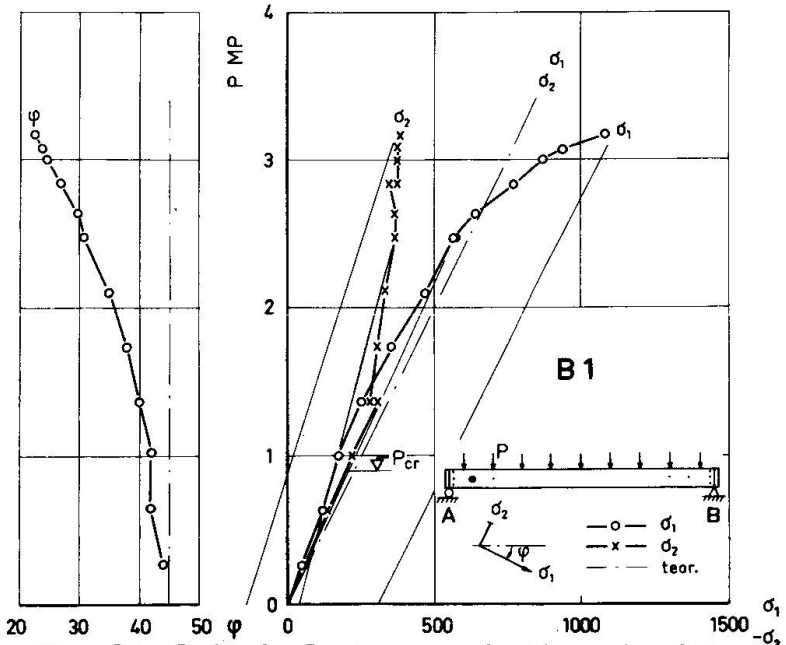

Fig. 10 Principal stresses in the web of test girder B1 at support A as a function of the load P.

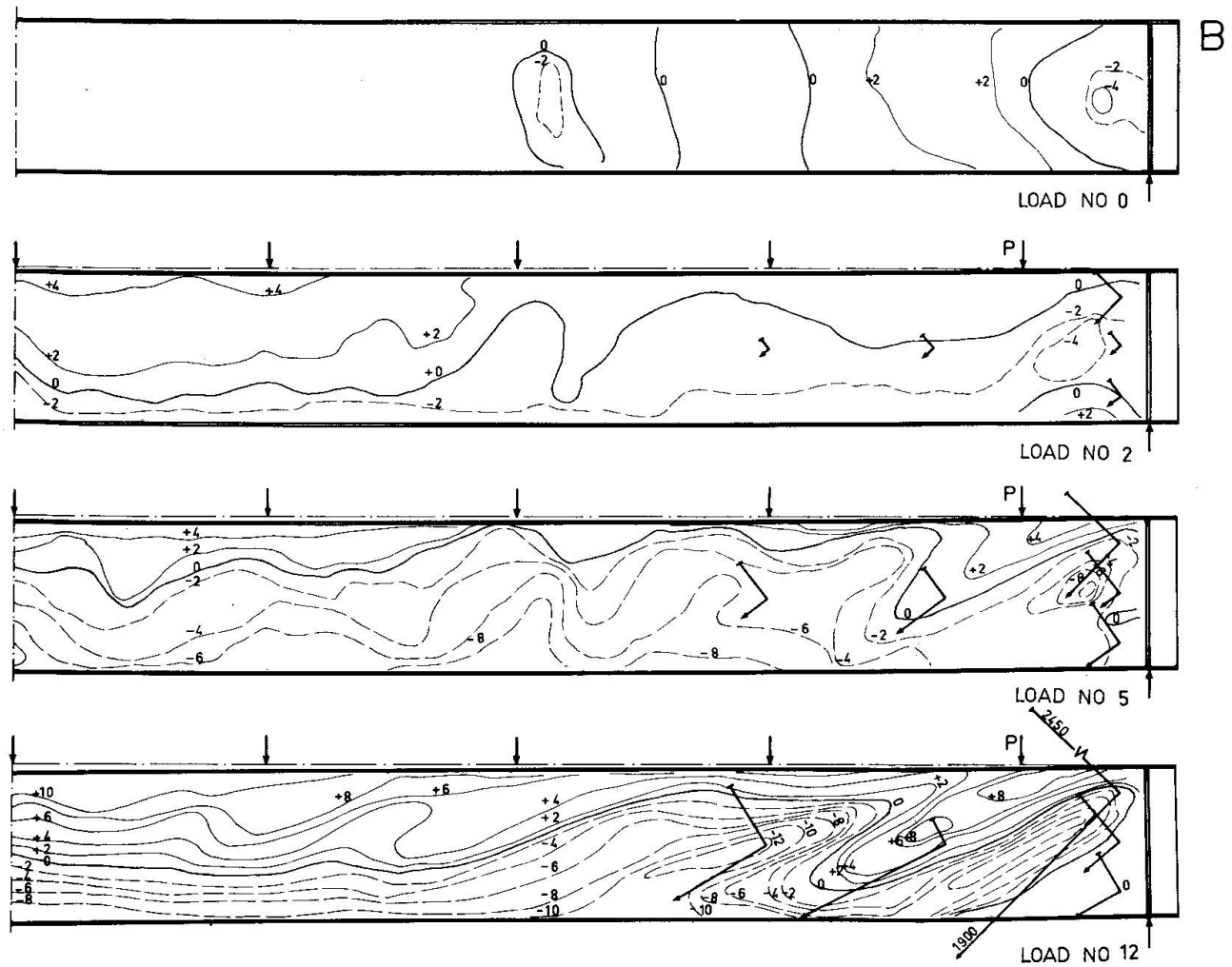

Fig. 11 Web deflection (in mm) and principal stresses in the web of test girder B1 at support B.

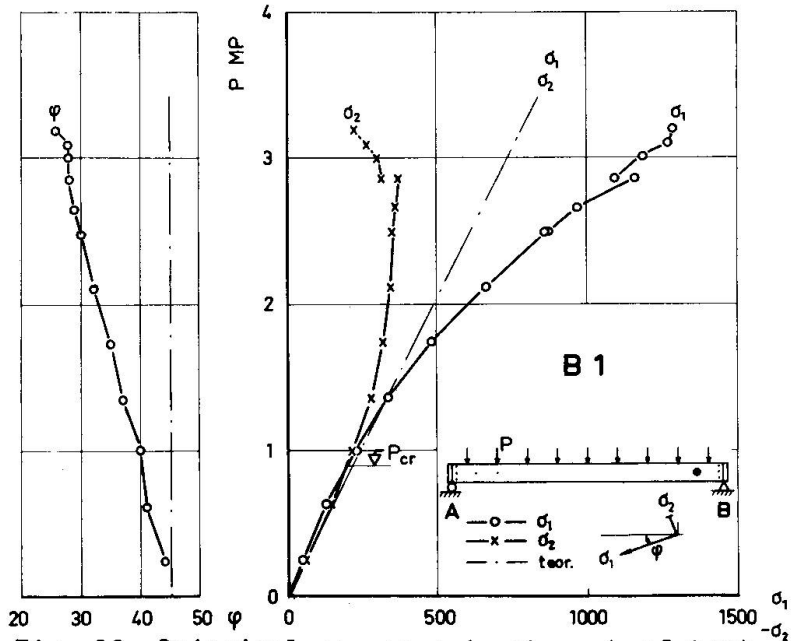

Fig. 12 Principal stresses in the web of test girder B1 at support B as a function of the load P.

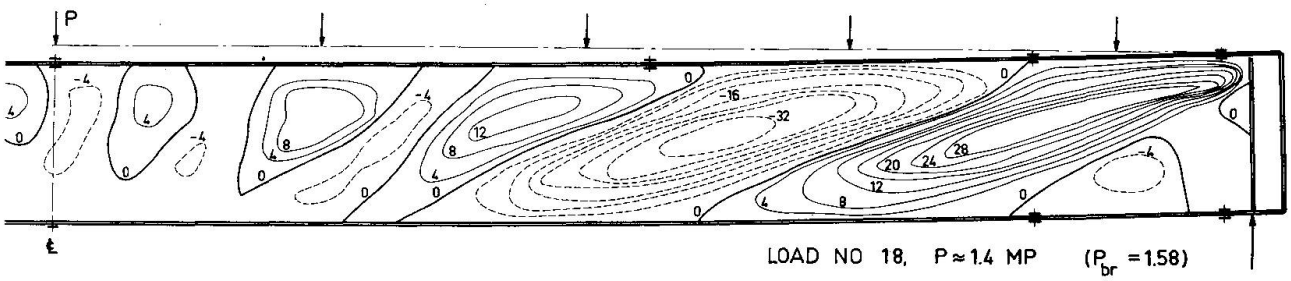

Fig. 13 Web deflection (in mm) of the test girder B4.

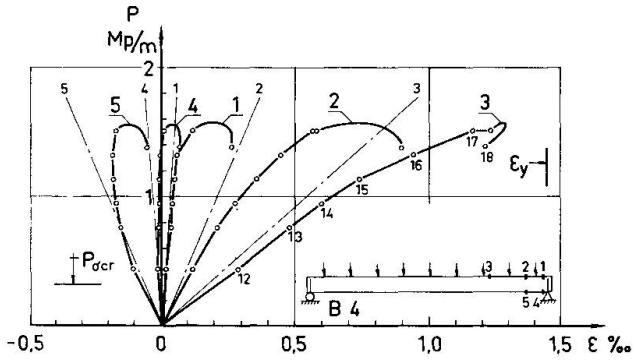

Fig 14 Flange strains in test girder B4.

Table 2. Summary of test results

Test girder	$\frac{h}{d}$	τ_y kp/cm²	τ_{cr} kp/cm²	α	P_{br} Mp	τ_u	$\frac{\tau_u}{\tau_y}$	$\frac{\tau_u}{\tau_{cr}}$
B1	210	2420	231	3.24	3.25	853	0.35	3.69
B4	300	1620	113	3.78	1.58	529	0.37	4.68
K1	210	2420	231	3.24	5.28	924	0.38	4.00

$\tau_y = \sigma_y/\sqrt{3}$; $\alpha = \sqrt{\tau_{cr}/\tau_y}$; P_{br} = ultimate load (1Mp = 2205 ℔b)

τ_u = maximum shear force at ultimate load.(1 kp/cm²=14,2 ℔b/sq in)

4. THEORY

In order to obtain an intelligible model of the shear loaded girder the web is replaced with a system of bars shown in fig. 15. The angle between the tension bars and the flanges is denoted β and the compression bars are perpendicular to the tension bars.

When the angle β is decreased the buckling load T_{cr} for the bar system is increased. The stress σ_c in the compression bars for the buckling load is almost

independent of β and approximately the same as the shear buckling stress τ_{cr} for the infinitly long web plate. This is still valid then the deflections become large. For a given bar system the load increases only a little when the deflections become large.

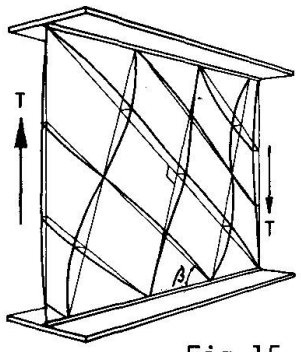

Fig 15

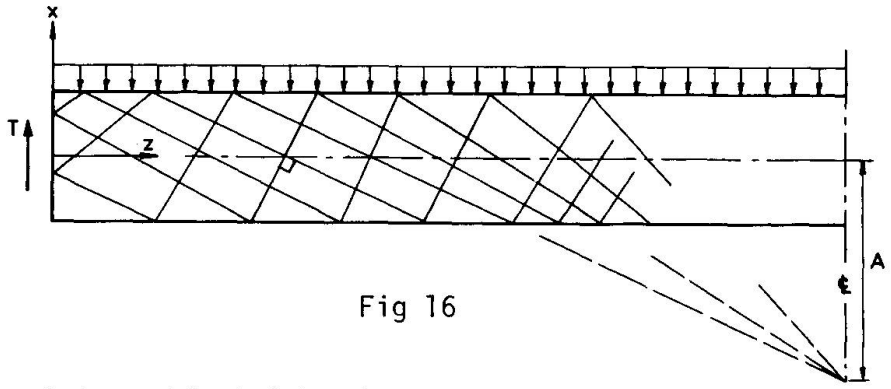

Fig 16

Fig. 15 Bar system for a girder subjected to shear.

Fig. 16 Bar system for a simply supported girder with distributed transverse load.

For the simply supported girder with distributed load the inclination of the bars is varied along the girder length because the shear force varies. The stresses in the compression bars are assumed to be less than or equal to τ_{cr} except at the upper corners at the supports where the bars are shorter and can resist stresses larger than τ_{cr}.

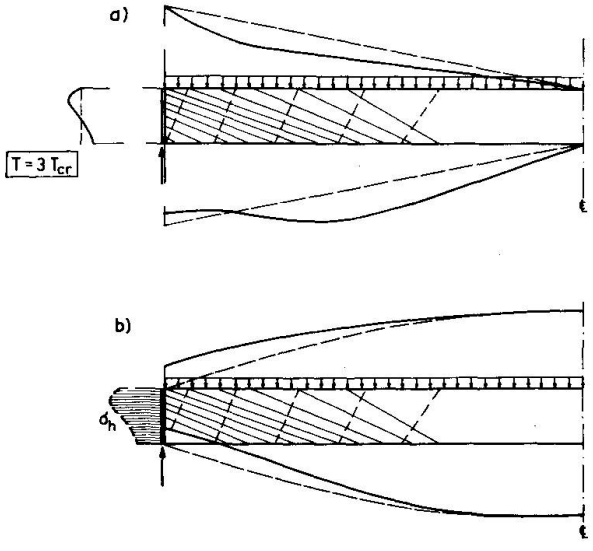

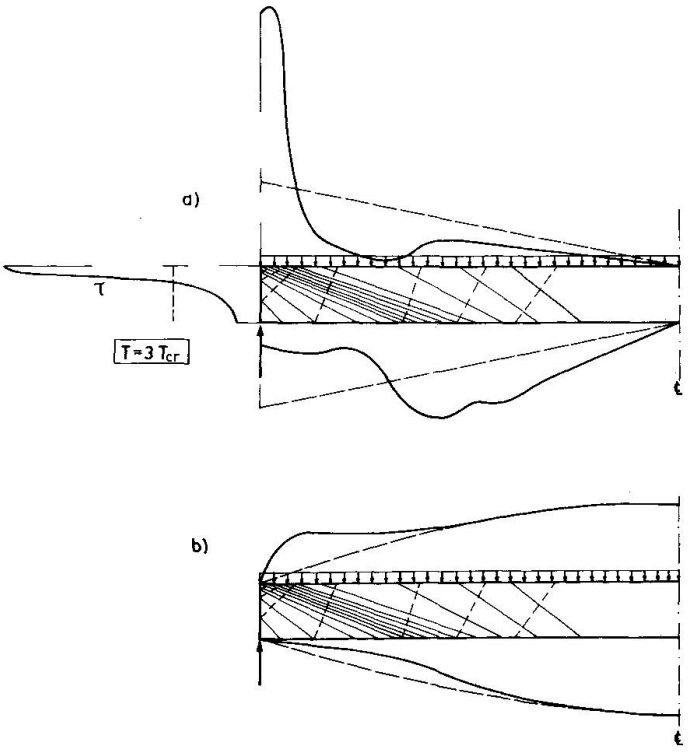

Fig. 17 Strong web stiffener

Fig. 18 Weak web stiffener

a) Calculated distribution of shear stresses between the flanges and the web. b) Distribution of flange stresses.

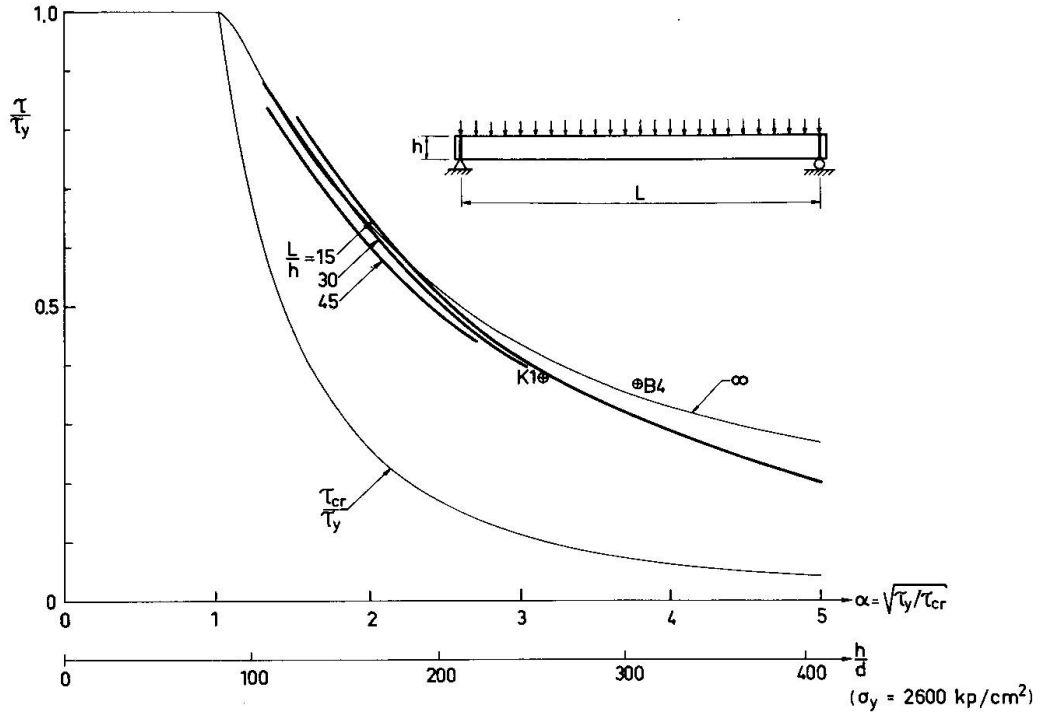

Fig. 19 Calculated ultimate load for girders with strong web stiffeners at the supports.

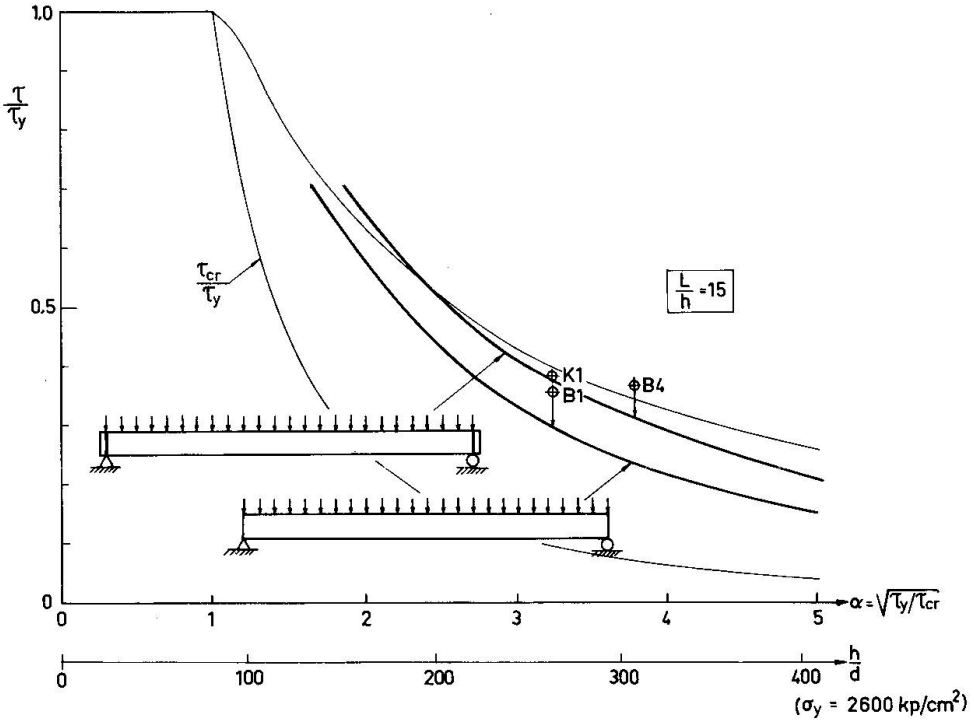

Fig. 20 Calculated ultimate load for girders with weak web stiffeners and strong web stiffeners at the supports.

Some results of the calculations for two cases are shown in fig. 17 and 18. The distribution of the shear forces between the web and the flanges, the web and the stiffeners (fig. 17a and 18a) is different for the two cases depending on the different bending stiffness of the web stiffeners at the supports. The strong web stiffeners (fig. 17) can resist the horisontal stress components of the tension and compression bars and the tension bars can be distributed over the girder depth. When the stiffeners are weak (fig. 18) the tension bars must be concentrated to the upper corners at the supports. Fig. 17b and 18b show the corresponding flange forces.

The tests confirm the theory with regard to stresses in the web, the flanges and the web stiffeners except in one respect:
The measured principal compression stresses are greater than the shear buckling stress for a long, simply supported panel with constant shearing force, which may be part of the explanation of the fact that the theory underestimates the ultimate load, see fig. 19 and 20.

5. ACKNOWLEDGEMENT

This report is based on research work performed at the Department of Building Statics and Structural Engineering of the Royal Institute of Technology, Stockholm, Sweden. Head of the department is Professor Henrik Nylander whom the author wishes to thank for valuable support. The author also wishes to thank Professor Bertil Hallert, the Department of Photogrammetry of the Royal Institute of Technology, Stockholm for helping with the photogrammetric determination of the web deflection surfaces, the Swedish Council for Building Research for sponsoring the investigation and Gränges Hedlund AB, Stockholm for donating the test girders.

6. REFERENCES

[1] Basler, K.& Yen, B.T.& Mueller, J.A.& Thürlimann, B. Web buckling Tests on Welded Plate Girders. Welding Research Council, Bulletin No 64, New York, Sept. 1960.

[2] Basler, K.& Thürlimann, B. Strength of plate girders in bending. Journal of the structural Division, ASCE, Aug. 1961.

[3] Basler, K. Strength of Plate Girders in Shear. Journal of the Structural Division, ASCE, Oct. 1961.

[4] Basler, K. Strength of plate girders under combined bending and shear. Journal of the structural division, ASCE, Oct. 1961.

[5] Bergfelt, A.& Hövik, J. Thin walled deep plate girders under static loads. IABSE, Eighth Congress, New York, 1968.

[6] Bergman, S.G.A. Behaviour of buckled rectangular Plates under the Action of shearing Forces, Stockholm 1948.

[7] Cooper, P.B.& Lew, H.S.& Yen, B.T. Welded constructional alloy steel plate girders. Journal of the Structural Division, ASCE, Febr. 1964.

[8] Fujii, T. On an Improved Theory for Dr. Basler's Theory. IABSE, Eighth Congress, New York 1968.

[9] Granholm, C.-A. Lättbalkar (Light girders). Teknisk Tidskrift, Stockholm 1961 and other not published reports.

[10] Kromm, A.& Marguerre, K. Verhalten eines von Schub- und Druckkräften beanspruchten Plattenstreifens oberhalb der Beulgrenze. Luftfahrtforschung, Vol. 14, 1937.

[11] Massonet, C. Thin-walled deep plate girders. Preliminary Publications, Eighth Congress, IABSE, New York 1968.

[12] Nishino, F.& Okumara, T. Experimental investigation of strength of plate girders in shear. Eighth Congress, IABSE, New York 1968.

[13] Rockey, K.& Skaloud, M. Influence of flange stiffeners upon the load carrying capacity of webs in Shear. Final Report Eighth Congress, IABSE, New York 1968.

[14] Rockey, K.& Skaloud, M. Influence of the flexural rigidity of flanges upon the load-carrying capacity and failure mechanism of webs in shear. Acta Technica Csav No3, Praha 1969.

[15] Skaloud, M. Comportement postcritique des ames des potres en acier livre. NCSAV, Praha 1962.

[16] Wagner, H. Ebene Blechwandträger mit sehr dünnem Stegblech, Zeitschrift für Flugtechnik und Motorluftschiffahrt, Vol. 20, 1929.

[17] Wästlund, G.& Bergman, S.G.A. Buckling of webs in deep steel I-girders. Statens Kommitté för Byggnadsforskning, Meddelande nr 8, Stockholm, 1947.

[18] Specifications for the design, fabrication & erection of structural steel for buildings. AISC, New York 1969.

[19] Provisoriska Normer för svetsade stålbalkar, typ HSI (Specifications for the design of welded steel girders, type HSI). Gränges Hedlund AB, Stockholm 1966 (in Swedish).

SUMMARY

Tests were performed on long simply supported thin plate I-girders with web stiffeners only at the supports. The girders were loaded with nine or six gravity loads. The depth to thickness ratio of the web ranged from 200 to 300. A theory is briefly presented where the web is assumed to be composed of a system of compression and tension bars.

RESUME

Des essais ont été effectués sur des poutres à âme mince simplement appuyées, avec raidisseurs aux appuis seulement. On a chargé les poutres par neuf ou six charges concentrées. Le rapport entre la hauteur et l'épaisseur de l'âme variait entre 200 et 300. On en présente une théorie en supposant que l'âme soit composée d'un système de barres de tension et de compression.

ZUSAMMENFASSUNG

Es wurden Versuche an langen, dünnen, einfach gelagerten I-Vollwandträgern durchgeführt, welche lediglich an den Enden Stegaussteifungen besassen. Man belastete die Träger mit sechs oder neun konzentrierten Kräften. Das Verhältnis der Höhe zur Dicke variierte zwischen 200 und 300. Es wird kurz eine Theorie vorgelegt, unter der Annahme, der Steg bestehe aus einem System von Zug- und Druckstäben.

Leere Seite
Blank page
Page vide

Vollwandträger: Berechnung im überkritischen Bereich

Plate-Girders: Design in the Post-Critical Range

Poutres à âme pleine: Calcul dans le domaine post-critique

K. BASLER
Dipl. Bauingenieur ETH/SIA
Zürich, Schweiz

In der Publikation*) "Vollwandträger, Berechnung im überkritischen Bereich" der Schweizer Stahlbau-Vereinigung hat der Autor die Resultate der theoretischen und der experimentellen Forschung, die in den Jahren 1957 bis 1960 im Fritz Engineering Laboratory der Lehigh University durchgeführt wurden, in einer für den schweizerischen Stahlbau nutzbaren Form zusammengestellt, begründet und darauf beruhende Bemessungsregeln aufgestellt.

Mit diesen Grossversuchen konnte man nicht nur zeigen, dass die Festigkeit eines Vollwandträgers in keiner Weise von der Beullast des Steges vorausgesagt werden kann, sondern auch belegen, dass Flanschen und Quersteifen Stegfunktionen übernehmen, indem sie einen Teil der Biegemomente und Querkräfte tragen. Dadurch entsteht aber ein neues Konzept für die Bemessung von Vollwandträgern, das hier dargestellt wird.

---

*) Diese Publikation ist bei der Schweizer Stahlbau-Vereinigung erhältlich.

BIEGUNG

Im Gegensatz zu Walzprofilen sind Vollwandträger Bauglieder, deren Gestaltung dem entwerfenden Ingenieur noch offensteht. Bei vorwiegend auf Biegung beanspruchten Blechträgern wird er - um den Hebelarm der inneren Kräfte zu vergrössern - die Flanschen so weit wie möglich auseinander halten oder - bei gegebener Bauhöhe - möglichst viel Material aus dem Steg in die Flanschen verlegen.

Mit Hilfe der Beultheorie werden für diese Bemessungsaufgaben klare Grenzen gezogen. Dieser Theorie ist aber für den Trägersteg eine zu grosse Bedeutung beigemessen worden, denn die Biegetragkapazität eines Vollwandträgers ist erst erreicht, wenn einer seiner Flansche versagt.

Abgesehen vom Sprödbruch wird in einem Vollwandträger mit gleichen Gurtflächen stets der Druckflansch versagen. Daher wird in diesem ersten Teil, der sich mit der Biegekapazität befasst, die Stabilität des Druckgurtes im Vordergrund stehen.

Wird der Obergurt eines Vollwandträgers wie in Figur 1 als losgelöster Stab betrachtet, so hat dieser hinsichtlich Knicken drei Freiheitsgrade. Dementsprechend wird auch der Inhalt dieses ersten Teiles gegliedert.

Figur 1
Knickrichtungen

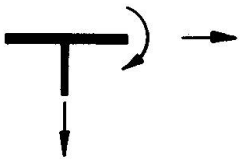

Um nun die Kapazität eines Trägers hinsichtlich Biegung zu ermitteln, bedarf es der Kenntnis über die kleinste der drei möglichen Lasten, die bei vertikalem Einknicken, bei seitlichem Knicken oder bei Torsionsknicken des Druckgurtes entstehen.

Für vertikales Einknicken des Druckflansches in den Steg wird hier keine Abschätzung der Tragkapazität versucht, sondern vielmehr verlangt, dass es nicht zur Ursache eines Versagens werde. Dementsprechend werden Grenzen für den Stegschlankheitsgrad $\beta = b/t$, d.h. Steghöhe zu Stegstärke, abgeschätzt, über die hinaus querausgesteifte Vollwandträger nicht mehr ohne Längssteifen gebaut werden sollten. Mit Eigenspannungen von der Grösse der halben Fliessspannung

liegt diese Grenze bei $\beta = 360$ für einen Stahl mit der Fliessspannung $\sigma_{fl} = 2{,}4$ t/cm2 und $\beta = 240$ für $\sigma_{fl} = 3{,}6$ t/cm2.

Bei direkter Flanschbelastung muss sowohl dem lokalen Einfluss der Last als auch dem globalen Zusammenbruch des Steges Rechnung getragen werden, was zu einer Begrenzung der Druckspannungen unter der Halsnaht führt. (Siehe Seite 16 der eingangs erwähnten Publikation.)

Was das seitliche Knicken des Druckgurtes oder das Kippen des Trägers anbetrifft, so hat der Verfasser verschiedentlich gezeigt*), dass es in vielen Einzelfällen genügt, nur einen der beiden Torsionswiderstände zu berücksichtigen, d.h. St. Venantsche Torsion oder Wölbtorsion. In diesem Fall befindet man sich immer auf der sicheren Seite. Will man beide Widerstände nutzen, so werden die beiden kritischen Spannungen vektoriell addiert, um die resultierende kritische Spannung zu finden. Im unelastischen Bereich werden die Spannungen abgemindert, was zum bekannten Knickdiagramm führt.

Das Torsionsknicken des Druckgurtes entspricht dem Beulen einer langen, dreiseitig gelagerten Rechteckplatte, wenn von einer Einspannung des Flansches im Steg abgesehen wird. Um das Beulen des Druckgurtes als Ursache des Zusammenbruches auszuschliessen, soll das Verhältnis von Flanschbreite zu Flanschstärke zwölf plus das Verhältnis von Kipplänge zu Flanschbreite nicht übersteigen.

Im überkritischen Bereich hat der Steg die Möglichkeit, durch seitliches Ausweichen sich der erhöhten Beanspruchung zu entziehen. Um den dadurch entstehenden, zusätzlichen Flanschspannungen Rechnung zu tragen, werden die Druckflanschspannungen in hohen Stegschlankheitsgraden reduziert.

Die zulässigen Druckspannungen im Flanschschwerpunkt sind in Tabelle 1 zusammengestellt.

---

*) KOLLBRUNNER/BASLER: Torsion
Springer-Verlag, Berlin/Heidelberg/New York, 1966

Englische Uebersetzung: Torsion in Structures
Springer-Verlag, Berlin/Heidelberg/New York, 1969

Französische Uebersetzung: Torsion
Edition Spes, Lausanne, 1970

SCHUBFESTIGKEIT

Um die Schubfestigkeit zu bestimmen, wird angenommen, der Vollwandträger übernehme die Querkraft nach der Stabtheorie bis zur Beullast und darüber hinaus in Zugfeldweise bis zum Fliessen des Steges. Denkt man aber an die ursprünglichen Stegverformungen und die Eigenspannungen aus Schweissen, so erscheint es fragwürdig, zwischen diesen beiden Tragarten eine klare Grenze zu ziehen. Diese Annahme sollte daher als eine Schätzung für die Grösse des auftretenden Druckfeldes genommen werden und nicht als eine Grenze, die sich tatsächlich beobachten lässt.

Was aus Versuchen jedoch ganz klar hervorgeht, ist erstens, dass sich ein Zugfeld entwickelt; zweitens, dass die hohe Schubtragkraft ohne ein zugehöriges Druckfeld unerklärbar wird und drittens, dass ein ausgedehntes Fliessen des Steges die Grenze für die Schubtragkapazität ergibt.

Diese Festigkeitsberechnung basiert daher auf folgenden drei wesentlichen Annahmen. Einmal, dass der Schubbeitrag aus dem Diagonaldruckfeld dadurch in Rechnung gesetzt wird, dass eine Stabtragweise bis zur Beulbelastung vorhanden sei; weiter, dass mindestens über einen Teil des Steges ein reines Zugfeld überlagert werden könne und letztlich, dass die Tragkraft erreicht sei, wenn die Ueberlagerung der beiden Spannungszustände unbegrenztes Fliessen ergebe.

Ob sich ein aus Membranspannungen gebildetes Zugfeld überhaupt entwickeln kann, hängt von den Rändern des Feldes ab. Bezüglich Membranspannung ist beim Steg eines Vollwandträgers zwischen zwei sehr verschiedenen Rändern zu unterscheiden, einerseits Ränder längs den Flanschen und anderseits Ränder längs den Quersteifen. Der Flansch eines üblichen, geschweissten Vollwandträgers hat so geringe Biegesteifigkeit in Stegrichtung, dass er keine nennenswerten Vertikalspannungen aus dem Steg aufnehmen kann. Solche Flansche sollen daher gar nicht als Verankerungsmöglichkeit für ein Zugfeld in Betracht gezogen werden. Ganz anders verhält es sich längs den Steggrenzen bei den Quersteifen. Zugstreifen können dort ihre Spannungen an die Quersteife und an das anschliessende Stegfeld weitergeben.

Abgesehen von der Pfostenfunktion, d.h. Einleitung konzentrierter Lasten in den Steg, ist die Aufgabe einer Quersteife eine zweifache, nämlich den Trägerquerschnitt zu erhalten und eine überkritische Festigkeit zu erzeugen. Mit Berücksichtigung der Details längs den Flanschen, die in Figur 2 zusammengefasst werden, fordert die erste Aufgabe eine gewisse minimale Steifigkeit, die zweite dagegen eine minimale Querschnittsfläche.

Unter der Annahme einer aus zwei Teilen bestehenden Schubtragkapazität - Stabtragweise bis zur kritischen Schubspannung und Zugfeldtragweise bis zum Fliessen des Steges - ist es möglich, die Steifigkeits- und Festigkeitsanforderungen für die Quersteifen voneinander zu trennen. Da ein Spannungszustand gemäss der klassischen Festigkeitslehre, also entsprechend der Stabtragweise, keine Normalkraft in einer Quersteife erzeugt, wird von dieser nur verlangt, dass sie steif genug sei, um an dieser Stelle eine Knotenlinie in der Beulfigur zu erzwingen. Die Steifigkeitsanforderungen beruhen gemäss den bisherigen Normen auf solchen Ueberlegungen, und so ist durch ihre Beachtung eine hinreichende Steifigkeit gewährleistet. Für den Zugfeldanteil muss die Quersteife jedoch die Vertikalkomponente der geneigten Zugspannungen aus dem Steg entnehmen und auf die andere Trägerseite übertragen.

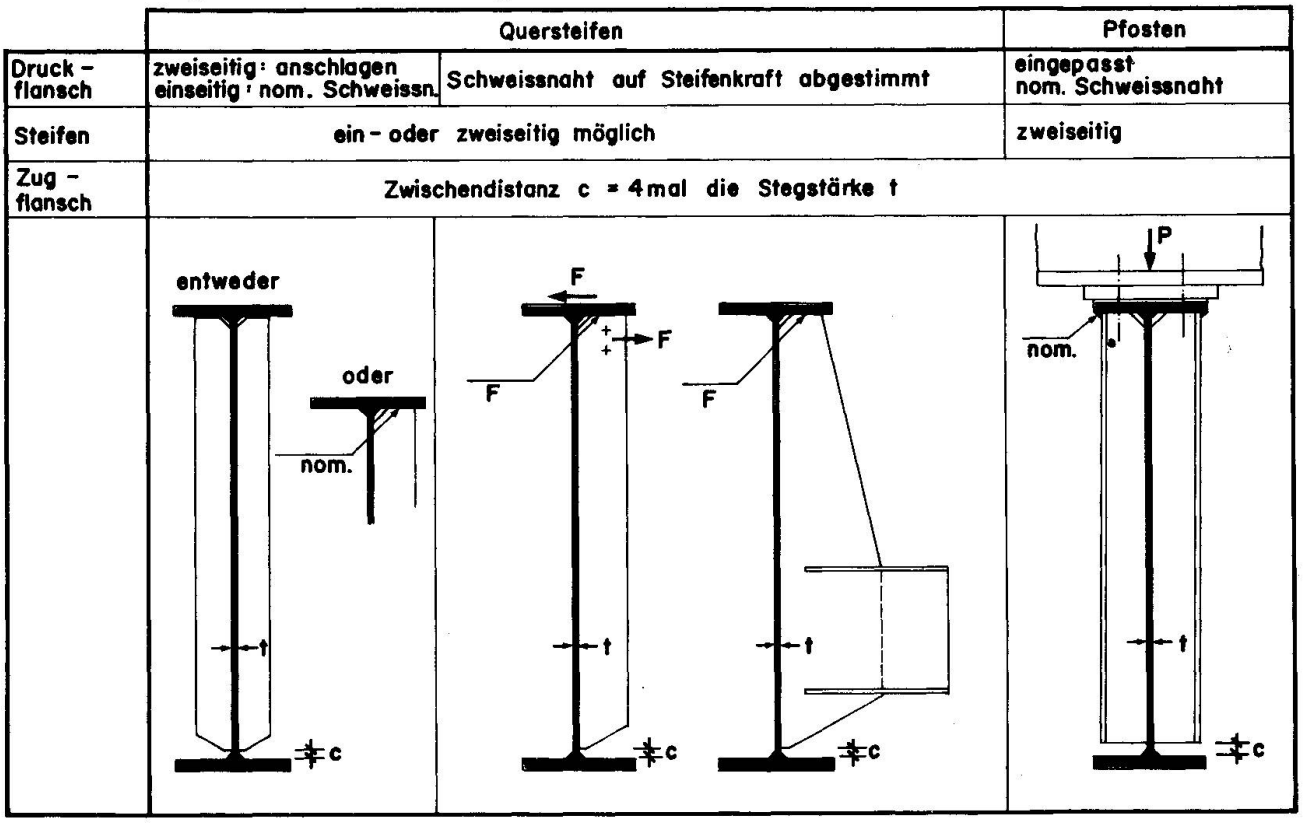

Figur 2 Zusammenfassung der Empfehlungen für die Ausbildung von Steifen

Die zulässigen Schubspannungen und die erforderlichen Quersteifenflächen sind in Tabelle 2 zusammengestellt. Im Bereich sehr hoher Schlankheitsgrade sollte der Quersteifenabstand nicht beliebig gross gewählt werden, auch dann nicht, wenn der Steg in der Lage wäre, die hier berechnete Querkraft mit dem vorgesehenen Sicherheitsgrad zu übernehmen. Die Verformungen bei der Herstellung, zum Teil aber auch unter der Belastung, werden schwierig zu begrenzen sein. In Anlehnung an amerikanische Erfahrungen wird daher für den hohen Bereich der Schlankheitsgrade eine Begrenzung gemäss folgender Ungleichung vorgeschlagen:

$$\beta \leq 150 + \frac{100}{\alpha}$$

Ob die hier abgesteckten Grenzen ausgenützt werden sollen, kann erst die Erfahrung in der Fabrikation und Montage lehren. Es sei betont, dass diese Grenzen hinsichtlich Festigkeitseigenschaften sogar überschritten werden könnten.

Für das Endfeld eines Trägers liegen andere Randbedingungen vor als in Zwischenfeldern. Hier ist kein anschliessendes Stegfeld, in welches das Zugfeld einmünden könnte. Deshalb muss ein Trägerende so ausgebildet werden, dass die Schubspannungen im Endfeld kleiner bleiben als die zulässigen Beulspannungen, oder dass bei Ueberschreiten der Schubspannungen über die zulässigen Beulspannungen diese Differenz näherungsweise als gleichmässig verteilte horizontale Belastung vom Endpfosten aufgenommen werden kann.

KOMBINATION VON BIEGUNG MIT SCHUB

Beim Zusammenwirken von Biegung mit Schub ist die Neuverteilung der Spannungen und Kräfte über einen Querschnitt aus zwei Gründen möglich. In sehr schlankem Steg ist die Veränderung der Spannungsverteilung auf die Stegdurchbiegungen zurückzuführen. Kleine Ausbiegungen des Steges aus seiner Ebene bewirken, dass der Widerstand des Steges gegenüber Biegemomenten abnimmt und die Flanschen dafür aufkommen. Das geschieht ohne Verlust der Schubtragkapazität, welche aus einem Zugfeld entsteht. In Trägern mit kräftigeren Stegen wird das Biegemoment, welches der Steg, da er die Schubfunktion zu übernehmen hat, nicht mehr aufnehmen kann, durch Fliessen in die Flanschen übertragen.

Aus diesen Gründen können die Verträglichkeitsbedingungen bei der Bemessung von Vollwandträgern unbeachtet gelassen werden. Das Verfahren entspricht daher demjenigen der plastischen Berechnungsmethoden, bei denen ein unterer Grenzwert der Tragkapazität erhalten wird, indem mögliche Gleichgewichtszustände konstruiert werden, die an keinem Ort die Fliessbedingung verletzen.

Das Zusammenwirken von Biegung und Schub in Vollwandträgern wird nur dann in Betracht gezogen, wenn sowohl die Schubspannung 60 % des zulässigen Wertes überschreitet als auch die Biegespannung über drei Vierteln des zugestandenen Wertes liegt. In diesem Bereich werden die Spannungen reduziert. Die Interaktionskurve ist eine Gerade. Bei diesen Ueberlegungen wird angenommen, der Flansch werde durch reines Fliessen versagen, oder die Flanschen können, ohne vorher instabil zu werden (sei es durch Kippen, Beulen oder senkrechtes

Einknicken des Druckflansches) bis zum Fliessen gestaucht werden. Diese Einschränkung wird nun aufgehoben und die Frage aufgeworfen, wie die unter reiner Biegung hergeleiteten drei Stabilitätsfälle geändert werden müssen, um dem Fall der kombinierten Beanspruchung von Biegung und Schub gerecht zu werden.

Die Anwesenheit von Schub gegenüber reiner Biegung hat sowohl einen Nachteil wie einen Vorteil. Der Vorteil ist dadurch bedingt, dass Vorhandensein von Schubkräften nur möglich ist, wenn ein Abfallen der Momente vorkommt, so dass immer nur ein kurzes Trägerstück dem grössten Biegemoment, das bei der Bemessung betrachtet wird, unterworfen ist. Der Nachteil besteht darin, dass der Steg, der bereits durch Schub voll ausgenützt ist, nicht gleichzeitig das ihm zugewiesene Biegemoment übernehmen kann; deshalb ist es den Flanschen überlassen, dafür aufzukommen. Das führt zur vorstehend angegebenen Reduktion bei Interaktion.

Hinsichtlich Kippen entsteht der ungünstigste Fall, wenn ein ganzes Trägerstück unter gleichem Biegemoment steht. Sobald ein Momentengradient vorhanden ist, kann die kritische Spannung - errechnet am meistbeanspruchten Querschnitt - gegenüber derjenigen, die sich für reine Biegung ergäbe, erhöht werden, und zwar um einen Multiplikationsfaktor C, der in Tabelle 1 angegeben ist.

Um vorzeitiges Versagen infolge Beulen und senkrechtes Einknicken des Druckgurtes auszuschliessen, müssen die oben genannten Bedingungen eingehalten werden.

VERSCHIEDENES

Alle bisherigen Betrachtungen beziehen sich auf die statische Tragkapazität von querausgesteiften, symmetrisch ausgebildeten Vollwandträgern, die ganz aus ein und demselben Material angefertigt sind. Allerdings ist der Fall mit unendlich grossem Steifenabstand dabei eingeschlossen, d.h. ohne Quersteifen ausgebildete I-Profile. Die folgenden Abschnitte geben nun einen Ausblick in Bereiche, in denen diese Einschränkungen aufgehoben werden. Es sei hier auf die ausführlichen Literaturangaben in der obengenannten Publikation "Vollwandträger" hingewiesen.

1. Hybride Träger

Träger, die aus Stählen verschiedener Qualität zusammengesetzt sind, werden als hybrid bezeichnet. Praktisch sind es geschweisste I-Profile oder Vollwandträger, deren Stege aus einem Stahl mit geringerer Fliessgrenze bestehen als die Flanschen. Die Anwendung hybrider Träger darf nach den amerikanischen Versuchen durchaus empfohlen werden, wobei die Fliessgrenzen der Stähle in bescheideneren Verhältnissen gehalten werden als die für die Versuchsträger gewählten. Für die Bemessung wird hier erstmals folgender, auf der sicheren Seite liegender Vorschlag gemacht:

An Vollwandträgern oder I-Profilen, deren Stegmaterial eine Fliessgrenze $\sigma_{fl,s}$ besitzt, die kleiner ist als diejenige der Flanschen, $\sigma_{fl,f}$, soll der Spannungsnachweis am entsprechenden nichthybriden Träger mit den Materialeigenschaften der Flanschen möglich sein. Hierbei ist für den Spannungsnachweis die Stegstärke mit einem im Verhältnis der Stegfliessspannung zur Flanschfliessspannung abgeminderten Wert einzusetzen.

$$\text{hybride Träger:} \qquad t_s^* = t_s \, \frac{\sigma_{fl,s}}{\sigma_{fl,f}}$$

Diese Formulierung bewirkt nicht nur einen stetigen Uebergang von gewöhnlichen zu hybriden Trägern, sondern sie schätzt die Grenzkapazität Q_p und M_p richtig ein. Ausserdem führt diese Auffassung bei schlanken Stegen zu etwas konservativeren Werten als wenn die effektive Stegstärke und die entsprechend kleinere Fliessgrenze dem Nachweis zugrunde gelegt würden. Das wäre ein Entgegenkommen bei Zusammenwirken von Biegung und Schub, das – wenn auch nicht aus Versuchen erforderlich, so doch in unserer Vorstellung wünschenswert erscheint.

2. Längssteifen

Längssteifen sollten eingeschweisst werden, wenn der Stegschlankheitsgrad über der in der Tabelle 2 für $\tau_{zul} = 0$ angegebenen Schranke liegt. Auch schon unterhalb dieser Grenze kann die Längssteife wirtschaftlich werden, weil sie verhindert, dass sich die im Druckbereich liegenden Stegstreifen der Spannungsaufnahme aus Biegemomenten entziehen. Man sollte sich auf eine Längssteife nur dann verlassen, wenn sie der Biegetragkapazität der Träger entsprechend bemessen wird.

Ein auf der sicheren Seite liegendes Konzept wird nachstehend beschrieben. Dabei wird die Axialspannung in der Steife berücksichtigt. Diese ist bestimmt durch die Knickspannung des Druckgurtes. Die Längssteife mit dem zu stabilisierenden Stegstreifen von etwa zweimal 30 t_s (wobei t_s die Stegstärke ist) sollten einen Schlankheitsgrad aufweisen, der garantiert, dass die Normalspannung aus Biegung, die in ihrem Abstand von der neutralen Achse vorkommt, bis

zum Versagen des Druckflansches erhalten bleibt. Man geht vom Schlankheitsgrad des Druckgurtes aus, der auch dann noch über den Flanschquerschnitt zusammen mit einem Sechstel der Stegfläche ermittelt werden soll, wenn die Stabilisierung der Längssteife über Zwischenquersteifen erfolgt (diese wiederum müssen von den Flanschen gehalten werden) und bestimmt so die Knickspannung, die Normalspannung auf der Höhe der Längssteife und mit dieser minimal erforderlichen Knickspannung den Steifenschlankheitsgrad.

Diese Auffassung wird im allgemeinen kräftigere Längssteifen erfordern als dies nach der Beultheorie verlangt wird, um eine Knotenlinie am Ort der Steife in der Beulfigur zu erzwingen. Es geht aber nicht an, dass für Beulen an eine Spannungsumlagerung appelliert wird, um kleine Sicherheitsfaktoren einzuführen und gleichzeitig die das Beulfeld einfassenden Glieder nach derselben Theorie zu bemessen. Weil die Tragkapazität eines Vollwandträgers zur Beullast eines Stegfeldes nicht in einer festen Beziehung steht, ist es auch nicht richtig, diese erhöhte Steifenanforderung auf Beulberechnungen allein zu bemessen: sie sollen bis zum Erschöpfen des ganzen Trägerabschnittes ihre Funktion erfüllen - oder aber nicht in Rechnung gestellt werden, d.h. die sich in der Nähe der Traglast einstellende Spannungsumlagerung mit der Abminderung der zulässigen Gurtspannung gemäss Tabelle 1 ist auch im Falle unzureichender Längssteifen anzuwenden. Der Stegschlankheitsgrad des gesamten Trägers mit einer Längssteife soll den Wert 450 nicht überschreiten.

Der Schubsicherheitsnachweis besteht darin, die zulässigen Schubspannungen der einzelnen Stegfelder zu bestimmen, mit ihren Teilquerschnitten des Steges zu multiplizieren und die Teilquerkräfte aufzusummieren. Ein einfacherer Schubnachweis am gesamten Steg würde darin bestehen, die günstige Wirkung der Längssteifen auf die Schubtragkapazität zu vernachlässigen.

Der neueste Vorschlag des American Iron and Steel Institute für den Entwurf von Strassenbrücken sieht vor, dass mit Rücksicht auf Ermüdung eine Längssteife im Fünftelspunkt des Steges eingebaut werden soll, wenn der Stegschlankheitsgrad $\beta = 200$ für Stahl 24/37 und $\beta = 160$ für Stahl 36/52 überschritten wird. Als obere Grenze mit einer Längssteife wird $\beta = 400$ für Stahl 24/37 und $\beta = 320$ für Stahl 36/52 angegeben. Der Schubnachweis wird am gesamten Stegfeld ohne Berücksichtigung der Längssteife durchgeführt.

3. Ermüdung

Ermüdung braucht im Stahlhochbau selten beachtet zu werden. Es ist umstritten, ob sie im Strassenbrückenbau ein Problem darstellt, denn in letzter Zeit sind praktisch keine Ermüdungsbrüche an Strassenbrücken bekannt geworden. Die nachfolgenden Gedanken haben daher mehr Bedeutung für den Eisenbahnbrückenbau.

Gegenüber Walzprofilen besteht ein Unterschied in Vollwandträgern mit schlanken Stegen darin, dass der Steg unter Belastung seitlich ausbiegt. Bei wiederholter Belastung bewegt er sich seitlich synchron mit der Belastung. Zufolge dieses Pumpeffektes ist es möglich, längs den Schweissnähten an einem Stegfeldrand Ermüdungsrisse zu erzeugen, die auf Plattenbiegung und nicht auf Membranspannungen zurückzuführen sind. Ob und wo solche Ermüdungsrisse auftreten hängt von der ursprünglichen Form der seitlichen Stegausbiegung ab, aber auch von der Art der Beanspruchung des Stegfeldes.

Es ist sehr schwierig, trotz dieser langjährigen Forschung, bei der Vollwandträger mit schlanken Stegen in natürlicher Grösse auf Ermüdung beansprucht wurden, zu einem abschliessenden Urteil zu kommen, weil zahlreiche Aspekte einen Einfluss ausüben. Immerhin liegen genügend Daten vor um festzustellen, dass diese Art Ermüdung nicht von grösserer Bedeutung ist als Details in jeder geschweissten Konstruktion, wie dies z.B. längs Quersteifen oder am Ende von Lamellen der Fall ist. Wenn also mit den in den Schweizer Stahlbaunormen festgelegten Ermüdungsvorschriften zufriedenstellende Erfahrungen gemacht worden sind, so dürfen sie in unveränderter Form auch für Vollwandträger mit Zugfeldtragweise angewendet werden. Als zusätzliche Massnahmen wird vorgeschlagen, den Bereich der Stegschlankheitsgrade gegenüber dem im Stahlhochbau üblichen etwas einzuschränken.

Unter den vielen Details, die im Laboratoriumsversuch an geschweissten Vollwandträgern zu Ermüdungsbrüchen Anlass geben können, sind es nach wie vor Enden von aufgeschweissten Lamellen, welche am raschesten versagen. Die Lamellen müssen über das theoretische Ende hinaus entsprechend ihrer Lamellenkraft angeschlossen werden, und zwar über eine Länge von 1,5 mal die Lamellenbreite, falls eine Stirnnaht gewählt wird, oder zweimal die Lamellenbreite, wenn auf eine solche verzichtet wird. Hinsichtlich Ermüdung ist zwischen den beiden Ausführungsarten kein merklicher Unterschied zu erkennen; im allgemeinen lohnt es sich auch nicht, verschiedene Lamellenverjüngungen vorzunehmen.

4. Verbundträger

Durch den Verbund verschiebt sich die neutrale Achse namhaft aus der Stegmitte heraus. Bezüglich der Schubtragkapazität hat das aber keinen Einfluss, und die dort hergeleiteten Formeln haben auch für Verbundträger Gültigkeit. Im Bereich der positiven Momente ist der Druckgurt durch die Betonplatte ideal gestützt. Der Obergurt kann weder seitlich ausknicken noch beulen. Bezüglich Querbelastung des Vollwandträgers aus der Fahrbahnplatte darf angenommen werden, dass der Lastüberschuss, der nicht durch den Steg direkt in den Träger eingeleitet werden kann, über die Quersteifen, welche in diesem Falle durch Schweissnähte am Druckgurt angeschlossen werden sollten, in den Vollwandträger eingeleitet werden. Die Platte müsste dann über den Steifenabstand für diesen Belastungsüberschuss selbsttra-

gend sein. Im Bereich der negativen Momente entsteht eine umhüllende Kurve aller Stegdruckspannungen, die weit über die halbe Trägerhöhe hinaufreicht. Hinsichtlich seitlichem Knicken als auch Spannungsabminderung sollte in solchen Fällen mit einem fiktiven Steg von der doppelten Grösse des Neutralachsenabstandes vom Druckgurt gerechnet werden. Es kann sein, dass sich in solchen Zonen der Einbau einer Längssteife lohnt; im allgemeinen ist auch ein näherer Abstand der Queraussteifung angezeigt.

BEMESSUNGSREGELN

Die nachstehenden Bemessungsregeln basieren auf dem üblichen Konzept der zulässigen Spannungen. Diese sind so angesetzt, dass ein Sicherheitsfaktor s gegenüber der Traglast eingehalten ist. Die Bezeichnung St.37 und St.52 wird entsprechend einer Neufassung der SIA-Norm No. 161 durch die Angabe der Fliessspannung ergänzt, somit: Stahl 24/37 bzw. 36/52. Der übliche Sicherheitsfaktor s = 1,5 für die Biegefestigkeit kann für den normalen Spannungsnachweis beibehalten werden. Für die zulässigen Schubspannungen wird s = 1,65 eingesetzt, um jene Fälle auszuschliessen, bei denen ein Schubversagen vor Erreichen der Biegetragkapazität eintreten könnte.

Die Bauwerksklassen II (Strassenbrücken) und III (Eisenbahnbrücken) unterscheiden sich in der Schweiz von Klasse I (Hochbauten) durch Berücksichtigung der Ermüdung. Hier wie in den DIN-Normen ist das Verhältnis der Grenzbeanspruchungen A/B = $\min\sigma/\max\sigma$ für die Ermüdung massgebend, wobei Zugspannungen positive und Druckspannungen negative Werte aufweisen.

Die Festsetzung zulässiger Spannungen des Dauerfestigkeitsnachweises geht dahin, die für den normalen Spannungsnachweis gültigen Werte mit den nachstehend zusammengestellten Reduktionsfaktoren zu verkleinern.

Nach den zurzeit in der Schweiz beachteten Regeln ist die Spannungsabminderung infolge Ermüdung für die beiden Stahlqualitäten St.37 und St.52 nach SIA-Norm No. 161, Art. 23 bzw. den TKSSV-Empfehlungen (Stahlbaubericht No. 21, September 1965) durchzuführen.

Gemäss der jüngsten, erst im Entwurf vorliegenden Fassung der Schweizer Stahlbaunormen, sind für Bauwerksklasse II nur 60 % der gleichmässig verteilten Nutzlast, also 0,6 p, für die Erhebung des Verhältnisses A/B einzuführen, wohl aber die vollen Achslasten, somit: g, 0,6 p, P.

Aus diesem Vorschlag entnimmt man folgende Reduktionsfaktoren der zulässigen Spannungen infolge Ermüdung, R_{erm}(Stahl,Kl.): (Werte $R_{erm} > 1$ sind nicht massgebend)

	Stahl 24/37	Stahl 36/52
Bauwerksklasse II	$R_{erm} = \frac{1,4/1,6}{1 - 0,4\ A/B}$	$R_{erm} = \frac{1,8/2,4}{1 - 0,55\ A/B}$
Bauwerksklasse III	$R_{erm} = \frac{1,2/1,4}{1 - 0,4\ A/B}$	$R_{erm} = \frac{1,5/1,9}{1 - 0,55\ A/B}$

Für den Lastfall HZ werden die zulässigen Spannungen erhöht. Bei den Bauwerksklassen I und III ist die Erhöhung ein Achtel, unabhängig von der Stahlqualität. Bei Bauwerksklasse III sind die Erhöhungsfaktoren 1,6/1,4 für Stahl 24/37 und 2,1/1,9 für Stahl 36/52.

Zusammenfassend kann gesagt werden, dass die Bemessung querausgesteifter Vollwandträger in der Einhaltung nachstehend gegebener zulässiger Spannungswerte besteht.

a) Ausgangswerte (Bauwerksklasse I, Fall Hauptbelastung)

1. Die zulässige Schwerpunktspannung des Druckgurtes ist für einen Stahl mit beliebiger Fliessgrenze aus den in Tabelle 1, Zeile 1, analytisch festgehaltenen Werten mit s = 1,5 zu bestimmen. Damit ist eine Kippsicherheit von mindestens 1,5 garantiert. Ein Beulnachweis ist nicht durchzuführen. Dagegen sind im Bereiche hoher Schlankheitsgrade β (über β_o = 180 bei Stahl 24/37 oder β_o = 150 bei Stahl 36/52) - falls keine Längssteifen hinreichender Festigkeit eingezogen werden - die zulässigen Druckspannungen um $0,05(\beta - \beta_o)F_S/F_f$ Prozent zu reduzieren. Dabei bedeuten F_S die Stegfläche und F_f die Fläche des Druckflansches.

2. Die beiden extremen Faserspannungen dürfen σ_{zul} = 1,6 t/cm2 für Stahl 24/37 und 2,4 t/cm2 für Stahl 36/52 nicht überschreiten. Allgemein formuliert sollen sie höchstens $\sigma_{zul} = \sigma_{fl}$ /1,5 werden.

3. Die durchschnittlichen Schubspannungen im Steg, $\tau = Q/F_S$, müssen kleiner bleiben als die zulässigen Schubspannungen, die aus der Aufstellung in Tabelle 2 mit s = 1,65 zu berechnen sind.

4. Bei kombinierter Beanspruchung durch Biegung und Schub ist die Einhaltung nachstehender Bedingung dann zu überprüfen, wenn im gleichen Trägerquerschnitt $\sigma_{vorh} \geq 0,75\ \sigma_{zul}$ als auch $\tau_{vorh} \geq 0,6\ \tau_{zul}$ sind:

$$\frac{\sigma}{\sigma_{zul}} = 1.375 - 0.625\,\frac{\tau}{\tau_{zul}}$$

Hierin sind σ und τ ein gleichzeitig auftretendes Paar von Flansch- und Stegspannungen, und σ_{zul} und τ_{zul} die unter Punkt 2 und 3 festgelegten Werte.

In der eingangs erwähnten Publikation "Vollwandträger" sind die unter 1 und 3 genannten zulässigen Spannungen für Stahl 24/37 und für Stahl 36/52 tabelliert.

b) Bauwerksklassen und Lastfälle

Werden die unter a) festgelegten zulässigen Spannungen als Ausgangswerte mit S und die in oben zusammengestellten Reduktionsfaktoren für Ermüdung mit R_{erm} bezeichnet, so sind die Ausgangswerte σ_{zul} und τ_{zul} unter obigen Punkten 2, 3 und 4 mit diesen Reduktionsfaktoren zu multiplizieren, um der Ermüdung Rechnung zu tragen. Die in Punkt 1 des Abschnittes a) festgehaltenen Druckspannungen sind nicht mit R_{erm} zu multiplizieren, da sie auf Stabilitätskriterien und nicht auf Festigkeitsbetrachtungen basieren.

Um auch andere Bauwerksklassen und Lastfälle zu erfassen, entsteht - bezogen auf die Ausgangswerte S - folgender Abänderungsschlüssel für die verschiedenen Bauwerksklassen und Lastfälle.

Abänderungsschlüssel für Bauwerksklassen und Lastfälle, bezogen auf Klasse I, Fall Hauptbelastung: S(Stahl) = zulässige Normal- und Schubspannungen nach a), R_{erm}(Stahl,Kl.) = Reduktionsfaktor für Ermüdung, der auf die σ_{zul} und τ_{zul} der Punkte 2, 3 und 4 anzuwenden ist.

Bauwerksklasse	Fall	Lastfall H Eigengewicht, Nutzlast Schnee, dyn. Belastung	Lastfall HZ H + Windlast Bremskr.,Temp. Schwinden
I	Stahl 24/37	S(24/37)	$\frac{9}{8}$S(24/37)
	Stahl 36/52	S(36/52)	$\frac{9}{8}$S(36/52)
II	Stahl 24/37	S(24/37)·R_{erm}(24/37,II)	$\frac{9}{8}$S(24/37)
	Stahl 36/52	S(36/52)·R_{erm}(36/52,II)	$\frac{9}{8}$S(24/37)
III	Stahl 24/37	$\frac{1,4}{1,6}$S(24/37)·R_{erm}(24/37,III)	S(24/37)
	Stahl 36/52	$\frac{1,9}{2,4}$S(36/52)·R_{erm}(36/52,III)	$\frac{2,1}{2,4}$S(36/52)

c) Konstruktive Gesichtspunkte

(Zusammenfassung der wichtigsten Gestaltungsregeln)

- Druckflansche mit Rechteckquerschnitten sollen mit ihrem Flanschbreite- zu Flanschstärkeverhältnis "zwölf plus das Verhältnis von Kipplänge zu Flanschbreite" nicht übersteigen.

- Querausgesteifte Vollwandträger sollen nicht über ein Stegschlankheitsverhältnis von $\beta_{Grenz} = 360$ bei Stahl 24/37 oder $\beta_{Grenz} = 240$ bei Stahl 36/52 ohne Längssteifen gebaut werden, um Einknicken des Druckgurtes in den Steg zu vermeiden. Wird die äussere Belastung nicht durch Quersteifen in den Träger eingeleitet, sondern der Steg direkt querbelastet, so ist diese Grenze entsprechend weiter zu reduzieren. Im Brückenbau sollen, mit Rücksicht auf Ermüdung, die im Abschnitt über Längssteifen angegebenen Grenzen nicht überschritten werden.

- Unabhängig von Bauwerksklasse oder Lastfall sollten symmetrisch angeordnete Quersteifen zusammen einen Querschnitt aufweisen, der den in der Tabelle 2 eingetragenen Prozentsatz der Stegfläche erreicht. Für einseitige Winkelsteifen mit am Steg anliegendem Schenkel ist dieser Wert auf das 1,8fache zu vergrössern, für eine einseitige Steife mit Rechteckquerschnitt auf das 2,4fache. Bei ungleichen Stählen sind diese Steifenquerschnitte noch mit dem Verhältnis von Stegfliessspannung zu Steifenfliessspannung zu multiplizieren. Wenn die grösste Schubspannung in einem die Steife flankierenden Stegfeld den zulässigen Wert nicht erreicht, so dürfen alle Werte im entsprechenden Verhältnis reduziert werden. In jedem Falle darf ein Stegstreifen von 12 t zum Steifenquerschnitt mitgerechnet werden.

- Ausserdem sollen Quersteifen die nach DIN 4114/2 Ri 18.1 geforderten Mindeststeifigkeiten aufweisen oder, nach AISC/Art. 1.10.5, $I_{erf} = (b/50)^4$ für symmetrische und unsymmetrische Steifen bezüglich der Stegachse aufweisen, wobei b die Steghöhe ist.

- In Endfeldern ist der Quersteifenabstand so zu wählen, dass $\tau_{vorh} = \tau_{cr}/1{,}65$ ist, oder der Endpfosten soll gemäss Abschnitt "Schubfestigkeit" ausgebildet werden.

- Eine Längssteife ist in folgenden Fällen erforderlich:

  a) Wenn der Stegschlankheitsgrad $\beta \geq 150 + 100/\alpha$ ist, um Fabrikationsschwierigkeiten bei allzu schlanken Stegen zu vermeiden.

  b) Wenn Ermüdung massgebend ist bei $\beta = 200$ für Stahl 24/37 bzw. $\beta = 160$ für Stahl 36/52.

- Bei unsymmetrischen Trägern sind die unter Punkt 1 des Abschnittes a) festgelegten Spannungen an einem fiktiven Steg der doppelten Höhe des Neutralachsenabstandes vom Druckgurt zu erheben.

Tabelle 1 Kippnachweis

Torsions-widerstand	Zulässige Druckspannungen im Flanschschwerpunkt	
	unelastischer Bereich	elastischer Bereich
Wölbtorsion	$\frac{\sigma_{fl}}{s}\left(1-\left(\frac{l}{r}\right)^2\frac{\varepsilon_{fl}}{4C\pi^2}\right)$ für $\frac{0.17\pi}{\sqrt{\varepsilon_{fl}}}<\frac{l}{r}<\sqrt{\frac{2C\pi^2}{\varepsilon_{fl}}}$ $\frac{\sigma_{fl}}{s}$ für $\frac{l}{r}<\frac{0.17\pi}{\sqrt{\varepsilon_{fl}}}$	$\frac{\sigma_{fl}}{s}\frac{C\pi^2}{\left(\frac{l}{r}\right)^2\varepsilon_{fl}}$ für $\frac{l}{r}>\sqrt{\frac{2C\pi^2}{\varepsilon_{fl}}}$
St. Venantsche Torsion	$\frac{\sigma_{fl}}{s}\left(1-\frac{\varepsilon_{fl}\, l\, b}{2.6\, F_f\, C}\right)$ für $0<\frac{lb}{F_f}<\frac{1.3C}{\varepsilon_{fl}}$	$\frac{\sigma_{fl}}{s}\frac{0.65\, F_f\, C}{\varepsilon_{fl}\, l\, b}$ für $\frac{lb}{F_f}>\frac{1.3C}{\varepsilon_{fl}}$
Gemischte Torsion	$\frac{\sigma_{fl}}{s}\left[1-\frac{\sigma_{fl}}{4C\sqrt{\left(\frac{0.65E}{\frac{lb}{F_f}}\right)^2+\left(\frac{\pi^2E}{\left(\frac{l}{r}\right)^2}\right)^2}}\right]$ für $0<\lambda<\sqrt{2C}$	$\frac{C}{s}\sqrt{\left(\frac{0.65E}{\frac{lb}{F_f}}\right)^2+\left(\frac{\pi^2E}{\left(\frac{l}{r}\right)^2}\right)^2}$ für $\lambda>\sqrt{2C}$
	darin bedeutet $\lambda=\sqrt{\frac{\sigma_{fl}}{\sqrt{\left(\frac{0.65E}{\frac{lb}{F_f}}\right)^2+\left(\frac{\pi^2E}{\left(\frac{l}{r}\right)^2}\right)^2}}}$	

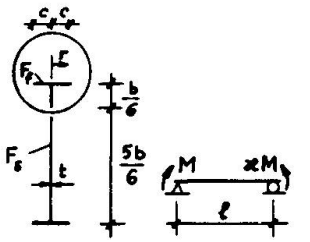

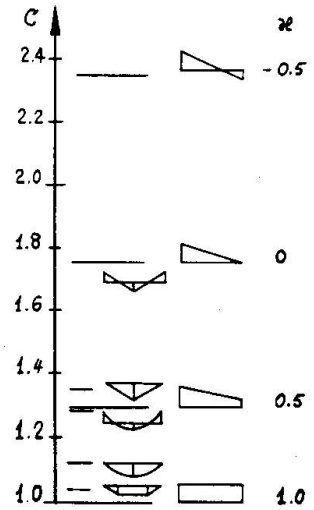

Spannungsreduktion im Stegschlankheitsbereich $6.0\sqrt{\frac{E}{\sigma_{fl}}}<\beta<\frac{0.5\,E}{\sqrt{\sigma_{fl}(\sigma_{fl}+\sigma_r)}}$: $0.05\frac{F_s}{F_f}\left(\beta-6.0\sqrt{\frac{E}{\sigma_{fl}}}\right)$ %

Es bedeuten:
- s = Sicherheitsfaktor
- σ_{fl} = Streckgrenze
- σ_r = Eigenspannung = $\sigma_{fl}/2$
- β = b/t
- r = Trägheitsradius des Druckgurtes ($F_f + F_s/6$)

K. BASLER

Tabelle 2 Schubnachweis

Zulässige Schubspannungen τ_{zul}		
wenn keine Längssteife dann = 0	$\frac{\sigma_{fl}}{s\sqrt{3}}\left(\frac{\tau_{cr}}{\tau_{fl}} + \frac{1-\frac{\tau_{cr}}{\tau_{fl}}}{\frac{2}{\sqrt{3}}\sqrt{1+\alpha^2}}\right)$	$\frac{\sigma_{fl}}{s\sqrt{3}}\frac{\tau_{cr}}{\tau_{fl}} = \frac{\tau_{cr}}{s} \leq 0.4\,\sigma_{fl}$
für $\beta > 150 + \frac{100}{\alpha}$	für $\frac{\tau_{cr}}{\tau_{fl}} \leq 1$	für $\frac{\tau_{cr}}{\tau_{fl}} > 1$

Darin bedeutet: $\frac{\tau_{cr}}{\tau_{fl}} = \frac{\pi^2\sqrt{3}\,E}{12(1-\nu^2)\sigma_{fl}}\frac{k}{\beta^2}$ gültig für $\frac{\tau_{cr}}{\tau_{fl}} \leq 0.8$

$\frac{\tau_{cr}}{\tau_{fl}} = \sqrt{\frac{0.8\,\pi^2\sqrt{3}\,E}{12(1-\nu^2)\sigma_{fl}}\frac{k}{\beta^2}}$ gültig für $\frac{\tau_{cr}}{\tau_{fl}} > 0.8$

mit: $k = 4.00 + \frac{5.34}{\alpha^2}$ wenn $\alpha \leq 1$

$k = 5.34 + \frac{4.00}{\alpha^2}$ wenn $\alpha \geq 1$

s = Sicherheitsfaktor

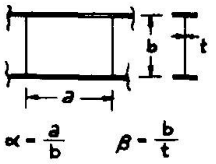

Erforderliche Gesamtquerschnittsfläche eines Quersteifenpaares:

$$F_{erf} \geq b\,t\left(1-\frac{\tau_{cr}}{\tau_{fl}}\right)\frac{\alpha}{2}\left(1-\frac{\alpha}{\sqrt{1+\alpha^2}}\right)YD$$

mit: $Y = \frac{\text{Streckgrenze des Stegmaterials}}{\text{Streckgrenze des Steifenmaterials}}$

D = 1,0 bei Steifenpaaren (= Fläche beider Steifen)
1,8 bei einseitig anliegenden Winkelsteifen
2,4 bei einseitiger Rechtecksteife

Ausserdem gilt: Mindeststeifigkeit nach DIN 4114/2, Ri 18.1

oder $I_{min} \geq \left(\frac{b}{50}\right)^4$ bez. Stegachse nach AISC

F_{erf} darf stets im Verhältnis $\frac{\tau_{vorh}}{\tau_{zul}}$ reduziert werden.

Stegsteifen von 12 t können zur Quersteifenfläche gezählt werden:
$F = (F_{erf} - 12\,t^2)$

Ultimate Load and Failure Mechanism of Thin Webs in Shear

Charge ultime et mécanisme de ruine des âmes minces cisaillées

Traglast und Tragmechanismus dünner schubbeanspruchter Stegbleche

MIROSLAV ŠKALOUD
Doc., CSc., Ing.
Senior Research Fellow
Czechoslovak Academy of Sciences
Institute of Theoretical and Applied Mechanics
Prague, Czechoslovakia

1. Introductory Remarks

This research project was designed as a continuation to the tests conducted jointly by K.C.Rockey and the writer during the stays of the latter in University Colleges of Swansea and Cardiff in 1966-9 /1/.

The objective was to obtain more detailed evidence regarding the stress state in the webs and flanges of steel plate girders in shear. Further it was regarded as useful to obtain some information about the behaviour of webs of higher width-to-thickness ratios than those tested in Swansea and Cardiff, since in modern metal structures deep and thin plate elements are encountered more and more frequently.

2. Test Girders and Apparatus

The general details of the test girders are given in Fig. 1, and Table 1a.

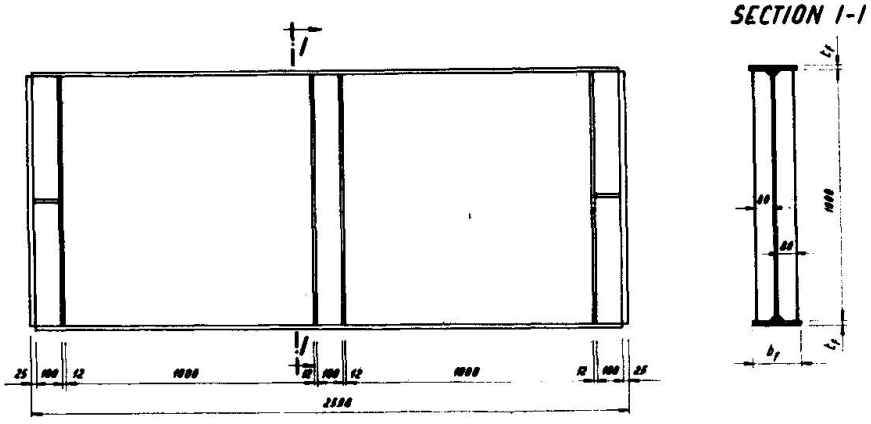

Test girder	b_f (mm)	t_f (mm)
T0 1, T0 1'	100	5
T0 2, T0 2'	200	10
T0 3, T0 3'	200	10
T0 4, T0 4'	300	20
T0 5, T0 5'	250	30

Fig. 1.

Table Ia.

Actual Geometrical Characteristics of the Flanges

Test Girder	b [mm]	t_f [mm]		I_f/a^3t		
		Lower flange	Upper flange	Lower flange	Upper flange	Average
TG 1	160	5,06	5,15	$0,69 \times 10^{-6}$	$0,729 \times 10^{-6}$	$0,709 \times 10^{-6}$
TG 1'	160	5,26	5,20	$0,775 \times 10^{-6}$	$0,75 \times 10^{-6}$	$0,762 \times 10^{-6}$
TG 2	200	10,08	10,00	$6,84 \times 10^{-6}$	$6,68 \times 10^{-6}$	$6,76 \times 10^{-6}$
TG 2'	200	10,12	10,17	$6,92 \times 10^{-6}$	$7,01 \times 10^{-6}$	$6,96 \times 10^{-6}$
TG 3	200	16,43	16,51	$29,5 \times 10^{-6}$	$29,9 \times 10^{-6}$	$29,7 \times 10^{-6}$
TG 3'	200	16,42	16,46	$29,5 \times 10^{-6}$	$29,6 \times 10^{-6}$	$29,55 \times 10^{-6}$
TG 4	200	20,16	20,18	$54,5 \times 10^{-6}$	$54,7 \times 10^{-6}$	$54,6 \times 10^{-6}$
TG 4'	200	20,13	20,20	$54,2 \times 10^{-6}$	$54,9 \times 10^{-6}$	$54,55 \times 10^{-6}$
TG 5	250	29,73	29,68	$218,5 \times 10^{-6}$	218×10^{-6}	$218,25 \times 10^{-6}$
TG 5'	250	29,72	29,73	$218,5 \times 10^{-6}$	$218,5 \times 10^{-6}$	$218,5 \times 10^{-6}$

The girders are of welded construction and manufactured from Czechoslovak mild steel of the series 37. The depth b and the thickness t of the web were kept constant, whereas the dimensions of the flange varied from girder to girder to obtain various flexural rigidities of the flange. The reader will notice that the width-to-thickness ratio b/t of the web was 400, and, therefore, larger than that of the above mentioned Swansea and Cardiff shear panels ($\frac{b}{t}$ = 150, 230 and 300). The aspect ratio was constant for all web panels; $\alpha = 1$.

All test girders were manufactured in two specimens; both having the same number, but one of them being differentiated by a dash.

The buckled pattern of the web was measured by means of a device consisting of nine rectangular frames on to which 81 dial gauges, graduated in units of 0,01 mm and capable of recording deflections up to 25 mm, were attached.

To evaluate the redistribution of stresses in the web in the post-buckled range, three sets of electric resistance strain gauges were mounted on to both sides of the web plate. Further batteries of strain gauges were attached to both sides of the upper and lower flanges, the objective being to study the influence of flange stiffness upon the bending and axial stresses in the flanges.

The material characteristics were determined by means of tensile tests and conducted in an Instron testing machine. The average material characteristics (yield point σ_y and ultimate stress σ_{ult}) are listed in Table Ib.

Table Ib.

Material Characteristics

Girder element	Yield stress σ_y [kp/mm²]	Ultimate stress σ_{ult} [kp/mm²]	Elongation (%)
Web plate	20,37	30,92	26,19 (δ_w)
Flange plate	28,62	42,67	34,05 (δ_f)

3. Buckled Pattern

We noted that the shape of the buckled surface was considerably affected by the flange stiffness. While in the case of a girder with flexible flanges merely one predominant buckling half wave forms, frequently accompanied with two small buckles at the web corners, the number of the buckling waves grows with the flexural rigidity of the flange. For a web fixed into very heavy flanges the buckles are more numerous so that they almost cover the whole web panel. Such a web thereby exhibits a tendency to behave as a tension field.

An analysis of the results also indicates that there is a certain tendency for the maximum web deflection w_{max} to diminish with the enlargement of flange stiffness. This is demonstrated in Fig. 2, where the ordinates w_{max} of girders TG 1,1 and TG 5, 5, are plotted. This over-all tendency appeared, however, to be disturbed by the effect of initial curvature and residual stress pattern, which resulted in the webs of not all test girders behaving correspondingly. For this reason it was not possible to define an optimum (from the point of view of web deflection) flange stiffness; as was so remarkably done by Rockey /2/ for his bolted test panels.

As the initial curvature and residual stress pattern in ordinary welded steel plate girders is likely to be similar to that of the author's test girders, it can be anticipated that for such structure elements it might frequently be difficult to base an optimum design of webs on the afore said elastic deflection approach. It is more promising to base the optimum design on the ultimate, plastic, behaviour of the girder. This concept was already used by Rockey and the author in /1/, /3/, and it is again followed below.

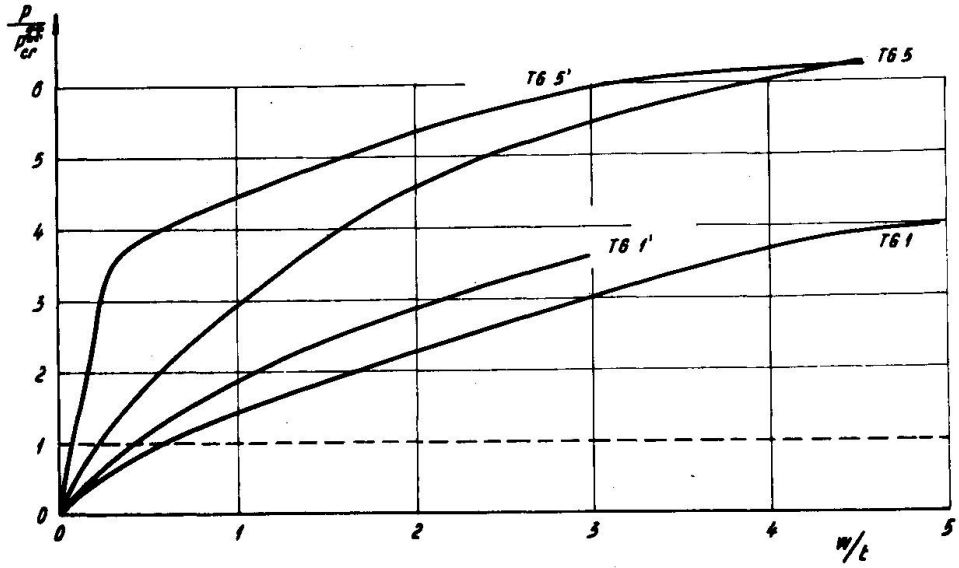

Fig. 2.

4. Stress State

4.1. Web

The strains in the web were evaluated by means of the

electric resistance strain gauges mounted on to both sides of the web of the test girders. The results relating to girders TG 1 (very flexible flanges) and TG 5 (very rigid flanges) are plotted in Fig. 3. The value ε_{cr} , corresponding to the critical load τ_{cr} of a simply supported web, and the value ε'_y , equal to σ_y / E and, therefore, relating to the yield stress σ_y of the web material, are also given in the figures for the sake of comparison. The progression of the plastification of the web is demonstrated in Fig. 4, in which the zones with plastic strain of 2 000 microstrains are plotted. Fig. 4a relates to girder TG 1, Fig. 4b to TG 3, and Fig.4 to TG 5.

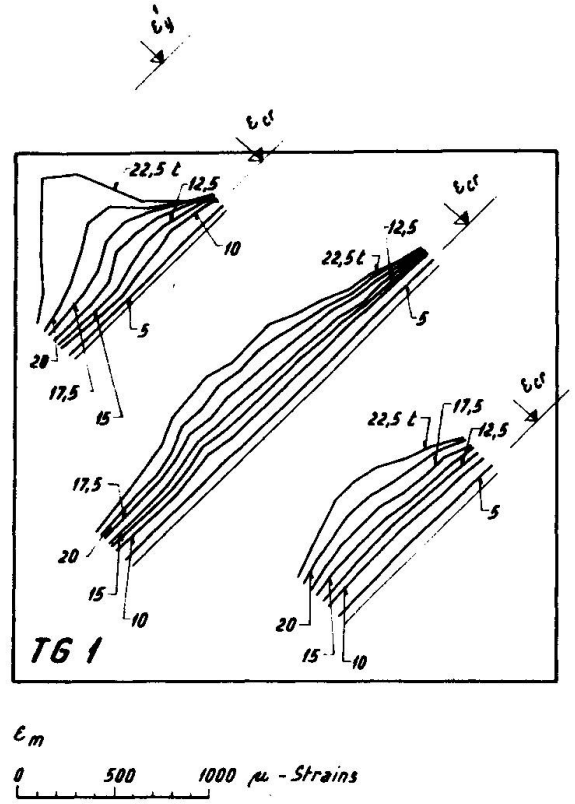

Fig. 3a.

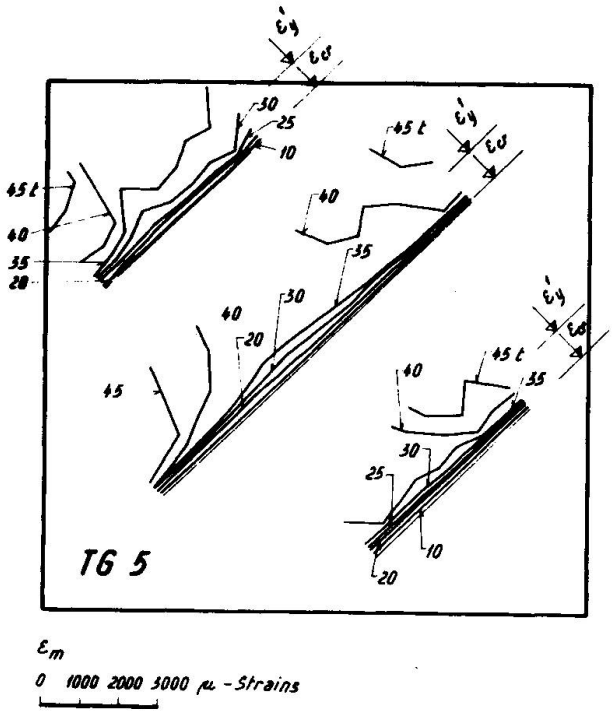

Fig. 3b.

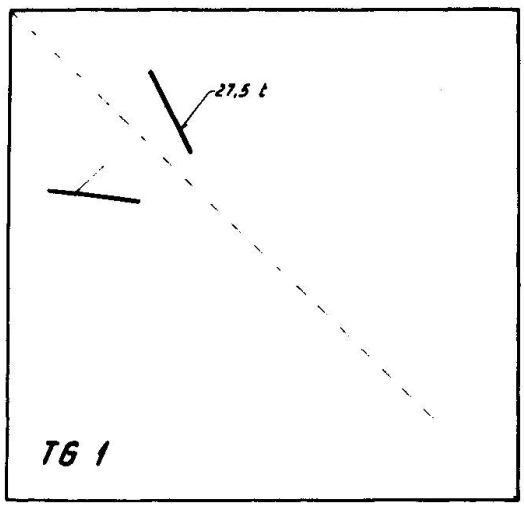

Fig. 4a.

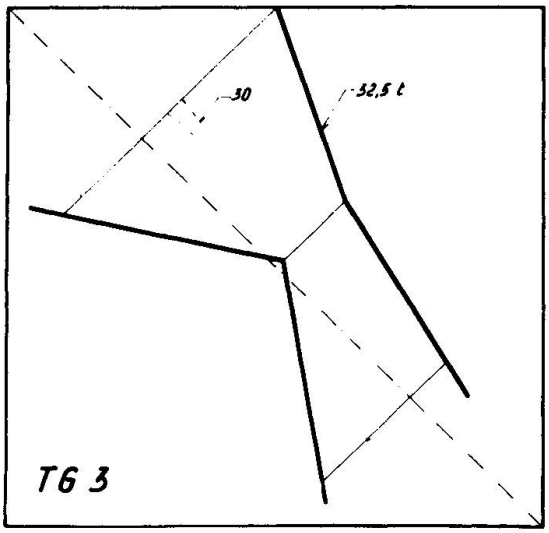

Fig. 4b.

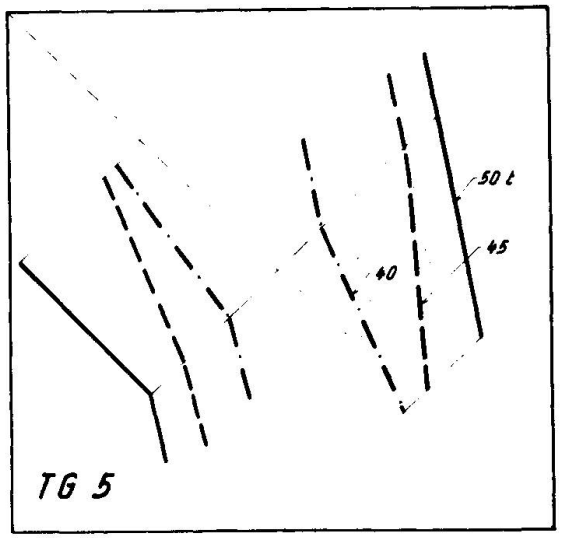

Fig. 4c.

An analysis of the results shows that a pronounced redistribution of stresses occurs in the web in the post-buckled range of its behaviour. Whereas at loads up to about the buckling load τ_{cr}, the stresses are uniformly distributed over the web ($\sigma_1 = -\sigma_2 = \tau$, σ_1 and σ_2 denoting the principal tension and compression stresses, respectively), in the postbuckled range it is the principal tension membrane stress that predominates.

Nevertheless, in the case of webs attached to flexible flanges, the stress pattern is far from a uniform tension field, whether complete or incomplete. It manifests a tendency to concentrate in a more or less narrow tension band following the tension diagonal, whereas the other web corners, situated at the ends of the compression diagonal, are idle. The more flexible are the flanges, the narrower is the tension band. As the flange stiffness increases, the width of the tension strip grows.

In the case of very heavy flanges, there is a tendency for the behaviour of the web to converge to an incomplete tension field covering the whole web. None the less, in spite of the flanges of girders TG 5 and TG 5' being very bulky, a classical incomplete tension field action has not been attained. This is a sign that the classical version of the incomplete tension field theory, established for webs fixed into completely rigid boundary elements, can very rarely be applied in the design of ordinary welded plate girders.

On the other hand, the experimental evidence shows that the tension band suggested by Basler in his very interesting contribution /4/ and assuming that its inclination equals one half of the angle of the geometrical diagonal, and that its border lines pass through the ends of the vertical stiffeners, is not fully compatible with the actual distribution of stress in a wide range of plate girder webs.

As in the preceding paragraph, where the web deformation was studied, the aforementioned analysis demonstrates the beneficial effect of flange stiffness on the post-buckled efficiency of webs in shear.

4.2. Flanges

The batteries of electric resistance strain gauges attached to both sides of each flange of the test girders enabled the bending- and axial strain occurring in the flange to be determined. The former are plotted in Fig. 5 and the latter in Fig. 6.

The bending strains demonstrate the flexure of the flange,

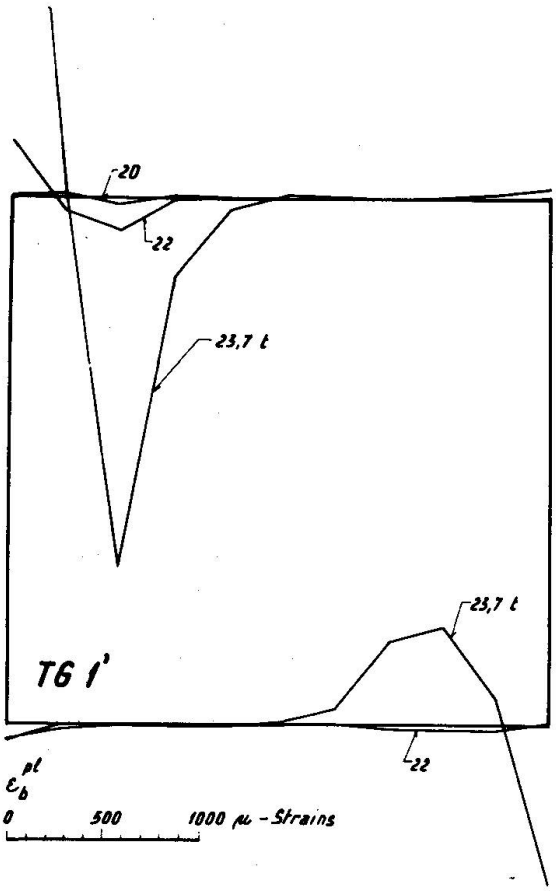

Fig. 5a.

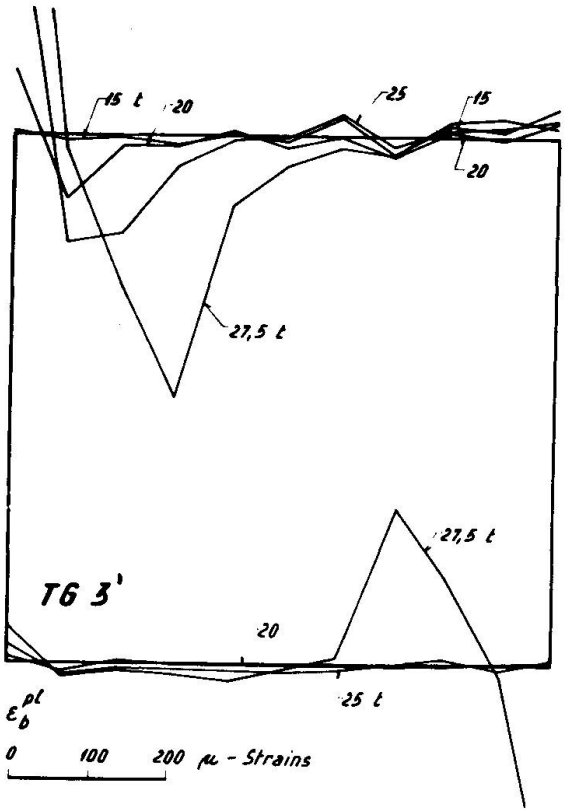

Fig. 5b.

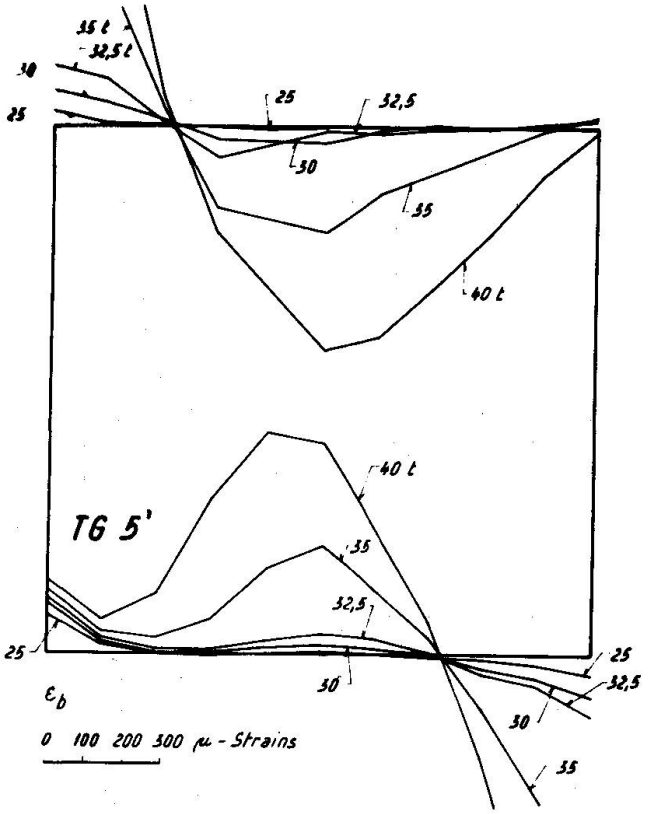

Fig. 5c.

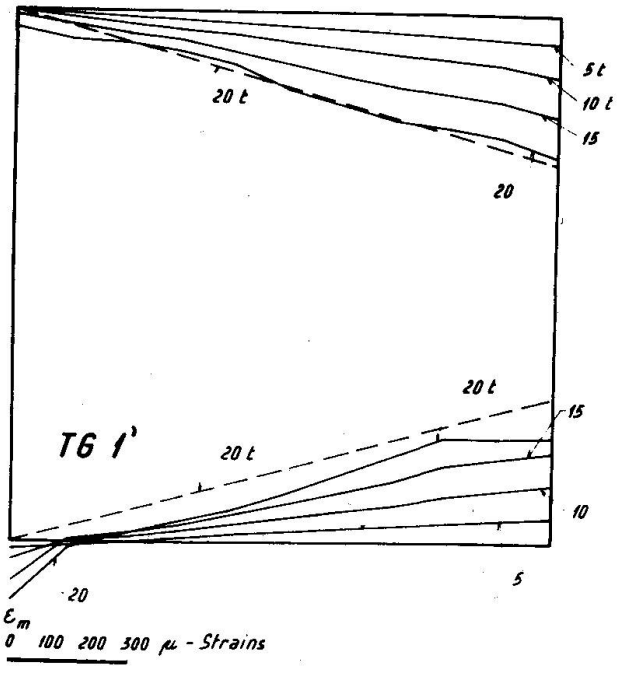

Fig. 6a.

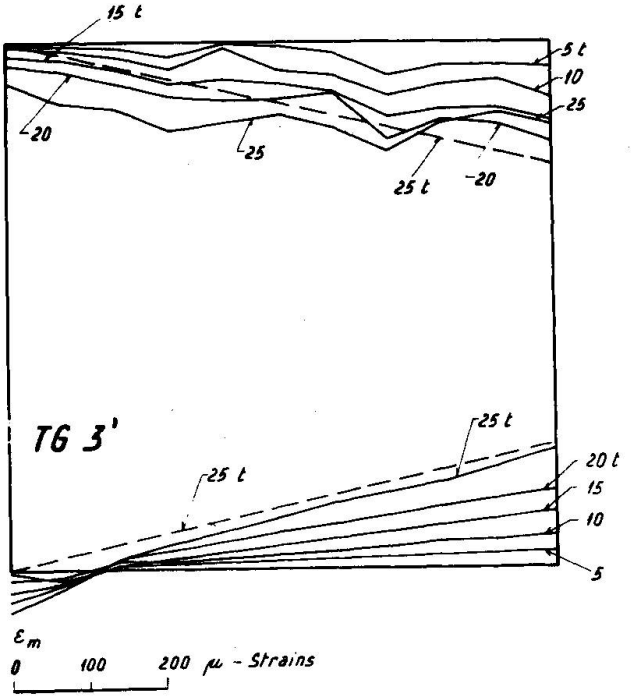

Fig. 6b.

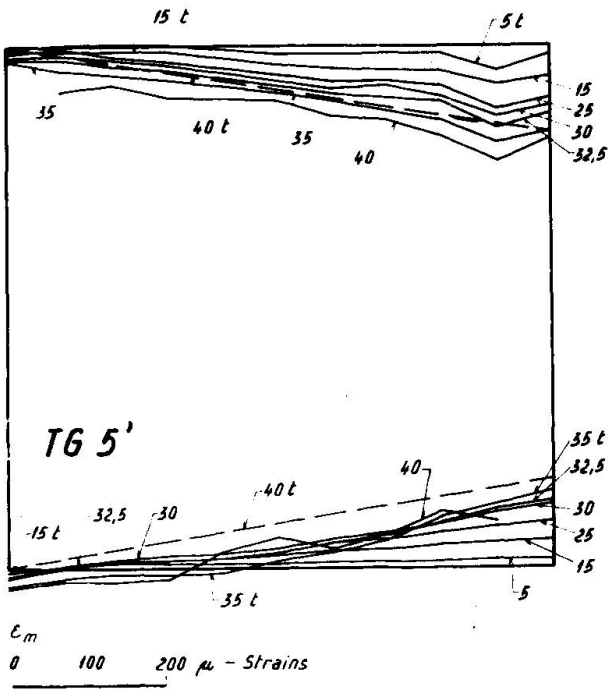

Fig. 6c.

in the middle plane of the web, under the load which is brought about by the membrane effect of the web in the post-buckled range. The bending effect is more pronounced in the compression flange than in the tension one: since compression contributes to the flange deformation and tensile stresses retard it. It can be seen that the curves have a more or less sharply defined peak, which indicates a concentration of stress in a limited portion of the flange. The more flexible is the flange, the nearer to the web corner is the stress peak. As will be shown in par. 6, plastic hinges in the flanges, playing an important part in the failure mechanism of the test girder, develop from the afore said sections of stress concentration.

The axial strains in the flanges indicate that a plate girder, with a slender web subjected to shear, is in general neither in a state of "beam action", nor in one of "truss action". Beam action would be encountered only in the case of a perfectly rigid, utterly buckling-resistant web. Then the distribution of the axial stress in the flange would be linear, as follows from the elementary formulae of "Strength od Materials" (Fig. 7). If, on the contrary, the web is extremely thin and behaves like a truss (Fig. 8), the axial force in the upper flange is uniform, and the force in the lower one is nil. The test girders exhibited the tendency to behave between the two boundary cases. It was noticed that the part played by the truss action increased with the flange stiffness. This can be explained in the light of the fact that for such girders the post-buckled strength is considerably greater (see par. 5), and, therefore, the tension field action is more developed.

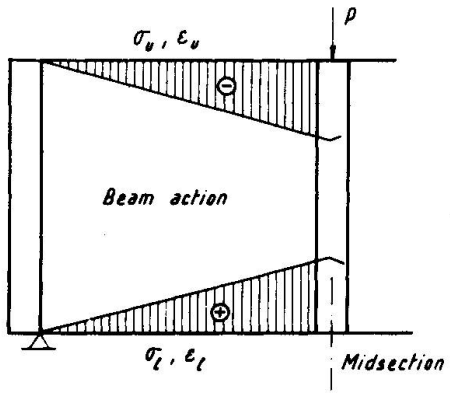

Fig. 7.

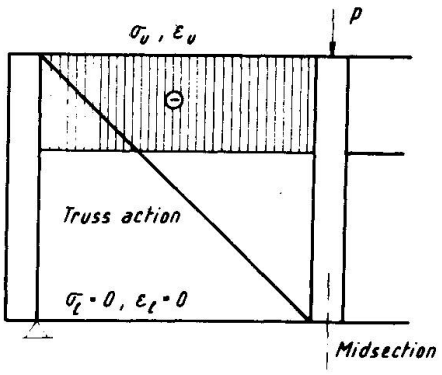

Fig. 8.

5. Ultimate Load.

The load-carrying capacities of the test girders are plotted in Fig. 9 in comparison with a) the critical loads of a simply supported web (P_{cr} ▭) and of a web fixed into flanges and simply supported at vertical stiffeners (P_{cr} ▭), b) the yield load in pure shear (P_y^s), c) the ultimate load determined by the theory of incomplete tension field for a web attached to perfectly rigid boundary elements ($^rP_{ult}$), d) the ultimate strength P_{ult} evaluated by Kuhn's approach to the effect of flange flexibility in tension field theories, and, e) the load-carrying capacity P_{ult}^B established by Basler's theory.

An analysis of the figure shows that the ultimate loads of the test girders very significantly grew with the flange stiffness, so indicating the benefical effect of flanges of large moment of inertia. The difference in strength between girder TG 1 and TG 5 was as great as 127 %.

Furthermore, it can be seen that the experimental load-carrying capacities of the girders with heavy flanges tend to

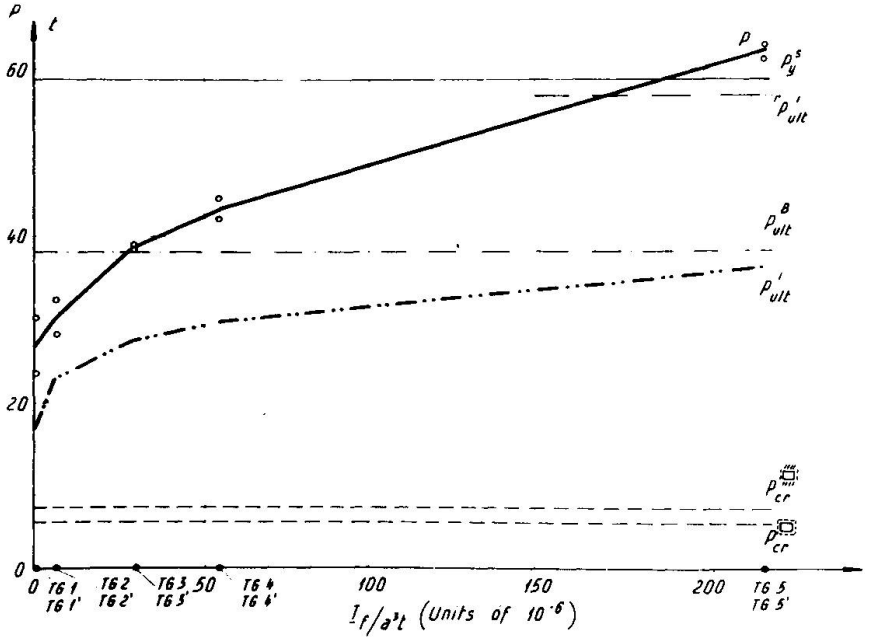

Fig. 9.

converge to the value $^{r}P_{ult}{}^{i}$; or, as this value is only slightly less than the yield load in pure shear, to $P_y{}^{s}$.

An inspection of the figure indicates, that the ultimate loads P_{ult} , which were calculated by Kuhn's approach /5/, based on the incomplete tension field theory and with due regard to flange flexibility, were considerably lower than the experimental results and, therefore, too conservative.

On the other hand, Basler's theory appeared to give too high load-carrying capacities when flanges are flexible (the reader will recall that this theory was established for girders of this kind), but it significantly underestimates the girder strength when the flanges are heavy.

It was also of interest to find out how the beneficial effect of increased flange rigidity was affected by the width-to-thickness ratio of the web. For this reason girders with higher b/t ratio than those tested in Swansea and Cardiff were tested. The resulting P_{ult}/P_{cr}-ratios, indicating the post-buckled reserve of strength of the respective girders, are plotted in Fig. 10; compared to the same ratios for the Swansea and Cardiff experimental girders. An inspection of the figure indicates that the beneficial effect of increased flange stiffness grows with the width-to-thickness ratio of the web.

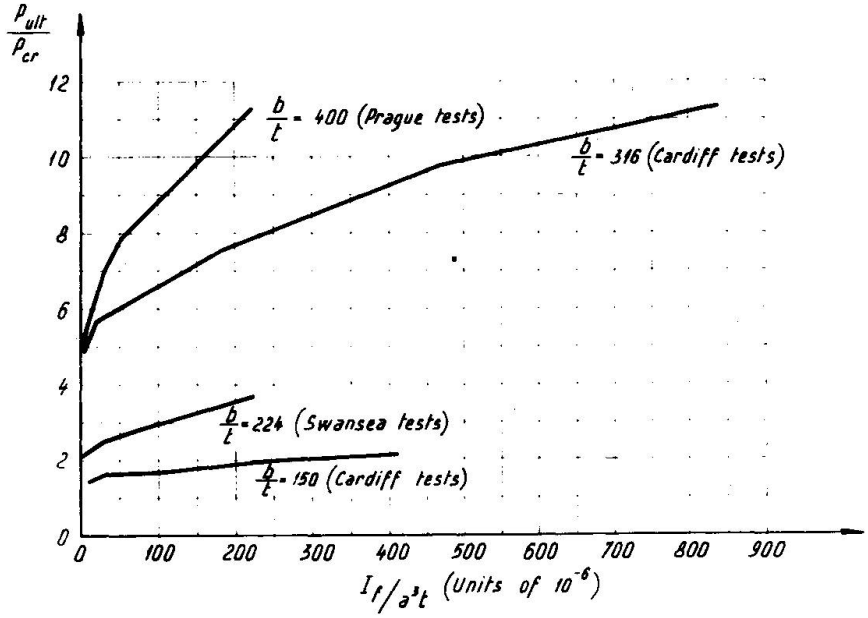

Fig. 10.

Plate girders with a web in shear and having a b/t-ratio as high as 400, as was the case for the author's test girders, can be used in ordinary steel structures (of course, subject to the fulfilment of other design requirements) provided that their flanges have a sufficient flange stiffness. Such slender webs may frequently be profitable in the case of deep large-span plate girders, where the web represents a predominant part of the weight of the whole girder.

6. Failure Mechanism

Rockey and the author discovered in Swansea and Cardiff in 1966-9 that the failure mechanism of a web panel in shear consisted of a diagonal plastic flow in the web and a system of plastic hinges in each flange.

The present experimental study has supported this finding.

In addition to it, thanks to measuring thoroughly the deformation and stress states in the web and flanges of the test girders, it was possible to obtain some evidence regarding the progression of yielding in various parts of the girder, and about its limiting state. The main conclusions will now be discussed.

6.1. Progression of Yielding and the Limiting State

The strain measurements discussed in par. 4 demonstrate the progression of yielding in a plate girder having web pannels subjected to shear. In ordinary welded steel plate girders, where initial curvature and residual stresses significantly influence their performance, the critical load P_{cr} can be exceeded, without any classical buckling phenomenon being observed (Fig.11). The load then grows on; at a value $P_{el\ max}$ the web buckling stops being elastic, and a permanent wave pattern forms.

After further increment of load, the web starts to yield at a point (or in a small zone) of one of its two surfaces; this being due to the combined action of membrane and bending stresses. The corresponding load is plotted in Fig. 11. Membrane yielding then begins over the whole web thickness, the relating load being slightly higher than that at which the aforementioned onset of surface plastification occurred. The membrane plastification propagates as the load is further increased. The force at which a plastic strain $\varepsilon_{pl} = 2\ 000$ microstrains was attained is also given in Fig. 11. When the load is further increased, a diagonal plastic band forms in the web, the web thereby losing any

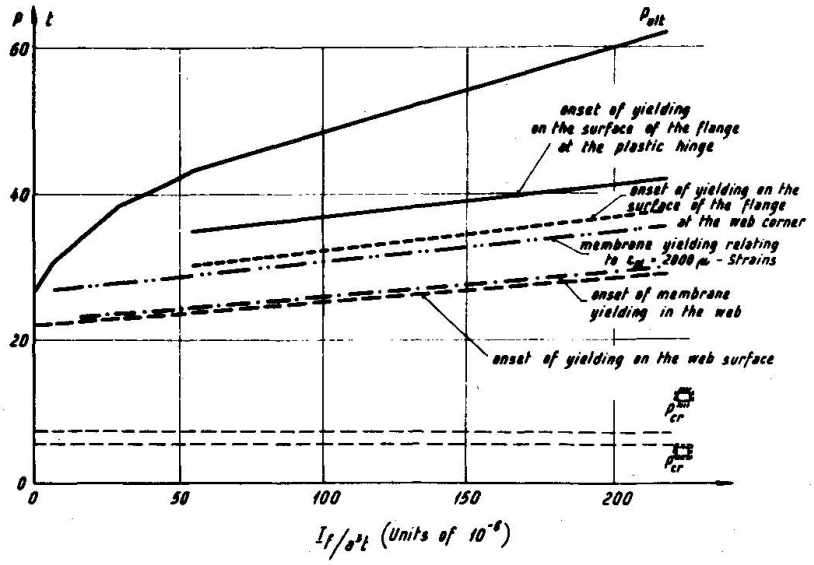

Fig. 11.

capacity to sustain any higher load; so that any additional increment in load has to be carried by the boundary frame consisting of flanges and vertical stiffeners.

The boundary framework fails when a collapse mechanism forms. Usually it is a mechanism of local failure of each flange; consisting of two plastic hinges at the frame corners (i.e. at the junctions of the flanges to the vertical stiffeners), and of another hinge between the stiffeners, situated more or less close to the web corner. The loads marking the onset of surface yielding of the flange at a) the web corners, and b) the inner plastic hinge are shown in Fig. 11. The difference between these loads on one side and the experimental collapse load curve on the other indicates a further reserve of strength provided by the stiffness of each flange.

An analysis of Fig. 11 shows that all respective loads discussed above increase with flange stiffness. thereby demonstrating the important part played by the flexural rigidity of flanges. It can also be seen there that the onset of yielding of any kind, or the sheer formation of a diagonal plastic strip in the web, does not yet mean that the limiting state of the girder has been attained. The limiting state of the girder is reached only when the aforementioned collapse mechanism forms.

6.2. Description of the Failure Mechanism

The failure mechanism of a web panel attached to flanges and vertical stiffeners, and subjected to shear, consists of a diagonal plastic band in the web and a system of plastic hinges in the boundary frame. The number of the hinges is such that a kinematic mechanism forms in the boundary framework. Usually this is a mechanism of local failure of each flange as shown in Fig. 12.

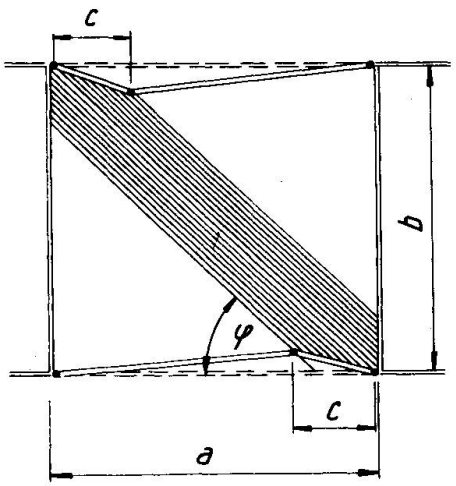

Fig. 12.

Plastic Buckled Pattern in the Web.

The contour plots of the post-failure plastic residues in web panel W_1 of girders TG 1, TG 3, and TG 5 are plotted in Fig. 13.

It will be noted there that the shape of the plastic buckled pattern is considerably affected by the flange stiffness. In the case of flexible flanges only one predominant buckling half wave forms (often accompanied by two small half waves, each of them situated near one end of the tension diagonal and on different sides of the predominant buckle). Moreover, the yielded strip is narrow. A larger number of buckling half waves, and a wider plastified area, frequently covering the whole web, occurs when the flanges are heavy.

The inclination φ of the diagonal buckles also demonstrates a tendency to grow somewhat with the moment of inertia I_f of the flange. It appears that the inclination converges to the value $\varphi_i = 45^o$, which results from the incomplete tension field theory for webs fixed into perfectly rigid boundary

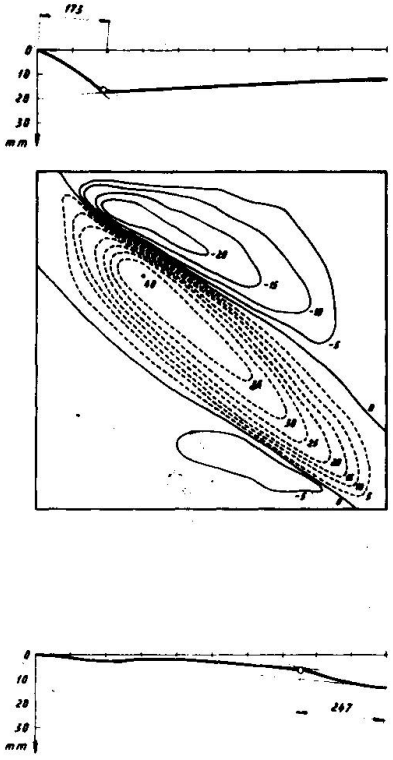

Test girder T6 1 - panel W1
(post-failure plastic residue)

Fig. 13a

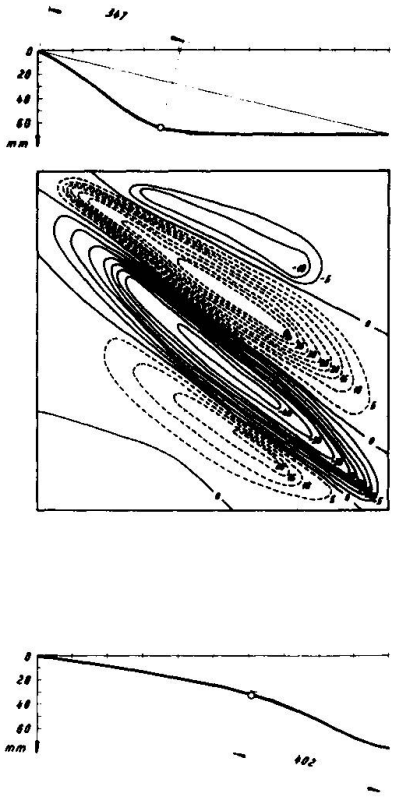

Test girder T6 3 - panel W1
(post-failure plastic residue)

Fig. 13b

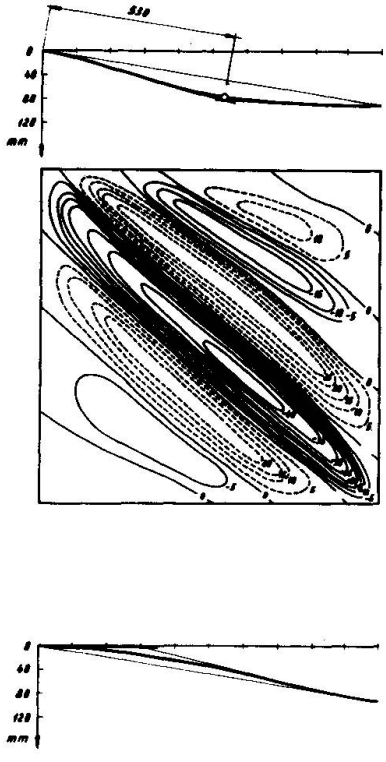

Test girder T6 5 - panel W1
(post-failure plastic residue)

Fig. 13c

elements. Nevertheless, the difference between the experimental φ -values and the angle φ_d of the geometrical diagonal is small for all test girders. (Fig. 14).

Plastic Hinges in the Flanges.

A typical flange plastic hinge is shown in Fig. 15. As in the previous tests by Rockey and the author of the present paper, it was noted that the distance c of the inner plastic hinge from the web corner grew with the flange rigidity. This is illustrated in Fig. 16, where the values of c/a are plotted, in terms of I_f/a^3t, for all test girders.

Design Procedure

Using the afore said failure mechanism, Rockey and the author of the present paper established in /3/ a design procedure for webs in shear and attached to flanges of various flexural rigidities.

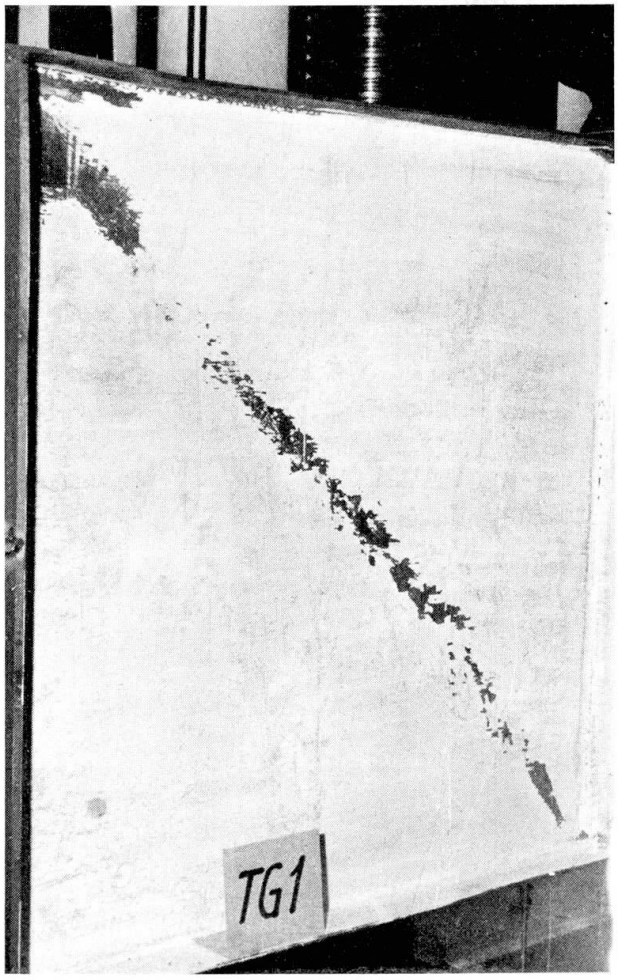

Fig. 13 d

Fig. 13 f

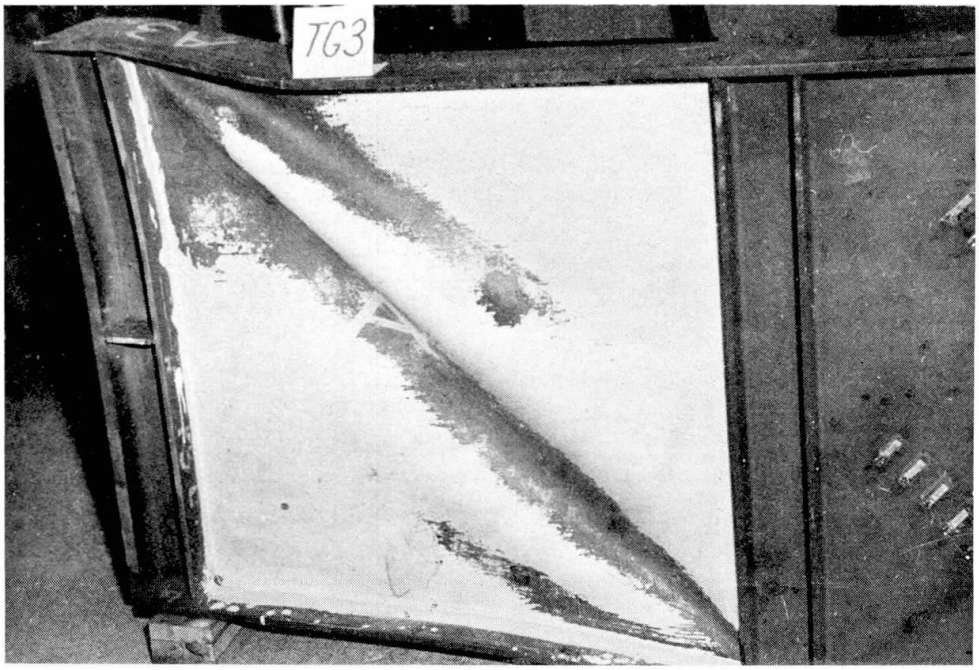

Fig. 13 e

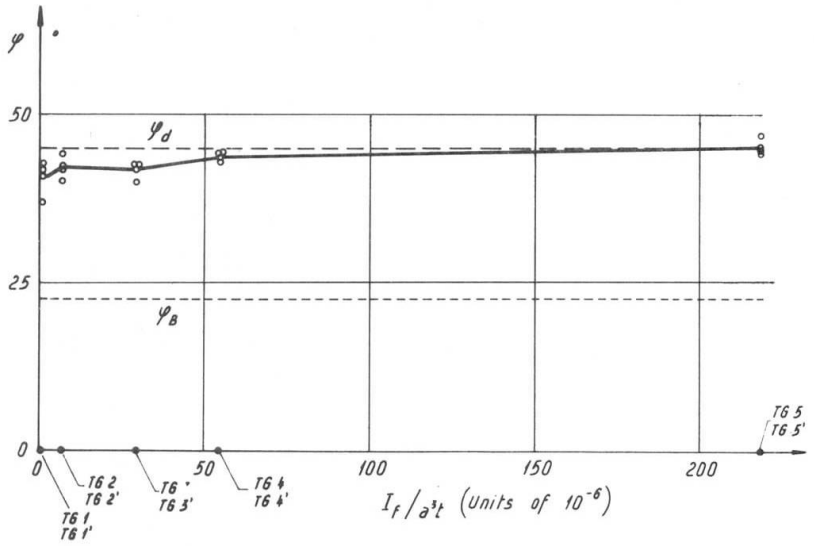

Fig. 14

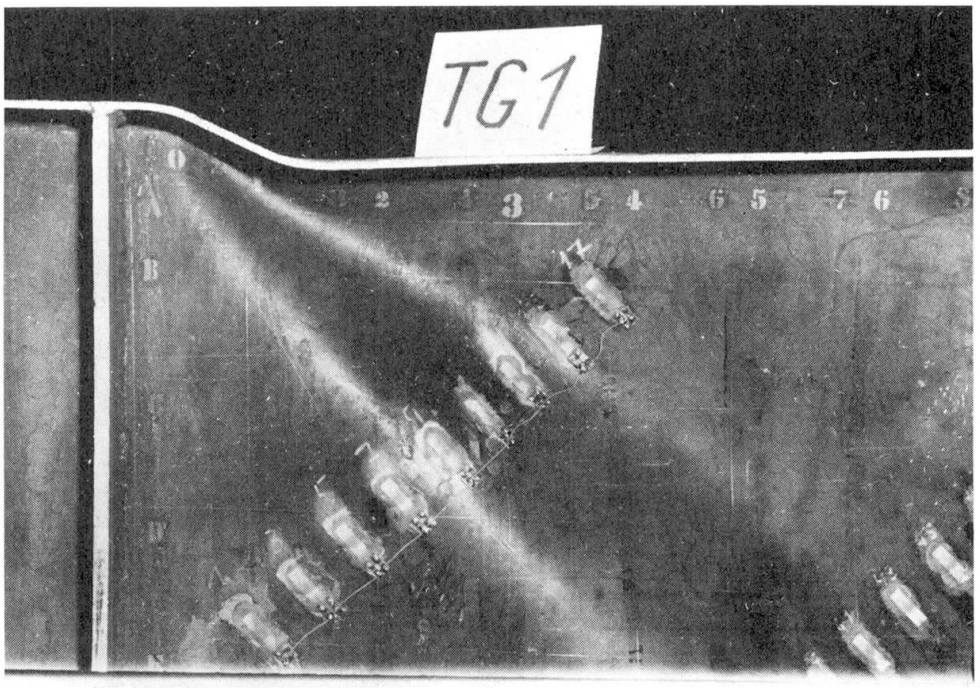

Fig. 15

This design procedure can serve as a suitable basis of an optimum design of webs in shear with regard to their post-buckled behaviour.

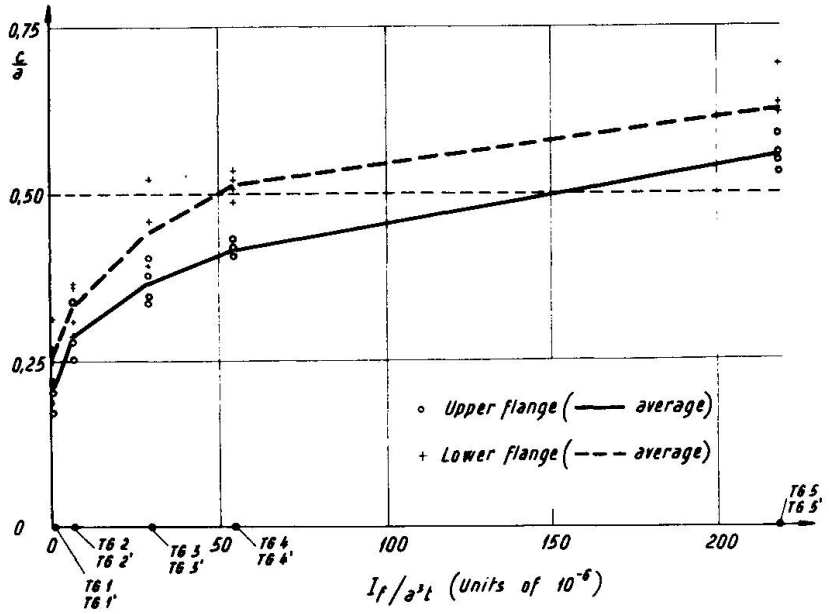

Fig. 16

References

/1/ Rockey,K.C., Škaloud,M.: Influence of Flange Stiffness upon the Load-Carrying Capacity of Webs in Shear; Report presented at the 8th Congress of IABSE, New York, September,1968

/2/ Rockey,K.C.: Plate Girder Design - Flange Stiffness and Web Plate Behaviour; Engineering, December, 1957

/3/ Rockey,K.C., Škaloud,M.: The Ultimate Load Behaviour of Plate Girders Loaded in Shear; Report of the University College Cardiff, 1970

/4/ Basler,K.: Strength of Plate Girders in Shear; Fritz Engineering Lab. Report No. 251-20, 1960

/5/ Kuhn,P., Patterson,J.O., Levin, L.R.: A Summary of Diagonal Tension - Part I - Method of Analysis; NACA - Technical Note 1952

SUMMARY

It was shown in the paper that flange stiffness very considerably affects the deformation and stress state of a web panel in shear, and the failure mechanism and ultimate load of the whole girder. A 127% increase in load-carrying capacity was achieved when the web was attached to flanges of high moment of inertia. Therefore, webs of large width-to-thickness ratios can be used provided that the flange rigidity is sufficiently high.

Leere Seite
Blank page
Page vide

I

Limit Design of Aluminium Shear Webs

Calcul à la ruine des âmes cisaillées en aluminium

Bemessung von Aluminiumstehblechen auf Traglast

J.W. CLARK
Chief, Engineering
Design Division

M.L. SHARP
Senior Research
Engineer

Alcoa Research Laboratories
New Kensington, Pennsylvania, USA

Introduction

The object of this investigation was to develop equations for analyzing thin-web aluminum girders loaded in shear, taking into account the effect of elastic flexural rigidity of the flanges on the ultimate strength of the web, stiffeners and fasteners. Flange stiffnesses varying from zero to complete rigidity are included. Consideration is also given to the effect of web buckles on the appearance of the girder. Results are compared with experimental data for thin-web aluminum girders.

The authors believe that the factors considered in this investigation are the areas of primary importance relative to the shear strength of thin-web aluminum girders in current applications, probably the most common of which are highway van trailers and shipping containers. However, it should be noted that a number of potentially interesting areas for investigation are not included, such as combined shear and bending, longitudinal stiffeners, and plastic hinge formation in the flanges.

Analysis of Girder Web

Figure 1 illustrates three types of idealized stress distribution that can act in the web of a girder under shear loading [1, 11]. It is assumed in this analysis that at loads above the shear buckling stress, the girder continues to carry a component of pure shear equal to the shear buckling stress. Superimposed on the shear buckling stress is a component of diagonal tension of the kind shown

in Figure 1B and an additional component like that shown in Figure 1C, the ratio between the latter two components depending on the flange flexibility. It is assumed that the stresses introduced in the flanges by the tension field action are roughly of the same magnitude as stresses introduced in the stiffeners, with the result that the component of the tension field stress corresponding to rigid flanges is at an angle of $\pi/4$. The stress distributions assumed are considerable oversimplifications of the actual distribution [2, 8, 13], but are believed to be satisfactory for the purposes of this analysis.

The total shear capacity of a girder, V_T, is assumed to be the sum of the contributions from the three stress components illustrated in Fig. 1.

$$V_T = V_{cr} + V_1 + V_2 \tag{1}$$

where V_{cr} is the total shear corresponding to the shear buckling stress, τ_{cr}, and V_1 and V_2 are the shearing forces contributed by the tensions σ_1 and σ_2, respectively. These three components are [1, 11]

$$V_{cr} = \tau_{cr} ht \tag{2}$$

$$V_1 = \frac{\sigma_1 ht}{2\sqrt{1 + \alpha^2}} \tag{3}$$

$$V_2 = \frac{\sigma_2 ht}{2} \tag{4}$$

in which h is the depth of web (distance between centroids of flange fasteners), t the web thickness, and α the aspect ratio (ratio of length of shear panel s to depth of panel, h).

The total shear carried by the web is thus

$$V_T = \tau_{cr} ht + \frac{\sigma_1 ht}{2\sqrt{1 + \alpha^2}} + \frac{\sigma_2 ht}{2} \tag{5}$$

All quantities in Eq. 5 are known for a given case except σ_1 and σ_2. Reference [19] shows how σ_1 and σ_2 can be evaluated, based on a consideration of the deformations of the web and assuming that the total shear is limited by the combination of stresses which causes general yielding in the web. The following relationships result:

$$\sigma_2 = K\sigma_1 \tag{6}$$

$$K = \frac{770\sqrt{1 + \alpha^2}}{\alpha} \left(\frac{I}{s^3 t}\right) \tag{7}$$

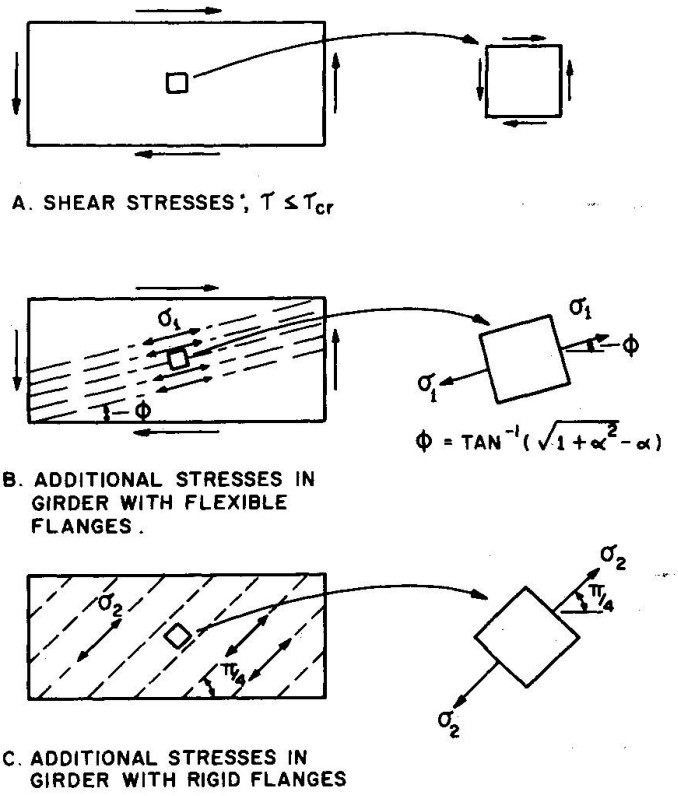

ASSUMED STRESSES IN BUCKLED GIRDER WEB

FIGURE 1

in which I is the flange moment of inertia.

As shown in Ref. [19], the following equations can be derived for the average shear stress in the web at yielding, τ_T, the corresponding compressive force in the stiffeners, F_s, and the increment in flange force, F_f, due to diagonal tension:

$$\tau_T = \tau_{cr} + C_1 \frac{\sqrt{3}}{2} (\tau_y - \tau_{cr}) \tag{8}$$

$$F_s = C_2 (s - s_e)\, t\, (\tau_T - \tau_{cr}) \tag{9}$$

$$F_f = \frac{C_3 h t}{2} (\tau_T - \tau_{cr}) \tag{10}$$

The coefficients in these equations are (see Fig. 2)

$$C_1 = \left(\frac{1}{K+1}\right) \left(\frac{1}{\sqrt{1+\alpha^2}} + K\right) \tag{11}$$

$$C_2 = \frac{\sqrt{1+\alpha^2} - \alpha + K\sqrt{1+\alpha^2}}{1 + K\sqrt{1+\alpha^2}} \tag{12}$$

$$C_3 = \frac{(K+1)\sqrt{1+\alpha^2}}{1+K\sqrt{1+\alpha^2}} \qquad (13)$$

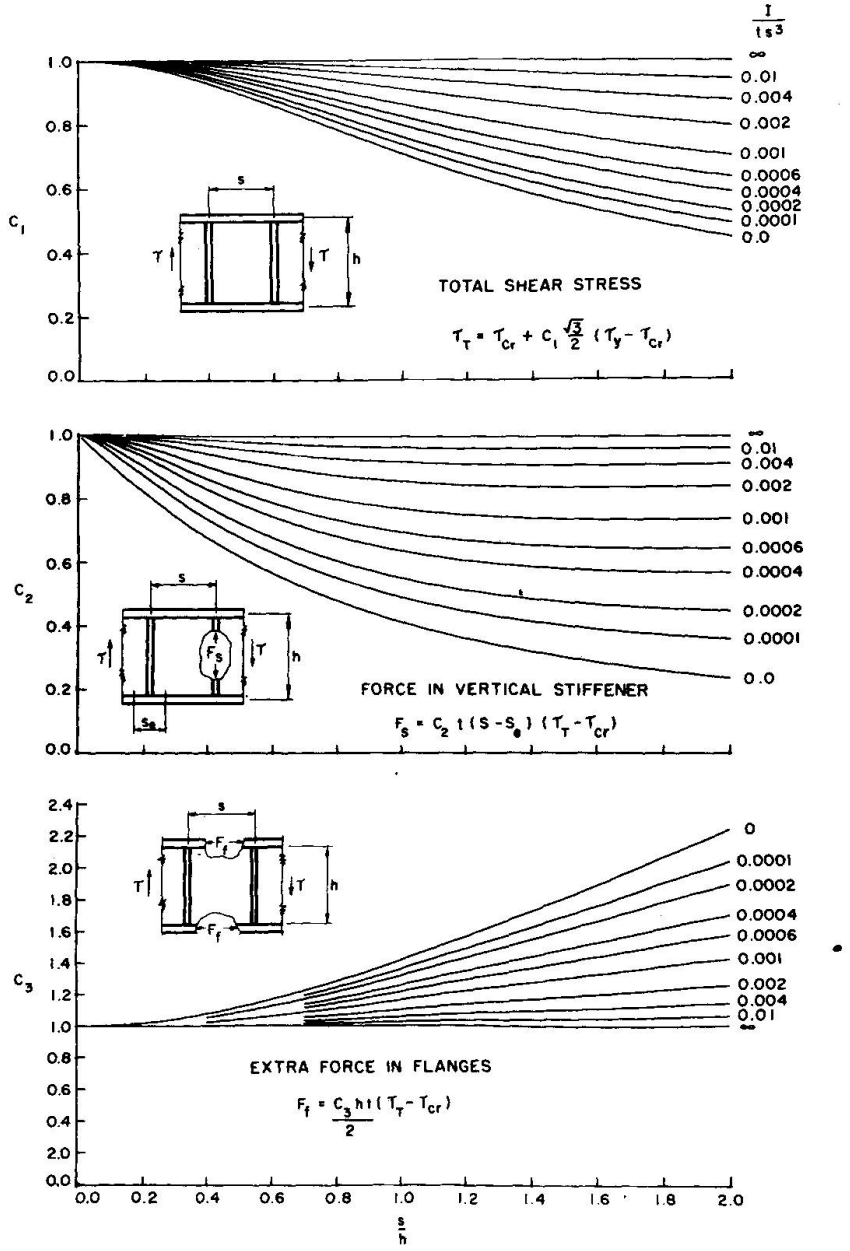

FIGURE 2

In Equation 9, the effective width of web acting with the stiffener, s_e, is given by

$$\text{If } \frac{s}{h} \leq 0.3,\ s_e = \frac{s}{2} \qquad (14a)$$

$$\text{If } \frac{s}{h} > 0.3,\ s_e = 0.15h \qquad (14b)$$

The experimental basis for Eq. 14a and 14b is discussed in Ref. [19].

If the ratio I/ts^3 exceeds 0.01, little accuracy is lost by considering the flanges to be completely rigid and letting $C_1 = C_2 = C_3 = 1.0$. This is true for many applications of aluminum girders.

Shear Buckling of Web

Although practical webs have some initial out-of-flatness and thus do not undergo true buckling, tests on aluminum girders [14, 15] have shown that the theoretical buckling stress gives an approximate indication of the load at which the web deflections become large and appreciable diagonal tension develops. For design purposes, the shear buckling stress can be expressed [3]:

In the elastic range: $\lambda > C_s$

$$\tau_{cr} = \frac{\pi^2 E}{\lambda^2} \tag{15}$$

In the inelastic range: $\lambda \leq C_s$

$$\tau_{cr} = B_s - D_s\lambda \tag{16}$$

where E is the modulus of elasticity, λ the equivalent slenderness ratio for shear buckling, and B_s and D_s are coefficients that depend on the yield strength and type of alloy [3].

Cook and Rockey have discussed the numerous factors that affect buckling behavior [4, 5, 6, 17]. The value of λ which is numerically about halfway between values corresponding to fixed and simply supported edges is [3]:

$$\lambda = \frac{a}{t}\sqrt{\frac{1.6}{1 + 0.7(a/b)^2}} \tag{17}$$

where a = smaller dimension of shear panel
b = larger dimension of shear panel

When the web plate is sandwiched between flange members or between stiffener members, a and b are equal to the clear distances between flanges and between stiffeners. For one-sided flanges or stiffeners, a and b are equal to the distance between fastener centerlines.

Intermediate Stiffeners

Stiffeners on thin-web girders perform two functions. They divide the web into panels, thereby increasing the buckling strength of the web; and when the shear stress is above the buckling stress, the stiffeners act as compression struts.

The following formulas for the stiffener moment of inertia, I_s, required to develop the shear buckling strength of the panels correspond to the design equations used in current United States specifications for aluminum structures [10, 20]:

$$\text{For } \frac{s}{h_c} \leq 0.4, \quad I_s = \frac{V_{cr} h_c^2}{0.154} \left(\frac{s}{h_c}\right) \tag{18a}$$

$$\text{For } \frac{s}{h_c} > 0.4, \quad I_s = \frac{V_{cr} h_c^2}{0.96} \left(\frac{h_c}{s}\right) \tag{18b}$$

where I_s in mm^4 is measured about the face of the sheet for stiffeners on one side and h_c is the clear height of the web in mm. V_{cr} is the shear buckling load in MN.

For many girders, stiffeners designed in accordance with Eqs. 18a and 18b will have adequate column strength in the post-buckling range. For example, if s/h is 0.4 or less and the average web stress, τ_T, does not exceed about 10 τ_{cr}, there is no need to check column strength of the stiffeners, provided that Eq. 18a is satisfied. For more severe loading the stiffener should be checked to insure that it can carry the force F_s given by Eq. 9, acting as a column with a length h_c. The use of the depth of web as the effective length of stiffener is conservative because the lateral support provided by the web is neglected [11]. In one-sided stiffeners the combined axial plus bending stress should be less than the yield stress of the material divided by a suitable factor of safety.

Kuhn [11] has noted that thin-walled stiffeners may be deformed by the buckle waves in the web and subsequently fail locally by "forced crippling" under the compression in the stiffener. Figure 3 shows that forced crippling can be avoided if the thickness of the stiffener, t_s, is:

$$t_s \geq t \left(0.65 + 0.35 \sqrt{\frac{\tau}{\tau_{cr}}}\right) \tag{19}$$

where τ is the average shear stress on the web.

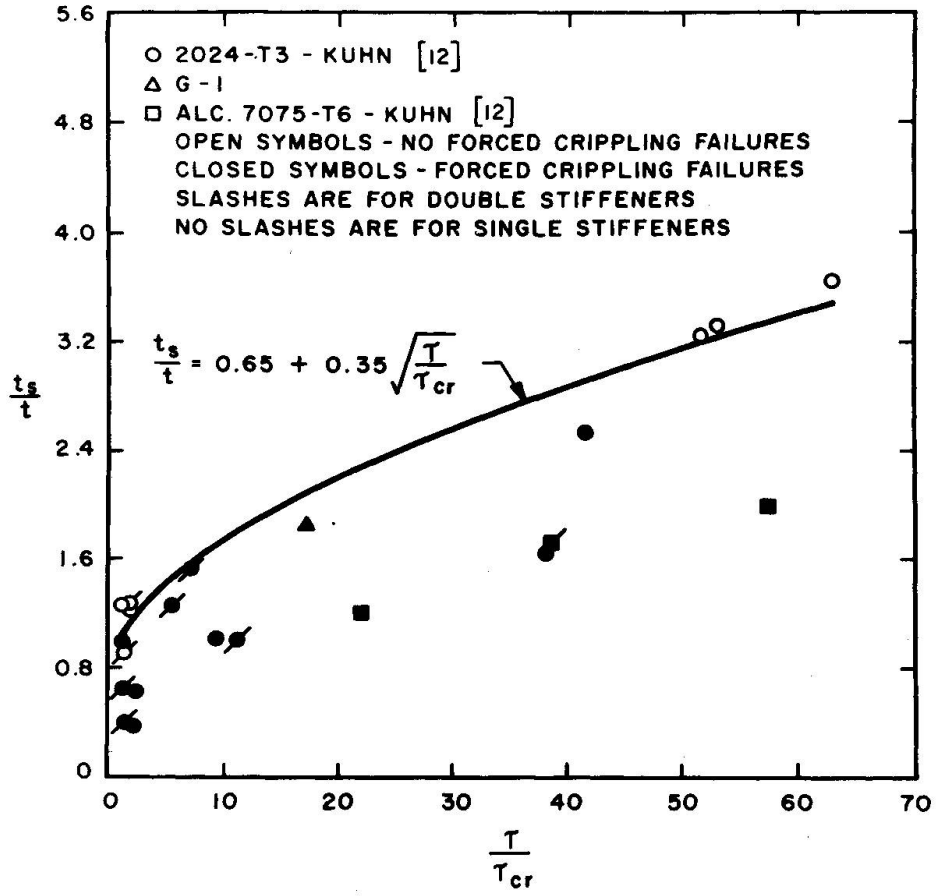

THICKNESS OF STIFFENER TO PROHIBIT FORCED CRIPPLING FAILURE OF STIFFENER

FIGURE 3

Flanges

The total axial force on the flange is that from Eq. 10 plus that from beam action. The flange should be checked for local buckling of the components, torsional buckling, lateral buckling and in the case of very thin webs, flexural buckling in the plane of the web between intermediate stiffeners. In the absence of a precise analysis, it is conservative to treat the flange as a column with an unsupported length equal to the stiffener spacing.

In the analysis in Ref. [19], an expression is developed for the lateral force on the flange exerted by the web. This force causes bending of the flange in the plane of the web. In practice this bending is generally ignored, as indicated by steel design rules [1, 21] and also aircraft experience [11]. The analysis of Fujii [7] and the tests of Rockey et al [18], however, tend to show that these forces are significant for design.

Connection of Web to Flanges and Stiffeners

An extensive survey of average stresses in the web near boundary members in steel girders [22] showed that these stresses were adequately given by calculations based on shear resistant behavior. Other recent tests [9] also indicate that membrane stresses near the edges of the panel are between values calculated for tension field and shear resistant behavior but nearer to the latter. This has been corroborated by strain measurements on an aluminum girder discussed later in this paper. Thus, it should be satisfactory to calculate the strength of the connection of web to flange members as though the web were shear resistant.

The load per unit length, R_f, is:

$$R_f = \tau_T t \tag{20}$$

The fastening between web and stiffener must at least be sufficient to develop the total load in the stiffener over one-half the length of the stiffener. To allow for some concentration of load, it has been proposed [1] to develop the load in one-third the length of the stiffener. The load per unit length, R_s, is thus:

$$R_s = \frac{3F_s}{h} \tag{21}$$

The framing at the ends of the girder must provide anchorage for the horizontal component of the web tension force at the end. This problem may be handled by making the end panel a shear resistant panel [1].

Appearance of Girder Web

In some cases it is desirable to proportion the girder so that the buckle waves present at working loads are small and not readily noticeable [16]. Reference [19] shows that this can be accomplished by limiting the average shear stresses on the web to a value equal to the shear buckling stress plus 10 MN/m^2.

While fatigue strength is not treated in this paper, it should be borne in mind that if the shear buckling stress is exceeded at working loads, the girder will be more susceptible to fatigue cracking than would a shear resistant web [22].

Test Results

Figure 4 shows details of a riveted aluminum girder having an h/t ratio of 532. The value of I/ts^3 for this girder was 0.027, so that its flanges were relatively rigid. The web material had a tensile strength of 450 MN/m^2. Figure 5 shows that the principal stresses at the centers of

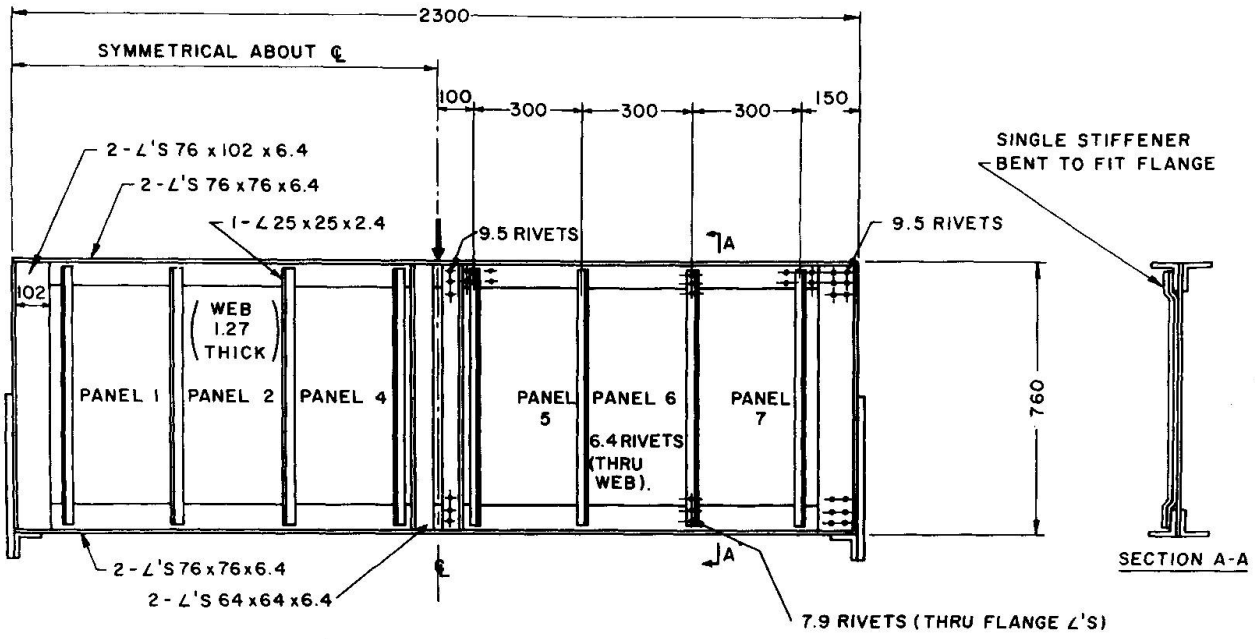

NOTES : 1.-MATERIAL
ALL RIVETS 2017-T31
ALL ANGLES 2024-T4
WEB PLATE 2024-T3

2.- FAILURE BY TEARING OF WEB AT LOAD OF 320 KILO NEWTON; INTERMEDIATE STIFFENERS FAILED BY CRIPPLING AT A LOAD OF 294 KILO NEWTON.

3.- ALL DIMENSIONS IN MILLIMETERS.

GIRDER G-I

FIGURE 4

the panels calculated using Eq. 5 are in agreement with the values from test. The stresses at the edge of the panel for this girder were intermediate to the calculated values for tension field and shear resistant webs but nearer to the values corresponding to shear resistant behavior. Figure 6 presents the portion of flange stress due to diagonal tension in the web. Equation 10 is seen to give reasonably conservative values of flange stress.

In most of the tests on aluminum girders or shear panels, the ultimate strength has been measured but not the load to cause general yielding. Shear stress values given by Eq. 8, which is based on yielding, would be expected to be conservative in comparison to the ultimate strengths, and this is generally found to be the case, as illustrated by data [12] for riveted panels given in Fig. 7.

Figure 8 compares test strengths of aluminum girders reported by Moore [14, 15] and Girder G1 with those calculated by the use of Eq. 8. In some cases the ultimate load for the girders was limited by torsional or local buckling of the compression flange so that the test values are a "lower bound" to web strength. The test data, however, tend to confirm that Eq. 8 provides a reasonable estimate of the variation of strength with flange rigidity for these girders.

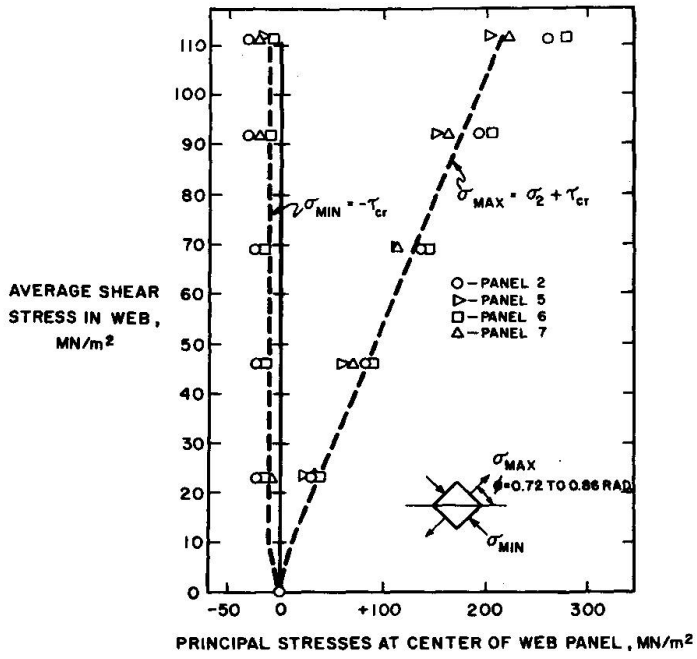

CALCULATED AND MEASURED STRESSES AT THE CENTER OF A PANEL – GIRDER G-I

FIGURE 5

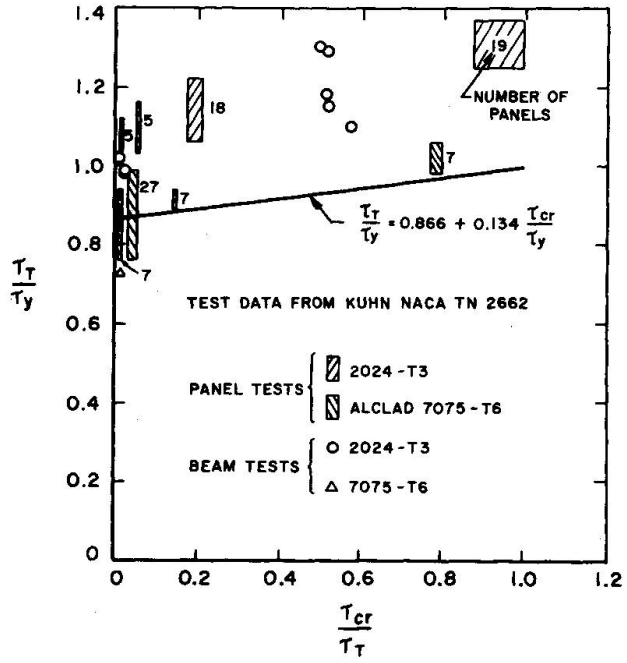

SHEAR STRENGTH OF PANELS AND BEAMS WITH RIGID FLANGES

FIGURE 7

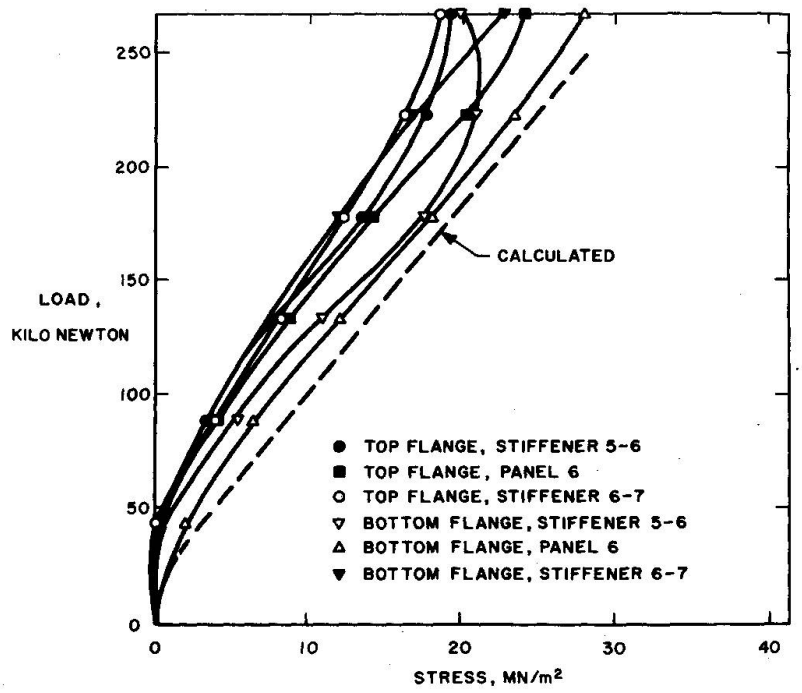

COMPRESSION STRESS IN FLANGE DUE TO DIAGONAL TENSION IN WEB

FIGURE 6

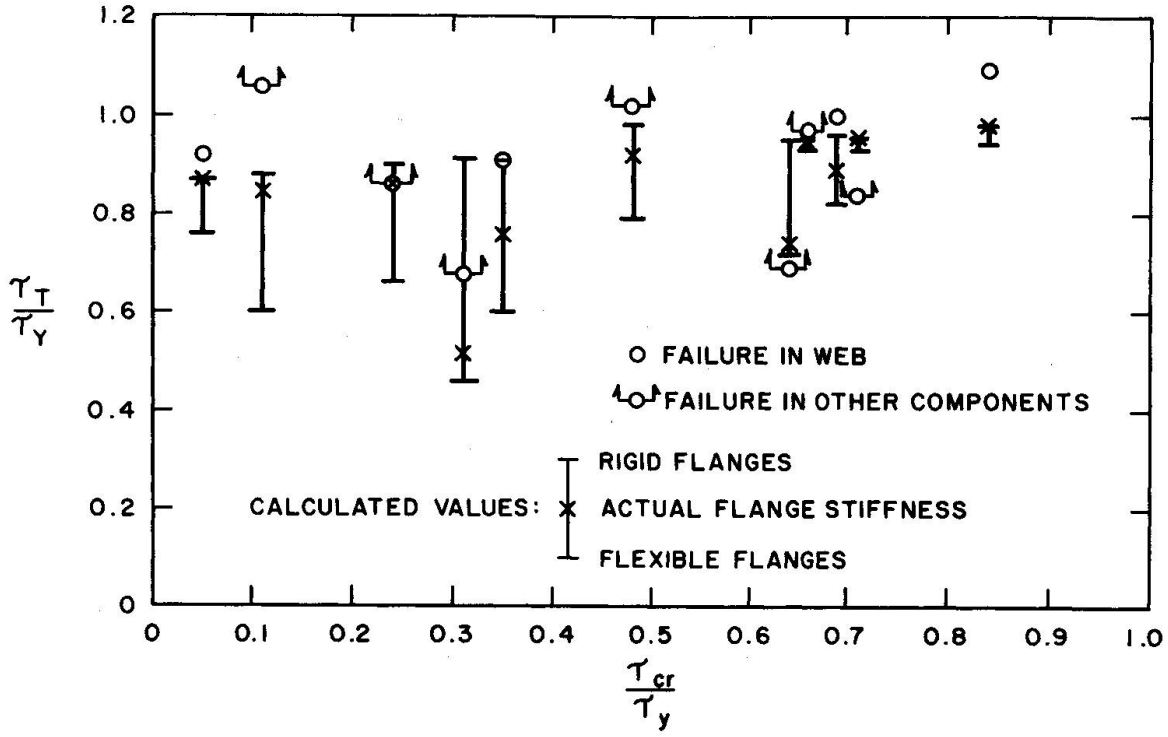

COMPARISON OF MEASURED AND CALCULATED SHEAR STRENGTHS OF ALUMINUM GIRDERS

FIGURE 8

Conclusions

Methods have been developed in this paper for analyzing the strength of thin aluminum shear webs in girders with flanges that are either flexible, rigid, or of intermediate stiffness. The steps to be taken in the analysis are summarized in Table 1.

Table 1

Steps in Analyzing Thin Web Aluminum Girders

1. Calculate τ_{cr} (Eq. 15-17). If fatigue is a major consideration, the web shear stress should not exceed τ_{cr}. If the web must not appear too wavy at design loads, the allowable shear stress in MN/m^2 should not exceed $(\tau_{cr} + 10)$, divided by a suitable factor of safety such as 1.2.

2. Calculate I/ts^3. If it exceeds 0.01, the flange is relatively rigid, and the coefficients C_1, C_2, and C_3 in Eqs. 8, 9, and 10 can be considered as unity. If $I/ts^3 < 0.01$, C_1, C_2, and C_3 can be determined from Fig. 2.

3. Calculate τ_T from Eq. 8 and Fig. 2. The average shear stress in the web should not exceed τ_T divided by a suitable factor of safety, such as 1.65.

4. Check the stiffener moment of inertia I_s to make sure that it meets the requirements of Eqs. 18a and 18b. Check the stiffener thickness by Eq. 19 to avoid forced crippling of the stiffener due to web buckling.

5. If $\tau_T/\tau_{cr} > 10$ or if $s/h > 0.4$, calculate the stiffener stress from Eq. 9 and Fig. 2. Compare with allowable column stresses.

6. Calculate the increment in flange stress from Eq. 10 and Fig. 2. Add the beam stress (Mc/I). The total flange stress must be within allowable limits for compression flanges of beams.

7. Check the spacing of flange and stiffener fasteners, using Eq. 20 and 21.

References

1. Basler, Konrad, "Strength of Plate Girders in Shear," Journal of the Structural Division, Proceedings, ASCE, Vol. 87, No. ST7, October, 1961, p. 151.

2. Basler, Konrad, "Strength of Plate Girders in Shear," closing discussion, Journal of the Structural Division, Proceedings, ASCE, Vol. 88, No. ST5, October, 1962, Part 1, p. 175.

3. Clark, J. W., and Rolf, R. L., "Buckling of Aluminum Columns, Plates and Beams," Journal of the Structural Division, Proceedings, ASCE, Vol. 92, No. ST3, June, 1966, p. 17.

4. Cook, I. T., and Rockey, K. C., "Shear Buckling of Clamped and Simple-Supported Infinitely Long Plates Reinforced by Transverse Stiffeners," The Aeronautical Quarterly, Vol. XIII, August, 1962.

5. Cook, I. T., and Rockey, K. C., "Shear Buckling of Clamped and Simply Supported Infinitely Long Plates Reinforced by Transverse Stiffeners," The Aeronautical Quarterly, Vol. XIII, February, 1962.

6. Cook, I. T., and Rockey, K. C., "Shear Buckling of Rectangular Plates With Mixed Boundary Conditions," The Aeronautical Quarterly, Vol. XIV, November, 1963.

7. Fujii, T., Minimum Weight Design of Structures Based on Buckling Strength and Plastic Collapse, (3rd report) - An Improved Theory on Post Buckling Strength of Plate Girders in Shear -, Journal of Society of Naval Architects (Japan) No. 122, December, 1967, p. 119-128.

8. Gaylord, E. H., "Strength of Plate Girders in Shear," discussion, Journal of the Structural Division, Proceedings, ASCE, Vol. 88, No. ST2, April, 1962, p. 151.

9. Goodpasture, D. W., and Stallmeyer, J. E., "Fatigue Behavior of Welded Thin Web Girders as Influenced by Web Distortion and Boundary Rigidity," Civil Engineering Studies, Structural Research Series No. 328, University of Illinois, August, 1967.

10. Hartmann, E. C., and Clark, J. W., "The U. S. Code," Proceedings, Symposium on Aluminum in Structural Engineering, The Institute of Structural Engineers and the Aluminum Federation, London, June 11-12, 1963.

11. Kuhn, P., Peterson, J. P., and Levin, L. R., "A Summary of Diagonal Tension, Part I - Methods of Analysis," National Advisory Committee for Aeronautics Technical Note 2661, May, 1952.

12. Kuhn, P., Peterson, J. P. and Levin, L. R., "A Summary of Diagonal Tension, Part II - Experimental Evidence," National Advisory Committee for Aeronautics Technical Note 2662, May, 1952.

13. Levy, S., Fienup, K. L., Woolley, R. M., "Analysis of Square Web Above Buckling Load, National Advisory Committee for Aeronautics Technical Note 962, February, 1945.

14. Moore, R. L., "Observations on the Behavior of Aluminum Alloy Test Girders," Transactions ASCE, Vol. 112, 1947, p. 901.

15. Moore, R. L., "An Investigation of the Effectiveness of Stiffeners on Shear-Resistant Plate-Girder Webs," National Advisory Committee for Aeronautics Technical Note No. 862, September, 1942.

16. Rockey, K. C., "Web Buckling and the Design of Webplates," The Structural Engineer, February, 1958.

17. Rockey, K. C., "Influence of Stiffener Thickness and Rivet Position Upon the Effectiveness of Single-Sided Stiffeners on Shear Webs," The Aeronautical Quarterly, Vol. XV, February, 1964.

18. Rockey, K., and Skaloud, M., "Influence of the Flexural Rigidity of Flanges Upon the Load-Carrying Capacity and Failure Mechanism of Webs in Shear." Acta Technica Csau, No. 3, 1969.

19. Sharp, M. L., and Clark, J. W., "Thin Aluminum Shear Webs," Journal of the Structural Division, Proceedings, ASCE, Vol. 97, No. ST4, April, 1971.

20. "Specifications for Aluminum Structures," Aluminum Construction Manual, The Aluminum Association, 1967.

21. "Specification for the Design, Fabrication and Erection of Structural Steel For Buildings," American Institute of Steel Construction, adopted February 12, 1969.

22. Yen, B. T., and Mueller, J. A., "Fatigue Tests of Large-Size Welded Plate Girders," Welding Research Council Bulletin 118, November, 1966.

Das überkritische Verhalten von Aluminium-Vollwandträgern mit Quersteifen (I. Bericht (1970) aus der "Versuchsanstalt für Stahl, Holz und Steine", Universität Karlsruhe)

Post-Critical Behaviour of Aluminium Plate Girders with Transverse Stiffeners (1st Report 1970)

Comportement post-critique des poutres à âme pleine en aluminium, munies de raidisseurs transversaux (1er rapport 1970)

O. STEINHARDT
Prof.Dr.-Ing., Dr.sc.techn.h.c.

W. SCHRÖTER
Dipl.-Ing., Wiss.Ass.

Karlsruhe, BRD

1. Einführung

Im überkritischen Bereich interessiert seit dem JVBH-Kongreß in New York (1968) das optimale Zusammenwirken der Gurte, des Steges und der Quer- und Längssteifen, wobei letztgenannte die Felder a x b gemäß a x (b_1+b_2+...) unterteilen können; auch geneigte oder gekrümmte Steifen sind möglich.- Die Art der Verbindung zwischen den genannten Bauelementen eines Vollwandträgers und deren Querschnittsformen (torsionsweich bzw.-steif und biegeweich bzw.-steif) bleibt überdies wesentlich.

In d i e s e r Untersuchung sollen ausschließlich Einfeldträger unter mittiger Einzellast betrachtet werden, die beiden (symmetrischen) Felder a x b sind durch biegeelastische Gurte und Steifen begrenzt; dabei sind für sämtliche Versuchsträger bei den Stegen die Voraussetzungen der klassischen (linearen) Beultheorie n i c h t erfüllt (also es ist insbesondere die Stegverformung w > 0,3·t).- Wie "starr" die Steifen auszubilden sind (z.B. Längssteifen gemäß k·γ^*= k·EJ/b·D o.ä.) und wie weit die kritischen Beulspannungen des Steges überschritten werden dürfen (z.B. gemäß $(\tau/\tau_{Kr})^2 + (\sigma/\sigma_{Kr})^2 = 2{,}25$ o.ä.) soll erst später anhand spezieller Traglast-Versuche zu klären versucht werden; jedenfalls sind die Verfasser z.Zt. schon überzeugt davon, daß der "Sicherheitsfaktor" gegenüber σ_{Kr} bzw. τ_{Kr} jeweils $\nu_B < 1$ sein kann, weil einerseits (gerade auch bei Aluminium-Vollwandträgern) die "Traglast" relativ sehr hoch liegt und andererseits bis zur elastischen Grenslast P_{Gr}^{el} (siehe S.4) der Gebrauchszustand der Träger nicht beeinträchtigt erscheint.

2. Stand der Forschung

Ch. MASSONNET hat (zunächst im Vorbericht und späterhin im Schlußbericht zum New Yorker Kongreß [1,2]) einige allgemeingültige Folgerungen aus zahlreichen einschlägigen V e r s u c h e n und theoretischen Untersuchungen gezogen, die auch für unsere z u s ä t z l i c h e n Betrachtungen von Bedeutung sind: das Beulen des Stegbleches geht hiernach kontinuierlich, und weiterhin (dies bis zu P_{Gr}^{el}) elastisch vor sich; (der Quotient P_{Gr}^{el}/P_{Kr} wurde bei Stahlträgern bei 2,8 ermittelt, für Aluminiumträger fand ROCKEY einen Wert von 4,0). Ferner besteht keine proportionale Beziehung zwischen Traglast (P_{Tr}^{pl}) und klassischer Beullast (P_{Kr}); das die Gurte (und Steifen) auf Biegung beanspruchende unvollkommene "Zugfeld" wird von der "Rahmensteifigkeit" der Feldränder bestimmt.-

Die Traglast - sei sie nun dargestellt als "Versagenslast" P_{Tr}^{pl} oder als "elastische Grenzlast" P_{Gr}^{el} - bestimmt die "überkritische Tragreserve" (über P_{Kr} hinaus), die sicherlich mit dem Dünnheitsmaß des Steges b/t relativ ansteigt, und die zusätzlich (man vergleiche Stahl- mit Aluminium-Vollwandträgern) nach Maßgabe von σ_F/E bzw. $\sigma_{0,2}/E$ dabei zunimmt. Die Traglast erhöht sich bei zunehmender Biegesteifigkeit des "Feldrahmens", wobei K.C. ROCKEY [3] (für $\alpha = a/b = 2$) bei Bemessung der Gurte eine Begrenzung der Beulentiefen (des Steges) im Auge hat. Teilweises Nachgeben des Steges innerhalb der Biegedruckzone soll nach K. BASLER-B. THÜRLIMAN [4] eine Senkung der neutralen Faser bewirken, auch sollen die lotrechten Querpressungen der Gurte über den ganzen Steg möglich sein (hieraus resultiert der Bemessungsgrenzwert $b/t \leq 360$ für Stahl), außerdem wird dem Druckgurt eine teilweise Mitwirkung des Steges (gemäß $30 \cdot t$) zugewiesen. Zuletzt wird von ihnen angenommen, daß der Schubwiderstand eines Stegbleches als reines Schubfeld (τ_{Kr}) bis zum Versagen des Steges bestehen bleibt, und daß das angebliche WAGNER'sche Diagonalzugfeld diesem "reinen" Schubfeld überlagert werden kann. Aus allen diesen Annahmen erhält man die Traglast T_{ult} [8.2 des Vorberichtes [1]] .- Für die gleichzeitige Wirkung von Schub und Biegung schlägt BASLER-THÜRLIMAN das Gesetz der Spannungsüberlagerung [gemäß [1] 8.3 sowie Figur 8.3] vor.- Diese sogenannte amerikanische Bemessungsmethode wurde in den AJSC-Normen aufgenommen.

Zusammenfassend stellte Ch. MASSONNET 1968 [2] fest, daß zwar durch die Kongreß-Berichte der Herren T. FUJII [5], K.C. ROCKEY und M. ŠKALOUD [6] die Näherungstheorie nach K. BASLER-B. THÜRLIMAN zum Teil bestätigt scheint, aber auch offene Fragen noch sichtbar geworden sind, Sieht man dabei zunächst

wiederum vom Längssteifenproblem ab, so läßt sich feststellen, daß die amerikanische Bemessungsmethode hier (mit ihren beschriebenen theoretischen Voraussetzungen) nur dann wirklichkeitsnah sein kann (wie auch H. WAGNER schon 1929 [7] feststellte), falls der Einfluß von n i c h t biegesteifen Gurten vernachlässigt werden darf, d.h. wenn der Abstand der Vertikalsteifen in relativ engen Grenzen bleibt. ROCKEY und SKALOUD haben zwar auch für große $\alpha = a/b$ eine gewisse Übereinstimmung mit den Voraussagen der Traglasten nach BASLER-THÜRLIMAN versuchstechnisch festgestellt, doch muß man u.E. den zugrundeliegenden Tragmechanismus weiter aufhellen. Sicher ist jedenfalls, daß der "wirksamen Flanschsteifigkeit" EJ_W, insbesondere des Obergurtes, wesentliche Bedeutung zukommt; hierfür geben ROCKEY und SKALOUD in einem vergleichbaren Bestreben den Parameter $J/a^3 \cdot t$, der zur Beulentiefe in Beziehung gesetzt werden kann, an, wobei zu überlegen bleibt ob anstelle von J nicht genauer ein (noch zu definierendes) J_W gesetzt werden müßte (vgl. auch noch Abschnitt 6).

3. Voraussetzungen und Definitionen bei den Karlsruher Versuchen (Teil I, 1970)

Bei den symmetrischen Einfeldbalken aus AlMg3 F23 (Steg) und AlMgSi0,5 F22 (Gurte und Quersteifen) mit mittiger Einzellast und den α-Werten 2 bzw. 3 sind die Q u e r s t e i f e n (an den Auflagern und in Trägermitte) so biegefest ausgebildet, daß sie als Bauteil bis zur Versagenslast nicht kritisch werden. Die Gurte sind gegen seitliches Ausweichen abgesichert. Die Stegbleche sollen, auch im überkritischen Bereich, höchstens örtlich begrenzte Plastizierungen erleiden. Eigenspannungen werden nicht berücksichtigt; bei dem geschweißten Träger (Nr. 3) wurde bei 250° C spannungsfrei geglüht, die übrigen 4 Träger wurden HV-verschraubt, wobei Träger Nr. 5 eine spezielle Behandlungsweise (zwecks abminderung der Biegesteifigkeit der Gurte) erfuhr.

Die Last-Eintragung in Trägermitte erfolgte über seitlich gleitfest angeschlossene Steifen direkt in den Steg. Eine Vierendeel-Rahmenwirkung für die geschraubten Träger wird dadurch vermieden, daß nur die abstehenden Winkelschenkel (mit Beilagen verstärkt) durch Druckkontakt die Kraft aus dem Gurt aufnehmen; die anliegenden Winkelschenkel der Quersteifen sind dabei einmal abgeschrägt, außerdem ist das erste Loch dieses Schenkels größer gebohrt und die darin angeordnete HV-Schraube jeweils nur gering angezogen.

Die "klassische Beullast" P_{Kr} (Schub-Biegung, einschl. Randbiegung) liefert einen Maßstab für die Prognosen im "überkritischen Bereich". So

wird mit $n = P_{Gr}^{el}/P_{Kr}$ die Erhöhung bis zur "elastischen Grenzlast" P_{Gr}^{el}, bei der die Stegverformungen gerade noch elastisch bleiben, beschrieben, während $n^* = P_{Tr}^{pl}/P_{Kr}$ den entsprechenden ert bis zur plastischen Traglast gleich Versagenslast charakterisiert.

4. Zielsetzungen und Durchführung der Versuche

Es sollen vor allem die Lastwerte P_{Kr}, P_{Gr}^{el} und P_{Tr}^{pl} auf versuchstechnischem Weg ermittelt werden, auch sind - zwecks Entwicklung eines brauchbaren Berechnungsverfahrens - laufend die Spannungen σ_x, σ_y und τ_{xy} (über geeignete Dehnungsmessungen) und die senkrechten und waagrechten Verformungen markierter Punkt des Steges und der Gurte festzustellen (nachdem auch die geometrischen V o r v e r f o r m u n g e n an zwei Trägern bestimmt worden waren).- Bei den Gurten sollen insbesondere auch über die gesamte Trägerlänge $l = 2a$ die jeweiligen Eigenverformungen (z.B.ihre Biegelinien) meßtechnisch beobachtet werden.

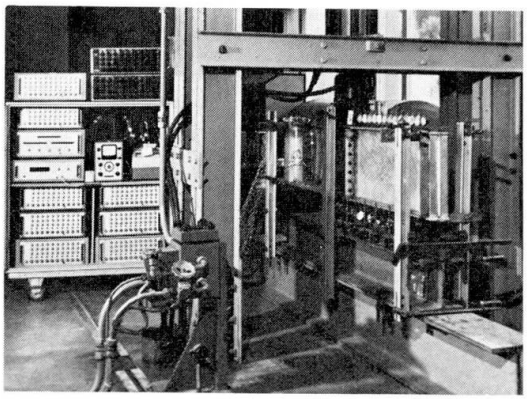

Bild 1: Versuchsträgeraufbau

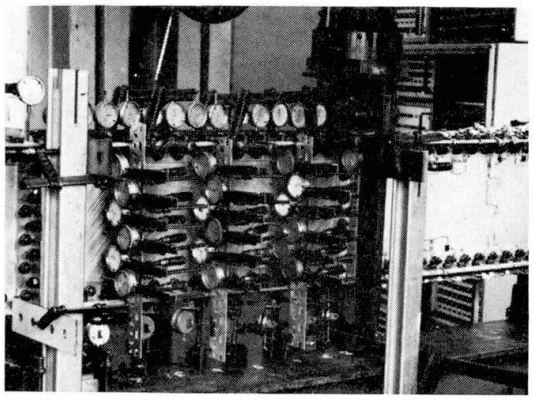

Bild 2: Meßeinrichtung für Stegverformungen

Die V e r s u c h s a n o r d n u n g als Ganzes ist aus den Fotos der Bilder 1 und 2 ersichtlich. Die Träger waren über beidseitige Rollenlager abgestützt und mittig belastet ("Gabellagerungen"). Verdrehungen und seitliche Verformungen der Gurte traten späterhin nicht auf. Infolge der (richtungstreuen) Lasteintragung über am Steg angeklemmte Steifen entfielen örtliche Pressungen am Obergurt. Zur Spannungsermittlung wurden auf e i n e r Trägerhälfte zahlreiche Dehnungsmeßstreifen angebracht, u.a. auf der Achse der Gurte und Rosetten beiderseits am Stegblech unterhalb der Gurte sowie neben den Aussteifungen. Die am Steg beidseitig gemessenen Dehnungen wurden jeweils gemittelt, um (erkannte) Biegebeanspruchungen zu eliminieren. Die z w e i t e Trägerhälfte blieb der Messung geometrischer Größen (Verschiebungen) vorbehalten; sie war mit Reißlack überzogen, um einen Überblick über die (mit der Be-

lastung veränderlichen!) Hauptdehnungsfelder zu gewinnen.- Meßuhrenketten gaben laufend die Distanz zwischen den Gurten wieder, auch wurden (über das ganze Feld a x b) die "Ausbeulungen" des Steges mit einer Genauigkeit von 1/100 [mm] gemessen.

In der vorliegenden V e r s u c h s r e i h e I wurden die Träger-Typen nach Tabelle 1, die zunächst ihre Abmessungen und Teil-Querschnitte enthält, geprüft.- Die Belastungssteigerung erfolgte in Stufen $\Delta P = 1$ Mp (bzw. in der Nähe von charakteristischen Lastwerten von $\Delta P = 0{,}5$ Mp). Bis zum Erreichen von P_{Gr}^{el} waren jeweils Entlastungen (bis auf eine geringe Vorlast) notwendig, um das Vorhandensein von nur elastischen Stegverformungen zu überprüfen.

5. Versuchsergebnisse und -beobachtungen

Zur Feststellung der Werkstoffkennwerte der beiden gleichzeitig verwendeten Legierungen AlMg3 (F23) und AlMgSi0,5 (F22) wurden je 2 Zugproben untersucht. Wie aus Bild 3 erkennbar, verlaufen die σ-ε-Diagramme in dem als Biegeträger mit Navier'scher Spannungsverteilung beanspruchten Bereich mit befriedigender Übereinstimmung.

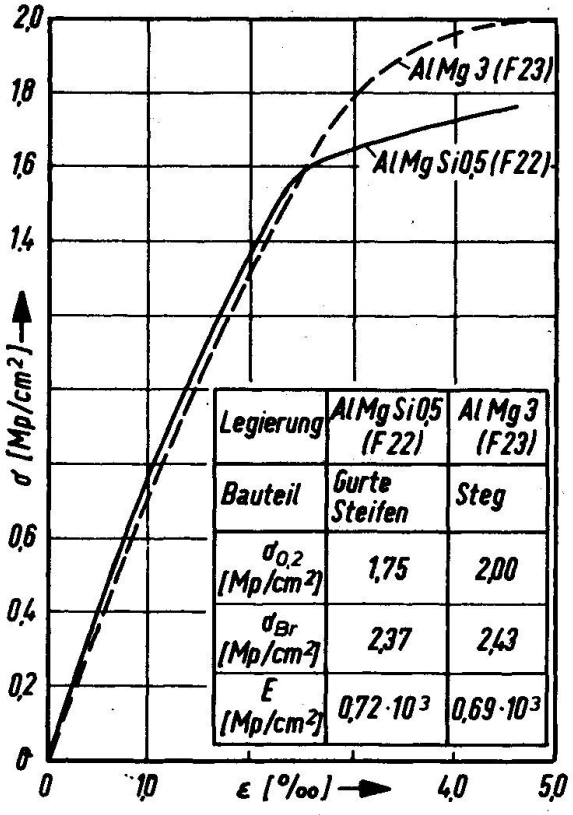

Legierung	AlMgSi0,5 (F22)	AlMg3 (F23)
Bauteil	Gurte Steifen	Steg
$\sigma_{0,2}$ [Mp/cm²]	1,75	2,00
σ_{Br} [Mp/cm²]	2,37	2,43
E [Mp/cm²]	$0{,}72 \cdot 10^3$	$0{,}69 \cdot 10^3$

Bild 3: Werkstoffkennwerte

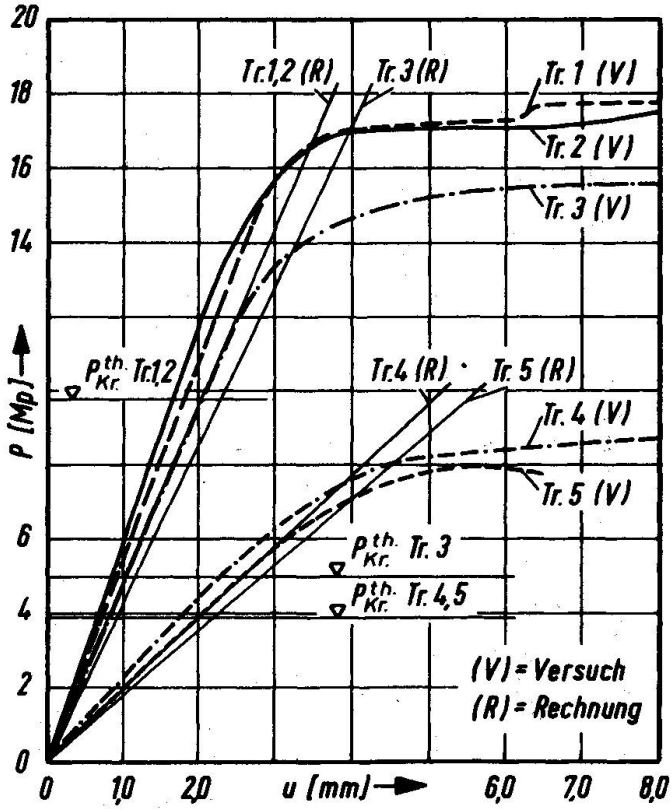

Bild 4: Last-Durchbiegungskurven der Träger (Tr) 1 bis 5

Tabelle 1: Abmessungen und Ergebnisse der Versuchsreihe I

Träger Nr.	Trägeraufbau	Abmessungen					Lasten				Krit. Spannungen		Laststeigerungen	
	Erläuterungen: $l = 2a = 900$ mm, $\ddot{u} = 100$ mm, $e = 23$ mm (Schraubenrißlinie), $b' = b - 2e$, $a' = a - 2e - 12$	Gurtplatte $\Phi\, d \cdot c$ [mm]	Gurtwinkel/ Stegsteifen [mm]	Stegblech $\Phi\, b \cdot t$ [mm]	$\alpha = \frac{a}{b}$ bzw. $\alpha = \frac{a'}{b'}$	$\beta = \frac{b}{t}$ bzw. $\beta = \frac{b'}{t}$	$P_{Kr}^{theor.}$ je nach Randbed. [Mp]	$P_{Kr}^{DIN\,4114}$ [Mp]	P_{Gr}^{el} [Mp]	$P_{Tr.}^{pl}$ [Mp]	$\tau_{Kr}(P_{Kr}^{theor.})$ [Mp/cm²]	$\sigma_{Kr}^{Rand}(P_{Kr}^{theor.})$ [Mp/cm²]	$n = \frac{P_{Gr}^{el}}{P_{Kr}^{theor.}}$	$n^* = \frac{P_{Tr}^{pl}}{P_{Kr}^{theor.}}$
	a	b	c	d	e	f	g	h	i	k	l	m	n	o
1	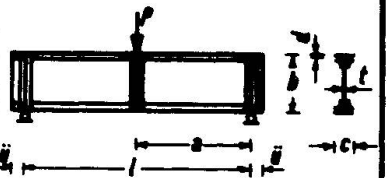	Φ120·10	⊤ 40·40·3	Φ450·3	1,98	135	9,8	(6,0)	14,0	17,6	0,34	0,53	1,43	1,80
2	Verbindungsmittel: HV M12		⊤ 40·40·3				9,8	(6,0)	15,0	18,0	0,34	0,53	1,52	1,84
3	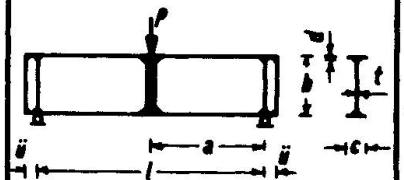 Verbindungsmittel: M16 – Schweißung	Φ120·10	Φ57·10	Φ450·3	1,94	150	5,0	(5,0)	12,0	16,1	0,16	0,36	2,40	3,22
4	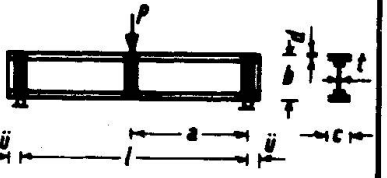	Φ 100·6	⊤ 40·40·3	Φ335·2	2,91	145	3,9	(2,3)	7,0	8,8	0,29	0,21	1,80	2,26
5	Verbindungsmittel: HV M12		⊤ 40·40·3				3,9	(2,3)	7,0	8,0	0,29	0,25	1,80	2,06

Bei den Verformungsmessungen in Tragwerksebene sind in Bild 4 die Lastverschiebungs-Diagramme für die Träger 1 bis 5 dargestellt. Hierbei ist festzustellen, daß die Verformungen sich noch in einem größeren Bereich über den jeweils kritischen Lasten nahezu linear verhalten und sich erst im Bereich von P_{Gr}^{el} die Abminderung des Schubmoduls G auswirkt. Die theoretischen Lastverformungslinien sind nur bis P_{kr} gültig und setzen sich aus der Summe der Biege- und Schubverformung zusammen; letztere hat infolge der geringen Stegfläche einen Anteil von 44 bis 57 % der Gesamtverformung, die hier – infolge der relativ kurzen Trägerstützweite – rechnerisch zu groß erscheint.

In Bild 5 für Träger 2 und in Bild 6 für Träger 5 sind die Verformungen u der Gurte für die drei maßgebenden Laststufen $P_{kr}^{theor.}$, P_{Gr}^{el}, P_{Tr}^{pl} (bzw. eine Last nahe bei P_{Tr}^{pl}) dargestellt. Es wird hierbei jeweils die überlagerte Biegelinie aus dem Anteil der Durchbiegung des gesamten Trägers und derjenigen aus der Zugfeldbeanspruchung u_o je Trägerhälfte wiedergegeben. Die maximalen Ordinaten bei a/2 wachsen erst nach Überschreiten der Last P_{Gr}^{el} stark an, zeigen jedoch von Anfang an kein proportionales Verhalten zur Laststeigerung. Aus dieser Gurtverformung im Bereich eines Stegfeldes wird dem Gurtquerschnitt neben der vorhandenen Normalkraft ein zusätzliches Biegemoment $\Delta M = P_G \cdot u_o$ zugewiesen. Weiterhin ist die durch die Zugfeldwirkung hervorgerufene Gegenkrümmung im Untergurt klar erkennbar. Der Unterschied der maximalen Werte u bei einem Vergleich der beiden Bilder sind hierbei abhängig von dem Überschreitungsgrad $vorh P/P_{Kr}$, dem Wert α sowie von der noch zu definierenden Gurtsteifigkeit EJ_W.

Verformungen w senkrecht zur Tragwerksebene sollten für die Gurte ausgeschlossen sein. In Bild 7 a–d für Träger 3 ($\alpha \approx 2$) sind nun die Stegverformungen für die maßgebenden Laststufen aufgezeichnet. Die große Vorverformung $w_o = 6{,}7$ mm $\approx 2{,}2$ t war bei diesem Träger aus dem Schweißvorgang entstanden. Alle weiteren wiedergegebenen Darstellungen (Bild 7b,c,d) nehmen diesen Zustand als Nullstellung an, zeigen jedoch, daß diese weitgehend spannungsfreie Vorbeule sich bei steigender Belastung in die Stegblechebene teilweise zurückbildet, um dann relativ früh wieder in ein nahezu klassisches Zugdiagonalfeld überzugehen. Ein verhältnismäßig schnelleres Anwachsen der Beultiefen sowie eine größere Traglastverminderung konnte bei einem Vergleich mit Träger 1 und 2 (gleiche Stegfläche, 1,29faches Trägheitsmoment) aus dem Vorhandensein einer Vorbeule nicht abgeleitet werden. Bei der Darstellung der Stegverformungen für den Träger 5 ($\alpha \approx 3$) in Bild 8 a–d zeigt sich ausgehend von einer sehr geringen Vorbeule $w_o = 0{,}6$ mm $\approx 0{,}3$ t – nach der Ausbildung typischer Beulfiguren in der Nähe der Last $P_{kr}^{theor.}$ (mit

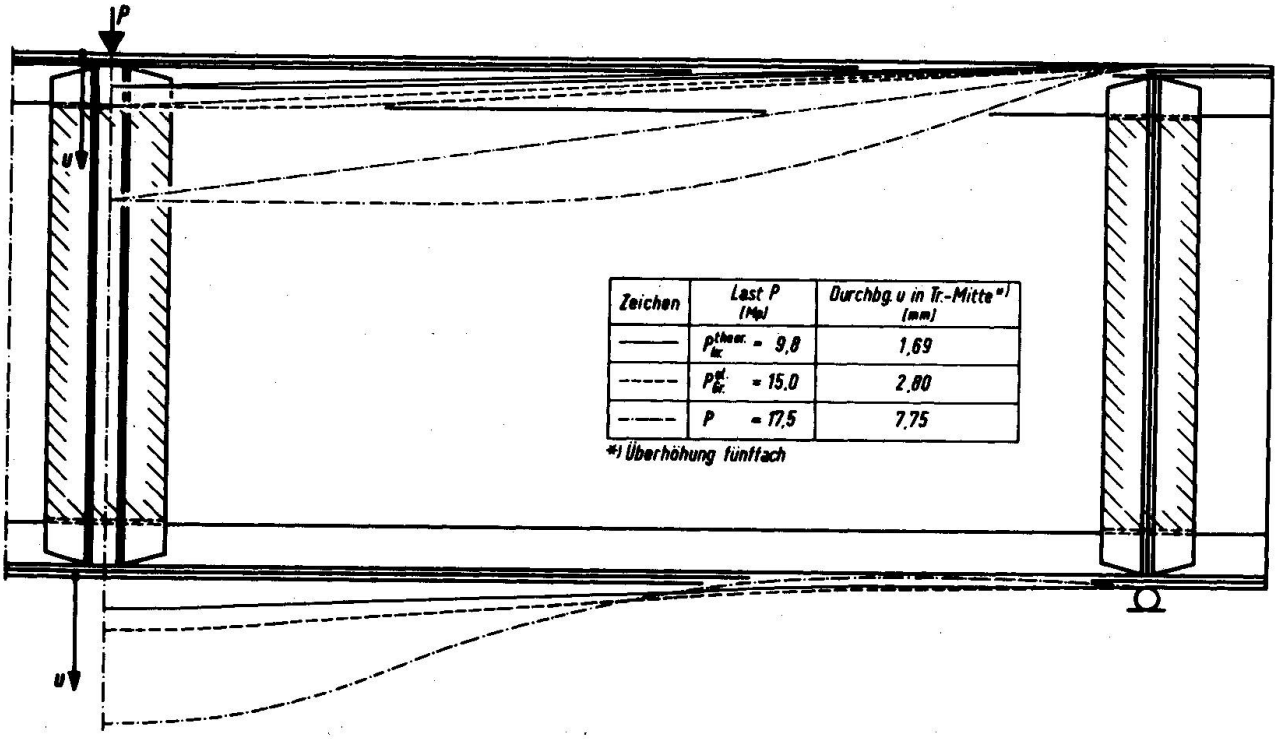

Zeichen	Last P (Mp)	Durchbg. u in Tr.-Mitte *) (mm)
———	$P_{kr.}^{theor.}$ = 9,8	1,69
- - - - -	$P_{Gr.}^{el.}$ = 15,0	2,80
—·—	P = 17,5	7,75

*) Überhöhung fünffach

Bild 5: Gurtverformungen u von Träger 2 (aus Versuch)

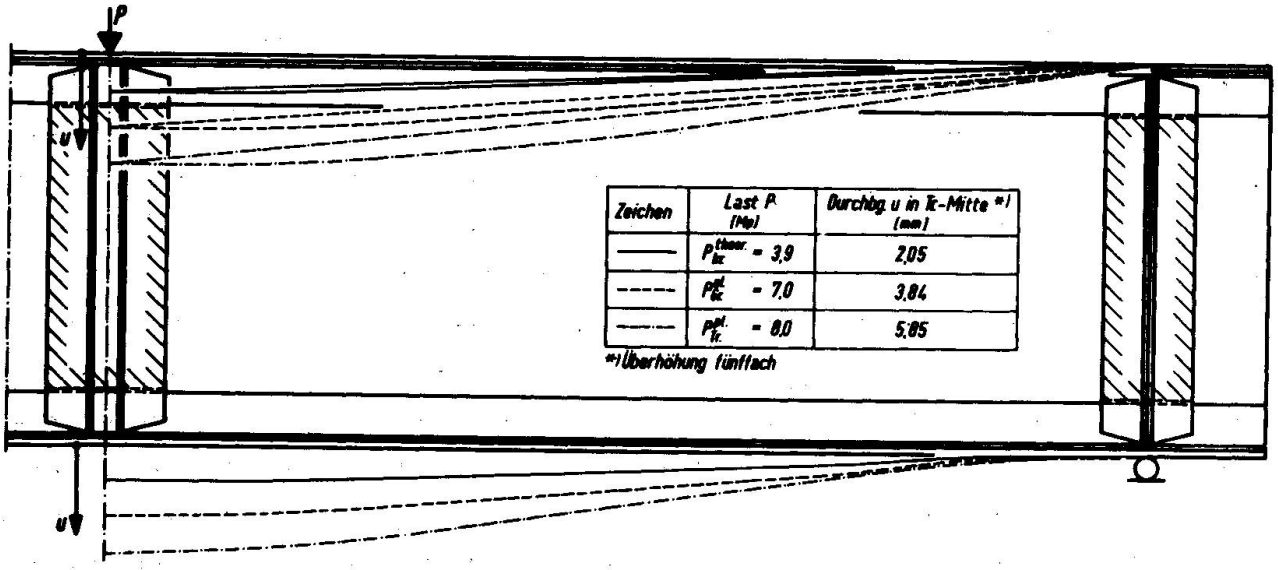

Zeichen	Last P (Mp)	Durchbg. u in Tr.-Mitte *) (mm)
———	$P_{kr.}^{theor.}$ = 3,9	2,05
- - - - -	$P_{Gr.}^{el.}$ = 7,0	3,84
—·—	$P_{Fl.}^{el.}$ = 8,0	5,85

*) Überhöhung fünffach

Bild 6: Gurtverformungen u von Träger 5 (aus Versuch)

einer Beulenbreite $b^* = 0{,}8$ bis $1{,}0\ b$) - wiederum das bekannte Zugdiagonalfeld, das ausgehend von der "klassischen" Zugfeldneigung $\phi = 40$ bis 45° sich erst später bei Lasten $P > P_{Gr}^{el}$ in die Neigung der geometrischen Diagonale des Stegfeldes dreht. Die Stegverformungen konnten (infolge Überschreitens des Meßbereiches an mehreren

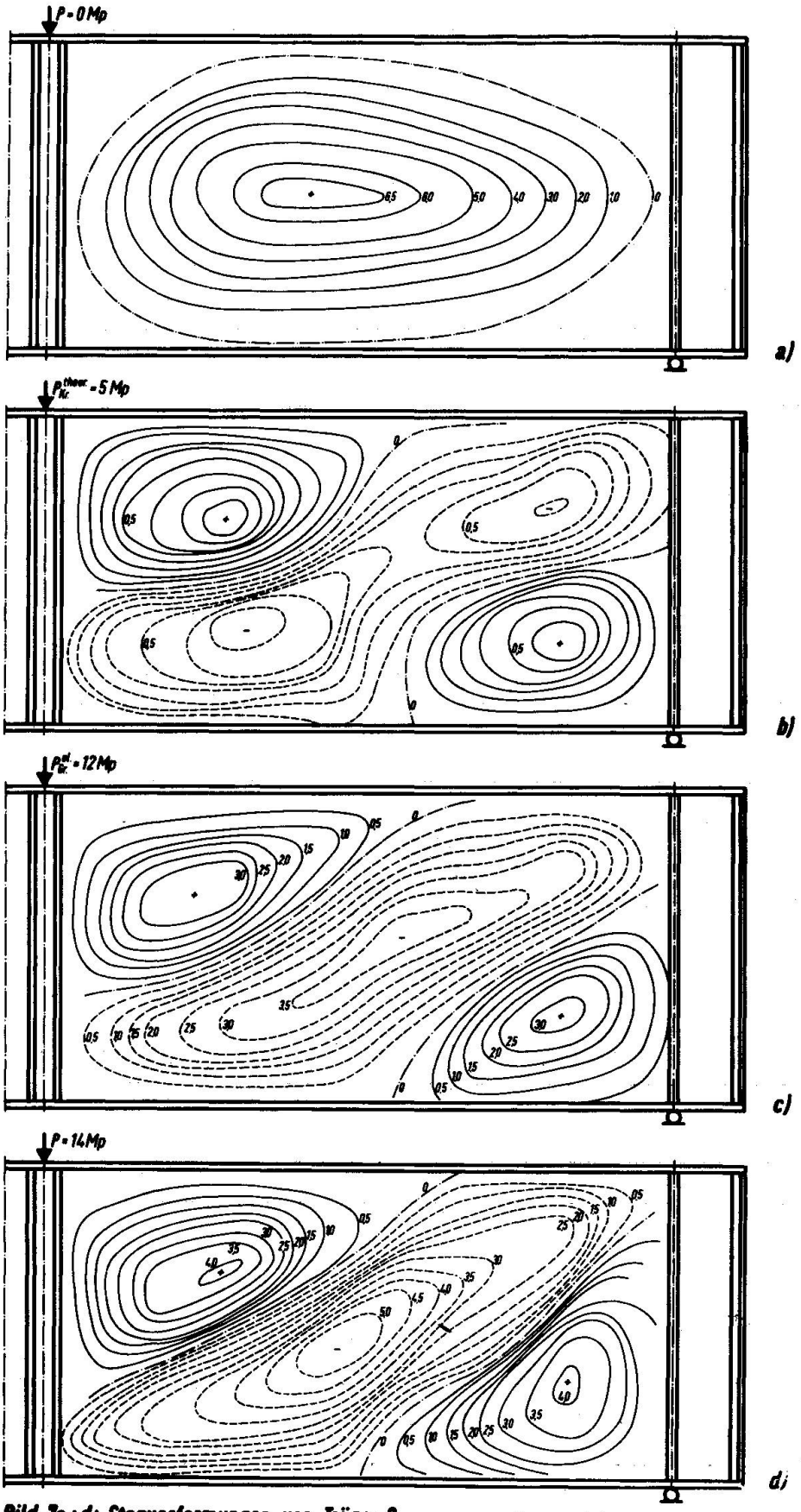

Bild 7a÷d: Stegverformungen von Träger 3
Höhenquoten in mm

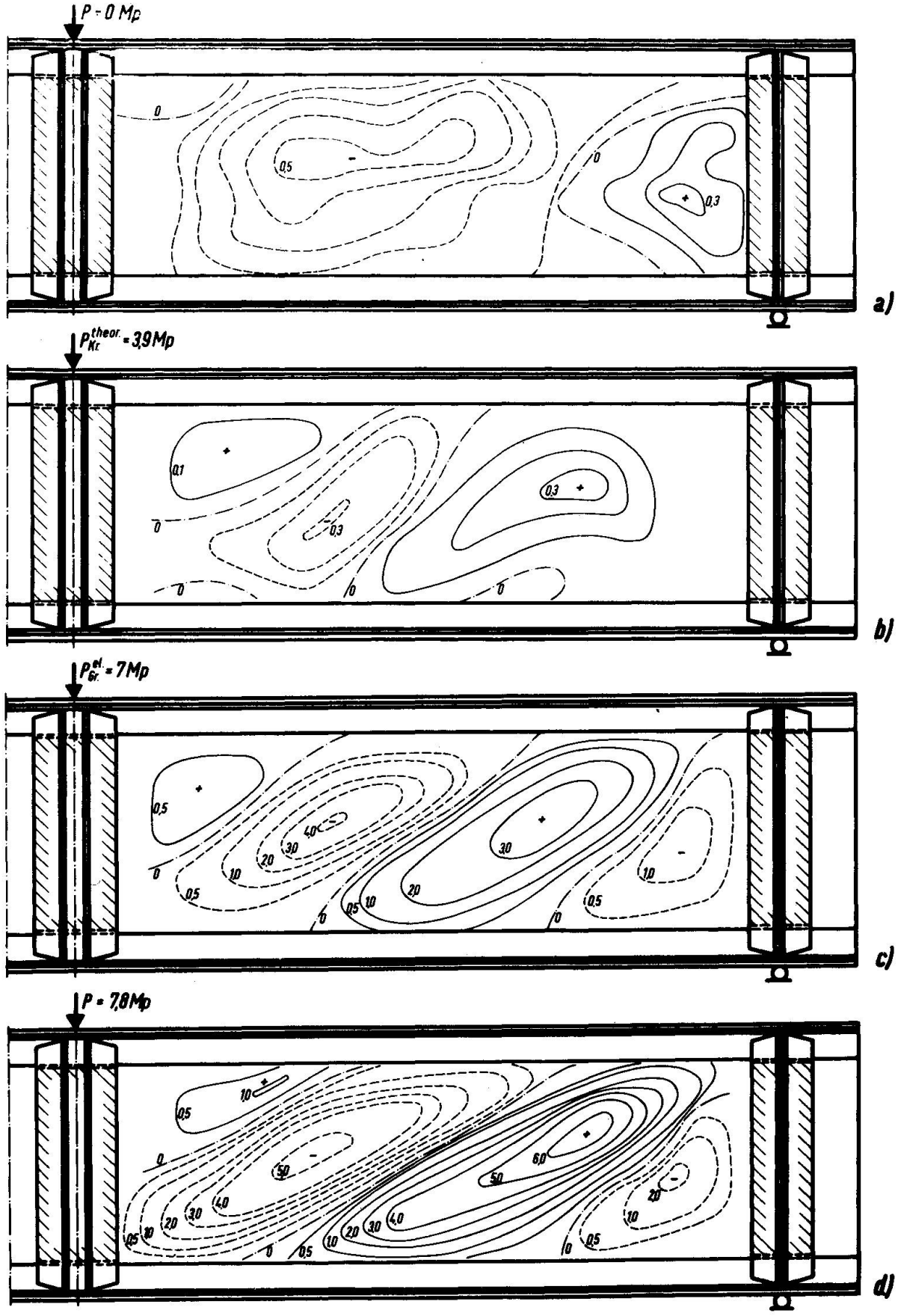

Bild 8a÷d: Stegverformungen von Träger 5

Höhenquoten in mm

Meßuhren) im Endzustand P_{Tr}^{pl} nicht mehr als vollständiges Bild (deshalb $P < P_{Tr}^{pl}$ für Bild 7d und Bild 8d), sondern nur an einzelnen Stellen gemessen werden. Tabelle 2 gibt eine Übersicht über die maximalen Stegverformungen w, die von der jeweiligen Vorverformung aus ermittelt wurden. (Für Träger 1 und 2 liegen keine Meßwerte vor.)

Tabelle 2: Maximale Stegverformungen w_{max} mm der Träger 3 bis 5

	a	b	c	d	e
1	Träger		3	4	5
2	Stegblechdicke t mm		3	2	2
2	nach ROCKEY $J_G/(a^3 \cdot t) \cdot 10^{-6}$		4,8	4,6	4,6
3	Stegverformungen in Abhängigkeit von den Lasten	P_o / w_{omax}	0 / 6,7	nicht gemessen	0 / 0,6
4		P_{Kr}^{theor} / w_{max}	5,0 / 0,8	3,9 / 0,6	3,9 / 0,3
5		P_{Gr}^{el} / w_{max}	12,0 / 3,3	7,0 / 3,0	7,0 / 4,0
6		P_{Tr}^{pl} / w_{max}	16,1 / 8,3	8,8 / 4,6	8,0 / 6,2

In Bild 9 werden für Träger 5 die in der Mitte der Gurte gemessenen Randspannungen σ_x (um 90° zur Spannungsrichtung gedreht) für die maßgebenden Lasten aufgetragen. Diesen Meßwerten sind die berechneten Spannungen nach der technischen Biegelehre gegenübergestellt. Hierbei ist deutlich eine Spannungsreduzierung für die Untergurte aber auch für die Obergurte eine Spannungszunahme festzustellen, die aus der horizontalen Komponente der Zugfelddiagonalen sowie aus der Änderung der Tragweise (Biegeträger-Schubfeldträger-Fachwerkträger) resultiert.- Zur Auftragung der σ_x-Spannungen am Querschnitt A B wurden zusätzlich Messungen in den Punkten A' und B' (56 mm von den Randfasern entfernt) vorgenommen. Die daraus sich ergebenden Spannungsverteilungen im Bereich der Gurte lassen für Laststufen $P > P_{Kr}^{theor.}$ keine Annahme (auch nicht im Bereich der Zugzone) nach Navier zu. Für die Spannungskomponenten in y-Richtung wurden meßtechnisch sehr kleine Werte festgestellt.

Bild 10 (für Träger 2) gibt eine Übersicht der τ_{xy}-Spannungen bei den maßgebenden Lasten, die im Abstand von 60 mm von der Randfaser sowie in zwei Querschnitten gemessen wurden und den rechnerischen Spannungen nach der technischen Biegelehre gegenübergestellt sind. Im Sinne des "unvollständigen" Zugfeldes ist hierbei ein dreistufiger Systemwandel zu be-

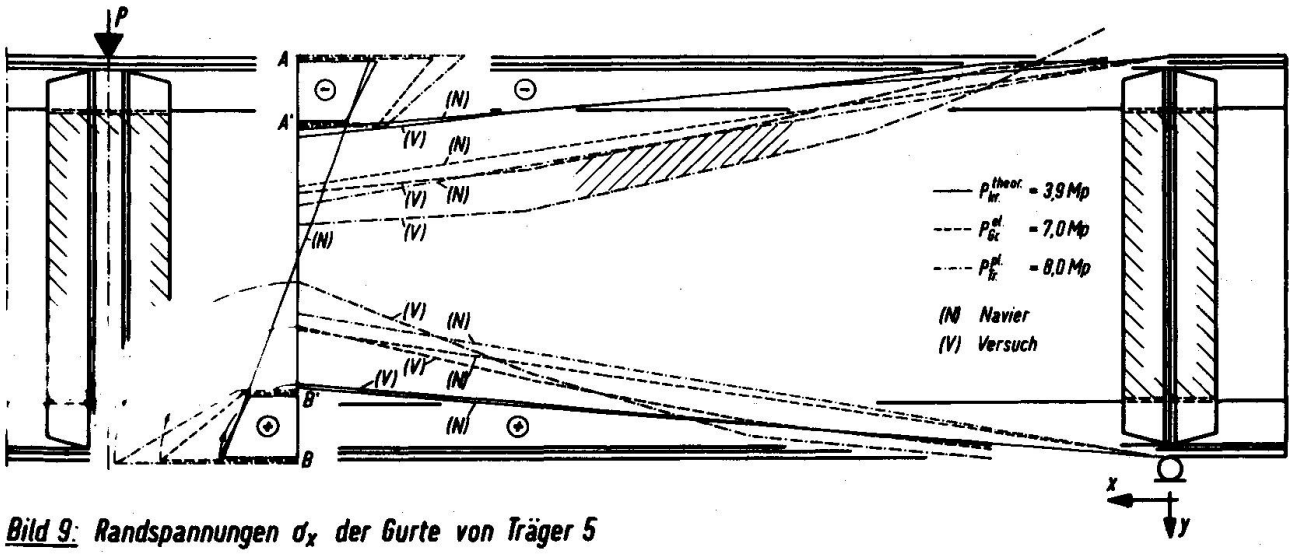

Bild 9: Randspannungen σ_x der Gurte von Träger 5

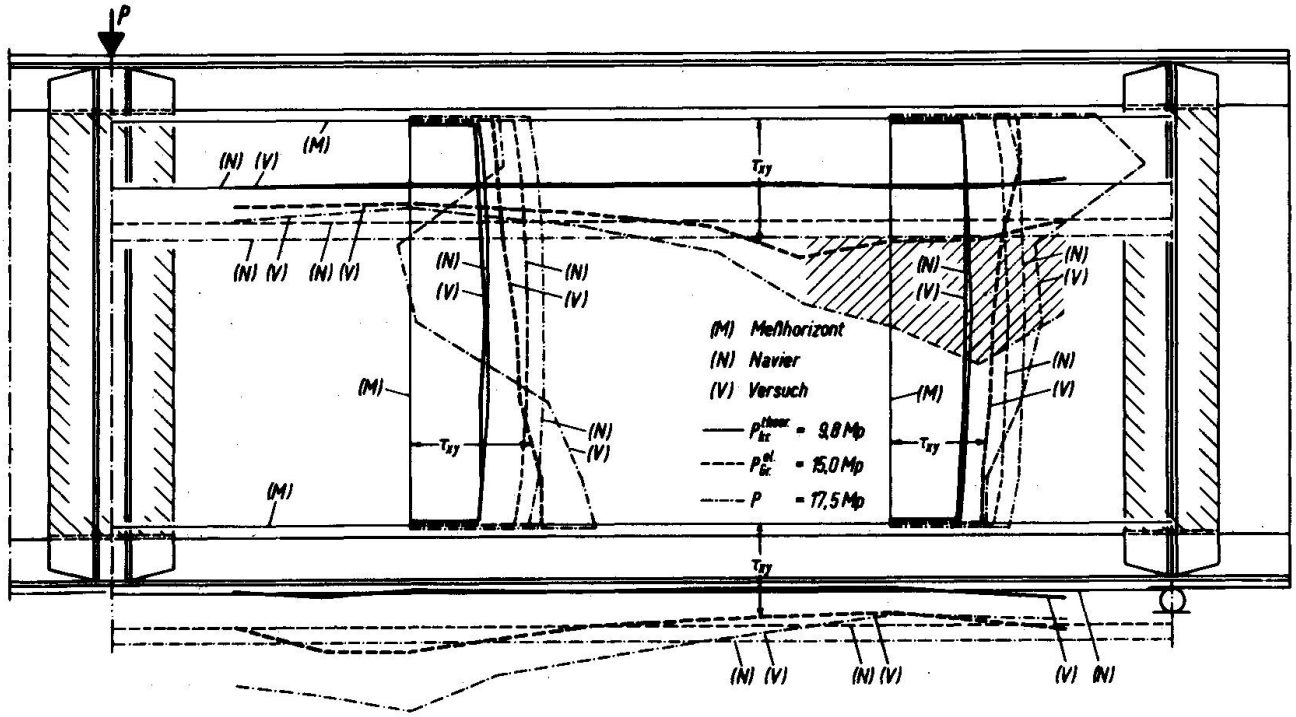

Bild 10: τ_{xy} - Spannungen von Träger 2

obachten. Ausgehend von der Berechnung nach der technischen Biegelehre ($P \leq P_{Krit}^{theor.}$) ist bei weiterer Laststeigerung in dem Stegbereich außerhalb des stärker wellenförmig verformten Zugfeldbandes eine proportionale Steigerung der Schubspannung zu beobachten. Man kann also bis etwa zur Laststufe P_{Gr}^{el} in einem größeren Bereich des Stegbleches von einer Sandwichtragweise (auch Schubfeldträger genannt) sprechen, wobei die Reduzierung des Schubmoduls im Bereich des Zugfeldbandes zu berücksichtigen wäre. Erst oberhalb P_{Gr}^{el} kommt es u.E. zur eigentlichen "Fachwerkträgerwirkung", d.h. das Zugband hat sich in die geometrische Diagonale gedreht. Diese Deutung befindet sich auch in Übereinstimmung mit der Drehung der Beulfiguren (z.B.Bild 7d) bei wachsenden Lasten in die geometrische Diagonale.

6. Theoretische Untersuchungen

In einer neueren Veröffentlichung gibt Ch. MASSONNET [8] eine kritische Beurteilung der bis jetzt bekanntgewordenen Traglastberechnungsmethoden. Darauf aufbauend läßt sich - unter Berücksichtigung mitgeteilter fremder und bisheriger eigener Versuche - u.E. das Tragverhalten von Vollwandträgern mit relativ sehr dünnen Stegen - in schrittweise zunehmender Genauigkeit - anhand der nachfolgend aufgeführten mechanischen Modelle baustatisch erfassen:

6.1 Vollwandträger ausschließlich mit Quersteifen

A. Über die (druckfesten) Quersteifen, die ausschließlich an ihren beiden Enden angeschlossen sind, verlaufen die (biegeelastischen) Gurte kontinuierlich durch.- Die feldweise Steigerung der Gurtkräfte infolge der Querkraft $Q = Q^{*} + Q^{**}$ erfolgt auf zweierlei Weise: Q^{*} wird (über τ_{krit} hinaus, jedoch bei etwas absinkendem Schubmodul G^{*}) kontinuierlich gemäß Navier's Theorie, Q^{**} gemäß einer Zugfeldtheorie örtlich in der Feldecke übertragen, welche ganz wesentlich erst zwischen P_{Gr}^{el} und P_{Tr}^{pl} zur Auswirkung gelangt. Für die vereinfachte Anwendung dieser letztgenannten Theorie darf die "Zugfelddiagonale" wie im Traglastfall unter einer Neigung $tg\,\phi = 1/\alpha = b/a$ angenommen werden; rechtwinklig zu dieser Diagonalen ergibt sich eine definierbare Zugspannungsverteilung σ_{dz} im Steg (Bild 11). Man erhält zuletzt eine mathematische Beziehung zwischen Q^{**} (bzw. den Parametern einer Verteilungsfunktion für σ_{dz}) und den Zwischenbiegelinien der Gurte über die Länge a, die von den jeweilig wirksamen Trägheitsmomenten J_{w} der Gurte selbst abhängen. Anstelle der Zugfeldneigung kann auch der für die Ausbildung des Beulfeldes wichtige Parameter α eingeführt werden (I. Bericht über die Karlsruher Untersuchungen).

B. In konsequenter Weiterführung des Gedankenganges, wie er unter A beschrieben wurde, kann der Einfluß einer stetig-festen Verbindung der Quersteifen mit dem Stegblech in Abhängigkeit von der Biegesteifigkeit dieser Steifen (in der Trägermittelebene) verfolgt werden. Es werden nun zusätzlich durch eine antimetrische Belastung der Steifen in genannter Ebene einerseits sprunghaft Zusatzbeträge der Gurtkräfte abgegeben, andererseits wird die Spannungsverteilung innerhalb des Zugfeldes in geringem Maße unsymmetrisch.

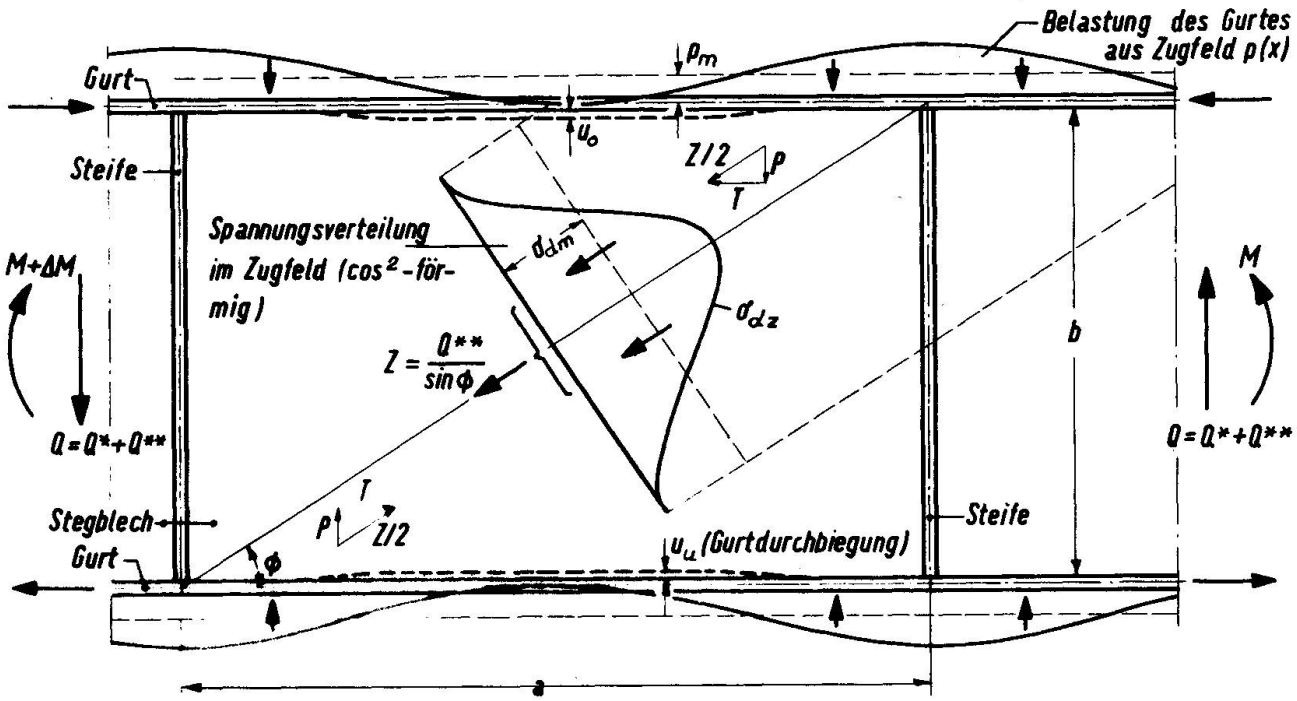

Bild 11: Gedankenmodell zur Spannungsverteilung im Zugfeld und resultierende Gurtbelastung

6.2 Vollwandträger mit Quersteifen und einer Längssteife (im Abstand b_1 vom Obergurt).

A. Bei zweckmäßiger Ausbildung einer Längssteife, die etwa bis $b_1 = b/3$ vom Obergurt entfernt ist, kann prinzipiell im Sinne der Ausführung unter 6.1 A verfahren werden. Infolge eines verhältnismäßig großen Trägheitsmomentes J_w für den Obergurtbereich ergibt sich ein verbreitertes und abgeflachtes Zugfeld innerhalb der größeren Stegfläche a x b_2. Es wird wahrscheinlich konstruktiv zweckmäßig sein, diesen einfachen Längssteifenstrang entweder aus hochfesterem Material herzustellen, oder ihn beispielsweise über HV-Verbindungen so anzuschließen, daß eine frühzeitige Plastizierung bzw. der Verlust der aussteifenden Wirkung senkrecht zur Trägerebene vermieden wird.

B. Eine weitergehende Untersuchung über Quersteifen mit erhöhter Steifigkeit (in Trägermittelebene) leitet über zu den nachfolgenden Betrachtungen (6.3). -

6.3 Vollwandträger mit Quer- und Längssteifen, die rahmenartig Stegblechfelder umfassen.

Das Problem eines einzelnen auf Biegung und Schub beanspruchten Stegfeldes, das durch einen biegesteifen, rechteckigen Rahmen begrenzt

wird, kann als Fortsetzung der Modellvorstellung gemäß 6.1 und 6.2 angesehen werden.- Falls die Gesamtansicht eines Vollwandträgers durch zahlreiche Einzelfelder $a_i \times b_i$ zusammengesetzt ist, bliebe zuletzt die Möglichkeit über ein größeres Rechenprogramm (z.B. mit Hilfe der Methode der Finiten Elemente) charakteristische Anwendungsfälle fallweise zu lösen.

8. Literatur

[1] MASSONNET, Ch.: Dünnwandige hohe Blechträger JVBH-Vorbericht, VIII. Kongreß New York (1968) S. 178.

[2] MASSONNET, Ch.: Bemerkungen des Verfassers des Einführungsberichtes. JVBH-Schlußbericht, VIII. Kongreß New York (1968) S. 493.

[3] ROCKEY, K.C.: The Influence of Flange Stiffness upon the Post-buckled Behaviour of Web Plates subjected to Shear. Engineering Vo. 184, (1957) S. 788.

[4] BASLER K. und B. THÜRLIMAN: Strength of Plate Girders in Bending Proc. ASCE, Journal Structural Div. St. 6 S. 153 Août 1962.

[5] FUJII, T.: On an Improved Theory for Dr. BASLER's Theory. JVBH-Schlußbericht, VIII. Kongreß New York (1968) S. 479.

[6] ROCKEY, K.C. u. M. ŠKALOUD: Influence of Flange Stiffness upon the Load Carrying Capacity of Webs in Shear. JVBH-Schlußbericht, VIII. Kongreß New York (1968) S. 429.

[7] WAGNER, H.: Ebene Blechwandträger mit sehr dünnem Stegblech. Zeitschrift für Flugtechnik u. Motorluftschiffahrt, 20. Jahrgang, 8. Heft (1929), S. 200.

[8] MASSONNET Ch.: Grandes poutres à âme mince, tendances actuelles dans la conception et le calcul; Construction métallique, Nr. 2, Paris, 1969.

ZUSAMMENFASSUNG

Die in unserem vorliegenden Bericht I in den Abschnitten 3, 4 und 5 beschriebenen Versuche an Aluminium-Vollwandträgern mit Quersteifen erlauben einige Rückschlüsse auf ihren Tragmechanismus. Abschnitt 6 gibt hierzu (in Bild 11) erste einfache mathematisierbare Ansätze, die in ihrer Auswertung anhand weiterer Diskussionsbeiträge unsererseits auf dem Colloquium erläutert werden sollen. - In diesem Abschnitt wird darüber hinaus für zukünftige Untersuchungen ein systematisches Fortschreiten beschrieben. Es ist zu erwarten, dass in Karlsruhe im Laufe des Jahres 1971 die unter 6.1 B und 6.2 A beschriebenen Ausführungsfälle versuchstechnisch erforscht werden können.

SUMMARY

The tests described in this report in the chapters 3, 4 and 5 allow some conclusions about the load behaviour of aluminium-plate girders with transverse stiffeners. Chapter 6 gives first points of application to find a mathematic solution that will be discussed by us at the Colloquium. In this chapter a systematic advancement for further research is also given. It is expected that during 1971 the two cases described in 6.1.B and 6.2.A will be tested at Karlsruhe.

RESUME

Les auteurs décrivent des essais effectués sur des poutres à âme pleine en aluminium, raidies transversalement; ces essais permettent d'établir quelques conclusions relatives au comportement des poutres sous charge. On donne également un modèle simple des sollicitations, qui sera discuté lors du Séminaire. On décrit pour terminer un programme systématique de recherches futures; il est probable que l'on pourra réaliser en 1971 les essais décrits sous 6.1B et 6.2A.